UNIVERSITY OF UDINE

PhD COURSE IN BIOMEDICAL SCIENCES AND BIOTECHNOLOGY

XXVIII CYCLE

DOCTORAL DISSERTATION

BLUU-TRAMP DATA ANALYSIS: THERMODYNAMIC LANDSCAPE OF LOCAL UNFOLDING PROCESSES

TUTOR: Prof. Gennaro Esposito   **PhD STUDENT: Marco Vuano**

ACADEMIC YEAR 2015/2016

INDEX

ABSTRACT

Isotopic exchange probed through NMR spectroscopy has been a precious source of information regarding local protein unfolding processes due to its ability to observe the exchange rate of single residues' amide sites. BLUU-Tramp extends this information allowing to follow, through two series of experiments, how the exchange constants vary over temperature.

In this thesis a novel approach is introduced by means of an ad hoc calculation routine which is able to extract thermodynamic parameters from the decays of the amide signals, obtained through suitable treatment of the experimental data by another original routine (TinT) of the suite devised in our laboratory. By assuming that the isotopic exchange rates can be approximated with the EX2 limit, it is possible to estimate both the ΔG of local unfolding and other underlying thermodynamic parameters, in particular the ΔCp.

The method is used to obtain these parameters in two human proteins, β2-microglobulin and lysozyme.

Furthermore, a similar computational approach is presented which is able to extract thermodynamic parameters from classical isotopic exchange experiments carried out at various different temperatures. Comparisons among the results extracted from BLUU-Tramp series and classical exchange experiments are drawn and critical aspects in the latter kind of experiments are discussed.

INTRODUCTION

THE BLUU-TRAMP METHOD

The BLUU-Tramp (Biophysical Laboratory of the University of Udine - Temperature ramp) method is a method to perform NMR isotope exchange experiments while varying one aspect of the system under study (typically temperature) in order to obtain results that are functions of that aspect[1].

Its current implementation consists in fully deuterating the molecule to be studied, lyophilizing it, putting it in an aqueous solution and then put the solution in an NMR tube that itself is put in an NMR spectrometer in order to acquire NMR spectra, in which hydrogen is in the direct dimension, at regular intervals. After each spectrum is acquired, the temperature is raised by a defined amount and, after a set amount of time needed for the system to equilibrate at the new temperature, a new spectrum is acquired. The resulting signal in the spectrum is therefore expected to increase due to the hydrogen exchange. Since the intensity and volume of the signal is affected by the temperature at which the spectrum is acquired, after the exchange is completed and the maximum temperature is reached, to evaluate the contribution of temperature to signal intensity and volume a new series of spectra, called the "reference series" is acquired using the same acquisition parameters, the same increase in temperature after each experiment and the same amount of time to equilibrate used in the first series of spectra, known as "exchange series".
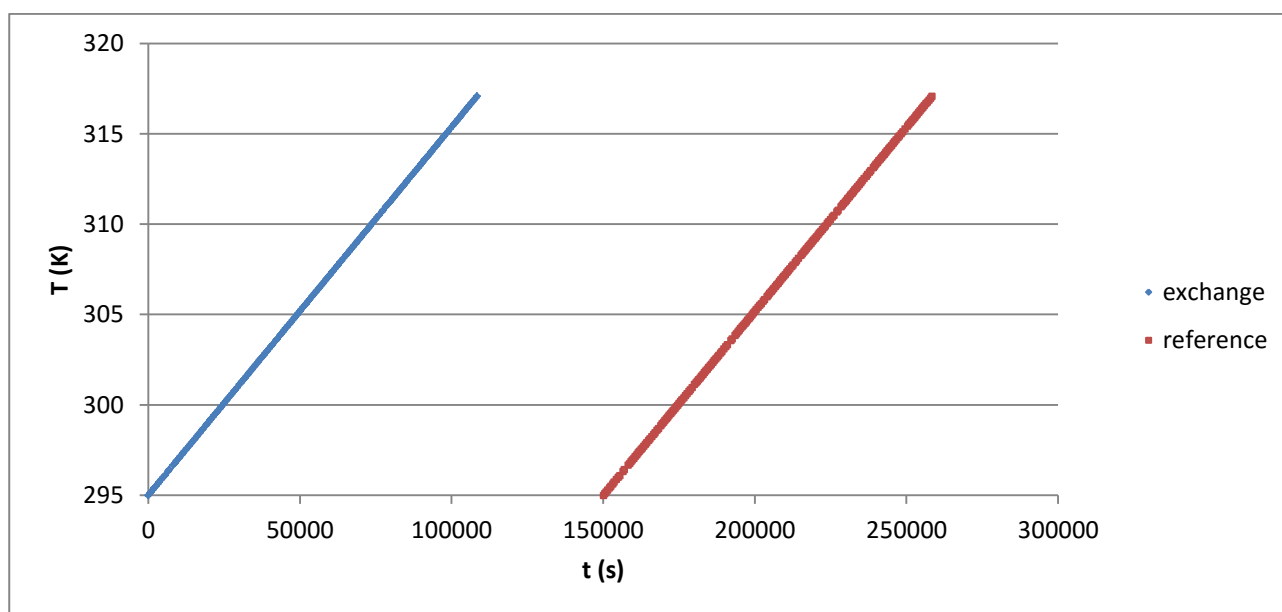
Figure 1 Example of the time elapsed from the first experiment of the exchange series and the temperature at which each experiment is acquired in a BLUU-Tramp experiment. Each experiment of the exchange series is indicated by a blue symbol, each experiment of the reference series is indicated by a red symbol.

Until now, mainly two dimensional ^{15}N-^{1}H spectra, such as SOFAST-HMQC spectra[2], have been acquired during the BLUU-Tramp experiments[1], although the method can be potentially used with any kind of spectra used to follow conventional isotope exchange experiments through NMR spectroscopy.

From the evolution of the signal in the exchange series and the evolution of the signal in the reference series it is possible to create a derivative signal I that decays over time:

THE BLUU-TRAMP METHOD

$$I_i = \frac{I_i^{ref} - I_i^{exc}}{I_i^{ref}} \qquad (1)$$

where I_i^{ref} is the signal intensity or volume in the i-th spectrum of the reference series, I_i^{exc} is the signal intensity or volume in the i-th spectrum of the exchange series and I_i is the i-th value of the derivative signal.
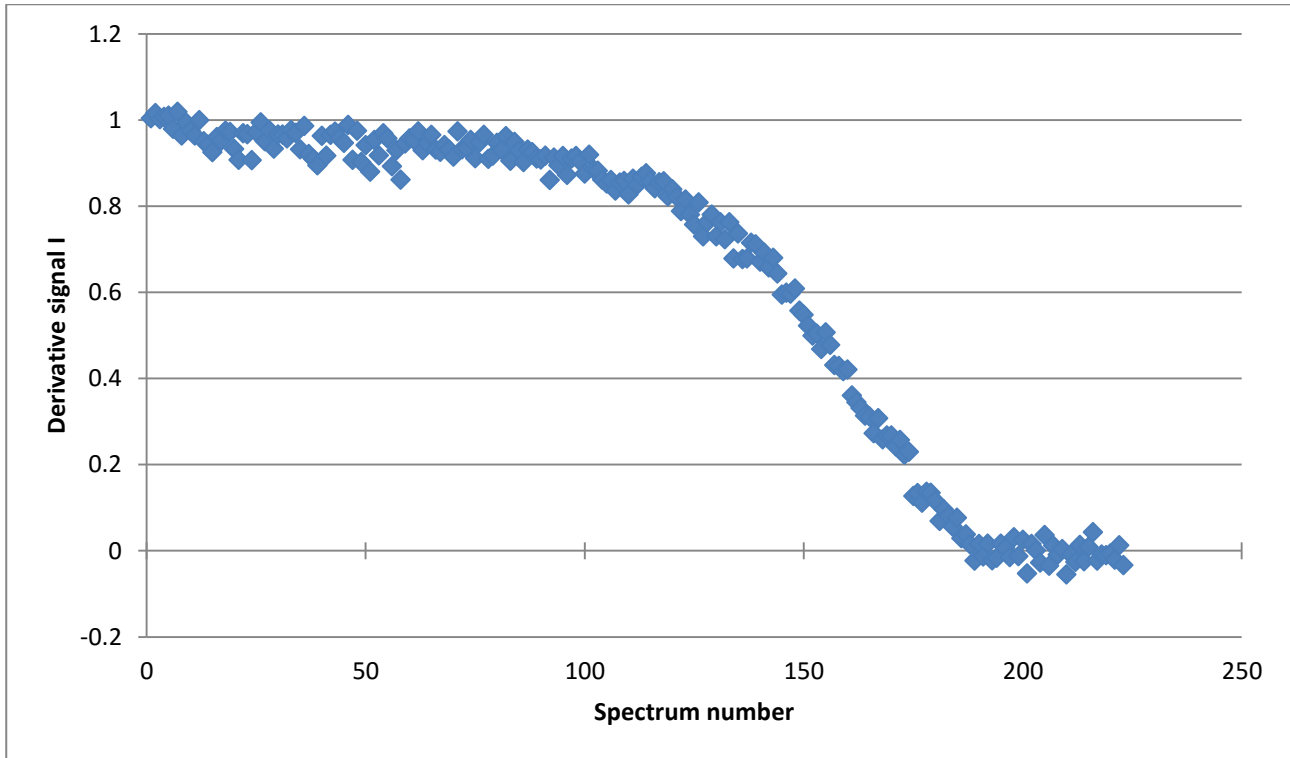
Figure 2 The derivative signal I of the Cysteine 25 of human β$_2$-microglobulin in the BLUU-Tramp experiment analyzed in this thesis.

Since the temperature is constantly changing over time, the derivative signal I is expected to follow this equation:

$$I = I_0 e^{-\int_o^t k_{ex}(T(t))dt} \qquad (2)$$

where I is the intensity of the decay, I_0 is the intensity of the decay in the first experiment, k_{ex} is the exchange constant, T is temperature (in K) and t is the time elapsed from the beginning of the first experiments (in seconds).

It is therefore possible to perform an analysis on the derivative signals I in order to estimate the value of the exchange constant as a function of time and temperature.

HUMAN β₂-MICROGLOBULIN

The human β₂-microglobulin is a small globular protein composed of 99 residues and having a molecular weight of around 11731.1 Da.
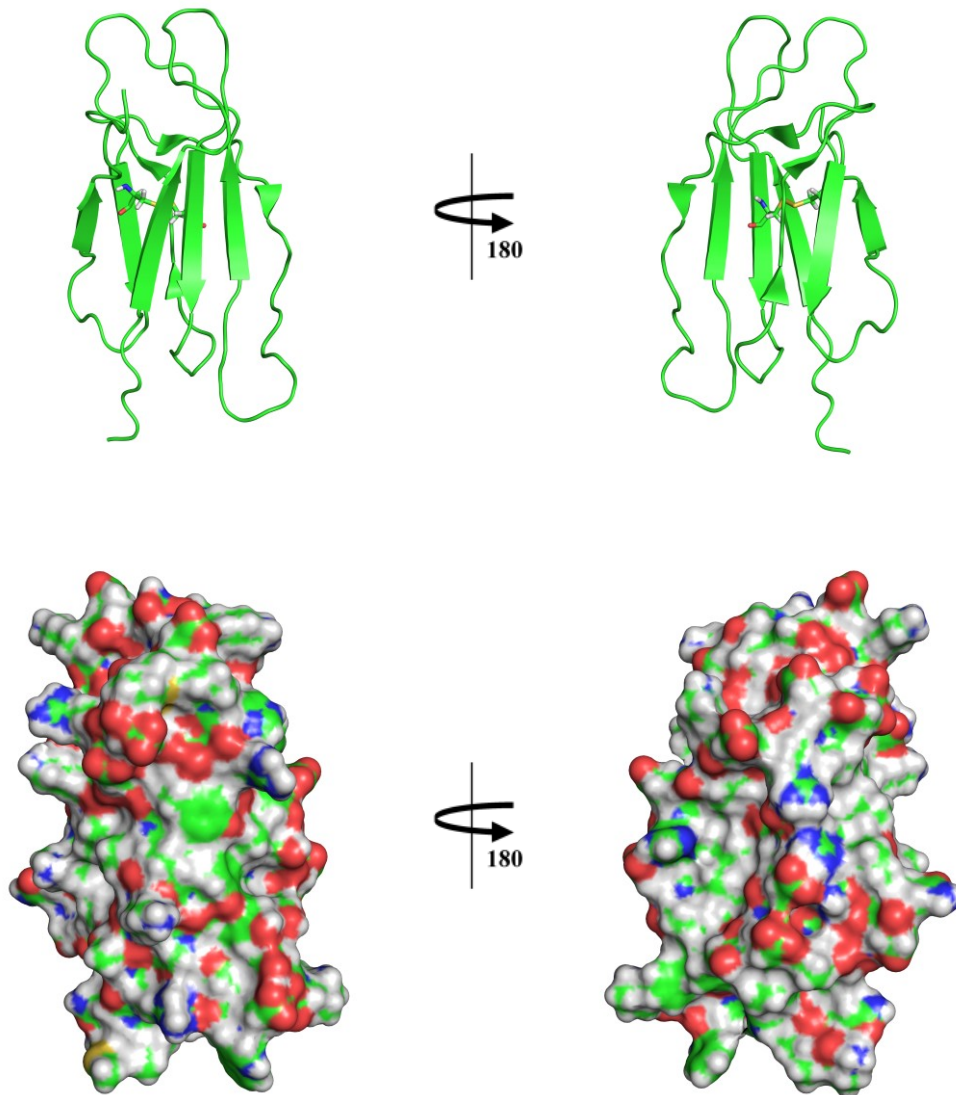
Figure 3 The structure of human β₂-microglobulin according to the first conformer of the RCSB Protein Data Bank entry 1JNJ[3] in both cartoon and surface representation. In the cartoon representation the cysteines involved in the disulfide bond are represented with sticks. The color reflects the element: carbon is green, hydrogen is white, oxygen is red, nitrogen is blue and sulfur is yellow. These representations of molecular structures and all the following representations of molecular structures in this thesis have been obtained using Pymol version 1.8.0[4].

Its solution structure has a single Ig-like Type C1 domain, with either 7 or 8 β strands forming two β sheets and a single disulfide bond[3].

Its gene, B2M, is located outside of the MHC locus, on the q arm of chromosome 15[5]. It presents 4 exons, the last of which only contains the 3' untranslated region.

The protein is translated with a 20 residues signal peptideat the N-terminal that gets cleaved as the protein enters in the Rough Endoplasmic Reticulum.

HUMAN β2-MICROGLOBULIN

The sequence of the protein after cleavage is reported here:

1	2	3	4	5	6	7	8	9	10	11	12	13	14	15	16	17	18	19	20
I	Q	R	T	P	K	I	Q	V	Y	S	R	H	P	A	E	N	G	K	S
21	22	23	24	25	26	27	28	29	30	31	31	33	34	35	36	37	38	39	40
N	F	L	N	C	Y	V	S	G	F	H	P	S	D	I	E	V	D	L	L
41	42	43	44	45	46	47	48	49	50	51	52	53	54	55	56	57	58	59	60
K	N	G	E	R	I	E	K	V	E	H	S	D	L	S	F	S	K	D	W
61	62	63	64	65	66	67	68	69	70	71	72	73	74	75	76	77	78	79	80
S	F	Y	L	L	Y	Y	T	E	F	T	P	T	E	K	D	E	Y	A	C
81	82	83	84	85	86	87	88	89	90	91	92	93	94	95	96	97	98	99	
R	V	N	H	V	T	L	S	Q	P	K	I	V	K	W	D	R	D	M	

Figure 4 The amino-acid residues sequence of human β₂-microglobulin. The background has been colored to underline which residues are part of β strands, while the two cysteines involved in the disulfide bond have an additional yellow background.

The β strands are named with letters in ascending order starting from the N-terminal. According to the solution structure derived from NMR data, they are composed of the following residues:

β strand	β sheet	Residues
A	1	K6-S11
B	1	L23-S28
C	2	I35-E36 and L39-L40
C'	2	R45-I46
D	1	V49-H51
E	1	Y63-T68
F	2	A79-H84
G	2	K91-K94

Table 1 The residues that form the 8 β strands. The β sheet to which each β strand belongs is reported as well.

BIOLOGICAL ROLE

The human β₂-microglobulin is a protein whose biological role is mainly structural: it is part of the Major Histocompatibility Complex I, that presents peptides found in the cytoplasm to T CD8 cells[6] and binds the KIR receptor of NK cells[7], inhibiting their cytotoxic activity.

Figure 5 Cartoon representation of the human class I Major Histocompatibility Complex, according to the conformer of the RCSB Protein data Bank 3HLA[8]. The α chain is colored in green, the β_2-microglobulin is colored in red.

The Major Histocompatibility Complex is formed by two chains. The first chain is a 43 kDa α chain composed of a cytoplasmic region, a transmembrane region and three domains: an α_3 domain, which is an Ig-like type C1 domain, and two α domains, α_1 and α_2, that form the peptide binding groove used to present the peptide. The second chain is β_2-microglobulin. The interaction, that happens in the Endoplasmic Reticulum where the α chain stays bound to calnexin until the complex with β_2-microglobulin is formed[9], has been shown to stabilize both the structure of the α chain and the structure of β_2-microglobulin[3].

After the complex is degraded, β_2-microglobulin ends up in the blood and is typically cleared by the kidneys[10].

β_2-microglobulin also interacts with other complexes, such as class IB Major Histocompatibility Complexes, the neonatal Fc Receptor (FcRn)[11], the CD1 receptor[12] and the HFE complex[13].

HUMAN β2-MICROGLOBULIN

INVOLVEMENT IN DISEASES

Dialysis- related Amyloidosis

Dialysis-related amyloidosis is one of the complications of chronic haemodialysis. It is characterized by an accumulation of amyloid, especially in the joints, causing pathological states such as Carpal tunnel Syndrome, trigger finger, cervical destructive spondyloarthropathy and the formation of amyloid-filled cysts in the femoral neck area[14].

The amyloid fibrils contains mainly β_2-microglobulin[15], along with amyloid P component[16] and modified forms of β_2-microglobulin, such as advanced glycation products[17], oxidized forms[18] and cleaved forms[19], such as ΔN6, a variant of β_2-microglobulin devoid of its first 6 residues at the N-terminal which constitutes the 26% of all the isoforms of β_2-microglobulin found in the fibrils[20].

Even though the concentration of β_2-microglobulin in patients undergoing haemodialysis is high[16], its monomer at pH 7.0 is stable and unable to form fibrils[21],[20]. For this reason, various hypotheses are being advanced in order to explain this phenomenon.

It has been noted that copper ions (Cu^{2+}) are able to induce fibrillation of monomers at 37 °C and pH 7[22], a similar effect is observed with glycosaminoglycans with Trifluoroethanol at pH 7.5[23] and with lysophosphatidic acid[24]. Type I collagen is also able to induce fibrillation at 40 °C and pH 6.4, conditions similar to those found in inflamed joints[25], and the addition of heparin to type I collagen allows fibrillation at 37 °C[26].

The ΔN6 variant has a free energy of stabilization that is 2.5 kcal/mol lower than that of the wild type form[27] and it also presents a trans-peptide bond between histidine 31 and proline 32[28]. However, its role in fibrillogenesis is not yet clear.

Despite the many hypotheses advanced so far, the event that starts fibrillogenesis is not known.

Hypercatabolic Hypoproteinemia

Hypercatabolic Hypoproteinemia is a rare disease characterized by chemical diabetes mellitus and scheletal deformities due to low concentration of albumin and IgG in the blood[29]. This low concentration is caused by a rapid degradation due to a mutation in the signal peptide of β2-microglobulin, A11P, that leads to lower expression of FcRn[30], which is able to bind the Fc of IgG and albumin, prolonging their half-lives[31].

Autosomal Dominant β_2 –microglobulinic amyloidosis

Autosomal Dominant β_2- microglobulinic amyloidosis is a rare disease characterized by chronic diarrhea, sicca syndrome and in the longer term loss of weight, postural dizziness, neuropathy and orthostatic hypotension. It is caused by amyloid deposits in the colon, spleen, salivary glands and, successively, also in the liver, heart and nerves[32].

These amyloid deposits are caused by a mutant form of β_2-microglobulin, D76N, whose mutation is generated by a point mutation from guanosine to adenosine of the 286th nucleotide of the coding sequence[32]. Monomers of this mutant form are able to form fibrils at 37 °C without other inducing factors, especially when the solution is agitated at 225 rpm, possibly due to an unfolding $\Delta \bar{G}^0$ that is around 2 kcal/mol lower than that of the wild type form[32].

HUMAN LYSOZYME C

The human lysozyme C is a small enzyme, member of the family 22 of Glycoside hydrolases, composed of 130 residues with a molecular weight of around 14700.6 Da.
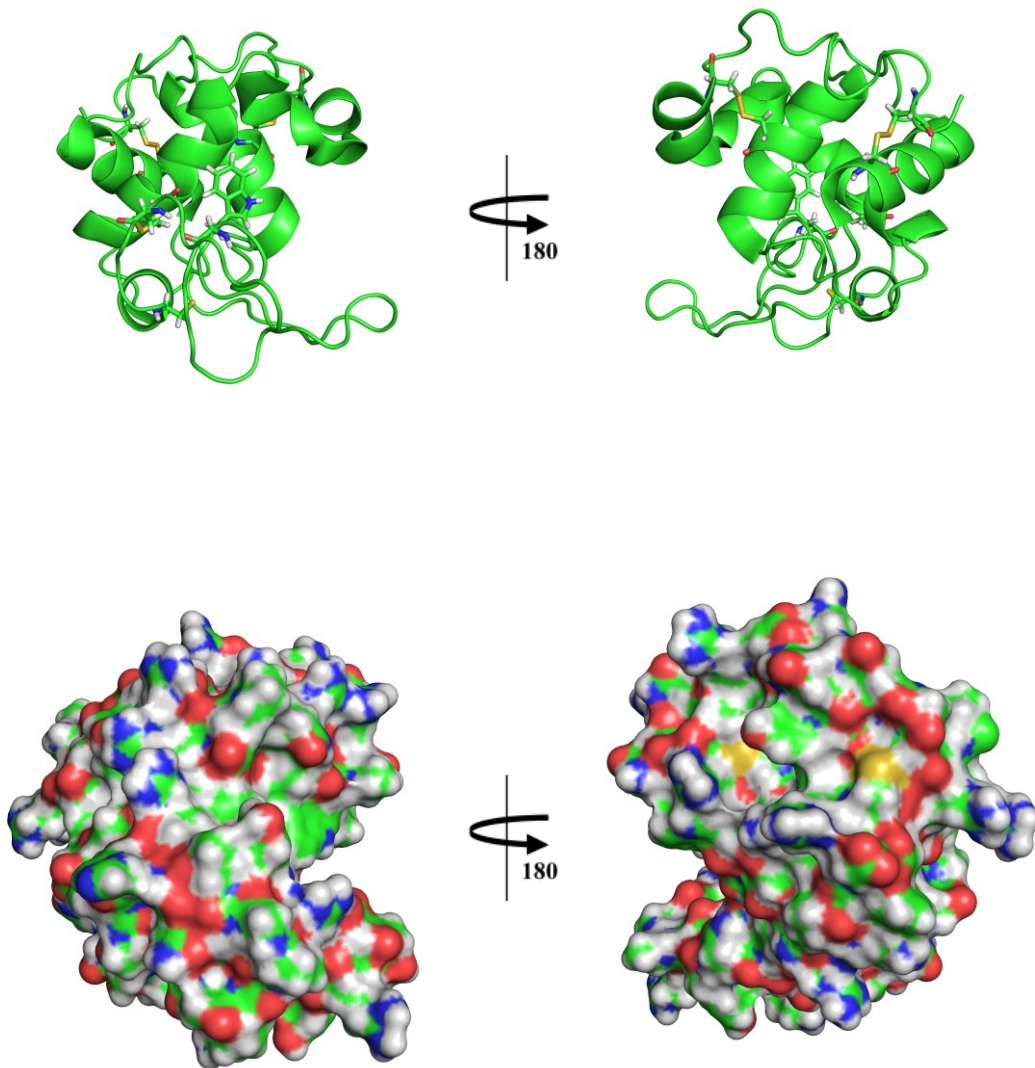
Figure 6 The solution structure of human lysozyme according to the conformer of the RCSB Protein Data Bank entry 1IY4[33] in both cartoon and surface representation. In the cartoon representation the cysteines involved in the disulfide bonds are represented with sticks. The color reflects the element: carbon is green, hydrogen is white, oxygen is red, nitrogen is blue and sulfur is yellow.

Its solution structure has two domains, an α-helix-rich domain, that includes the residues from Lysine 1 to Threonine 40 and from Alanine 90 to Valine 130, and a β-strand-rich domain, that includes the residue from Arginine 41 to Isoleucine 89. It presents four α-helices, three β-strands, two 3_{10} helices and four disulfide bonds[33].

Its gene, LYZ, is located in the q arm of chromosome 12. It has four exons and three introns.

HUMAN LYSOZYME C

The protein is translated with a 18 residues-long signal peptide at the N-terminal, that gets cleaved as the protein enters in the Rough Endoplasmic Reticulum.

The sequence of the protein after cleavage is reported here:

1	2	3	4	5	6	7	8	9	10	11	12	13	14	15
K	V	F	E	R	C	E	L	A	R	T	L	K	R	L
16	17	18	19	20	21	22	23	24	25	26	27	28	29	30
G	M	D	G	Y	R	G	I	S	L	A	N	W	M	C
31	32	33	34	35	36	37	38	39	40	41	42	43	44	45
L	A	K	W	E	S	G	Y	N	T	R	A	T	N	Y
46	47	48	49	50	51	52	53	54	55	56	57	58	59	60
N	A	G	D	R	S	T	D	Y	G	I	F	Q	I	N
61	62	63	64	65	66	67	68	69	70	71	72	73	74	75
S	R	Y	W	C	N	D	G	K	T	P	G	A	V	N
76	77	78	79	80	81	82	83	84	85	86	87	88	89	90
A	C	H	L	S	C	S	A	L	L	Q	D	N	I	A
91	92	93	94	95	96	97	98	99	100	101	102	103	104	105
D	A	V	A	C	A	K	R	V	V	R	D	P	Q	G
106	107	108	109	110	111	112	113	114	115	116	117	118	119	120
I	R	A	W	V	A	W	R	N	R	C	Q	N	R	D
121	122	123	124	125	126	127	128	129	130					
V	R	Q	Y	V	Q	G	C	G	V					

Figure 7 The amino-acid residues sequence of human β_2-microglobulin. The background has been colored to underline which residues are part of secondary structures, while the cysteines involved in disulfide bridges have an additional yellow background. The residues that are part of the β-strand-rich domain have their one letter code and number in red.

According to the solution structure[33], the secondary structures and the disulfide bonds involve the following residues:

Structure/bridge	Domain	Residues
A-helix	α-helix-rich	R5-R14
B-helix	α-helix-rich	L25-E35
β_1-strand	β-strand-rich	A42-N46
β_2-strand	β-strand-rich	S51-I56
β_3-strand	β-strand-rich	I59-S61
3_{10}-helix (i)	β-strand-rich	C81-L85
C-helix	α-helix-rich	A90-V99
D-helix	α-helix-rich	V110-C116
3_{10}-helix (ii)	α-helix-rich	R122-Y124
1st disulfide bond	α-helix-rich	C6-C128
2nd disulfide bond	α-helix-rich	C30-C116
3rd disulfide bond	β-strand-rich	C65-C81
4th disulfide bond	β-strand-rich/α-helix-rich	C77-C95

Table 2 The residues that form the secondary structures and disulfide bonds. The domains in which the structures are found are reported as well. The residues that form the 3_{10}-helices were inferred from the DSSP annotation[34] of the conformer of the RCSB PDB entry 1LZ1[35].

BIOLOGICAL ROLE

The human lysozyme C is a peptidoglycan N-acetylmuramoylhydrolase, whose primary function is to split the bond between N-acetylglucosamine and N-acetylmuramic acid in the peptidoglycans, multiple layers of which are found in the cell wall of Gram positive bacteria[36].

Two residues have catalytic activity: the Glutammate 35 and the Aspartate 53[36]. Furthermore, there are six subsites that accommodate the oligosaccharide units. The subsites are formed by the following residues[33]:

Subsite	Domain	Residues
A	β-strand-rich	T43, N44, N46, I56-I59
B	α-helix-rich	W34-S36
C	α-helix-rich	R98, R101-P103
D	α-helix-rich	R107-V110, W112
E	β-strand-rich	R62, Y63
F	β-strand-rich	A73

Table 3 The residues that form the catalytic subsites. The domains in which the subsites are found are reported as well.

Lysozyme mainly causes cell lysis through the hydrolysis of the peptidoglycans layers of the bacteria and through the induction of autolysins that cause autolysis in the bacteria[36], although there are also mechanisms of anti-bacterial activity that do not depend on the catalytic activity of lysozyme, but rather on its structural features[37].

Lysozyme is also reportedly able to enhance phagocytic activity of polymorphonuclear leukocytes and macrophages[37] and to enhance the tumoricidal activity of monocytes[38].

INVOLVEMENT IN DISEASES

Hereditary Amyloidosis
Various mutated forms of the human lysozyme, including forms mutated in only one residue such as I56T[39], D67H[39], W64R[40] and F57I[41], and forms mutated in two residues such as the double mutant form T70N and W112R[42], are involved in hereditary Amyloidosis that commonly involve the kidneys[40],[41],[42],[43] but, depending on the mutations, may also involve other organs such as spleen[43], liver[39],[43], colon[39],[42] and upper gastrointestinal tract[42] and may also cause sicca syndrome[40].

Four of the variants known to cause amyloidosis, I56T, F57I, W64R and D67H, present a lower thermostability when compared to the wild type protein[43], furthermore the I56T and D67H variants unfolds 30 times and 160 times faster than the wild type form respectively in presence of high concentration of guanidinium chloride and the I56T also refolds at a slower pace[44].

It has also been shown that the I56T and D76H variants form amyloid fibrils in denaturating conditions much more easily than the wild type protein[43].

AIMS OF THE PROJECT

The main aim of the project was the analysis of data from BLUU-Tramp experiments, in particular experiments involving proteins whose unfolding events are linked to diseases such as amyloidosis, like the human β_2-microglobulin and the human lysozyme C. In order to analyze the data it was important to develop a routine able to derive relevant thermodynamic parameters related to the unfolding process from derivative signal decays obtained through the processing of BLUU-Tramp data.

Once such a routine has been developed, it was applied to data obtained from BLUU-Tramp experiments performed on human β_2-microglobulin and human lysozyme C. Such an application can demonstrate whether or not the output of the routine can be correlated to structural features of the proteins, showing the viability of this routine in the analysis of relevant structural changes of the system under study when it is perturbed by external factors such as ligands or denaturing conditions.

Finally, in order to confirm the correctness of the values obtained, another aim of the project was the development of a routine to obtain similar thermodynamic parameters from conventional isotope exchange experiments followed through NMR spectroscopy, its application to preexisting data, and the comparison of the values obtained from the analysis of the data from conventional isotope exchange experiments with the values obtained from the analysis of the data from BLUU-Tramp experiments.

MATERIALS AND METHODS

ANALYSIS OF BLUU-TRAMP DATA

THEORETICAL PRINCIPLES

The decays are currently fitted with the following function:

$$\hat{I} = ae^{be^{ct}} \tag{3}$$

where $\hat{I}$ is the estimated intensity of the decays, t is the time elapsed from the beginning of the first experiment (in seconds) and a, b and c are fitting parameters.

Due to the specific implementation of the BLUU-Tramp method, the decay of each individual amide signal follows this equation:

$$I = I_0 e^{-\int_o^t k_{ex}(T(t))dt} \tag{2}$$

where I is the intensity of the decay, I_0 is the intensity of the decay in the first experiment, k_{ex} is the exchange constant and T is temperature (in K).

Therefore, the exchange constant can be derived in the following way:

$$k_{ex} = -\frac{d \ln I}{dt} \tag{4}$$

that can be expanded, based on eq. (2), as

$$\widehat{k_{ex}} = -\frac{d \ln \hat{I}}{dt} = -\frac{d(\ln a + be^{ct})}{dt} = -bce^{ct} \tag{5}$$

Where the circumflex superscript indicates that the value is estimated.

Following the classical formalism[45], the exchange constant of an amide hydrogen can be expressed as:

$$k_{ex} = \frac{k_{op} \times k_{rc}}{k_{op} + k_{cl} + k_{rc}} \tag{6}$$

where k_{op} and k_{cl} are the kinetic constants of the opening and closing processes, respectively, and k_{rc} is the kinetic constant of exchange in random coil conformation.

In the EX2 limit, we have that k_{cl} is significantly larger than k_{op} and k_{rc}, therefore the exchange constant can be expressed as:

$$k_{ex} = \frac{k_{op} \times k_{rc}}{k_{cl}} = K \times k_{rc} \tag{7}$$

where K is the equilibrium constant of the unfolding process.

With this simplification, an estimate of the equilibrium constant in the EX2 limit can be expressed as:

ANALYSIS OF BLUU-TRAMP DATA

$$\widehat{K} = \frac{\widehat{k_{ex}}}{k_{rc}} = \frac{-bce^{ct}}{k_{rc_r}e^{-\frac{E_a}{R}(\frac{1}{T}-\frac{1}{T_r})}} = -\frac{bc}{k_{rc_r}}e^{ct+\frac{E_a}{R}(\frac{1}{T}-\frac{1}{T_r})} \tag{8}$$

where k_{rc_r} is the kinetic constant of exchange in random coil conformation determined at temperature T_r, E_a is the activation energy of the exchange process in random coil conformation and R is the gas constant. In equilibrium conditions, the relation between equilibrium constant and the variation of molar Gibbs free energy in standard conditions, $\Delta\bar{G}^0$, is the following:

$$\Delta\bar{G}^0 = -RT \ln K \tag{9}$$

And an estimate of the $\Delta\bar{G}^0$ can be derived accordingly:

$$\widehat{\Delta\bar{G}^0} = -RT \ln \widehat{K} = -RT \ln\left(-\frac{bc}{k_{rc_r}}e^{ct+\frac{E_a}{R}(\frac{1}{T}-\frac{1}{T_r})}\right) = -RT \ln\left(-\frac{bc}{k_{rc_r}}\right) - RTct - E_a + \frac{TE_a}{T_r} \tag{10}$$

Since temperature and time are approximately related to each other according to the following formula:

$$T = T_o + mt \tag{11}$$

where T_o is the temperature of the first experiment and m is the difference quotient of the temperature versus time measured as $\frac{T_f - T_0}{t_f}$, where T_f is the temperature of the last experiment and t_f is the time interval between the beginning of the first experiment and the beginning of the last experiment, the formula for the estimation of the $\Delta\bar{G}^0$ can be further simplified:

$$\begin{aligned}
\widehat{\Delta\bar{G}^0} &= -RT \ln\left(-\frac{bc}{k_{rc_r}}\right) + RTct + E_a + \frac{TE_a}{T_r} \\
&= -RT \ln\left(-\frac{bc}{k_{rc_r}}\right) - RTc\left(\frac{T-T_0}{m}\right) - E_a + \frac{TE_a}{T_r} \\
&= -RT \ln\left(-\frac{bc}{k_{rc_r}}\right) - \frac{RT^2c}{m} + \frac{RTcT_0}{m} - E_a + \frac{TE_a}{T_r} \\
&= T^2\left(-\frac{Rc}{m}\right) + T\left(\frac{RcT_0}{m} + \frac{E_a}{T_r} - R\ln\left(-\frac{bc}{k_{rc_r}}\right)\right) - E_a = xT^2 + yT + z
\end{aligned} \tag{12}$$

where $x = -\frac{Rc}{m}$, $y = \frac{RcT_0}{m} + \frac{E_a}{T_r} - R\ln\left(-\frac{bc}{k_{rc_r}}\right)$ and $z = -E_a$.

This equation allows a straightforward estimation of other important thermodynamic parameters.

From the following relationship between Entropy and Gibbs free energy:

$$S = -\frac{\partial G}{\partial T} \tag{13}$$

The following equation can be derived:

$$\Delta\bar{S}^0 = -\frac{\partial \Delta\bar{G}^0}{\partial T} \tag{14}$$

The heat capacity at constant pressure can be related to Gibbs' Free Energy as well:

$$C_p = \frac{\delta Q}{\partial T} = T\frac{\partial S}{\partial T} = -T\frac{\partial^2 G}{\partial T^2} \tag{15}$$

17

MATERIALS AND METHODS
ANALYSIS OF BLUU-TRAMP DATA

From which, its molar variation in standard conditions related to the unfolding process can be calculated as well:

$$\Delta \bar{C}_p^0 = -T \frac{\partial^2 \Delta \bar{G}^0}{\partial T^2} \tag{16}$$

The aforementioned thermodynamic parameters can therefore be estimated:

$$\Delta \widehat{\bar{S}^0} = -\frac{\partial \Delta \widehat{\bar{G}}^0}{\partial T} = -2xT - y = T\left(\frac{2Rc}{m}\right) + R \ln\left(-\frac{bc}{k_{rc_r}}\right) - \frac{RcT_0}{m} - \frac{E_a}{T_r} \tag{17}$$

$$\widehat{\Delta \bar{H}^0} = \widehat{\Delta \bar{G}}^0 + T\,\widehat{\Delta \bar{S}^0} = -xT^2 + z = T^2\left(\frac{Rc}{m}\right) - E_a \tag{18}$$

$$\Delta \widehat{\bar{C}_p^0} = -T \frac{\partial^2 \Delta \widehat{\bar{G}}^0}{\partial T^2} = -2xT = T\left(\frac{2Rc}{m}\right) \tag{19}$$

It is interesting to note that, due to the fitting equation employed, $\Delta \widehat{\bar{C}_p^0}$ here is not constant but rather directly proportional to temperature, in contrast with other proposed models, and that $\Delta \widehat{\bar{S}^0}$ and $\Delta \widehat{\bar{C}_p^0}$ differ only by a constant value. $\Delta \bar{H}^0$ was estimated as well.

ACTUAL IMPLEMENTATION
The program written to perform the aforementioned calculations follows a workflow divided in 4 steps: data import, fitting of the data, estimation of the thermodynamics parameters and their associated error from the fitting parameters and their covariance matrix, writing of the final results. These steps will be thoroughly described.

PRELIMINARY OPERATIONS
Before data import, two structures are generated in order to better organize the data and facilitate both the import and the subsequent analysis:

1. An array of residue specific structures ("residuo") that contains the name of the residue, its raw data in ascending order according to spectrum number, the data structures needed for the fitting routine and the output values of the program;
2. A general parameter structure ("generale") containing the number of residues, the temperature of the first experiment, the difference quotient of the temperature with respect to time and the reference temperature at which the exchange rates in random coil conditions were calculated.

Furthermore, the arrays of values, the arrays of structures and the arrays of characters (strings) are allocated with predefined length. The current values for this preliminary allocation are 1024 residues, 1024 characters for each string variable and 2048 spectra per single ramp. In case future data exceed these limits, they can be easily changed in the source code.

DATA IMPORT
The data import is based on a file whose path is given via the second argument of the command. This file is structured as follows:

- the first line contains the reference temperature at which the exchange constants in random coil conditions are calculated;

- the second line contains the path of the file (which will be subsequently called "tT file") containing the temperature and time at which each spectrum was acquired, with the time reported as seconds passed from the beginning of the first experiment;
- the following lines are referred each to a single residue and report the name of the residue, the path of the file containing the raw data, the exchange rate constant in random coil condition, and the starting fitting parameters.

The raw data are organized in lines, one for each spectrum, in each line the number of the spectrum and the S value obtained in it are reported.

The program first check if the second argument is present, if not an error message is printed in the Standard Output. Then it attempts to read the main input file and extract the important information from the first and second line by assigning the relevant values to the appropriate variables. If it fails, it prints an error message and exits the program with an error (non 0) output. After reading the first two lines, the following lines are read one at a time until no line can be read, again assigning the relevant values of each line to the appropriate variables. After a line is read a counter, initialized at zero, is increased by one, this counter is then used to know the number of the residues to be analyzed.

After reading the main input file, the tT file is read, one line at a time and the values are stored in appropriate arrays of time values and temperature values. As before, an integer counter initialized at zero is increased after each line is read in order to know the actual number of spectra acquired. After the tT file is read, a message of successful read is printed.

At this point, the raw data pertaining to each residue are read one line at a time. First of all the S value and the spectrum at which it was obtained are stored in appropriate arrays within the residue specific structure, then the spectrum number is used to associate to each S value the correct temperature and time at which that value was obtained. If a residue has less than two data points, an error message is printed and the program exits with an error output.

After the raw data of all residues are read, four values are stored in the general structure: the number of residues, the starting temperature, the calculated different quotient of temperature over time and the temperature at which the exchange rate constants in random coil condition were calculated.

DATA FITTING
The imported data are then fitted using an implementation of the Levenberg-Marquardt minimization algorithm called lmder1 contained in C/C++ MINPACK, which is the version written in C language of the MINPACK library[46]. In the case of each residue, the initial fitting parameters and the number of data points is used to create the appropriate input variables for the algorithms. Furthermore, a routine is used to calculate both a vector of functions whose squares are minimized and the Jacobian matrix. At each data point i the function F_i whose square is to be minimized is the following:

$$F_i = S_i - x_0 e^{x_1 e^{x_2 t_i}}$$

Where S_i is the S value obtained in spectrum i, t_i is the moment when spectrum i was acquired, measured in seconds from the beginning of the acquisition of the first spectrum, and x_0, x_1, and x_2 are the fitting parameters.

The derivatives of said function, which are part of the Jacobian matrix, are:

$$\frac{\partial F_i}{\partial x_0} = -e^{x_1 e^{x_2 t_i}}$$

$$\frac{\partial F_i}{\partial x_1} = -e^{x_2 t_i} \times x_0 e^{x_1 e^{x_2 t_i}}$$

$$\frac{\partial F_i}{\partial x_2} = -x_1 e^{x_2 t_i} \times t_i \times x_0 e^{x_1 e^{x_2 t_i}}$$

After the fitting the covariance matrix of the fitting parameters σ is obtained:

$$\sigma = \begin{pmatrix} \sigma_{00} & \sigma_{01} & \sigma_{02} \\ \sigma_{10} & \sigma_{11} & \sigma_{12} \\ \sigma_{20} & \sigma_{21} & \sigma_{22} \end{pmatrix}$$

CALCULATION OF THERMODYNAMIC PARAMETERS

From the fitted values the thermodynamic parameters are obtained for each spectrum i. First of all the exchange constant is estimated:

$$\widehat{k_{ex_i}} = -x_1 x_2 e^{x_2 t_i}$$

Then the equilibrium constant in EX2 limit is derived:

$$\widehat{K_i} = \frac{\widehat{k_{ex_i}}}{k_{rc_r} e^{-\frac{E_a}{R}(\frac{1}{T_i} - \frac{1}{T_r})}}$$

The $\Delta \bar{G}_i^0$ is estimated with two methods. The first one simply uses the following formula:

$$\widehat{\Delta G_{1_i}^0} = -RT \ln \widehat{K_i}$$

The second uses the fitting parameters:

$$\widehat{\Delta G_{2_i}^0} = -Rx_2 \left(\frac{T_i^{\,2}}{m} \right) - \left(R \ln \left(-\frac{x_1 x_2}{k_{rc_r}} \right) - \frac{E_a}{T_r} - \frac{RT_0 x_2}{m} \right) T_i - E_a$$

A comparison of both methods allows the evaluations of differences due to rounding errors.

The other thermodynamic parameters are then calculated:

$$\widehat{\Delta S_i^0} = \frac{2Rx_2 T_i}{m} + R \ln \left(-\frac{x_1 x_2}{k_{rc_r}} \right) - \frac{E_a}{T_r} - \frac{RT_0 x_2}{m}$$

$$\widehat{\Delta H_i^0} = T_i^2 \left(\frac{Rc}{m} \right) - E_a$$

$$\widehat{\Delta C_{p_i}^0} = \frac{2T_i Rx_2}{m}$$

The uncertainty of each parameter is estimated using the coefficients of the covariance matrix:

ANALYSIS OF BLUU-TRAMP DATA

$$\widehat{\sigma_{k_{ex_i}}} = \sqrt{\sigma_{11}\left(\frac{\partial k_{ex}}{\partial x_1}\right)^2 + \sigma_{22}\left(\frac{\partial k_{ex}}{\partial x_2}\right)^2 + 2\sigma_{12}\left(\frac{\partial k_{ex}}{\partial x_1}\right)\left(\frac{\partial k_{ex}}{\partial x_2}\right)}$$

$$= \sqrt{\sigma_{11}(-x_2 e^{x_2 t_i})^2 + \sigma_{22}(-x_1 e^{x_2 t_i} - t_i x_1 x_2 e^{x_2 t_i}) + 2(-x_2 e^{x_2 t_i})(-x_1 e^{x_2 t_i} - t_i x_1 x_2 e^{x_2 t_i})}$$

$$\widehat{\sigma_{\Delta \bar{G}_i^0}} = \sqrt{\sigma_{11}\left(\frac{\partial \Delta \bar{G}_i^0}{\partial x_1}\right)^2 + \sigma_{22}\left(\frac{\partial \Delta \bar{G}_i^0}{\partial x_2}\right)^2 + 2\sigma_{12}\left(\frac{\partial \Delta \bar{G}_i^0}{\partial x_1}\right)\left(\frac{\partial \Delta \bar{G}_i^0}{\partial x_2}\right)}$$

$$= \sqrt{\sigma_{11}\left(\frac{-RT_i}{x_1}\right)^2 + \sigma_{22}\left(\frac{RT_i T_0 x_2 - RT_i^2 x_2 - mRT_i}{mx_2}\right)^2 + 2\sigma_{12}\left(\frac{-RT_i}{x_1} \times \frac{RT_i T_0 x_2 - RT_i^2 x_2 - mRT_i}{mx_2}\right)}$$

$$\widehat{\sigma_{\Delta \bar{S}_i^0}} = \sqrt{\sigma_{11}\left(\frac{\partial \Delta \bar{S}_i^0}{\partial x_1}\right)^2 + \sigma_{22}\left(\frac{\partial \Delta \bar{S}_i^0}{\partial x_2}\right)^2 + 2\sigma_{12}\left(\frac{\partial \Delta \bar{S}_i^0}{\partial x_1}\right)\left(\frac{\partial \Delta \bar{S}_i^0}{\partial x_2}\right)}$$

$$= \sqrt{\sigma_{11}\left(\frac{R}{x_1}\right)^2 + \sigma_{22}\left(\frac{2RT_i x_2 - RT_0 x_2 + mR}{mx_2}\right)^2 + 2\sigma_{12}\left(\frac{R}{x_1} \times \frac{2RT_i x_2 - RT_0 x_2 + mR}{mx_2}\right)}$$

$$\widehat{\sigma_{\Delta \bar{H}_i^0}} = \sqrt{\sigma_{22}\left(\frac{\partial \Delta \bar{H}_i^0}{\partial x_2}\right)^2} = \sqrt{\sigma_{22}\left(\frac{T_i^2 R}{m}\right)^2}$$

$$\widehat{\sigma_{\Delta \bar{C}_{p_i}^0}} = \sqrt{\sigma_{22}\left(\frac{\partial \Delta \bar{C}_{p_i}^0}{\partial x_2}\right)^2} = \sqrt{\sigma_{22}\left(\frac{2T_i R}{m}\right)^2}$$

Finally, the exchange constant and the thermodynamic parameters, along with their standard deviations, are calculated at a reference temperature, currently set at 300K, and the mean squared error of the fitting is computed:

$$MSE = \frac{\sum_i (y_i - \widehat{y_i})^2}{n}$$

CREATION OF THE OUTPUT FILES

The first step of the output process is the removal of the previous results file, if present, and the report on the standard output of the initial temperature, T_0, and of the different quotient of temperature versus time, m.

Then , for each residue a check is performed whether an error message from the fitting routine is present, and if it is present, the export of the data from that residue stops and the error in the fitting procedure is reported on the standard output.

If the error check doesn't find any error message, a summary containing the mean squared error of the regression, the fitting parameters and the thermodynamic parameters calculated at the reference temperature along with their estimated uncertainties is sent to the standard output, and then an attempt at adding a line with this information to a summary file is done. If the attempt fails, the program stops showing how to properly format the command to be input. After writing the summary line, two files are written:

1. a file containing, for each spectrum, the time and temperature at which it was acquired, the measured S-value, the S-value reconstructed from the fitting parameters and the difference between the two;

2. a file containing, for each spectrum, the temperature at which it was acquired, the measured exchange constant, the $\widehat{\Delta G^0_{1_\iota}}$, $\widehat{\Delta G^0_{2_\iota}}$, $\widehat{\Delta S^0_\iota}$ and $\widehat{\Delta C^0_{p_\iota}}$; all these parameters, with the exception of temperature and $\widehat{\Delta G^0_{1_\iota}}$, are reported with their estimated errors.

After outputting this information for all the residues, the program exits with status 0.

CONVENTIONAL EXCHANGE DATA ANALYSIS

The program to analyze data from conventional isotope exchange experiments follows a workflow similar to the one of the BLUU-Tramp data analysis software. This workflow can be divided in four parts: data import, data fitting, extraction of thermodynamic parameters and associated errors from the fitting parameters and their covariance matrix, output of results both on the standard output and on files.

PRELIMINARY OPERATIONS

Before data import, a structure is defined that stores for each residue the name of the residue, the number of data points which will be used for fitting, the initial values of the fitting parameters, the temperature at which each experiment was performed and the exchange constant measured in each experiment along with its uncertainty, the data structures needed for the fitting routine, the intermediate values used for the calculations and the parameters that will be part of the output, along with their uncertainty.

After the structure is defined, an array of structures is created and two global variables, that will be used to pass values to the fitting routine, are declared. Finally, the system memory is preallocated for each array defined. The current preallocations, that constitute the upper limits with regard to dimensions of the arrays, consist in 512 residues, 512 characters for each string and 512 exchange constants derived from conventional exchange experiments.

DATA IMPORT

The data import subroutine uses an input file organized in lines, one for each residue. In each lines the name of the residue, the location of the file containing the data to be fitted, the exchange constant in random coil conditions calculated at 293 K and the initial values for the fitting parameters are reported.

The files containing the data to be fitted are organized as well in lines, one for each experiment. In each line the temperature at which the exchange experiment was performed, the exchange rate measured in the experiment and its uncertainty are reported.

The subroutine first checks that the second argument is present, if it is not, the program exits while displaying on the standard output the proper syntax to run the program from the command line. Then the program reads the input file one line at a time and stores the read values in the proper variables. After that, all the files with the raw data are read one line at a time and the values are stored in the appropriate variables. If one residue has less than two data points, the program exits with an error message on the standard output. In the end, the number of residues read is put in a variable and the subroutine ends.

DATA FITTING

Each residue is treated separately.

The first step is to estimate, at each temperature, the $\Delta \bar{G}^0$ assuming the exchange happened in conditions that can be approximated with the EX2 limit.

To estimate the equilibrium constant of the local unfolding leading to the exchange, K, the exchange constant of the i-th experiment, k_{ex_i}, is divided by the exchange constant calculated in random coil condition, k_{rc_i}:

$$\widehat{K_\iota} = \frac{k_{ex_i}}{k_{rc_i}} = \frac{k_{ex_i}}{k_{rc_r} e^{-\frac{E_a}{R}\left(\frac{1}{T_i}-\frac{1}{T_r}\right)}}$$

Then, the $\Delta \bar{G}^0$ is estimated from the equilibrium constant:

MATERIALS AND METHODS
CONVENTIONAL EXCHANGE DATA ANALYSIS

$$\widehat{\Delta\bar{G}^0_{EX2_i}} = -RT_i \ln \widehat{K_i}$$

The $\Delta\bar{G}^0$ and temperature of each isotope exchange experiment are stored in global variables and the uncertainty of the $\Delta\bar{G}^0$ is estimated from the uncertainty of the exchange constants:

$$\sigma_{\widehat{\Delta\bar{G}^0_{EX2_i}}} = \sqrt{\left(\frac{-RT_i \sigma_{k_{obs_i}}}{k_{obs_i}}\right)^2}$$

where k_{obs_i} and $\sigma_{k_{obs_i}}$ are the observed exchange constant and its uncertainty in the i-th exchange experiment, respectively.

After this step, the functions whose squares are to be minimized are generated. A vector is created using for the i-th exchange experiment performed at temperature T_i the following function F_i [47]:

$$F_i = \widehat{\Delta\bar{G}^0_{EX2_i}} - \left(x_0 - T_i x_1 + x_2\left(T_i - T_r - \left(T_i \ln\frac{T_i}{T_r}\right)\right)\right)$$

where x_0, x_1 and x_2 are minimization parameters.

The Jacobian matrix is calculated as well using the following functions:

$$\frac{\partial F_i}{\partial x_0} = -1$$

$$\frac{\partial F_i}{\partial x_1} = T_i$$

$$\frac{\partial F_i}{\partial x_2} = -\left(T_i - T_r - \left(T_i \ln\frac{T_i}{T_r}\right)\right)$$

The fitting routine used is lmder1 contained in C/C++ MINPACK[46].

After the fitting the programs calculates the covariance matrix σ of the fitting parameters:

$$\sigma = \begin{pmatrix} \sigma_{00} & \sigma_{01} & \sigma_{02} \\ \sigma_{10} & \sigma_{11} & \sigma_{12} \\ \sigma_{20} & \sigma_{21} & \sigma_{22} \end{pmatrix}$$

CALCULATION OF THERMODYNAMIC PARAMETERS
After the fitting is completed, the thermodynamics parameters and their standard deviations are estimated for each exchange experiment from the fitting parameters:

$$\widehat{\Delta H^0_i} = x_0 + x_2(T_i - T_r)$$

$$\widehat{\sigma_{\Delta H^0_i}} = \sqrt{\sigma_{00} + \sigma_{22}(T_i - T_r)^2 + 2\sigma_{02}(T_i - T_r)}$$

$$\widehat{\Delta S^0_i} = x_1 + x_2 \ln\left(\frac{T_i}{T_r}\right)$$

$$\widehat{\sigma_{\Delta S^0_i}} = \sqrt{\sigma_{11} + \sigma_{22}\left(\ln\left(\frac{T_i}{T_r}\right)\right)^2 + 2\sigma_{12}\ln\left(\frac{T_i}{T_r}\right)}$$

CONVENTIONAL EXCHANGE DATA ANALYSIS

$$\widehat{\Delta \bar{C}_p} = x_2$$

$$\widehat{\sigma_{\Delta \bar{C}_p}} = \sqrt{\sigma_{22}}$$

$$\widehat{\Delta \bar{G}_i^0} = x_0 - T_i x_1 + x_2 \left(T_i - T_r - T_i \ln\left(\frac{T_i}{T_r}\right) \right)$$

$$\widehat{\sigma_{\Delta \bar{G}_i^0}}$$

$$= \sqrt{\sigma_{00} + \sigma_{11}(-T_i)^2 + \sigma_{22}\left(T_i - T_r - T_i \ln\left(\frac{T_i}{T_r}\right)\right)^2 - 2\sigma_{01}T_i + 2\sigma_{02}\left(T_i - T_r - T_i \ln\left(\frac{T_i}{T_r}\right)\right) - 2\sigma_{12}T_i\left(T_i - T_r - T_i \ln\left(\frac{T_i}{T_r}\right)\right)}$$

The thermodynamic parameters and their errors are also calculated at the reference temperature T_r and the mean square error is calculated as well:

$$MSE = \frac{\sum_{i=1}^{n}\left(\widehat{\Delta \bar{G}_{EX2_i}^0} - \widehat{\Delta \bar{G}_i^0}\right)^2}{n}$$

CREATION OF THE OUTPUT FILES

The first step of the last part of the program is removing the summary file having the same name, if present.

The routine works on each residue. It first checks if an error code from the minimization subroutine is present and outputs the appropriate error message in that case. If no error code is present, a summary line is sent to the standard output. This line contains the name of the residue, the mean squared error, the minimization parameters and their uncertainty inferred from the covariance matrix, the reference temperature and the thermodynamic parameters calculated at that temperature, along with their errors. An attempt at writing the same line in the results summary file is done, and if this is not possible, the programs outputs a line with the instruction to properly call the routine from the command line and exits with an error (non 0) output. A second file specific for the residue is then written, in which each line contains the temperature of the isotope exchange experiment, the observed exchange constant, the equilibrium constant and the relative variation in molar Gibbs Free Energy in equilibrium conditions derived according to the EX2 limit equations, the variation in molar Gibbs Free Energy in equilibrium conditions derived from the minimization parameters and the difference between the latter two. Finally, another file specific for the residue is written, in which the temperature and the thermodynamic parameters estimated for each exchange experiment, with the associated errors, are reported. If the program fails to write any of these files, the program exits with an error output and a line is sent to the standard output explaining how to properly call the routine from the command line.

After the output files for each residue have been created, the program exits with a normal execution output (code 0).

EXPERIMENTAL PROCEDURES

SAMPLES USED

$β_2$-microglobulin

The protein used, the human form of $β_2$-microglobulin, presents a methionine added at the N-terminal. The protein was deuterated and lyophilized. By adding an aqueous solution containing phosphate buffer and D_2O, a 600 µl aqueous sample having a pH of 7.12 and containing ^{15}N-enriched human $β_2$-microglobulin at a concentration of 295 µM, along with D_2O at a concentration of 5% v/v and phosphate buffer at a concentration of 20 mM was prepared and put in an NMR samples tube for the BLUU-Tramp experiment. The tube was inserted in an NMR spectrometer and the acquisition was started 324 seconds after the addition of the protein to the aqueous solution.

Lysozyme

The human Lysozyme was deuterated and lyophilized. By adding an aqueous solution containing phosphate buffer and D_2O, an aqueous sample having a pH of 7.12 containing ^{15}N-enriched human Lysozyme at a concentration of 267 µM, along with D_2O at a concentration of 5% v/v and phosphate buffer at a concentration of 20 mM was prepared and put in an NMR samples tube for the BLUU-Tramp experiment. The tube was inserted in an NMR spectrometer and the acquisition was started 305 seconds after the addition of the protein to the aqueous solution.

$β_2$-microglobulin for conventional exchange experiments

The protein used, the human form of $β_2$-microglobulin, presents a methionine added at the N-terminal. 3 mg of ^{15}N-enriched protein were put in 550 of a D_2O solution having a pH of 6.6 and containing phosphate buffer at a concentration of 70 mM and NaCl at a concentration of 100 mM and the resulting solution was put in an NMR sample tube. The sample tube was then inserted in an NMR spectrometer and the acquisition was started 4 minutes after the addition of the protein to the D_2O solution.

SPECTROMETERS USED

BLUU-Tramp experiments

A Bruker Avance III spectrometer having a ^{1}H base frequency of 600.13 MHz and equipped with a 5 mm CPTCI 1H-13C/15N/D Z-GRD probe was used. TOPSPIN version 3.2-p16 was used as acquisition software.

Conventional exchange experiments

A Bruker Avance spectrometer having a 1H base frequency of 500.13 MHz and equipped with a 5 mm TXI 1H/2H-13C/15N XYZ-GRD probe was used. TOPSPIN version 1.3 was used as acquisition software.

NMR EXPERIMENTS

ACQUISITION

$β_2$-microglobulin BLUU-Tramp experiments

223 best-TROSY[48],[49] experiments with sensitivity improvement and using Echo-Antiecho to obtain quadrature detection in the indirect dimension were performed per temperature ramp. The starting temperature was 273.28 K and in the first 27 experiments the temperature was increased by 0.36 K between one experiment and the next, while in the next 196 experiments the temperature was increased by 0.18 K between one experiment and the next. The overall temperature range was therefore 273.28 K - 318.1 K. After increasing the temperature, 50 seconds of delay were introduced to allow equilibration at the new temperature.

NMR EXPERIMENTS

The parameters used in the acquisition were the following:

First 27 experiments

PARAMETER	F1 (^{15}N)	F2 (^{1}H)
Number of dummy scans		32
Number of scans		64
Number of points	80	768
Base Frequency (MHz)	60.810645	500.13
Offset (Hz)	7175.66	2818.2
Spectral Width (Hz)	1946.28260023355	9009.00900900901

Other experiments

PARAMETER	F1 (^{15}N)	F2 (^{1}H)
Number of dummy scans		32
Number of scans		32
Number of points	80	768
Base Frequency (MHz)	60.810645	600.13
Offset (Hz)	7175.66	2818.2
Spectral Width (Hz)	1946.28260023355	9009.00900900901

Lysozyme BLUU-Tramp experiments

213 best-TROSY[48],[49] experiments with sensitivity improvement and using Echo-Antiecho to obtain quadrature detection in the indirect dimension were performed per temperature ramp. The starting temperature was 283 K and the temperature was increased by 0.125 K between one experiment and the next. The overall temperature range was therefore 283 K - 336 K. After increasing the temperature, 50 seconds of delay were introduced to allow equilibration at the new temperature.

The parameters used in the acquisition were the following:

PARAMETER	F1 (^{15}N)	F2 (^{1}H)
Number of dummy scans		32
Number of scans		32
Number of points	80	768
Base Frequency (MHz)	60.810645	600.13
Offset (Hz)	7175.65611000026	2818.2
Spectral Width (Hz)	1946.28260023355	9009.00900900901

MATERIALS AND METHODS
NMR EXPERIMENTS

β₂-microglobulin conventional exchange experiments

250 HSQC experiments with sensitivity improvement[50],[51],[52],[53] and using Echo-Antiecho-TPPI to obtain quadrature detection in the indirect dimension and flip-back pulse to suppress solvent were performed. The acquisition temperature was 293 K.

The parameters used in the acquisition were the following:

PARAMETER	F1 (^{15}N)	F2 (^{1}H)
Number of dummy scans		16
Number of scans		16
Number of points	80	2048
Base Frequency (MHz)	50.677733	500.13
Offset (Hz)	5928.99999999474	2352.6
Spectral Width (Hz)	1700.10200612037	7002.80112044818

PROCESSING

β₂-microglobulin BLUU-Tramp experiments

After being converted in the NMRPipe input format, the raw data was processed with NMRPipe[54] using the following parameters:

PARAMETER	F1 (^{15}N)	F2 (^{1}H)
Baseline correction	4th order polynomial subtract (only in the Frequency Domain)	4th order polynomial subtract (both in the Time Domain and Frequency Domain)
Window Function	Gaussian with g1= 10 and g2=25	Gaussian with g1= 10 and g2=25 and c=0.5
Linear prediction	Forward-backward linear prediction, 80 more points predicted	none
Number of points after zero filling	1024	1536

Lysozyme BLUU-Tramp experiments

After being converted in the NMRPipe input format, the raw data was processed with NMRPipe[54] using the following parameters:

PARAMETER	F1 (^{15}N)	F2 (^{1}H)
Baseline correction	4th order polynomial subtract (only in the Frequency Domain)	4th order polynomial subtract (both in the Time Domain and Frequency Domain)
Window Function	Gaussian with g1= 10 and g2=25	Gaussian with g1= 10 and g2=25 and c=0.5
Linear prediction	Forward-backward linear prediction, 80 more points predicted	none
Number of points after zero filling	1024	1536

NMR EXPERIMENTS

β₂-microglobulin conventional exchange experiments

After being converted in the NMRPipe input format, the raw data was processed with NMRPipe[54] using the following parameters:

PARAMETER	F1 (^{15}N)	F2 (^{1}H)
Baseline correction	4th order polynomial subtract (only in the Frequency Domain)	4th order polynomial subtract (both in the Time Domain and Frequency Domain)
Window Function	Gaussian with g1= 10 and g2=25	Gaussian with g1= 10 and g2=25 and c=0.5
Linear prediction	Forward-backward linear prediction, 80 more points predicted	none
Number of points after zero filling	1024	4096

ANALYSIS

BLUU-Tramp experiments

The processed data were analyzed using a routine developed in the Biophysical Laboratory of the University of Udine called TinT. The obtained decays were then assigned using Sparky[55].

Conventional isotope exchange experiment

The peaks were assigned using Sparky[55]. The Sparky save file and the spectrums were then loaded in NMRViewJ in order to obtain the decays using the "Rate Analysis" routine. Once the decays were obtained, they were fitted with the "Grace" software using the following fitting function F:

$$F = a_0 e^{-a_1 t}$$

Where t is the time passed from the first spectrum acquired, while a_0 and a_1 are minimization parameters.

The a_1 value was then added to the list of exchange rates already measured for the human β₂-microglobulin protein and these lists were used as input for the classical exchange experiments analysis software.

RESULTS

It is important to note that the values reported in the tables retain the figures obtained from fitting and calculations. The actual number of significant figures, however, is three at most, except for temperature values known to an accuracy of four significant figures.

β₂-MICROGLOBULIN BLUU-TRAMP EXPERIMENT

The analysis on the BLUU-Tramp data yielded results for 39 residues, summarized in the following tables.

β2-MICROGLOBULIN BLUU-TRAMP EXPERIMENT

Residue	$\Delta \bar{G}^0$ (kcal/mol)	$\Delta \bar{H}^0$ (kcal/mol)	$\Delta \bar{S}^0$ (kcal/(mol × K))	$\Delta \bar{C}_p^0$ (kcal/(mol × K))
R3	7.970313 ± 0.386207	-1.114641 ± 7.301295	-0.030283 ± 0.025587	0.079236 ± 0.048675
K6	4.885545 ± 0.746845	17.378207 ± 9.750194	0.041642 ± 0.034985	0.202521 ± 0.065001
V9	4.586833 ± 1.639609	19.130024 ± 21.981588	0.048477 ± 0.078723	0.2142 ± 0.146544
Y10	8.138548 ± 0.013714	31.907682 ± 0.887009	0.07923 ± 0.002918	0.299385 ± 0.005913
S11	7.970284 ± 0.323976	-4.078544 ± 5.054953	-0.040163 ± 0.017918	0.059476 ± 0.0337
H13	8.04543 ± 0.280905	-1.48583 ± 5.088301	-0.031771 ± 0.017875	0.076761 ± 0.033922
E16	6.795751 ± 0.223175	0.274971 ± 4.179506	-0.021736 ± 0.014656	0.0885 ± 0.027863
N17	8.003041 ± 0.194076	-8.121323 ± 0.977151	-0.053748 ± 0.003903	0.032525 ± 0.006514
G18	8.329893 ± 0.276694	-2.707631 ± 4.761344	-0.036792 ± 0.016776	0.068616 ± 0.031742
C25	9.874799 ± 0.010769	31.364336 ± 0.780935	0.071632 ± 0.002578	0.295762 ± 0.005206
Y26	9.171372 ± 0.015136	33.81162 ± 0.879046	0.082134 ± 0.002888	0.312077 ± 0.00586
D38	8.872414 ± 0.061137	80.217098 ± 7.174253	0.237816 ± 0.023727	0.621447 ± 0.047828
L39	4.918507 ± 0.253261	13.856644 ± 3.687007	0.029794 ± 0.01313	0.179044 ± 0.02458
L40	8.492698 ± 0.023404	43.757532 ± 0.888471	0.117549 ± 0.002887	0.378384 ± 0.005923
K41	8.580887 ± 0.021221	35.59002 ± 1.233741	0.09003 ± 0.004053	0.323933 ± 0.008225
E44	7.246711 ± 0.018205	18.443332 ± 0.809425	0.037322 ± 0.00275	0.209622 ± 0.005396
E47	6.697006 ± 0.050849	-8.095045 ± 0.264338	-0.049307 ± 0.00105	0.0327 ± 0.001762
K48	7.568547 ± 0.129654	-7.419283 ± 2.271122	-0.049959 ± 0.007991	0.037205 ± 0.015141
V49	4.171009 ± 2.029309	103.707305 ± 90.594803	0.331788 ± 0.308667	0.778049 ± 0.603965
S52	8.355197 ± 0.494492	-3.11854 ± 7.912922	-0.038246 ± 0.028005	0.065876 ± 0.052753
D59	5.950662 ± 1.794346	29.328693 ± 42.353706	0.077927 ± 0.147068	0.282191 ± 0.282358
L64	7.236692 ± 0.011672	13.119701 ± 1.121106	0.01961 ± 0.003754	0.174131 ± 0.007474
Y67	7.20736 ± 0.030582	10.929707 ± 0.854867	0.012408 ± 0.002945	0.159531 ± 0.005699
F70	7.522031 ± 0.056281	29.998839 ± 3.102521	0.074923 ± 0.01052	0.286659 ± 0.020683
T71	6.503178 ± 0.633883	8.447076 ± 9.744482	0.00648 ± 0.03458	0.142981 ± 0.064963
T73	7.145369 ± 0.237459	-3.58686 ± 4.082915	-0.035774 ± 0.014386	0.062754 ± 0.027219
K75	7.399089 ± 0.19851	-1.784832 ± 3.823115	-0.030613 ± 0.013384	0.074768 ± 0.025487
D76	7.162462 ± 0.24952	-0.508281 ± 4.336722	-0.025569 ± 0.015272	0.083278 ± 0.028911
E77	6.700189 ± 0.160867	-0.940461 ± 3.168113	-0.025469 ± 0.011078	0.080397 ± 0.021121
Y78	5.832353 ± 0.712457	9.081756 ± 10.724315	0.010831 ± 0.038108	0.147212 ± 0.071495
A79	9.031541 ± 0.011572	35.987977 ± 0.652086	0.089855 ± 0.002141	0.326587 ± 0.004347
R81	9.477786 ± 0.008141	30.889888 ± 0.552528	0.071374 ± 0.001822	0.292599 ± 0.003684
V82	8.243707 ± 0.027014	10.307075 ± 1.384427	0.006878 ± 0.004693	0.15538 ± 0.00923
N83	9.026461 ± 0.006847	27.657226 ± 0.554973	0.062103 ± 0.001838	0.271048 ± 0.0037
L87	6.55811 ± 0.097877	-1.764791 ± 1.434163	-0.027743 ± 0.005105	0.074901 ± 0.009561
Q89	8.067988 ± 0.169752	-2.612678 ± 3.01687	-0.035602 ± 0.010609	0.069249 ± 0.020112
K91	6.258958 ± 0.083409	8.099468 ± 1.326706	0.006135 ± 0.004698	0.140663 ± 0.008845
V93	7.542878 ± 0.008767	32.492744 ± 0.552014	0.083166 ± 0.001817	0.303285 ± 0.00368
W95	7.134201 ± 0.022946	23.927954 ± 1.235592	0.055979 ± 0.004186	0.246186 ± 0.008237
R97	7.287295 ± 0.201636	-2.715728 ± 3.302916	-0.033343 ± 0.011672	0.068562 ± 0.022019
D98	7.431917 ± 0.163221	-0.812008 ± 3.022383	-0.02748 ± 0.010605	0.081253 ± 0.020149
M99	4.876508 ± 0.130727	-2.054448 ± 2.414842	-0.023103 ± 0.008474	0.07297 ± 0.016099

Table 4 Results of the analysis on the β₂-microglobulin BLUU-Tramp experiment. Data are reported as value ± standard deviation and are relative to the reference temperature of 300K.

RESULTS
β2-MICROGLOBULIN BLUU-TRAMP EXPERIMENT

Residue	Lowest Temperature			Reference Temperature			Highest Temperature		
	T (K)	$\Delta\bar{G}^0$ (kcal/mol)	$\sigma_{\Delta\bar{G}^0}$ (kcal/mol)	T (K)	$\Delta\bar{G}^0$ (kcal/mol)	$\sigma_{\Delta\bar{G}^0}$ (kcal/mol)	T (K)	$\Delta\bar{G}^0$ (kcal/mol)	$\sigma_{\Delta\bar{G}^0}$ (kcal/mol)
R3	273.28	7.066862	0.26639	300	7.970313	0.386207	318.1	8.475175	0.869718
K6	273.28	5.757238	0.121513	300	4.885545	0.746845	318.1	4.021241	1.414847
Y10	290.74	8.829436	0.038375	300	8.138548	0.013714	318.1	6.541008	0.045238
S11	273.28	6.826363	0.126486	300	7.970284	0.323976	318.1	8.664755	0.664995
H13	273.28	7.105172	0.172822	300	8.04543	0.280905	318.1	8.57857	0.619504
E16	273.28	6.109659	0.148914	300	6.795751	0.223175	318.1	7.140849	0.500606
N17	273.28	6.528196	0.097797	300	8.003041	0.194076	317.74	8.939469	0.266658
G18	273.28	7.265169	0.147903	300	8.329893	0.276694	318.1	8.958358	0.595025
C25	273.28	11.436864	0.070548	300	9.874799	0.010769	318.1	8.416773	0.042794
Y26	273.28	10.994646	0.083168	300	9.171372	0.015136	318.1	7.514344	0.043756
D38	283.54	12.506243	0.425713	300	8.872414	0.061137	305.14	7.622678	0.072232
L39	273.28	5.501547	0.073338	300	4.918507	0.253261	318.1	4.281479	0.503779
L40	273.28	11.183369	0.092613	300	8.492698	0.023404	318.1	6.158449	0.034066
K41	273.28	10.601042	0.116892	300	8.580887	0.021221	318.1	6.774462	0.061107
E44	273.28	7.994521	0.052388	300	7.246711	0.018205	318.1	6.456724	0.068889
E47	273.28	5.340617	0.025026	300	6.697006	0.050849	318.1	7.571605	0.070778
K48	273.28	6.18936	0.074673	300	7.568547	0.129654	318.1	8.452498	0.280816
S52	273.28	7.254882	0.210277	300	8.355197	0.494492	318.1	9.011477	1.027188
L64	289.12	7.415695	0.03593	300	7.236692	0.011672	318.1	6.786672	0.077744
Y67	273.28	7.349066	0.044578	300	7.20736	0.030582	318.1	6.895672	0.085709
F70	283.54	8.625817	0.111624	300	7.522031	0.056281	299.74	7.541479	0.053687
T71	273.28	6.506178	0.228087	300	6.503178	0.633883	318.1	6.307827	1.293184
T73	273.28	6.114812	0.127062	300	7.145369	0.237459	318.1	7.758616	0.510356
K75	273.28	6.49214	0.143388	300	7.399089	0.19851	318.1	7.912362	0.451188
D76	273.28	6.38016	0.136274	300	7.162462	0.24952	318.1	7.579793	0.539416
E77	273.28	5.923995	0.122236	300	6.700189	0.160867	318.1	7.117277	0.369875
Y78	273.28	5.946595	0.23692	300	5.832353	0.712457	318.1	5.555925	1.439205
A79	273.28	11.043846	0.062182	300	9.031541	0.011572	318.1	7.226848	0.031828
R81	273.28	11.036717	0.050525	300	9.477786	0.008141	318.1	8.026158	0.029595
V82	273.28	8.242592	0.091989	300	8.243707	0.027014	303.34	8.217846	0.041499
N83	273.28	10.363313	0.04852	300	9.026461	0.006847	318.1	7.754408	0.032389
L87	273.28	5.727689	0.029842	300	6.55811	0.097877	318.1	7.019361	0.195177
Q89	273.28	7.034296	0.099552	300	8.067988	0.169752	318.1	8.674577	0.37079
K91	273.28	6.255507	0.033823	300	6.258958	0.083409	297.94	6.270602	0.073877
V93	273.28	9.404191	0.051336	300	7.542878	0.008767	318.1	5.871971	0.028535
W95	283.54	7.944452	0.046305	300	7.134201	0.022946	318.1	5.986556	0.101022
R97	273.28	6.314776	0.092553	300	7.287295	0.201636	318.1	7.853375	0.423522
D98	273.28	6.600972	0.106222	300	7.431917	0.163221	318.1	7.884935	0.363953
M99	273.28	4.172361	0.084939	300	4.876508	0.130727	318.1	5.254832	0.291041

Table 5 $\Delta\bar{G}^0$ of the amide sites of β$_2$-microglobulin at various temperatures. Isolated cases in which the lowest temperature is higher than the reference temperature or the highest temperature is lower than the reference temperature are highlighted in red.

β2-MICROGLOBULIN BLUU-TRAMP EXPERIMENT

Residue	Lowest Temperature			Reference Temperature			Highest Temperature		
	T (K)	$\Delta \bar{H}^0$ (kcal/mol)	$\sigma_{\Delta \bar{H}^o}$ (kcal/mol)	T (K)	$\Delta \bar{H}^0$ (kcal/mol)	$\sigma_{\Delta \bar{H}^o}$ (kcal/mol)	T (K)	$\Delta \bar{H}^0$ (kcal/mol)	$\sigma_{\Delta \bar{H}^o}$ (kcal/mol)
R3	273.28	-3.137535	6.058611	300	-1.114641	7.301295	318.1	0.362789	8.208895
K6	273.28	12.207822	8.090706	300	17.378207	9.750194	318.1	21.154424	10.962209
Y10	290.74	29.178167	0.833097	300	31.907682	0.887009	318.1	37.490011	0.997271
S11	273.28	-5.59698	4.194598	300	-4.078544	5.054953	318.1	-2.969546	5.683318
H13	273.28	-3.445547	4.22227	300	-1.48583	5.088301	318.1	-0.05454	5.720812
E16	273.28	-1.984435	3.468152	300	0.274971	4.179506	318.1	1.92514	4.699047
N17	273.28	-8.951676	0.81084	300	-8.121323	0.977151	317.74	-7.527279	1.096133
G18	273.28	-4.459397	3.950961	300	-2.707631	4.761344	318.1	-1.42822	5.353211
C25	273.28	23.813505	0.648019	300	31.364336	0.780935	318.1	36.879123	0.87801
Y26	273.28	25.84426	0.729432	300	33.81162	0.879046	318.1	39.630621	0.988318
D38	283.54	70.268691	6.408595	300	80.217098	7.174253	305.14	83.438701	7.422196
L39	273.28	9.285631	3.059477	300	13.856644	3.687007	318.1	17.195107	4.145327
L40	273.28	34.097373	0.737253	300	43.757532	0.888471	318.1	50.812877	0.998914
K41	273.28	27.319976	1.023757	300	35.59002	1.233741	318.1	41.630089	1.387103
E44	273.28	13.091663	0.67166	300	18.443332	0.809425	318.1	22.351952	0.910042
E47	273.28	-8.929871	0.219347	300	-8.095045	0.264338	318.1	-7.485326	0.297197
K48	273.28	-8.369124	1.884576	300	-7.419283	2.271122	318.1	-6.725562	2.553438
S52	273.28	-4.800369	6.566139	300	-3.11854	7.912922	318.1	-1.890208	8.896552
L64	289.12	11.259507	1.041263	300	13.119701	1.121106	318.1	16.366557	1.260467
Y67	273.28	6.856859	0.709368	300	10.929707	0.854867	318.1	13.904331	0.961133
F70	283.54	25.409875	2.77141	300	29.998839	3.102521	299.74	29.92434	3.097145
T71	273.28	4.796773	8.085966	300	8.447076	9.744482	318.1	11.113093	10.955787
T73	273.28	-5.188981	3.388001	300	-3.58686	4.082915	318.1	-2.416743	4.59045
K75	273.28	-3.693659	3.172419	300	-1.784832	3.823115	318.1	-0.39071	4.298354
D76	273.28	-2.634377	3.59861	300	-0.508281	4.336722	318.1	1.044525	4.875806
E77	273.28	-2.993	2.628898	300	-0.940461	3.168113	318.1	0.558622	3.56193
Y78	273.28	5.323431	8.899031	300	9.081756	10.724315	318.1	11.826668	12.05742
A79	273.28	27.6502	0.541101	300	35.987977	0.652086	318.1	42.077514	0.733145
R81	273.28	23.419809	0.458487	300	30.889888	0.552528	318.1	36.345699	0.621211
V82	273.28	6.3402	1.148797	300	10.307075	1.384427	303.34	10.828934	1.415425
N83	273.28	20.737347	0.460517	300	27.657226	0.554973	318.1	32.711194	0.62396
L87	273.28	-3.677029	1.190068	300	-1.764791	1.434163	318.1	-0.368179	1.612439
Q89	273.28	-4.380605	2.503397	300	-2.612678	3.01687	318.1	-1.321464	3.391887
K91	273.28	4.508328	1.1009	300	8.099468	1.326706	297.94	7.810696	1.308548
V93	273.28	24.749858	0.458061	300	32.492744	0.552014	318.1	38.1478	0.620633
W95	283.54	19.986892	1.103726	300	23.927954	1.235592	318.1	28.518349	1.389184
R97	273.28	-4.466116	2.740758	300	-2.715728	3.302916	318.1	-1.437323	3.71349
D98	273.28	-2.88641	2.507972	300	-0.812008	3.022383	318.1	0.703042	3.398086
M99	273.28	-3.917386	2.003834	300	-2.054448	2.414842	318.1	-0.693842	2.715023

Table 6 $\Delta \bar{H}^0$ of the amide sites of β$_2$-microglobulin at various temperatures. Isolated cases in which the lowest temperature is higher than the reference temperature or the highest temperature is lower than the reference temperature are highlighted in red.

RESULTS
β2-MICROGLOBULIN BLUU-TRAMP EXPERIMENT

Residue	Lowest Temperature			Reference Temperature			Highest Temperature		
	T (K)	$\Delta \bar{S}^0$ (kcal/(mol × K))	$\sigma_{\Delta \bar{S}^0}$ (kcal/(mol × K))	T (K)	$\Delta \bar{S}^0$ (kcal/(mol × K))	$\sigma_{\Delta \bar{S}^0}$ (kcal/(mol × K))	T (K)	$\Delta \bar{S}^0$ (kcal/(mol × K))	$\sigma_{\Delta \bar{S}^0}$ (kcal/(mol × K))
R3	273.28	-0.03734	0.021252	300	-0.030283	0.025587	318.1	-0.025503	0.028523
K6	273.28	0.023604	0.029195	300	0.041642	0.034985	318.1	0.053861	0.038906
Y10	290.74	0.069989	0.002736	300	0.07923	0.002918	318.1	0.097293	0.003275
S11	273.28	-0.04546	0.014917	300	-0.040163	0.017918	318.1	-0.036574	0.019951
H13	273.28	-0.038608	0.014854	300	-0.031771	0.017875	318.1	-0.02714	0.019922
E16	273.28	-0.029618	0.012175	300	-0.021736	0.014656	318.1	-0.016396	0.016337
N17	273.28	-0.056645	0.003323	300	-0.053748	0.003903	317.74	-0.051825	0.004288
G18	273.28	-0.042903	0.013949	300	-0.036792	0.016776	318.1	-0.032652	0.018691
C25	273.28	0.045289	0.002115	300	0.071632	0.002578	318.1	0.089476	0.002892
Y26	273.28	0.054338	0.002366	300	0.082134	0.002888	318.1	0.100963	0.003242
D38	283.54	0.203719	0.021103	300	0.237816	0.023727	305.14	0.248463	0.024547
L39	273.28	0.013847	0.010941	300	0.029794	0.01313	318.1	0.040596	0.014613
L40	273.28	0.083848	0.00236	300	0.117549	0.002887	318.1	0.140379	0.003245
K41	273.28	0.061179	0.00332	300	0.09003	0.004053	318.1	0.109574	0.004549
E44	273.28	0.018652	0.002269	300	0.037322	0.00275	318.1	0.049969	0.003075
E47	273.28	-0.052219	0.000893	300	-0.049307	0.00105	318.1	-0.047334	0.001156
K48	273.28	-0.053273	0.006643	300	-0.049959	0.007991	318.1	-0.047715	0.008905
S52	273.28	-0.044113	0.023306	300	-0.038246	0.028005	318.1	-0.034271	0.031187
L64	289.12	0.013295	0.003483	300	0.01961	0.003754	318.1	0.030116	0.004204
Y67	273.28	-0.001801	0.002437	300	0.012408	0.002945	318.1	0.022033	0.003289
F70	283.54	0.059195	0.009385	300	0.074923	0.01052	299.74	0.074674	0.010502
T71	273.28	-0.006255	0.028794	300	0.00648	0.03458	318.1	0.015106	0.0385
T73	273.28	-0.041363	0.011962	300	-0.035774	0.014386	318.1	-0.031988	0.016028
K75	273.28	-0.037272	0.011114	300	-0.030613	0.013384	318.1	-0.026102	0.014922
D76	273.28	-0.032986	0.012698	300	-0.025569	0.015272	318.1	-0.020545	0.017017
E77	273.28	-0.03263	0.009197	300	-0.025469	0.011078	318.1	-0.020618	0.012352
Y78	273.28	-0.00228	0.031741	300	0.010831	0.038108	318.1	0.019713	0.042422
A79	273.28	0.060767	0.001753	300	0.089855	0.002141	318.1	0.109559	0.002403
R81	273.28	0.045313	0.001494	300	0.071374	0.001822	318.1	0.089027	0.002044
V82	273.28	-0.006961	0.003871	300	0.006878	0.004693	303.34	0.008608	0.004795
N83	273.28	0.037961	0.001509	300	0.062103	0.001838	318.1	0.078456	0.002062
L87	273.28	-0.034414	0.004253	300	-0.027743	0.005105	318.1	-0.023224	0.005681
Q89	273.28	-0.04177	0.008818	300	-0.035602	0.010609	318.1	-0.031424	0.011823
K91	273.28	-0.006393	0.00391	300	0.006135	0.004698	297.94	0.005169	0.004637
V93	273.28	0.056154	0.001489	300	0.083166	0.001817	318.1	0.101464	0.002039
W95	283.54	0.042472	0.003734	300	0.055979	0.004186	318.1	0.070832	0.004683
R97	273.28	-0.03945	0.009711	300	-0.033343	0.011672	318.1	-0.029207	0.013001
D98	273.28	-0.034717	0.00881	300	-0.02748	0.010605	318.1	-0.022577	0.01182
M99	273.28	-0.029602	0.00704	300	-0.023103	0.008474	318.1	-0.018701	0.009445

Table 7 $\Delta \bar{S}^0$ of the amide sites of β$_2$-microglobulin at various temperatures. Isolated cases in which the lowest temperature is higher than the reference temperature or the highest temperature is lower than the reference temperature are highlighted in red.

β2-MICROGLOBULIN BLUU-TRAMP EXPERIMENT

Residue	Lowest Temperature			Reference Temperature			Highest Temperature		
	T (K)	$\Delta \bar{C}_p^0$ (kcal/(mol × K))	$\sigma_{\Delta \bar{C}_p^0}$ (kcal/(mol × K))	T (K)	$\Delta \bar{C}_p^0$ (kcal/(mol × K))	$\sigma_{\Delta \bar{C}_p^0}$ (kcal/(mol × K))	T (K)	$\Delta \bar{C}_p^0$ (kcal/(mol × K))	$\sigma_{\Delta \bar{C}_p^0}$ (kcal/(mol × K))
R3	273.28	0.072178	0.04434	300	0.079236	0.048675	318.1	0.084016	0.051612
K6	273.28	0.184483	0.059212	300	0.202521	0.065001	318.1	0.21474	0.068923
Y10	290.74	0.290144	0.005731	300	0.299385	0.005913	318.1	0.317447	0.00627
S11	273.28	0.054179	0.030698	300	0.059476	0.0337	318.1	0.063065	0.035733
H13	273.28	0.069924	0.030901	300	0.076761	0.033922	318.1	0.081392	0.035969
E16	273.28	0.080617	0.025382	300	0.0885	0.027863	318.1	0.093839	0.029544
N17	273.28	0.029628	0.005934	300	0.032525	0.006514	317.74	0.034448	0.0069
G18	273.28	0.062504	0.028915	300	0.068616	0.031742	318.1	0.072756	0.033657
C25	273.28	0.26942	0.004743	300	0.295762	0.005206	318.1	0.313607	0.00552
Y26	273.28	0.284282	0.005338	300	0.312077	0.00586	318.1	0.330906	0.006214
D38	283.54	0.587351	0.045204	300	0.621447	0.047828	305.14	0.632095	0.048648
L39	273.28	0.163097	0.022391	300	0.179044	0.02458	318.1	0.189847	0.026063
L40	273.28	0.344682	0.005396	300	0.378384	0.005923	318.1	0.401213	0.006281
K41	273.28	0.295082	0.007492	300	0.323933	0.008225	318.1	0.343477	0.008721
E44	273.28	0.190952	0.004916	300	0.209622	0.005396	318.1	0.222269	0.005722
E47	273.28	0.029787	0.001605	300	0.0327	0.001762	318.1	0.034673	0.001869
K48	273.28	0.033891	0.013792	300	0.037205	0.015141	318.1	0.039449	0.016054
S52	273.28	0.060009	0.048054	300	0.065876	0.052753	318.1	0.069851	0.055936
L64	289.12	0.167816	0.007203	300	0.174131	0.007474	318.1	0.184637	0.007925
Y67	273.28	0.145322	0.005192	300	0.159531	0.005699	318.1	0.169156	0.006043
F70	283.54	0.270931	0.019549	300	0.286659	0.020683	299.74	0.28641	0.020666
T71	273.28	0.130246	0.059177	300	0.142981	0.064963	318.1	0.151607	0.068883
T73	273.28	0.057165	0.024795	300	0.062754	0.027219	318.1	0.06654	0.028862
K75	273.28	0.068108	0.023217	300	0.074768	0.025487	318.1	0.079279	0.027025
D76	273.28	0.075861	0.026336	300	0.083278	0.028911	318.1	0.088303	0.030656
E77	273.28	0.073236	0.01924	300	0.080397	0.021121	318.1	0.085248	0.022395
Y78	273.28	0.1341	0.065128	300	0.147212	0.071495	318.1	0.156093	0.075809
A79	273.28	0.297499	0.00396	300	0.326587	0.004347	318.1	0.346291	0.00461
R81	273.28	0.266538	0.003355	300	0.292599	0.003684	318.1	0.310253	0.003906
V82	273.28	0.141541	0.008407	300	0.15538	0.00923	303.34	0.15711	0.009332
N83	273.28	0.246907	0.00337	300	0.271048	0.0037	318.1	0.287401	0.003923
L87	273.28	0.06823	0.00871	300	0.074901	0.009561	318.1	0.07942	0.010138
Q89	273.28	0.063081	0.018321	300	0.069249	0.020112	318.1	0.073427	0.021326
K91	273.28	0.128135	0.008057	300	0.140663	0.008845	297.94	0.139697	0.008784
V93	273.28	0.276272	0.003352	300	0.303285	0.00368	318.1	0.321583	0.003902
W95	283.54	0.232679	0.007785	300	0.246186	0.008237	318.1	0.26104	0.008734
R97	273.28	0.062455	0.020058	300	0.068562	0.022019	318.1	0.072698	0.023348
D98	273.28	0.074016	0.018355	300	0.081253	0.020149	318.1	0.086156	0.021365
M99	273.28	0.066471	0.014665	300	0.07297	0.016099	318.1	0.077373	0.01707

Table 8 $\Delta \bar{C}_p^0$ of the amide sites of β₂-microglobulin at various temperatures. Isolated cases in which the lowest temperature is higher than the reference temperature or the highest temperature is lower than the reference temperature are highlighted in red.
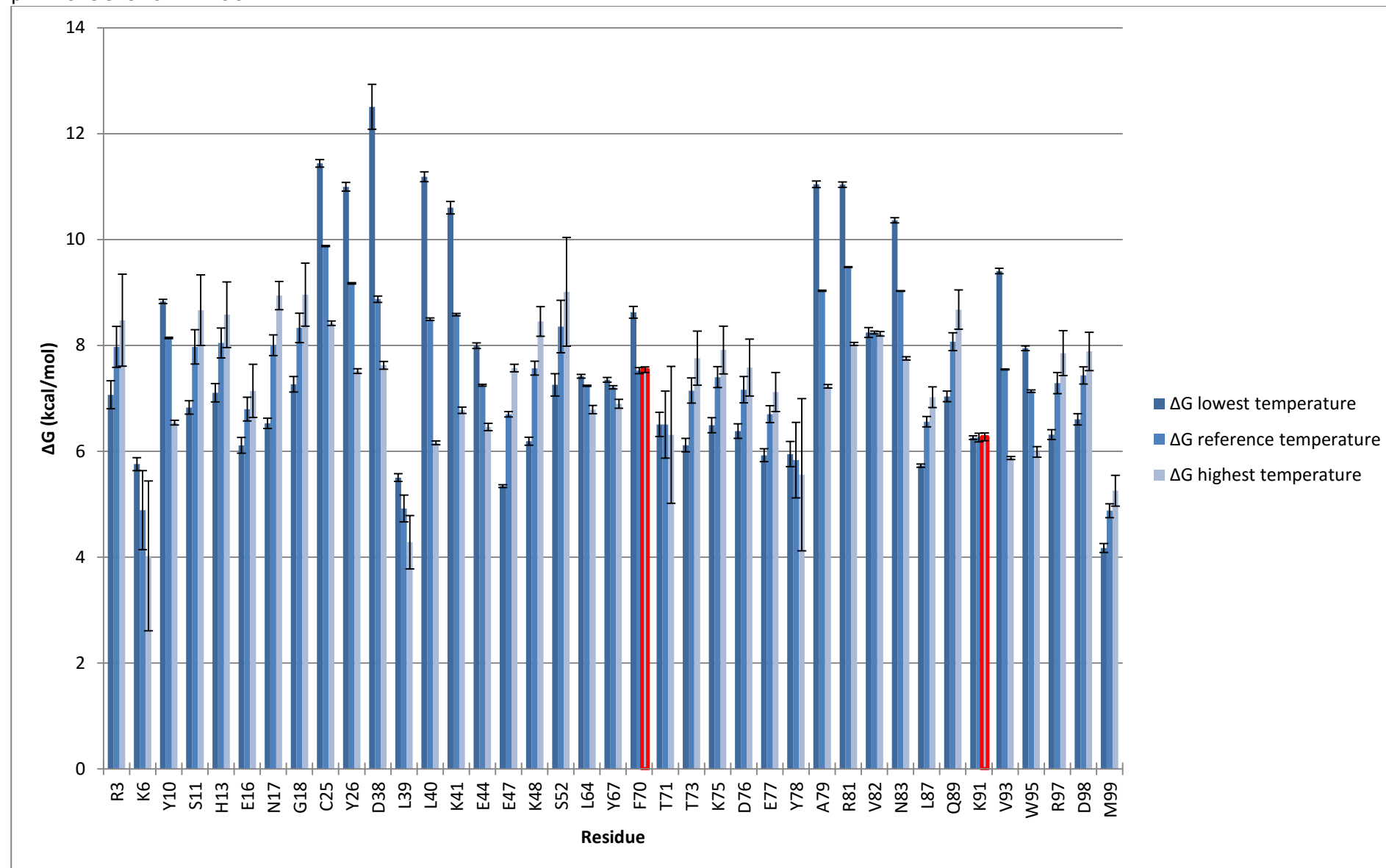
β2-MICROGLOBULIN BLUU-TRAMP EXPERIMENT

Figure 8 $\Delta \overline{G}^0$ **of the amide sites of β₂-microglobulin based on the results of the analysis on the BLUU-Tramp experiment. Half of the error bar corresponds to a standard deviation. The values highlighted in red in the tables are shown with a red border in this graph.**

Figure 9 $\Delta \overline{H}^0$ of the amide sites of β_2-microglobulin based on the results of the analysis on the BLUU-Tramp experiment. Half of the error bar corresponds to a standard deviation. The values highlighted in red in the tables are shown with a red border in this graph.
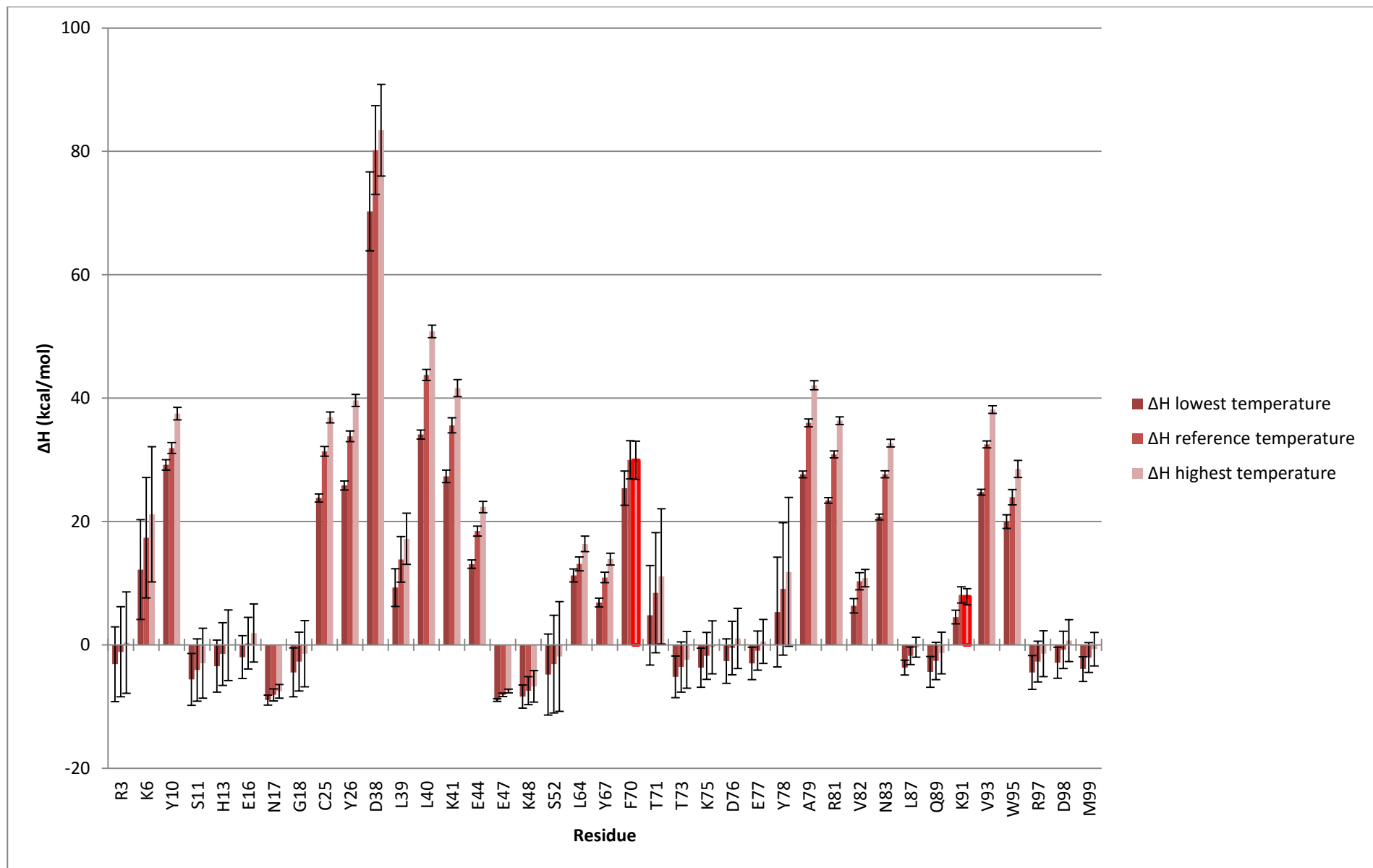
β2-MICROGLOBULIN BLUU-TRAMP EXPERIMENT

β2-MICROGLOBULIN BLUU-TRAMP EXPERIMENT

Figure 10 $\Delta\overline{S}^0$ of the amide sites of β$_2$-microglobulin based on the results of the analysis on the BLUU-Tramp experiment. Half of the error bar corresponds to a standard deviation. The values highlighted in red in the tables are shown with a red border in this graph.
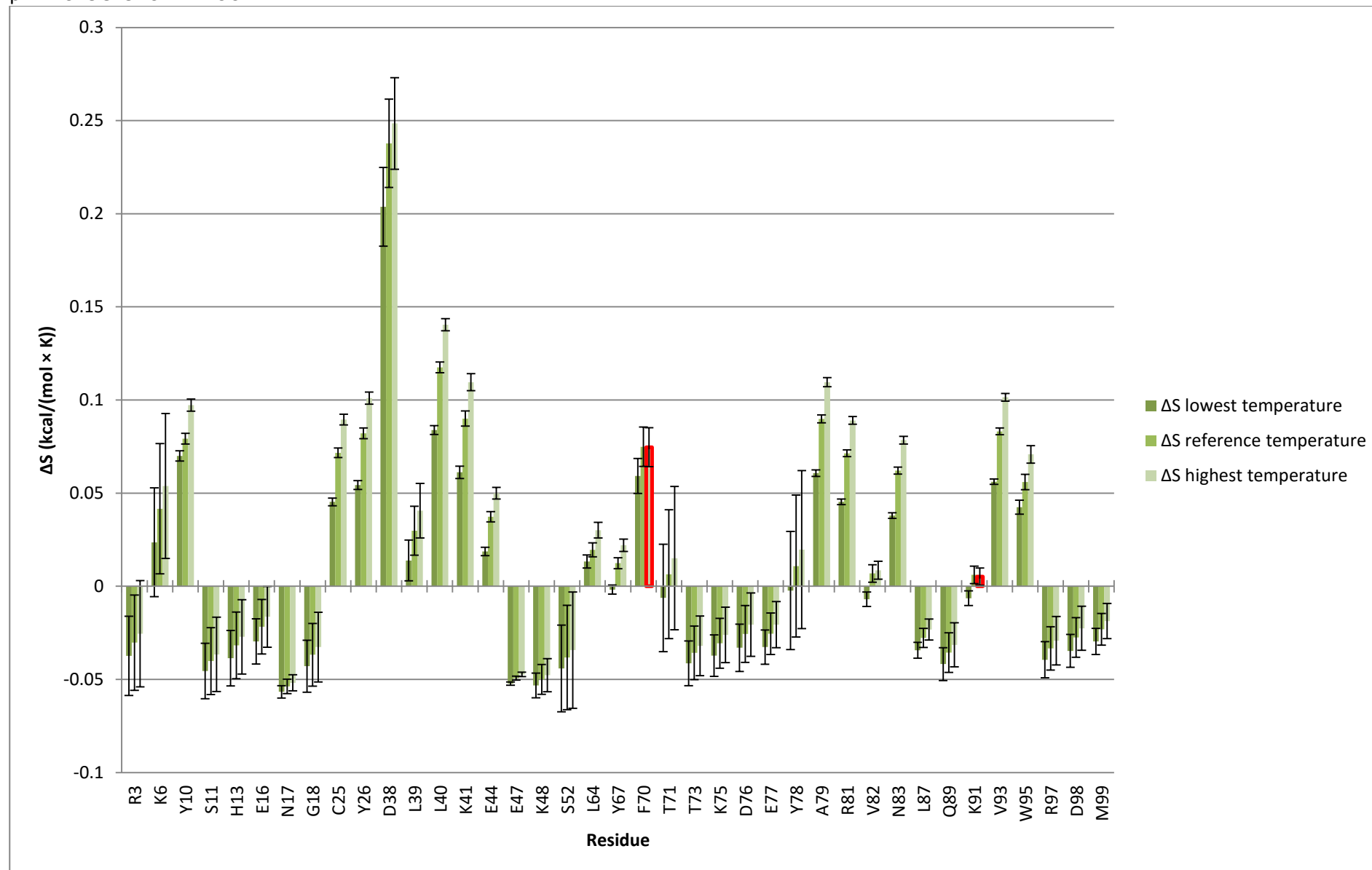
Figure 11 $\Delta \overline{C}_p^0$ of the amide sites of β_2-microglobulin based on the results of the analysis on the BLUU-Tramp experiment. Half of the error bar corresponds to a standard deviation. The values highlighted in red in the tables are shown with a red border in this graph.
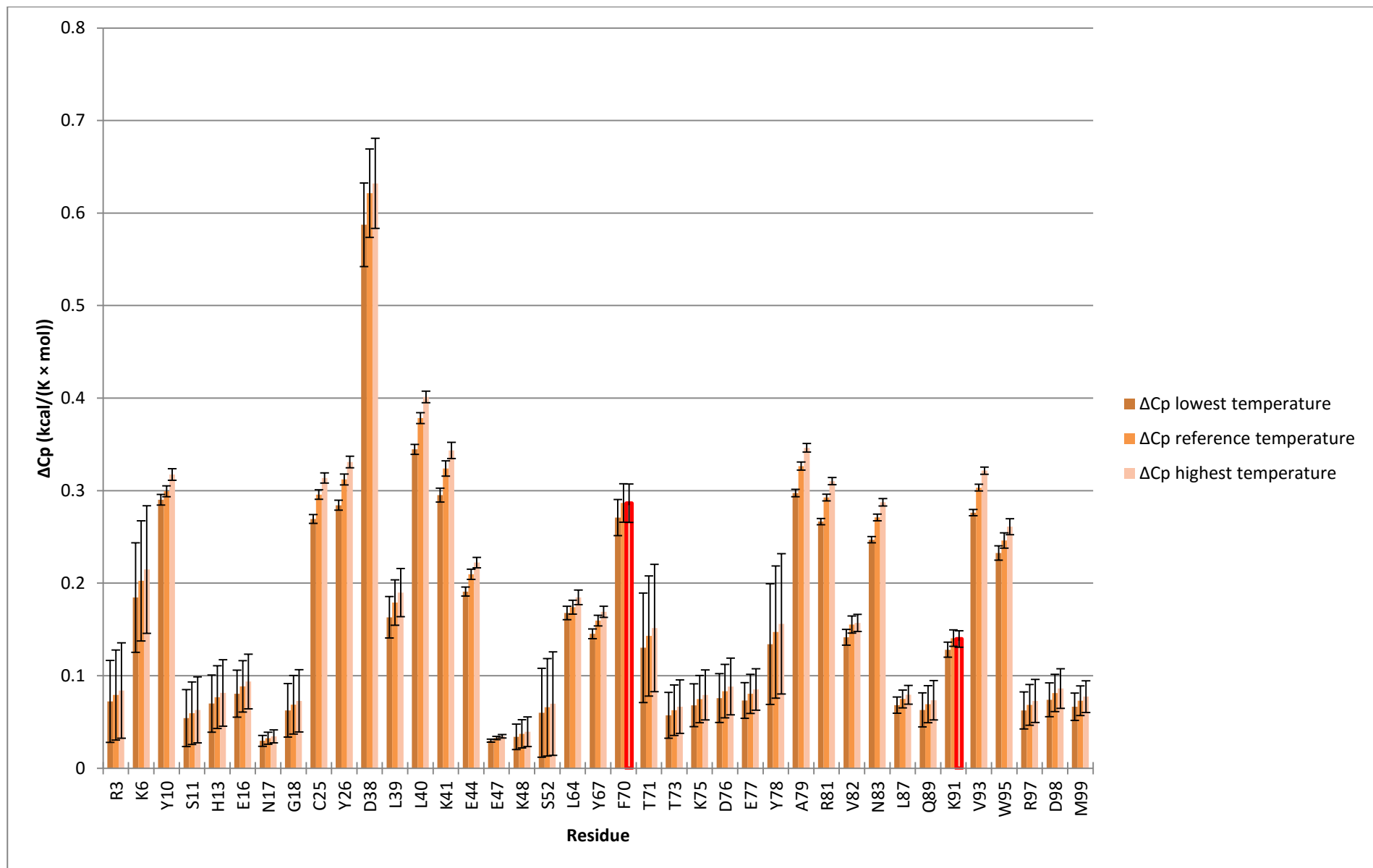
β2-MICROGLOBULIN BLUU-TRAMP EXPERIMENT

LYSOZYME

In the case of human lysozyme from the analysis results relative to 39 residues were obtained, which are summarized in the following tables and graphs.

Residue	$\Delta \bar{G}^0$ (kcal/mol)	$\Delta \bar{H}^0$ (kcal/mol)	$\Delta \bar{S}^0$ (kcal/(mol × K))	$\Delta \bar{C}_p^0$ (kcal/(mol × K))
E7	8.90102 ± 0.059883	-8.394398 ± 1.508151	-0.057651 ± 0.004871	0.030704 ± 0.010054
L8	7.026827 ± 0.007341	13.926862 ± 0.573587	0.023 ± 0.001919	0.179512 ± 0.003824
R10	9.598478 ± 0.015591	16.888488 ± 0.358934	0.0243 ± 0.001147	0.199257 ± 0.002393
T11	6.953466 ± 0.070864	13.743423 ± 1.878407	0.022633 ± 0.006495	0.178289 ± 0.012523
L12	13.096426 ± 0.112078	68.385533 ± 1.555337	0.184297 ± 0.004812	0.54257 ± 0.010369
G19	9.287495 ± 0.174117	-11.595485 ± 4.536169	-0.06961 ± 0.014639	0.009363 ± 0.030241
G22	10.371971 ± 0.373239	-8.267483 ± 7.641663	-0.062132 ± 0.024376	0.03155 ± 0.050944
I23	6.486453 ± 0.038458	7.777089 ± 1.257848	0.004302 ± 0.004315	0.138514 ± 0.008386
N27	8.589028 ± 0.018434	16.379743 ± 1.430172	0.025969 ± 0.004795	0.195865 ± 0.009534
W28	14.76335 ± 0.269324	83.687709 ± 3.622254	0.229748 ± 0.011179	0.644585 ± 0.024148
M29	7.818878 ± 0.055385	12.444223 ± 2.055894	0.015418 ± 0.007033	0.169628 ± 0.013706
C30	15.039956 ± 0.156171	80.306706 ± 2.270882	0.217556 ± 0.007051	0.622045 ± 0.015139
L31	12.227279 ± 0.157476	51.112037 ± 2.243686	0.129616 ± 0.006957	0.427414 ± 0.014958
A32	11.229655 ± 0.068934	45.108717 ± 1.10662	0.11293 ± 0.003461	0.387391 ± 0.007377
K33	9.594353 ± 0.046719	23.708657 ± 1.27695	0.047048 ± 0.004106	0.244724 ± 0.008513
W34	11.377278 ± 2.589344	23.833841 ± 27.175954	0.041522 ± 0.082003	0.245559 ± 0.181173
S36	11.215347 ± 1.054248	13.018996 ± 12.330649	0.006012 ± 0.037634	0.17346 ± 0.082204
T40	8.565328 ± 0.012894	10.485271 ± 0.930324	0.0064 ± 0.003097	0.156568 ± 0.006202
A42	8.703042 ± 0.010207	13.179207 ± 0.653489	0.014921 ± 0.002162	0.174528 ± 0.004357
D53	7.421296 ± 0.011713	-7.88211 ± 0.171975	-0.051011 ± 0.000612	0.034119 ± 0.001146
Y54	9.481784 ± 0.051973	38.739918 ± 1.255753	0.097527 ± 0.004017	0.344933 ± 0.008372
G55	10.189611 ± 0.045882	33.554852 ± 1.21738	0.077884 ± 0.00391	0.310366 ± 0.008116
F57	7.146938 ± 0.021434	12.297407 ± 1.317316	0.017168 ± 0.004441	0.168649 ± 0.008782
S61	11.254307 ± 0.123379	49.266786 ± 3.139908	0.126708 ± 0.010063	0.415112 ± 0.020933
R62	8.953921 ± 0.033875	14.956964 ± 2.330928	0.02001 ± 0.007866	0.18638 ± 0.01554
C65	10.861041 ± 0.501617	5.859994 ± 30.858118	-0.01667 ± 0.104324	0.125733 ± 0.205721
D67	8.932064 ± 0.058818	-12.027649 ± 0.095193	-0.069866 ± 0.000513	0.006482 ± 0.000635
T70	15.922857 ± 3.326312	92.259006 ± 42.71521	0.254454 ± 0.131317	0.701727 ± 0.284768
C77	8.739973 ± 0.01294	-11.367386 ± 0.032141	-0.067025 ± 0.00015	0.010884 ± 0.000214
L79	8.583837 ± 0.322008	8.736277 ± 22.843172	0.000508 ± 0.075229	0.144909 ± 0.152288
S80	8.55009 ± 0.111943	-1.872989 ± 6.514955	-0.034744 ± 0.021999	0.07418 ± 0.043433
A83	9.435745 ± 0.069629	-5.916729 ± 1.576114	-0.051175 ± 0.005061	0.047222 ± 0.010507
L84	8.142033 ± 0.01579	14.801767 ± 0.55212	0.022199 ± 0.001795	0.185345 ± 0.003681
V93	9.162524 ± 0.041591	23.913814 ± 0.934789	0.049171 ± 0.00298	0.246092 ± 0.006232
A94	7.368529 ± 0.017116	15.191564 ± 0.893324	0.026077 ± 0.003026	0.187944 ± 0.005955
A96	10.687136 ± 0.044814	20.261655 ± 4.767931	0.031915 ± 0.015802	0.221744 ± 0.031786
V100	9.294795 ± 0.054937	36.982259 ± 1.169296	0.092292 ± 0.003717	0.333215 ± 0.007795
Y124	16.088034 ± 3.121034	95.589875 ± 40.047359	0.265006 ± 0.123106	0.723933 ± 0.266982
Q126	8.782032 ± 0.050764	-4.684569 ± 1.235841	-0.044889 ± 0.003985	0.055436 ± 0.008239

Table 9 Results of the analysis on the lysozyme BLUU-Tramp experiment. Data are reported as value ± standard deviation.

LYSOZYME

Residue	Lowest Temperature			Reference Temperature			Highest Temperature		
	T (K)	$\Delta \bar{G}^0$ (kcal/mol)	$\sigma_{\Delta \bar{G}^0}$ (kcal/mol)	T (K)	$\Delta \bar{G}^0$ (kcal/mol)	$\sigma_{\Delta \bar{G}^0}$ (kcal/mol)	T (K)	$\Delta \bar{G}^0$ (kcal/mol)	$\sigma_{\Delta \bar{G}^0}$ (kcal/mol)
E7	283	7.906157	0.129982	300	8.90102	0.059883	336	10.910149	0.155167
L8	283	7.331364	0.029488	300	7.026827	0.007341	336	5.811076	0.079777
R10	283	9.915603	0.033443	300	9.598478	0.015591	336	8.293282	0.032219
T11	283	7.252354	0.035968	300	6.953466	0.070864	295.5	7.049298	0.042618
L12	288	15.177774	0.167197	300	13.096426	0.112078	336	5.289782	0.084505
G19	285.5	8.27487	0.358824	300	9.287495	0.174117	336	11.773227	0.459439
G22	283	9.300538	0.738763	300	10.371971	0.373239	336	12.540557	0.684497
I23	283	6.492871	0.034488	300	6.486453	0.038458	336	6.032386	0.210497
N27	283	8.93616	0.0703	300	8.589028	0.018434	336	7.231074	0.20241
W28	283	18.358589	0.447447	300	14.76335	0.269324	336	5.100124	0.186941
M29	283	7.999277	0.060291	300	7.818878	0.055385	298	7.848583	0.041889
C30	283	18.438787	0.268527	300	15.039956	0.156171	336	5.864329	0.131432
L31	283	14.224878	0.268133	300	12.227279	0.157476	336	6.637895	0.127439
A32	295.5	11.724766	0.084149	300	11.229655	0.068934	336	6.327402	0.07275
K33	290.5	10.004495	0.083758	300	9.594353	0.046719	318	8.615343	0.035327
W34	305.5	11.136528	2.132621	300	11.377278	2.589344	336	9.352084	0.820296
S36	283	11.234004	1.648908	300	11.215347	1.054248	336	10.624236	0.523234
T40	283	8.598711	0.052419	300	8.565328	0.012894	336	7.996746	0.124356
A42	283	8.872627	0.040573	300	8.703042	0.010207	336	7.788922	0.082764
D53	313	8.074833	0.01998	300	7.421296	0.011713	336	9.184007	0.036204
Y54	283	10.973603	0.11551	300	9.481784	0.051973	336	5.225754	0.112562
G55	283	11.364148	0.107496	300	10.189611	0.045882	336	6.715392	0.114675
F57	283	7.357565	0.058267	300	7.146938	0.021434	313	6.876248	0.076761
S61	285.5	12.946115	0.260705	300	11.254307	0.123379	336	5.796168	0.287399
R62	283	9.20432	0.09878	300	8.953921	0.033875	303	8.891095	0.055662
C65	283	10.517087	1.257362	300	10.861041	0.501617	303	10.909166	0.793555
D67	283	7.741224	0.050406	300	8.932064	0.058818	323	10.53326	0.071172
T70	308	13.812376	2.248598	300	15.922857	3.326312	336	5.24679	2.033477
C77	283	7.595313	0.01049	300	8.739973	0.01294	336	11.129346	0.018808
L79	293	8.575559	0.806014	300	8.583837	0.322008	310.5	8.551874	0.569701
S80	283	7.923718	0.277526	300	8.55009	0.111943	308	8.820126	0.27552
A83	283	8.543027	0.143768	300	9.435745	0.069629	336	11.176043	0.152715
L84	283	8.430143	0.043088	300	8.142033	0.01579	336	6.942519	0.059493
V93	283	9.879896	0.088722	300	9.162524	0.041591	320.5	7.982152	0.02645
A94	283	7.721308	0.035397	300	7.368529	0.017116	336	6.023806	0.136483
A96	283	11.122885	0.282634	300	10.687136	0.044814	308	10.408163	0.108788
V100	283	10.703252	0.113903	300	9.294795	0.054937	320.5	7.169429	0.029356
Y124	308	13.890765	2.110489	300	16.088034	3.121034	336	4.984119	1.902516
Q126	283	7.992222	0.108304	300	8.782032	0.050764	336	10.278281	0.125217

Table 10 $\Delta \bar{G}^0$ of the amide sites of lysozyme at various temperatures. Isolated cases in which the lowest temperature is higher than the reference temperature or the highest temperature is lower than the reference temperature are highlighted in red.

RESULTS
LYSOZYME

Residue	Lowest Temperature			Reference Temperature			Highest Temperature		
	T (K)	$\Delta\bar{H}^0$ (kcal/mol)	$\sigma_{\Delta\bar{H}^0}$ (kcal/mol)	T (K)	$\Delta\bar{H}^0$ (kcal/mol)	$\sigma_{\Delta\bar{H}^0}$ (kcal/mol)	T (K)	$\Delta\bar{H}^0$ (kcal/mol)	$\sigma_{\Delta\bar{H}^0}$ (kcal/mol)
E7	283	-8.901577	1.34207	300	-8.394398	1.508151	336	-7.222733	1.891824
L8	283	10.961616	0.510423	300	13.926862	0.573587	336	20.777056	0.719508
R10	283	13.597102	0.319407	300	16.888488	0.358934	336	24.49212	0.450247
T11	283	10.798378	1.671553	300	13.743423	1.878407	295.5	12.947138	1.822477
L12	288	62.004907	1.433399	300	68.385533	1.555337	336	89.090012	1.951015
G19	285.5	-11.727974	4.108269	300	-11.595485	4.536169	336	-11.238177	5.69017
G22	283	-8.788638	6.800146	300	-8.267483	7.641663	336	-7.063531	9.585702
I23	283	5.48907	1.119331	300	7.777089	1.257848	336	13.062781	1.577845
N27	283	13.144381	1.272678	300	16.379743	1.430172	336	23.85395	1.794007
W28	283	73.040243	3.223364	300	83.687709	3.622254	336	108.285062	4.543756
M29	283	9.642249	1.829494	300	12.444223	2.055894	298	12.106098	2.028574
C30	283	70.031564	2.020808	300	80.306706	2.270882	336	104.043932	2.848595
L31	283	44.051877	1.996606	300	51.112037	2.243686	336	67.422139	2.814479
A32	295.5	43.37853	1.07367	300	45.108717	1.10662	336	59.891574	1.388144
K33	290.5	21.420586	1.197357	300	23.708657	1.27695	318	28.245847	1.434781
W34	305.5	25.196795	28.181539	300	23.833841	27.175954	336	33.20437	34.089516
S36	283	10.153727	10.97277	300	13.018996	12.330649	336	19.638229	15.467566
T40	283	7.899021	0.827875	300	10.485271	0.930324	336	16.459924	1.166999
A42	283	10.296295	0.581525	300	13.179207	0.653489	336	19.839198	0.819736
D53	313	-7.42895	0.187202	300	-7.88211	0.171975	336	-6.580119	0.215725
Y54	283	33.042203	1.117466	300	38.739918	1.255753	336	51.902553	1.575216
G55	283	28.428128	1.08332	300	33.554852	1.21738	336	45.398406	1.527082
F57	283	9.5116	1.172251	300	12.297407	1.317316	313	14.537352	1.433957
S61	285.5	43.393125	2.843719	300	49.266786	3.139908	336	65.107456	3.938701
R62	283	11.878281	2.074241	300	14.956964	2.330928	303	15.518899	2.37778
C65	283	3.78309	27.459954	300	5.859994	30.858118	303	6.23908	31.478367
D67	283	-12.134727	0.08471	300	-12.027649	0.095193	323	-11.87284	0.110348
T70	308	97.94767	45.02373	300	92.259006	42.71521	336	119.036897	53.581959
C77	283	-11.547173	0.028602	300	-11.367386	0.032141	336	-10.952048	0.040318
L79	293	7.733751	21.789594	300	8.736277	22.843172	310.5	10.284443	24.470177
S80	283	-3.09832	5.797513	300	-1.872989	6.514955	308	-1.271636	6.867052
A83	283	-6.696755	1.402549	300	-5.916729	1.576114	336	-4.114745	1.977077
L84	283	11.740174	0.491319	300	14.801767	0.55212	336	21.874536	0.69258
V93	283	19.848783	0.831848	300	23.913814	0.934789	320.5	29.131069	1.066909
A94	283	12.087046	0.79495	300	15.191564	0.893324	336	22.363498	1.120586
A96	283	16.598808	4.242876	300	20.261655	4.767931	308	22.059263	5.025611
V100	283	31.478102	1.04053	300	36.982259	1.169296	320.5	44.046558	1.334559
Y124	308	101.458555	42.211696	300	95.589875	40.047359	336	123.215139	50.235407
Q126	283	-5.600283	1.099747	300	-4.684569	1.235841	336	-2.569124	1.550238

Table 11 $\Delta\bar{H}^0$ of the amide sites of lysozyme at various temperatures. Isolated cases in which the lowest temperature is higher than the reference temperature or the highest temperature is lower than the reference temperature are highlighted in red.

LYSOZYME

Residue	Lowest Temperature			Reference Temperature			Highest Temperature		
	T (K)	$\Delta\bar{S}^0$ (kcal/(mol × K))	$\sigma_{\Delta\bar{S}^0}$ (kcal/(mol × K))	T (K)	$\Delta\bar{S}^0$ (kcal/(mol × K))	$\sigma_{\Delta\bar{S}^0}$ (kcal/(mol × K))	T (K)	$\Delta\bar{S}^0$ (kcal/(mol × K))	$\sigma_{\Delta\bar{S}^0}$ (kcal/(mol × K))
E7	283	-0.059391	0.004301	300	-0.057651	0.004871	336	-0.053967	0.006077
L8	283	0.012828	0.001702	300	0.023	0.001919	336	0.044542	0.002378
R10	283	0.013009	0.001012	300	0.0243	0.001147	336	0.048211	0.001435
T11	283	0.01253	0.005785	300	0.022633	0.006495	295.5	0.019959	0.006307
L12	288	0.162594	0.004397	300	0.184297	0.004812	336	0.249405	0.006056
G19	285.5	-0.070062	0.013178	300	-0.06961	0.014639	336	-0.068486	0.018267
G22	283	-0.063919	0.02149	300	-0.062132	0.024376	336	-0.058345	0.030488
I23	283	-0.003547	0.00384	300	0.004302	0.004315	336	0.020924	0.005321
N27	283	0.01487	0.004255	300	0.025969	0.004795	336	0.049473	0.005939
W28	283	0.193221	0.00981	300	0.229748	0.011179	336	0.307098	0.014076
M29	283	0.005806	0.006256	300	0.015418	0.007033	298	0.014287	0.006941
C30	283	0.182307	0.006193	300	0.217556	0.007051	336	0.292201	0.008867
L31	283	0.105396	0.006109	300	0.129616	0.006957	336	0.180905	0.008752
A32	295.5	0.107119	0.00335	300	0.11293	0.003461	336	0.159417	0.004346
K33	290.5	0.039298	0.003836	300	0.047048	0.004106	318	0.061731	0.004616
W34	305.5	0.046024	0.085325	300	0.041522	0.082003	336	0.070989	0.103743
S36	283	-0.003817	0.032976	300	0.006012	0.037634	336	0.026827	0.047498
T40	283	-0.002472	0.002745	300	0.0064	0.003097	336	0.025188	0.003841
A42	283	0.005031	0.001915	300	0.014921	0.002162	336	0.035864	0.002684
D53	313	-0.049533	0.000662	300	-0.051011	0.000612	336	-0.046917	0.00075
Y54	283	0.077981	0.003542	300	0.097527	0.004017	336	0.138919	0.005021
G55	283	0.060297	0.00345	300	0.077884	0.00391	336	0.115128	0.004884
F57	283	0.007611	0.003943	300	0.017168	0.004441	313	0.024476	0.004821
S61	285.5	0.106645	0.009051	300	0.126708	0.010063	336	0.176522	0.012574
R62	283	0.009449	0.006986	300	0.02001	0.007866	303	0.021874	0.008022
C65	283	-0.023795	0.092667	300	-0.01667	0.104324	303	-0.015413	0.106382
D67	283	-0.070233	0.000477	300	-0.069866	0.000513	323	-0.069369	0.000562
T70	308	0.273167	0.138911	300	0.254454	0.131317	336	0.338661	0.165489
C77	283	-0.067641	0.000138	300	-0.067025	0.00015	336	-0.065718	0.000176
L79	293	-0.002873	0.071676	300	0.000508	0.075229	310.5	0.00558	0.080559
S80	283	-0.038947	0.019538	300	-0.034744	0.021999	308	-0.032765	0.023157
A83	283	-0.053851	0.004466	300	-0.051175	0.005061	336	-0.045508	0.006322
L84	283	0.011696	0.001586	300	0.022199	0.001795	336	0.044441	0.002237
V93	283	0.035226	0.002627	300	0.049171	0.00298	320.5	0.065987	0.003406
A94	283	0.015427	0.002688	300	0.026077	0.003026	336	0.04863	0.00374
A96	283	0.01935	0.014001	300	0.031915	0.015802	308	0.037828	0.01665
V100	283	0.073409	0.003276	300	0.092292	0.003717	320.5	0.115061	0.00425
Y124	308	0.284311	0.130225	300	0.265006	0.123106	336	0.351878	0.155143
Q126	283	-0.04803	0.003518	300	-0.044889	0.003985	336	-0.038236	0.004974

Table 12 $\Delta\bar{S}^0$ of the amide sites of lysozyme at various temperatures. Isolated cases in which the lowest temperature is higher than the reference temperature or the highest temperature is lower than the reference temperature are highlighted in red.

RESULTS
LYSOZYME

Residue	Lowest Temperature			Reference Temperature			Highest Temperature		
	T (K)	$\Delta \bar{C}_p^0$ (kcal/(mol × K))	$\sigma_{\Delta \bar{C}_p^0}$ (kcal/(mol × K))	T (K)	$\Delta \bar{C}_p^0$ (kcal/(mol × K))	$\sigma_{\Delta \bar{C}_p^0}$ (kcal/(mol × K))	T (K)	$\Delta \bar{C}_p^0$ (kcal/(mol × K))	$\sigma_{\Delta \bar{C}_p^0}$ (kcal/(mol × K))
E7	283	0.028964	0.009485	300	0.030704	0.010054	336	0.034388	0.011261
L8	283	0.16934	0.003607	300	0.179512	0.003824	336	0.201054	0.004283
R10	283	0.187965	0.002257	300	0.199257	0.002393	336	0.223167	0.00268
T11	283	0.168186	0.011813	300	0.178289	0.012523	295.5	0.175615	0.012335
L12	288	0.520867	0.009954	300	0.54257	0.010369	336	0.607679	0.011613
G19	285.5	0.008911	0.028779	300	0.009363	0.030241	336	0.010487	0.03387
G22	283	0.029762	0.048058	300	0.03155	0.050944	336	0.035336	0.057058
I23	283	0.130665	0.00791	300	0.138514	0.008386	336	0.155136	0.009392
N27	283	0.184766	0.008994	300	0.195865	0.009534	336	0.219369	0.010679
W28	283	0.608058	0.02278	300	0.644585	0.024148	336	0.721935	0.027046
M29	283	0.160016	0.012929	300	0.169628	0.013706	298	0.168497	0.013615
C30	283	0.586796	0.014281	300	0.622045	0.015139	336	0.69669	0.016956
L31	283	0.403193	0.01411	300	0.427414	0.014958	336	0.478703	0.016753
A32	295.5	0.381581	0.007267	300	0.387391	0.007377	336	0.433878	0.008263
K33	290.5	0.236975	0.008243	300	0.244724	0.008513	318	0.259408	0.009024
W34	305.5	0.250061	0.184495	300	0.245559	0.181173	336	0.275026	0.202914
S36	283	0.163631	0.077546	300	0.17346	0.082204	336	0.194275	0.092069
T40	283	0.147696	0.005851	300	0.156568	0.006202	336	0.175357	0.006946
A42	283	0.164638	0.00411	300	0.174528	0.004357	336	0.195471	0.004879
D53	313	0.035598	0.001196	300	0.034119	0.001146	336	0.038214	0.001284
Y54	283	0.325387	0.007897	300	0.344933	0.008372	336	0.386325	0.009376
G55	283	0.292778	0.007656	300	0.310366	0.008116	336	0.34761	0.00909
F57	283	0.159093	0.008284	300	0.168649	0.008782	313	0.175958	0.009163
S61	285.5	0.395048	0.019921	300	0.415112	0.020933	336	0.464925	0.023445
R62	283	0.175818	0.014659	300	0.18638	0.01554	303	0.188244	0.015695
C65	283	0.118608	0.194063	300	0.125733	0.205721	303	0.126991	0.207778
D67	283	0.006115	0.000599	300	0.006482	0.000635	323	0.006979	0.000683
T70	308	0.720439	0.292362	300	0.701727	0.284768	336	0.785934	0.31894
C77	283	0.010267	0.000202	300	0.010884	0.000214	336	0.01219	0.00024
L79	293	0.141527	0.148734	300	0.144909	0.152288	310.5	0.14998	0.157618
S80	283	0.069977	0.040972	300	0.07418	0.043433	308	0.076158	0.044591
A83	283	0.044546	0.009912	300	0.047222	0.010507	336	0.052888	0.011768
L84	283	0.174842	0.003472	300	0.185345	0.003681	336	0.207587	0.004122
V93	283	0.232147	0.005879	300	0.246092	0.006232	320.5	0.262908	0.006658
A94	283	0.177294	0.005618	300	0.187944	0.005955	336	0.210497	0.00667
A96	283	0.209179	0.029985	300	0.221744	0.031786	308	0.227658	0.032634
V100	283	0.314333	0.007354	300	0.333215	0.007795	320.5	0.355985	0.008328
Y124	308	0.743237	0.274102	300	0.723933	0.266982	336	0.810804	0.29902
Q126	283	0.052295	0.007772	300	0.055436	0.008239	336	0.062089	0.009228

Table 13 $\Delta \bar{C}_p^0$ of the amide sites of lysozyme at various temperatures. Isolated cases in which the lowest temperature is higher than the reference temperature or the highest temperature is lower than the reference temperature are highlighted in red.
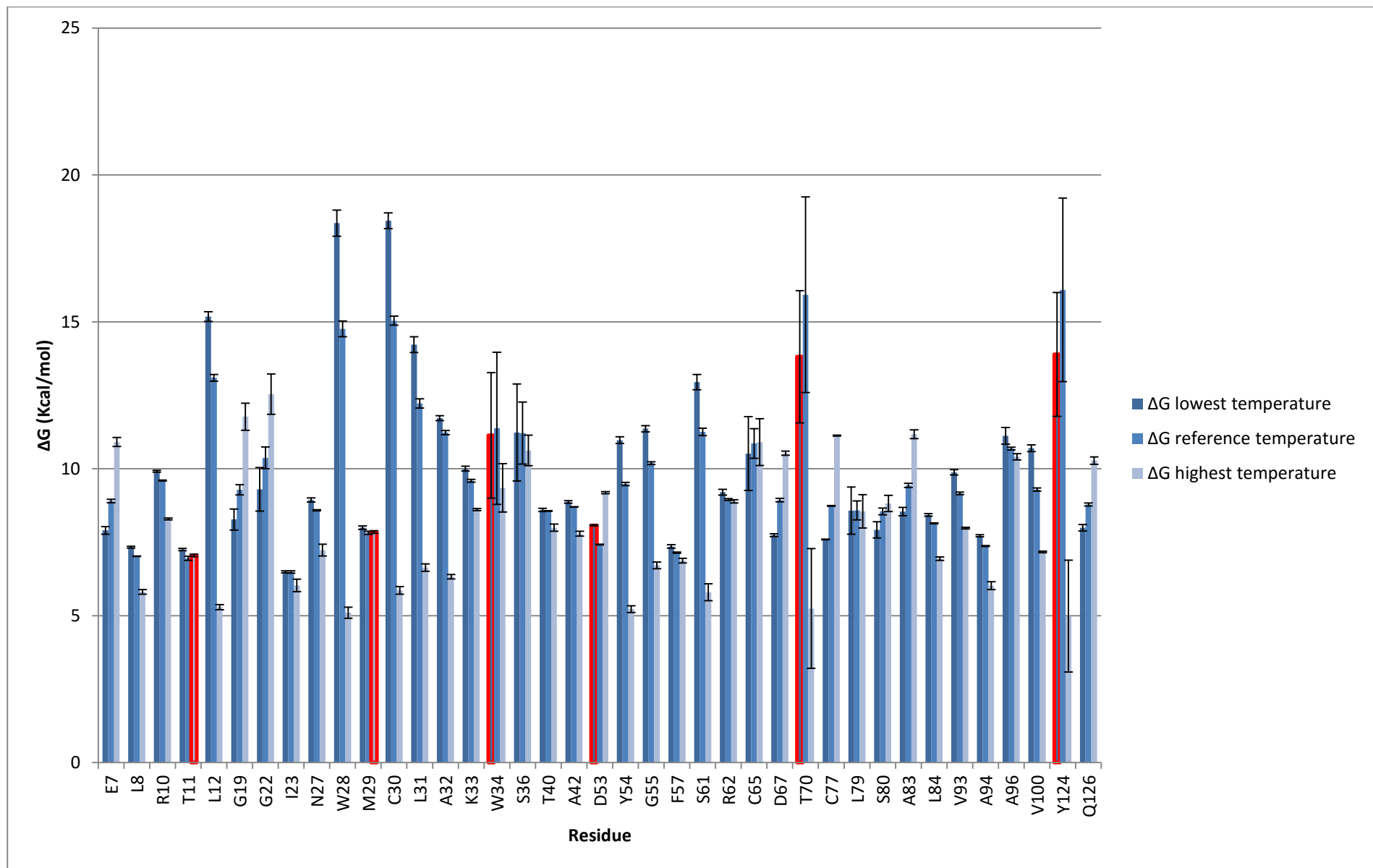
Figure 12 $\Delta \overline{G}^0$ of the amide sites of lysozyme based on the results of the analysis on the BLUU-Tramp experiment. Half of the error bar corresponds to a standard deviation. The values highlighted in red in the tables are shown with a red border in this graph.

Figure 13 $\Delta \overline{H}^0$ of the amide sites of lysozyme based on the results of the analysis on the BLUU-Tramp experiment. Half of the error bar corresponds to a standard deviation. The values highlighted in red in the tables are shown with a red border in this graph.

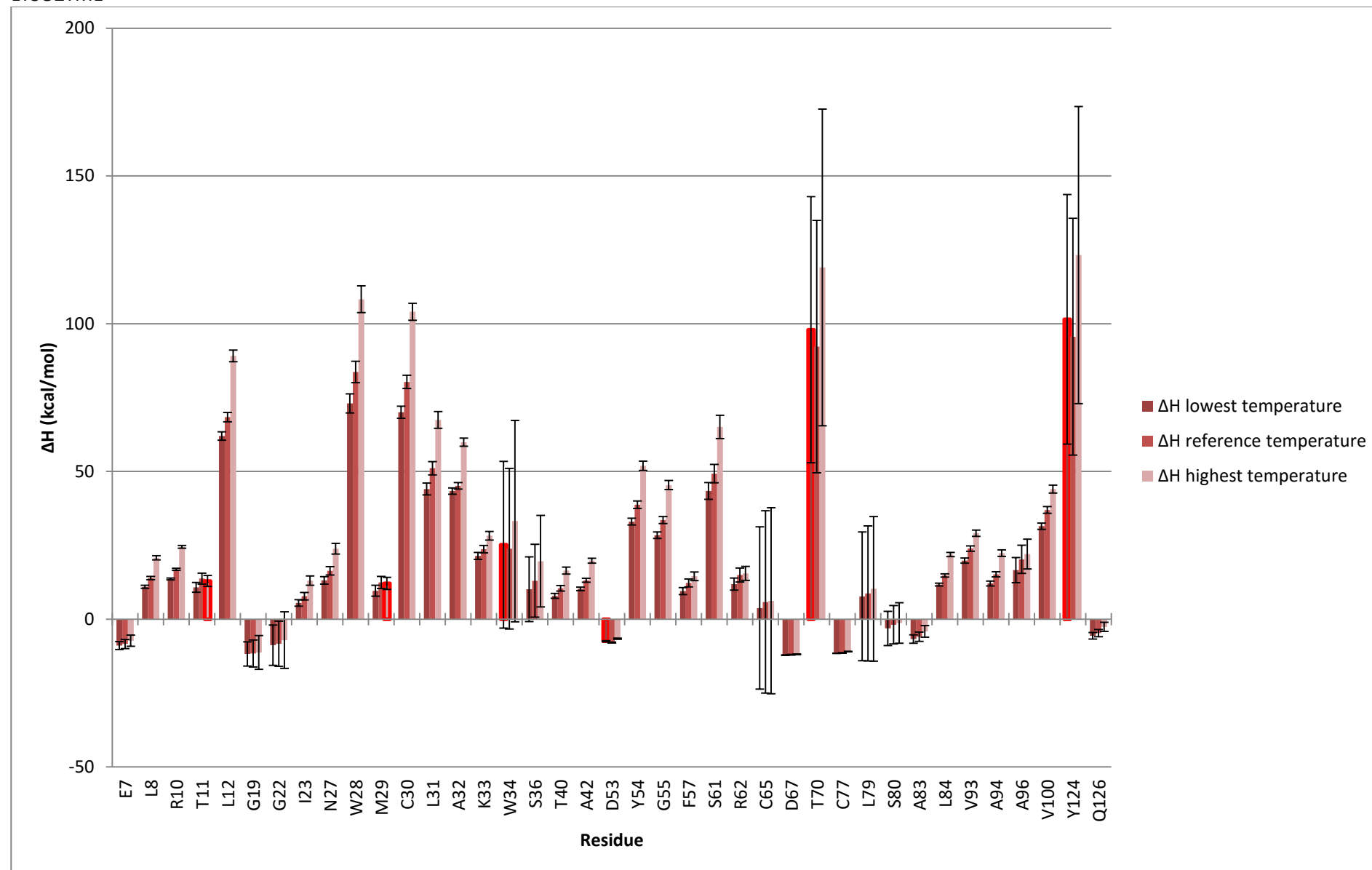**Figure 14** $\Delta \overline{S}^0$ of the amide sites of lysozyme based on the results of the analysis on the BLUU-Tramp experiment. Half of the error bar corresponds to a standard deviation. The values highlighted in red in the tables are shown with a red border in this graph.
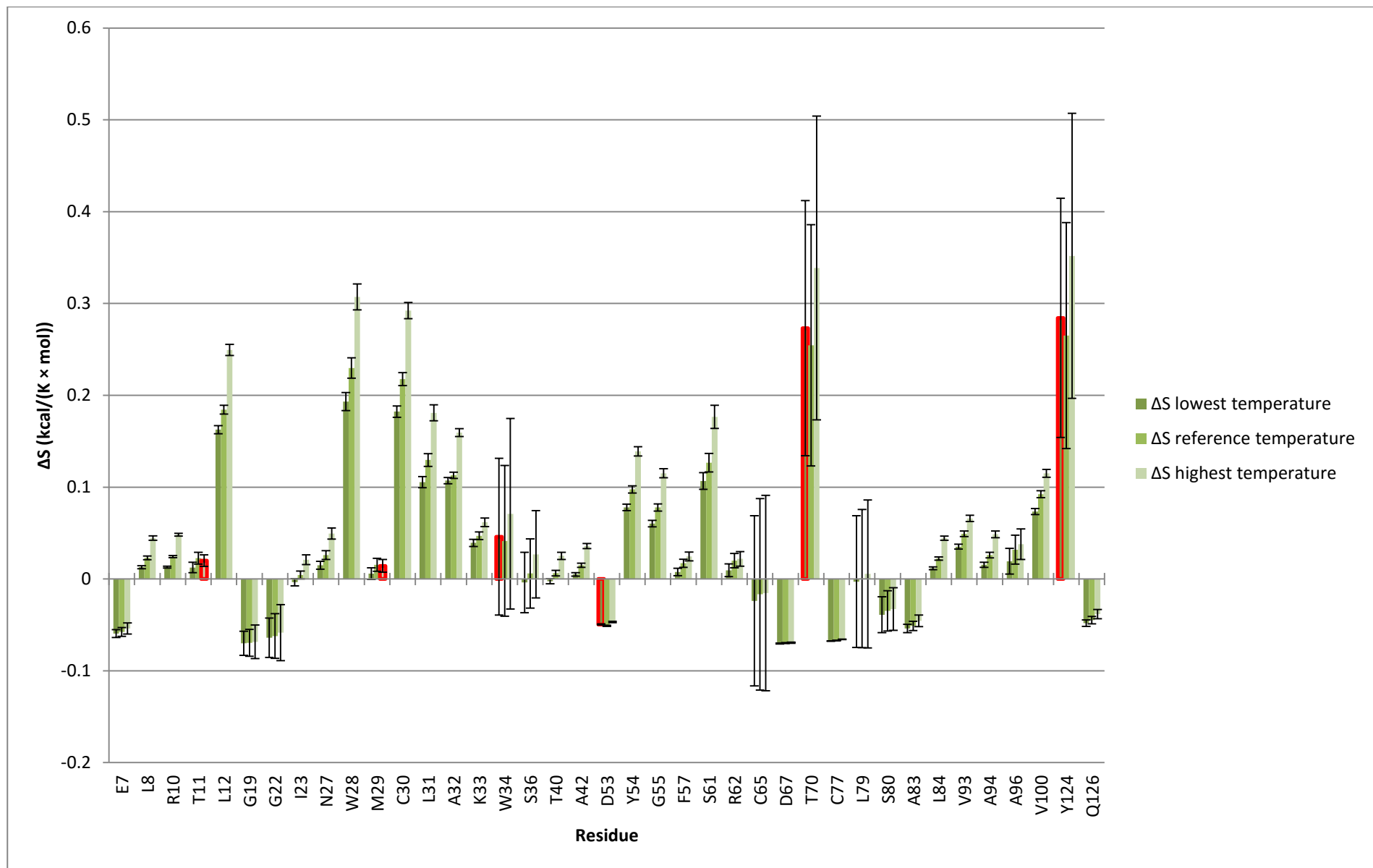
Figure 15 $\overline{C}_p^0$ **of the amide sites of lysozyme based on the results of the analysis on the BLUU-Tramp experiment. Half of the error bar corresponds to a standard deviation. The values highlighted in red in the tables are shown with a red border in this graph.**
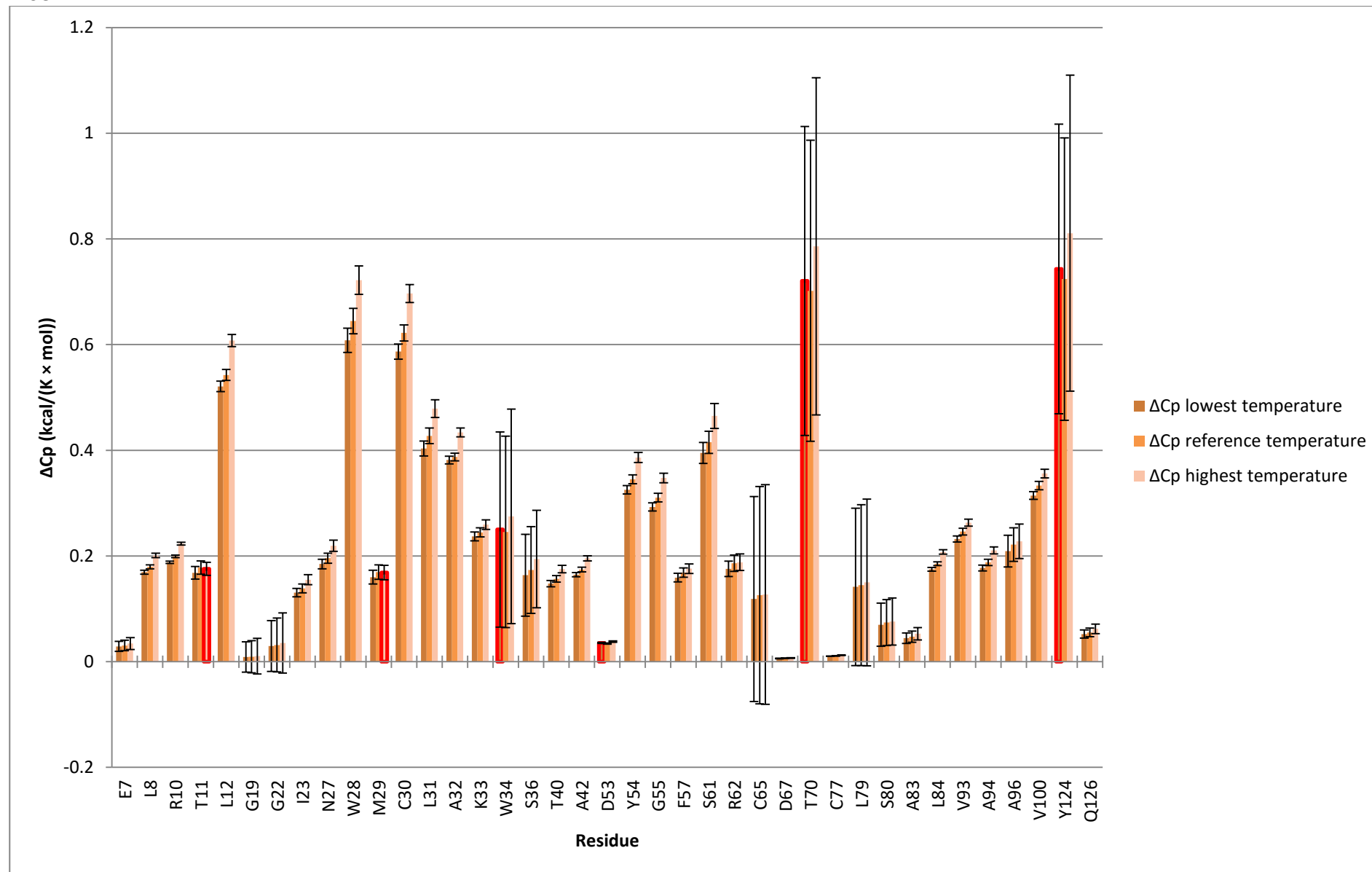
CONVENTIONAL ISOTOPE EXCHANGE EXPERIMENTS

The first analysis performed was on the data from a previously published isotope exchange study on β_2-microglobulin[56]. From these data it was possible to obtain the thermodynamic parameters in the case of 18 amide sites. It is important to note that the lowest temperature at which hydrogen exchange experiments were performed, 301 K, is higher than the reference temperature at which the thermodynamic parameters are calculated, 300K.

The following results were obtained:

Residue	$\Delta\bar{G}^0$ (kcal/mol)	$\Delta\bar{H}^0$ (kcal/mol)	$\Delta\bar{S}^0$ (kcal/(mol × K))	$\Delta\bar{C}_p^0$ (kcal/(mol × K))
Y10	8.14885 ± 0.051867	37.665053 ± 4.701538	0.098387 ± 0.015519	0.945281 ± 0.58762
C25	9.850581 ± 0.056428	42.479631 ± 5.114995	0.108763 ± 0.016884	0.200861 ± 0.639296
Y26	9.375117 ± 0.083553	45.274252 ± 7.573792	0.119664 ± 0.025	0.395621 ± 0.946608
S28	8.354108 ± 0.04867	23.490718 ± 4.411784	0.050455 ± 0.014563	1.015073 ± 0.551405
E36	7.623165 ± 0.050305	20.481734 ± 4.559973	0.042862 ± 0.015052	2.185498 ± 0.569927
D38	8.409392 ± 0.095924	41.083812 ± 8.695144	0.108915 ± 0.028701	0.757394 ± 1.086759
L39	5.382502 ± 0.037035	11.567684 ± 3.357083	0.020617 ± 0.011081	-0.248669 ± 0.419584
L40	8.707767 ± 0.07451	35.698716 ± 6.754077	0.08997 ± 0.022294	2.694421 ± 0.844156
E44	7.6506 ± 0.067525	23.42857 ± 6.120902	0.052593 ± 0.020204	1.373873 ± 0.765019
Y66	9.345367 ± 0.095624	38.315631 ± 8.667924	0.096568 ± 0.028612	1.943768 ± 1.083357
Y67	7.73804 ± 0.11321	9.191627 ± 10.262065	0.004845 ± 0.033874	2.322137 ± 1.2826
T68	7.620292 ± 0.044938	19.850891 ± 4.073468	0.040769 ± 0.013446	1.192457 ± 0.509121
F70	7.749214 ± 0.060965	17.391252 ± 5.526217	0.03214 ± 0.018241	2.661408 ± 0.690692
R81	9.558049 ± 0.061334	42.143407 ± 5.559673	0.108618 ± 0.018352	0.552641 ± 0.694874
N83	8.954296 ± 0.058222	39.159584 ± 5.277556	0.100684 ± 0.01742	0.322299 ± 0.659613
L87	6.014748 ± 0.052516	19.130623 ± 4.760364	0.04372 ± 0.015713	-0.445434 ± 0.594972
V93	7.568593 ± 0.075961	28.430278 ± 6.885553	0.069539 ± 0.022728	1.978979 ± 0.860588
W95	7.706903 ± 0.031471	27.868483 ± 2.85275	0.067205 ± 0.009417	0.950596 ± 0.35655

Table 14 Results of the analysis on the data from the original isotope exchange experiments performed on β_2-microglobulin. Data are reported as value ± standard deviation.

RESULTS
CONVENTIONAL ISOTOPE EXCHANGE EXPERIMENTS

Residue	Lowest Temperature			Reference Temperature			Highest Temperature		
	T (K)	$\Delta\bar{G}^0$ (kcal/mol)	$\sigma_{\Delta\bar{G}^0}$ (kcal/mol)	T (K)	$\Delta\bar{G}^0$ (kcal/mol)	$\sigma_{\Delta\bar{G}^0}$ (kcal/mol)	T (K)	$\Delta\bar{G}^0$ (kcal/mol)	$\sigma_{\Delta\bar{G}^0}$ (kcal/mol)
Y10	301	8.048889	0.039517	300	8.14885	0.051867	315	6.324324	0.042107
C25	301	9.741484	0.042992	300	9.850581	0.056428	315	8.145031	0.04581
Y26	301	9.254794	0.063658	300	9.375117	0.083553	315	7.434215	0.067831
S28	301	8.301962	0.037081	300	8.354108	0.04867	315	7.222815	0.039512
E36	301	7.576664	0.038327	300	7.623165	0.050305	315	6.174002	0.040839
D38	301	8.299216	0.073083	300	8.409392	0.095924	315	6.496267	0.077873
L39	301	5.362299	0.028216	300	5.382502	0.037035	315	5.164978	0.030066
L40	301	8.613312	0.056768	300	8.707767	0.07451	315	6.364243	0.060489
E44	301	7.595719	0.051446	300	7.6506	0.067525	315	6.354877	0.054819
Y66	301	9.245564	0.072854	300	9.345367	0.095624	315	7.179795	0.07763
Y67	301	7.729329	0.086253	300	7.73804	0.11321	315	6.80872	0.091907
T68	301	7.577538	0.034238	300	7.620292	0.044938	315	6.568863	0.036482
F70	301	7.712644	0.046448	300	7.749214	0.060965	315	6.285315	0.049493
R81	301	9.448511	0.046729	300	9.558049	0.061334	315	7.72491	0.049792
N83	301	8.853075	0.044358	300	8.954296	0.058222	315	7.325134	0.047266
L87	301	5.97177	0.040011	300	6.014748	0.052516	315	5.523276	0.042634
V93	301	7.49576	0.057873	300	7.568593	0.075961	315	5.795461	0.061667
W95	301	7.638115	0.023977	300	7.706903	0.031471	315	6.348147	0.025549

Table 15 $\Delta\bar{G}^0$ of the amide sites of β$_2$-microglobulin at various temperatures.

Residue	Lowest Temperature			Reference Temperature			Highest Temperature		
	T (K)	$\Delta\bar{H}^0$ (kcal/mol)	$\sigma_{\Delta\bar{H}^0}$ (kcal/mol)	T (K)	$\Delta\bar{H}^0$ (kcal/mol)	$\sigma_{\Delta\bar{H}^0}$ (kcal/mol)	T (K)	$\Delta\bar{H}^0$ (kcal/mol)	$\sigma_{\Delta\bar{H}^0}$ (kcal/mol)
Y10	301	38.610334	4.132386	300	37.665053	4.701538	315	51.844263	4.381694
C25	301	42.680492	4.495792	300	42.479631	5.114995	315	45.492548	4.767024
Y26	301	45.669873	6.656935	300	45.274252	7.573792	315	51.208567	7.05855
S28	301	24.505792	3.877709	300	23.490718	4.411784	315	38.716821	4.111652
E36	301	22.667232	4.007958	300	20.481734	4.559973	315	53.264208	4.249759
D38	301	41.841206	7.64254	300	41.083812	8.695144	315	52.444724	8.103617
L39	301	11.319016	2.950686	300	11.567684	3.357083	315	7.837653	3.128702
L40	301	38.393138	5.936452	300	35.698716	6.754077	315	76.115037	6.2946
E44	301	24.802444	5.379927	300	23.42857	6.120902	315	44.036672	5.7045
Y66	301	40.259398	7.618615	300	38.315631	8.667924	315	67.472145	8.078248
Y67	301	11.513764	9.019775	300	9.191627	10.262065	315	44.023681	9.563941
T68	301	21.043348	3.580348	300	19.850891	4.073468	315	37.737744	3.796352
F70	301	20.05266	4.857233	300	17.391252	5.526217	315	57.312366	5.150271
R81	301	42.696048	4.886639	300	42.143407	5.559673	315	50.433029	5.181451
N83	301	39.481883	4.638674	300	39.159584	5.277556	315	43.994073	4.918526
L87	301	18.685189	4.184091	300	19.130623	4.760364	315	12.449111	4.436519
V93	301	30.409257	6.052012	300	28.430278	6.885553	315	58.114961	6.417132
W95	301	28.819079	2.507406	300	27.868483	2.85275	315	42.127422	2.658678

Table 16 $\Delta\bar{H}^0$ of the amide sites of β$_2$-microglobulin at various temperatures.

CONVENTIONAL ISOTOPE EXCHANGE EXPERIMENTS

Residue	Lowest Temperature			Reference Temperature			Highest Temperature		
	T (K)	$\Delta\bar{S}^0$ (kcal/(mol × K))	$\sigma_{\Delta\bar{S}^0}$ (kcal/(mol × K))	T (K)	$\Delta\bar{S}^0$ (kcal/(mol × K))	$\sigma_{\Delta\bar{S}^0}$ (kcal/(mol × K))	T (K)	$\Delta\bar{S}^0$ (kcal/(mol × K))	$\sigma_{\Delta\bar{S}^0}$ (kcal/(mol × K))
Y10	301	0.101533	0.013623	300	0.098387	0.015519	315	0.144508	0.014023
C25	301	0.109432	0.014821	300	0.108763	0.016884	315	0.118564	0.015256
Y26	301	0.12098	0.021946	300	0.119664	0.025	315	0.138966	0.02259
S28	301	0.053833	0.012784	300	0.050455	0.014563	315	0.099981	0.013159
E36	301	0.050135	0.013213	300	0.042862	0.015052	315	0.149493	0.013601
D38	301	0.111435	0.025195	300	0.108915	0.028701	315	0.145868	0.025935
L39	301	0.01979	0.009727	300	0.020617	0.011081	315	0.008485	0.010013
L40	301	0.098936	0.019571	300	0.08997	0.022294	315	0.221431	0.020145
E44	301	0.057165	0.017736	300	0.052593	0.020204	315	0.119625	0.018257
Y66	301	0.103036	0.025116	300	0.096568	0.028612	315	0.191404	0.025853
Y67	301	0.012573	0.029735	300	0.004845	0.033874	315	0.118143	0.030608
T68	301	0.044737	0.011803	300	0.040769	0.013446	315	0.098949	0.01215
F70	301	0.040997	0.016013	300	0.03214	0.018241	315	0.161991	0.016483
R81	301	0.110457	0.01611	300	0.108618	0.018352	315	0.135581	0.016583
N83	301	0.101757	0.015292	300	0.100684	0.01742	315	0.116409	0.015741
L87	301	0.042237	0.013794	300	0.04372	0.015713	315	0.021987	0.014199
V93	301	0.076125	0.019951	300	0.069539	0.022728	315	0.166094	0.020537
W95	301	0.070369	0.008266	300	0.067205	0.009417	315	0.113585	0.008509

Table 17 $\Delta\bar{S}^0$ of the amide sites of β$_2$-microglobulin at various temperatures.

Residue	Lowest Temperature			Reference Temperature			Highest Temperature		
	T (K)	$\Delta\bar{C}_p^0$ (kcal/(mol × K))	$\sigma_{\Delta\bar{C}_p^0}$ (kcal/(mol × K))	T (K)	$\Delta\bar{C}_p^0$ (kcal/(mol × K))	$\sigma_{\Delta\bar{C}_p^0}$ (kcal/(mol × K))	T (K)	$\Delta\bar{C}_p^0$ (kcal/(mol × K))	$\sigma_{\Delta\bar{C}_p^0}$ (kcal/(mol × K))
Y10	301	0.945281	0.58762	300	0.945281	0.58762	315	0.945281	0.58762
C25	301	0.200861	0.639296	300	0.200861	0.639296	315	0.200861	0.639296
Y26	301	0.395621	0.946608	300	0.395621	0.946608	315	0.395621	0.946608
S28	301	1.015073	0.551405	300	1.015073	0.551405	315	1.015073	0.551405
E36	301	2.185498	0.569927	300	2.185498	0.569927	315	2.185498	0.569927
D38	301	0.757394	1.086759	300	0.757394	1.086759	315	0.757394	1.086759
L39	301	-0.248669	0.419584	300	-0.248669	0.419584	315	-0.248669	0.419584
L40	301	2.694421	0.844156	300	2.694421	0.844156	315	2.694421	0.844156
E44	301	1.373873	0.765019	300	1.373873	0.765019	315	1.373873	0.765019
Y66	301	1.943768	1.083357	300	1.943768	1.083357	315	1.943768	1.083357
Y67	301	2.322137	1.2826	300	2.322137	1.2826	315	2.322137	1.2826
T68	301	1.192457	0.509121	300	1.192457	0.509121	315	1.192457	0.509121
F70	301	2.661408	0.690692	300	2.661408	0.690692	315	2.661408	0.690692
R81	301	0.552641	0.694874	300	0.552641	0.694874	315	0.552641	0.694874
N83	301	0.322299	0.659613	300	0.322299	0.659613	315	0.322299	0.659613
L87	301	-0.445434	0.594972	300	-0.445434	0.594972	315	-0.445434	0.594972
V93	301	1.978979	0.860588	300	1.978979	0.860588	315	1.978979	0.860588
W95	301	0.950596	0.35655	300	0.950596	0.35655	315	0.950596	0.35655

Table 18 $\Delta\bar{C}_p^0$ of the amide sites of β$_2$-microglobulin at various temperatures.

Figure 16 $\Delta\overline{G}^0$ of the amide sites of β$_2$-microglobulin based on the results of the analysis on the conventional exchange experiments. Half of the error bar corresponds to a standard deviation.
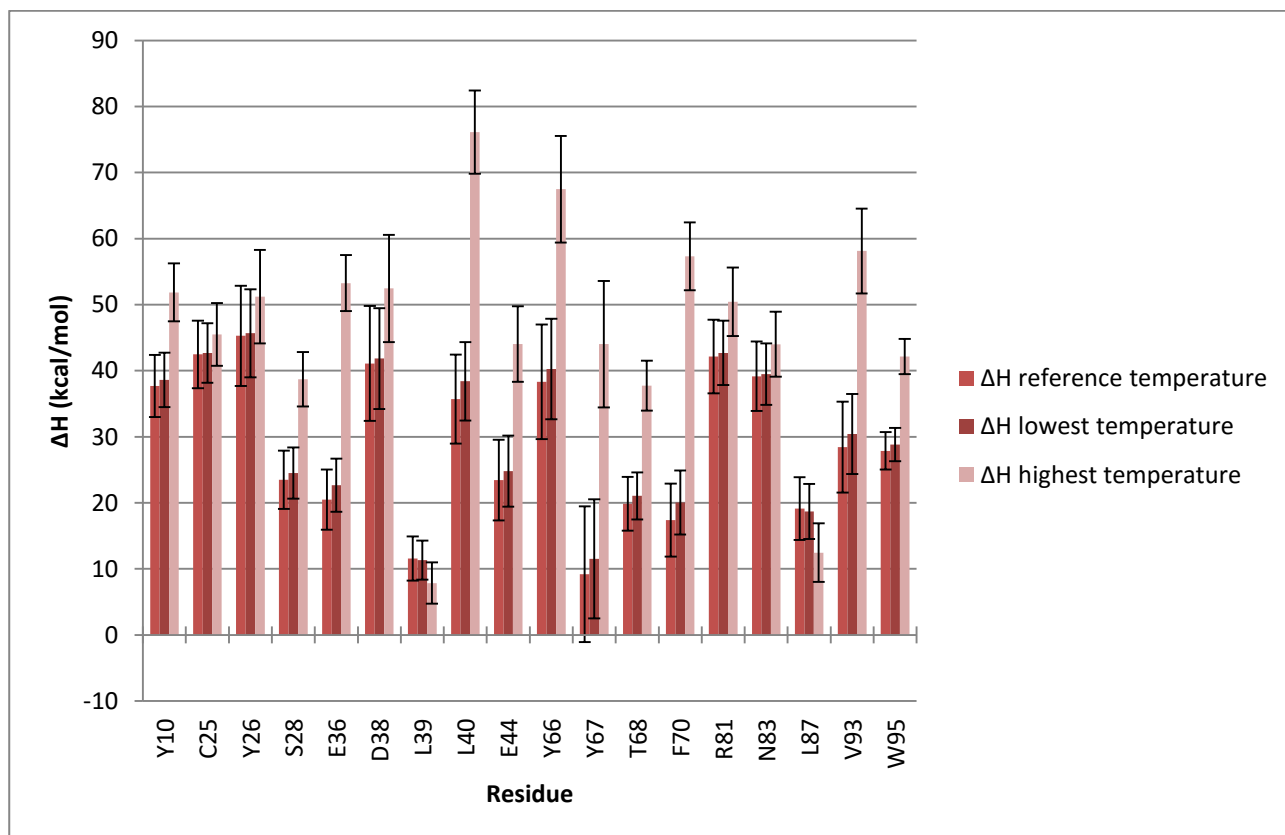
Figure 17 $\Delta\overline{H}^0$ of the amide sites of β$_2$-microglobulin based on the results of the analysis on the conventional exchange experiments. Half of the error bar corresponds to a standard deviation.

CONVENTIONAL ISOTOPE EXCHANGE EXPERIMENTS

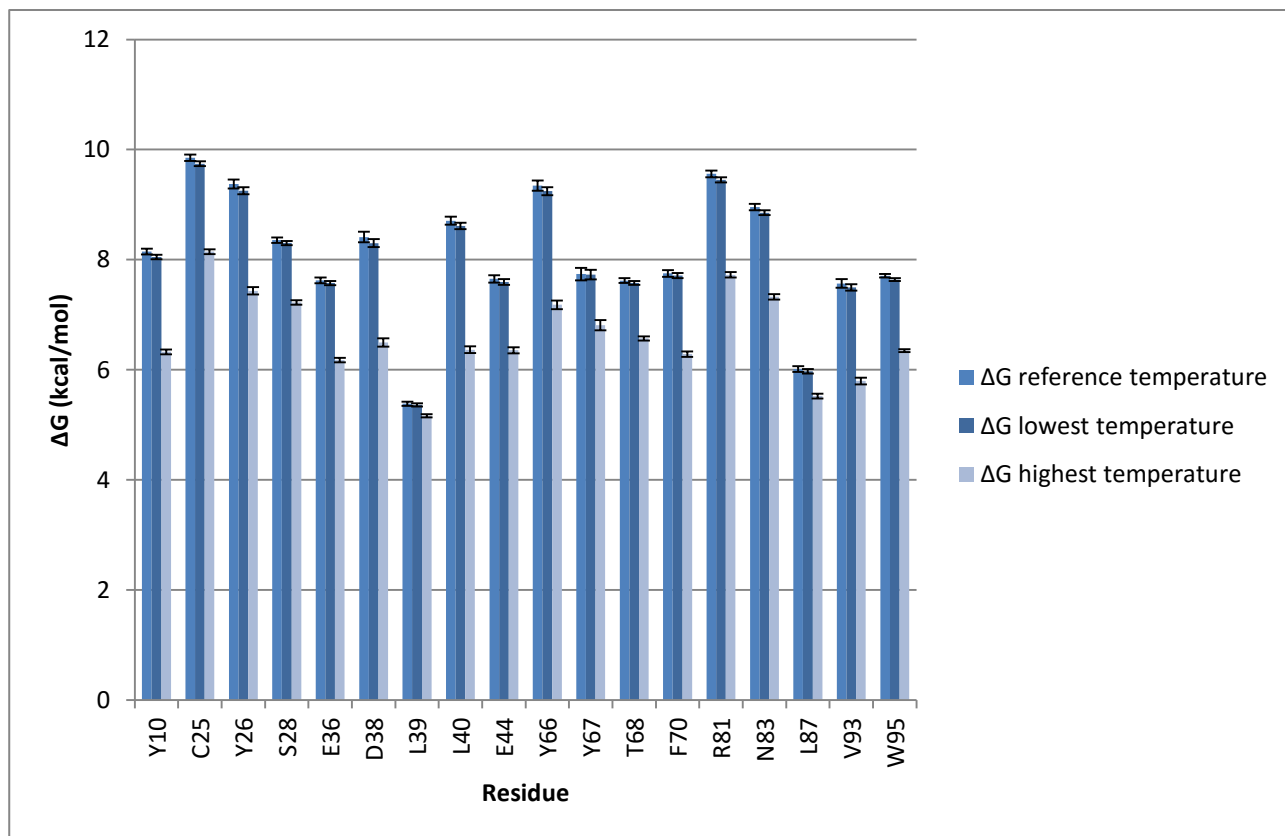**Figure 18** $\Delta \overline{S}^0$ of the amide sites of β$_2$-microglobulin based on the results of the analysis on the conventional exchange experiments. Half of the error bar corresponds to a standard deviation.

Figure 19 $\Delta \overline{C}_p^0$ of the amide sites of β$_2$-microglobulin based on the results of the analysis on the conventional exchange experiments. Half of the error bar corresponds to a standard deviation.
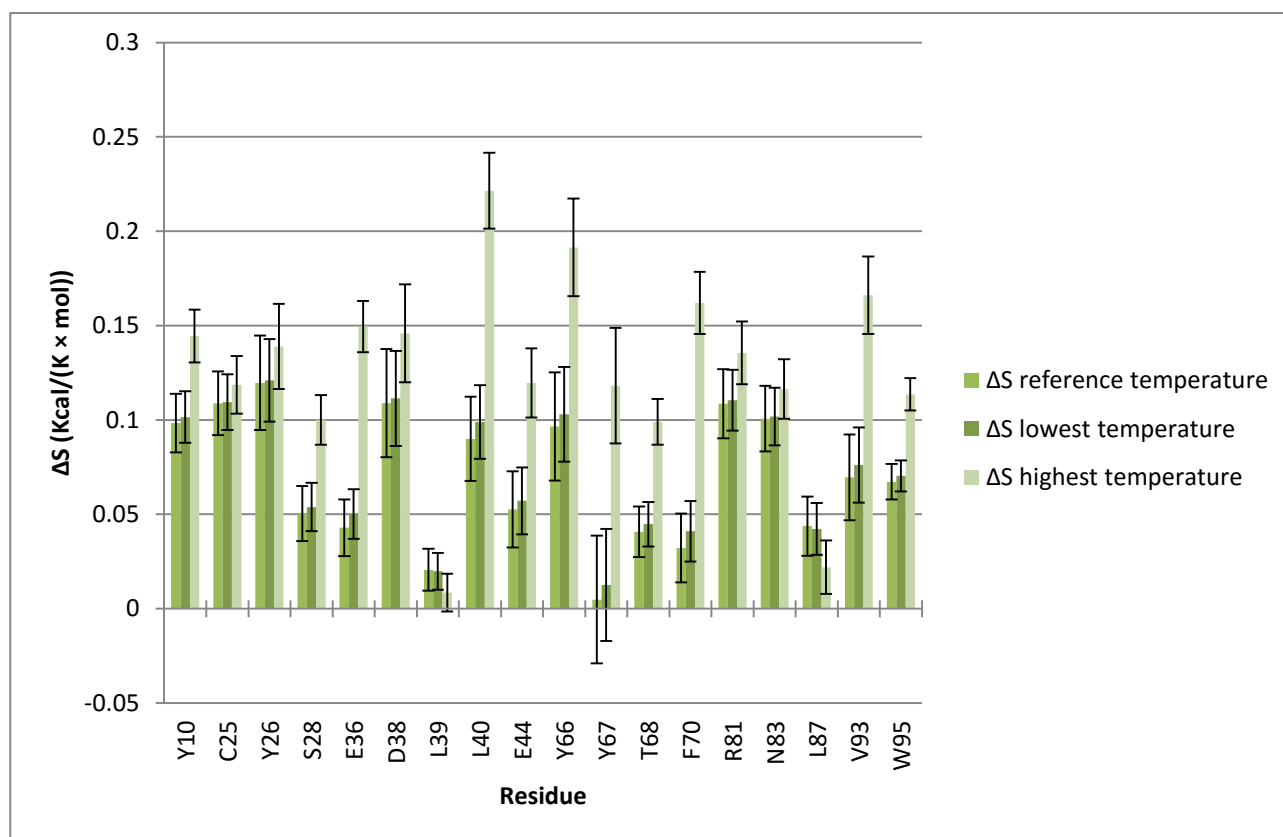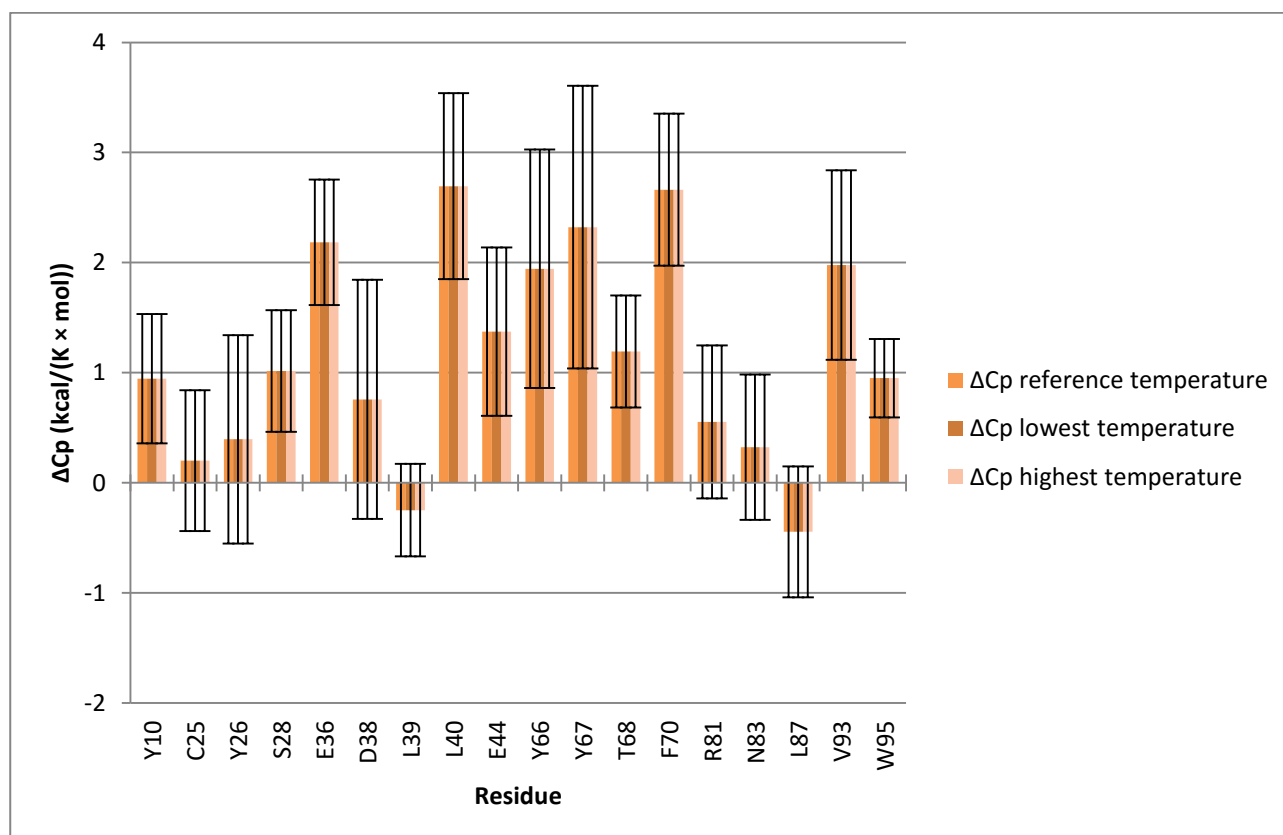
COMPARISON WITH THE RESULTS FROM THE BLUU-TRAMP EXPERIMENT

A comparison with the results obtained with the data from the BLUU-Tramp experiment at the reference temperature of 300 K reveals results in general agreement, while in the case of the $\Delta \bar{C}_p^0$ the conventional exchange experiments yields values with high variability and a considerable standard deviation, as opposed to the consistency obtained in the case of the BLUU-Tramp experiment.

Figure 20 Comparison on the $\Delta \bar{G}^0$ at 300 K of the amide sites of β$_2$-microglobulin obtained from the analysis of data from both the conventional isotope exchange experiments (in light blue) and the BLUU-Tramp experiment (in blue). Half of the error bar corresponds to a standard deviation.

CONVENTIONAL ISOTOPE EXCHANGE EXPERIMENTS
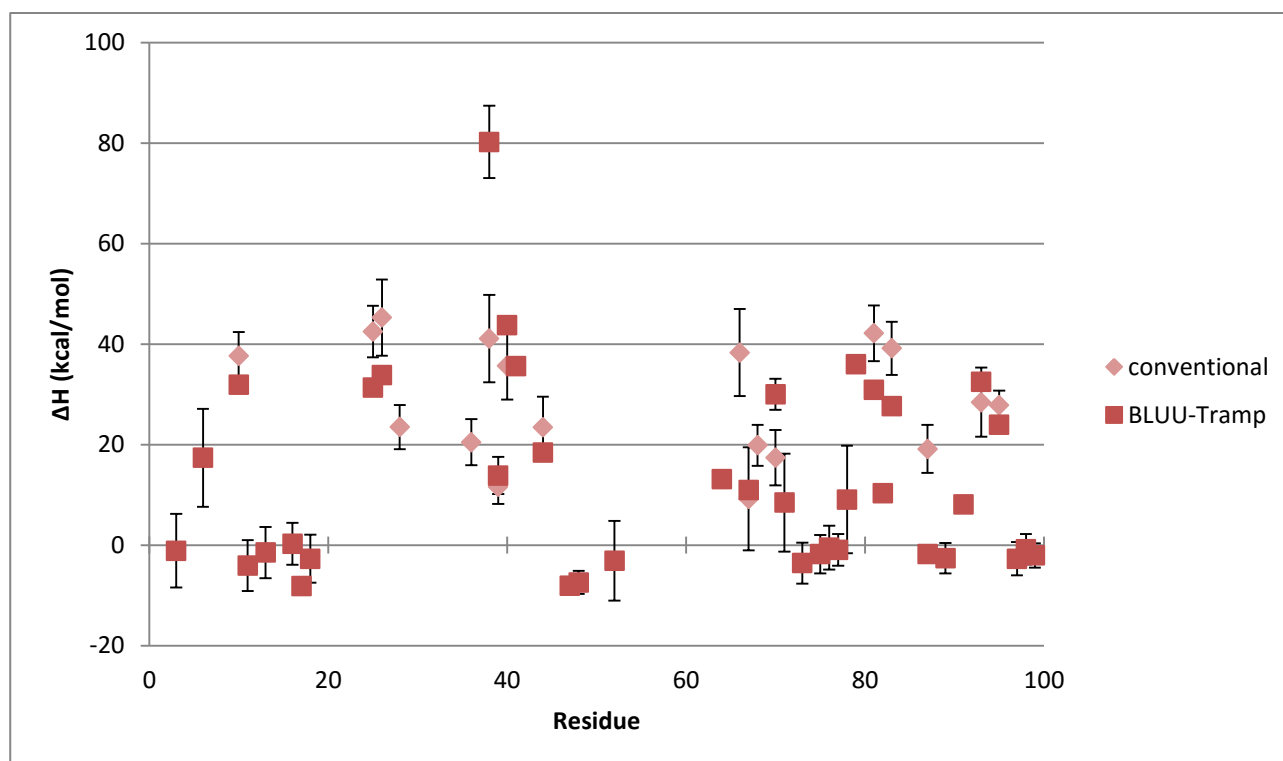
Figure 21 Comparison on the $\Delta\bar{H}^0$ at 300 K of the amide sites of β$_2$-microglobulin obtained from the analysis of data from both the conventional isotope exchange experiments (in light red) and the BLUU-Tramp experiment (in red). Half of the error bar corresponds to a standard deviation.
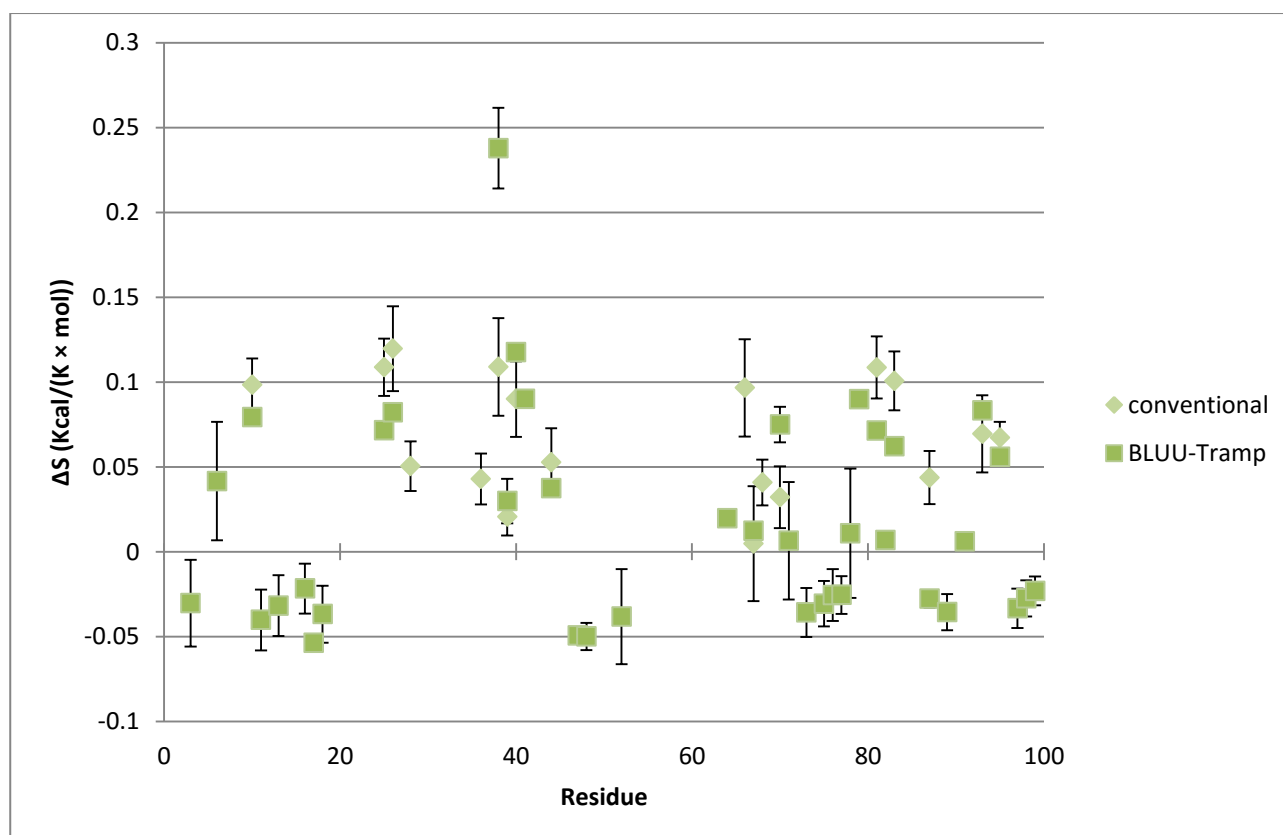
Figure 22 Comparison on the $\Delta\bar{S}^0$ at 300 K of the amide sites of β$_2$-microglobulin obtained from the analysis of data from both the conventional isotope exchange experiments (in light green) and the BLUU-Tramp experiment (in green). Half of the error bar corresponds to a standard deviation.
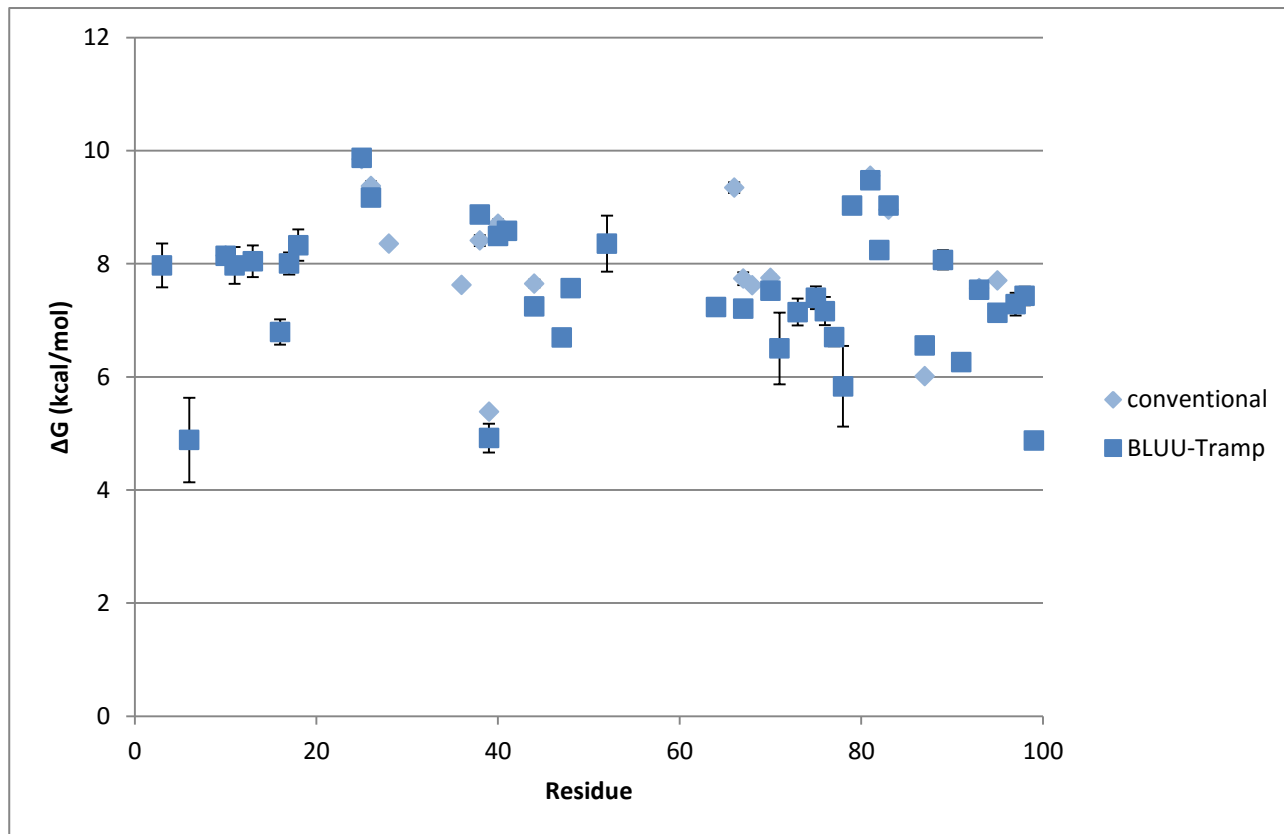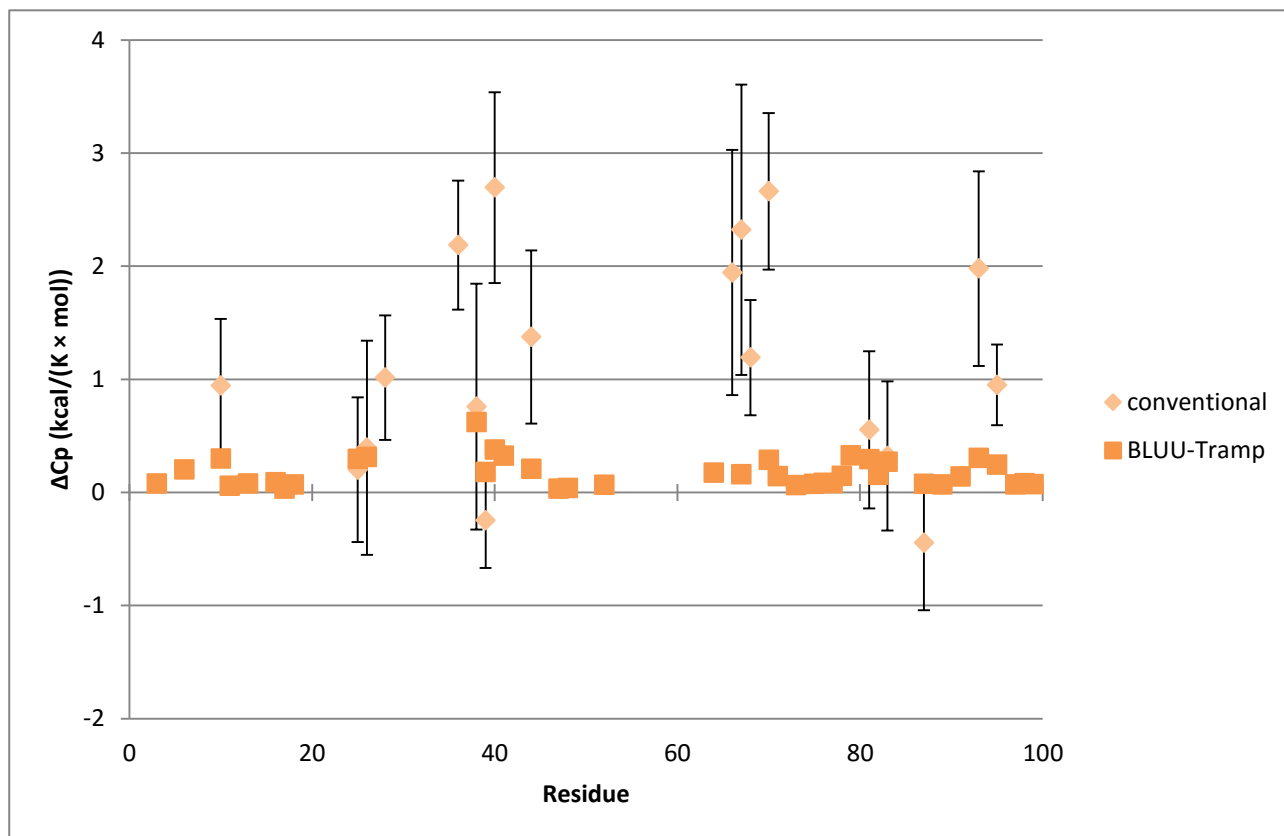
Figure 23 Comparison on the $\Delta \bar{C}_p^0$ at 300 K of the amide sites of β$_2$-microglobulin obtained from the analysis of data from both the conventional isotope exchange experiments (in light orange) and the BLUU-Tramp experiment (in orange). Half of the error bar corresponds to a standard deviation.

In order to check the reliability and the extent of the $\Delta \bar{C}_p^0$ assessment dispersion , an attempt was made to extend the data range by performing an additional hydrogen exchange experiment at lower temperature (293 K) and adding the obtained exchange constants to the published data.

CONVENTIONAL ISOTOPE EXCHANGE EXPERIMENTS WITH ADDED EXCHANGE CONSTANTS

The additional exchange experiment performed at 293 K allowed to obtain a new exchange constant for 14 residues. The analysis was performed again on the original data for these 14 residues with the addition of the newly measured exchange constants, and its results are shown in the following tables and graphs.

Residue	$\Delta \bar{G}^0$ (kcal/mol)	$\Delta \bar{H}^0$ (kcal/mol)	$\Delta \bar{S}^0$ (kcal/(mol × K))	$\Delta \bar{C}_p^0$ (kcal/(mol × K))
Y10	8.057846 ± 0.027566	28.686262 ± 1.411438	0.068761 ± 0.004684	2.027322 ± 0.24712
C25	9.727909 ± 0.03252	30.376345 ± 1.66508	0.068828 ± 0.005526	1.659438 ± 0.291529
Y26	9.231186 ± 0.044143	31.07354 ± 2.260193	0.072808 ± 0.007501	2.106961 ± 0.395724
S28	8.298493 ± 0.023293	18.003607 ± 1.192615	0.03235 ± 0.003958	1.67633 ± 0.208808
E36	7.578674 ± 0.023231	16.092085 ± 1.189455	0.028378 ± 0.003948	2.714499 ± 0.208255
L40	8.62174 ± 0.035723	27.210941 ± 1.829076	0.061964 ± 0.00607	3.71729 ± 0.320242
E44	7.57558 ± 0.032164	16.026873 ± 1.646839	0.028171 ± 0.005466	2.265858 ± 0.288335
Y67	7.747509 ± 0.049333	10.125835 ± 2.525927	0.007928 ± 0.008383	2.209555 ± 0.44225
F70	7.725689 ± 0.026864	15.070134 ± 1.375471	0.024481 ± 0.004565	2.941128 ± 0.240823
R81	9.447157 ± 0.032927	31.202418 ± 1.685924	0.072518 ± 0.005595	1.871149 ± 0.295178
N83	8.837708 ± 0.032445	27.656592 ± 1.661235	0.06273 ± 0.005513	1.708534 ± 0.290856
L87	5.917322 ± 0.028447	9.518137 ± 1.456529	0.012003 ± 0.004834	0.712975 ± 0.255015
V93	7.578081 ± 0.033124	29.366403 ± 1.695982	0.072628 ± 0.005629	1.866166 ± 0.29694
W95	7.609161 ± 0.021813	18.224973 ± 1.116879	0.035386 ± 0.003707	2.112743 ± 0.195548

Table 19 Results of the analysis on the original data with the addition of the exchange constants at 293 K of the β₂-microglobulin conventional isotope exchange experiment. Data are reported as value ± standard deviation.

Residue	Lowest Temperature			Reference Temperature			Highest Temperature		
	T (K)	$\Delta \bar{G}^0$ (kcal/mol)	$\sigma_{\Delta \bar{G}^0}$ (kcal/mol)	T (K)	$\Delta \bar{G}^0$ (kcal/mol)	$\sigma_{\Delta \bar{G}^0}$ (kcal/mol)	T (K)	$\Delta \bar{G}^0$ (kcal/mol)	$\sigma_{\Delta \bar{G}^0}$ (kcal/mol)
Y10	293	8.372308	0.057852	300	8.057846	0.027566	315	6.278543	0.040473
C25	293	10.073119	0.068248	300	9.727909	0.03252	315	8.083318	0.047746
Y26	293	9.567418	0.09264	300	9.231186	0.044143	315	7.361807	0.06481
S28	293	8.386968	0.048883	300	8.298493	0.023293	315	7.194837	0.034198
E36	293	7.553891	0.048753	300	7.578674	0.023231	315	6.15162	0.034107
L40	293	8.74952	0.07497	300	8.62174	0.035723	315	6.320965	0.052448
E44	293	7.586276	0.0675	300	7.57558	0.032164	315	6.317136	0.047223
Y67	293	7.621136	0.103532	300	7.747509	0.049333	315	6.813484	0.07243
F70	293	7.654977	0.056377	300	7.725689	0.026864	315	6.27348	0.039441
R81	293	9.800767	0.069102	300	9.447157	0.032927	315	7.669124	0.048343
N83	293	9.136187	0.06809	300	8.837708	0.032445	315	7.266482	0.047635
L87	293	5.942656	0.0597	300	5.917322	0.028447	315	5.474263	0.041766
V93	293	7.932873	0.069514	300	7.578081	0.033124	315	5.800234	0.048632
W95	293	7.682965	0.045778	300	7.609161	0.021813	315	6.298976	0.032026

Table 20 $\Delta \bar{G}^0$ of the amide sites of β₂-microglobulin at various temperatures.

RESULTS
CONVENTIONAL ISOTOPE EXCHANGE EXPERIMENTS WITH ADDED EXCHANGE CONSTANTS

Residue	Lowest Temperature			Reference Temperature			Highest Temperature		
	T (K)	$\Delta\bar{H}^0$ (kcal/mol)	$\sigma_{\Delta\bar{H}^0}$ (kcal/mol)	T (K)	$\Delta\bar{H}^0$ (kcal/mol)	$\sigma_{\Delta\bar{H}^0}$ (kcal/mol)	T (K)	$\Delta\bar{H}^0$ (kcal/mol)	$\sigma_{\Delta\bar{H}^0}$ (kcal/mol)
Y10	293	14.495005	2.960922	300	28.686262	1.411438	315	59.096098	2.761719
C25	293	18.760276	3.493015	300	30.376345	1.66508	315	55.26792	3.258014
Y26	293	16.324815	4.741446	300	31.07354	2.260193	315	62.677952	4.422454
S28	293	6.269298	2.501876	300	18.003607	1.192615	315	43.148556	2.333556
E36	293	-2.909405	2.495246	300	16.092085	1.189455	315	56.809563	2.327372
L40	293	1.189909	3.837047	300	27.210941	1.829076	315	82.970296	3.5789
E44	293	0.165865	3.454749	300	16.026873	1.646839	315	50.014746	3.222322
Y67	293	-5.341047	5.298905	300	10.125835	2.525927	315	43.269155	4.942408
F70	293	-5.51776	2.88547	300	15.070134	1.375471	315	59.187048	2.691343
R81	293	18.104374	3.536741	300	31.202418	1.685924	315	59.269657	3.298798
N83	293	15.696851	3.484949	300	27.656592	1.661235	315	53.284609	3.25049
L87	293	4.527315	3.055514	300	9.518137	1.456529	315	20.212757	2.849947
V93	293	16.303243	3.557842	300	29.366403	1.695982	315	57.358887	3.318479
W95	293	3.435768	2.342995	300	18.224973	1.116879	315	49.916125	2.185364

Table 21 $\Delta\bar{H}^0$ of the amide sites of β₂-microglobulin at various temperatures.

Residue	Lowest Temperature			Reference Temperature			Highest Temperature		
	T (K)	$\Delta\bar{S}^0$ (kcal/(mol × K))	$\sigma_{\Delta\bar{S}^0}$ (kcal/(mol × K))	T (K)	$\Delta\bar{S}^0$ (kcal/(mol × K))	$\sigma_{\Delta\bar{S}^0}$ (kcal/(mol × K))	T (K)	$\Delta\bar{S}^0$ (kcal/(mol × K))	$\sigma_{\Delta\bar{S}^0}$ (kcal/(mol × K))
Y10	293	0.020897	0.009941	300	0.068761	0.004684	315	0.167675	0.008875
C25	293	0.029649	0.011728	300	0.068828	0.005526	315	0.149792	0.01047
Y26	293	0.023063	0.015919	300	0.072808	0.007501	315	0.175607	0.014213
S28	293	-0.007228	0.0084	300	0.03235	0.003958	315	0.114139	0.007499
E36	293	-0.035711	0.008378	300	0.028378	0.003948	315	0.160819	0.00748
L40	293	-0.025801	0.012883	300	0.061964	0.00607	315	0.243331	0.011502
E44	293	-0.025326	0.011599	300	0.028171	0.005466	315	0.138723	0.010356
Y67	293	-0.04424	0.017791	300	0.007928	0.008383	315	0.115732	0.015883
F70	293	-0.044958	0.009688	300	0.024481	0.004565	315	0.16798	0.008649
R81	293	0.02834	0.011875	300	0.072518	0.005595	315	0.163811	0.010601
N83	293	0.022391	0.011701	300	0.06273	0.005513	315	0.146089	0.010446
L87	293	-0.004831	0.010259	300	0.012003	0.004834	315	0.046789	0.009159
V93	293	0.028568	0.011945	300	0.072628	0.005629	315	0.163678	0.010665
W95	293	-0.014496	0.007867	300	0.035386	0.003707	315	0.138467	0.007023

Table 22 $\Delta\bar{S}^0$ of the amide sites of β₂-microglobulin at various temperatures.

CONVENTIONAL ISOTOPE EXCHANGE EXPERIMENTS WITH ADDED EXCHANGE CONSTANTS

Residue	Lowest Temperature			Reference Temperature			Highest Temperature		
	T (K)	$\Delta \bar{C}_p^0$ (kcal/(mol × K))	$\sigma_{\Delta \bar{C}_p^0}$ (kcal/(mol × K))	T (K)	$\Delta \bar{C}_p^0$ (kcal/(mol × K))	$\sigma_{\Delta \bar{C}_p^0}$ (kcal/(mol × K))	T (K)	$\Delta \bar{C}_p^0$ (kcal/(mol × K))	$\sigma_{\Delta \bar{C}_p^0}$ (kcal/(mol × K))
Y10	293	2.027322	0.24712	300	2.027322	0.24712	315	2.027322	0.24712
C25	293	1.659438	0.291529	300	1.659438	0.291529	315	1.659438	0.291529
Y26	293	2.106961	0.395724	300	2.106961	0.395724	315	2.106961	0.395724
S28	293	1.67633	0.208808	300	1.67633	0.208808	315	1.67633	0.208808
E36	293	2.714499	0.208255	300	2.714499	0.208255	315	2.714499	0.208255
L40	293	3.71729	0.320242	300	3.71729	0.320242	315	3.71729	0.320242
E44	293	2.265858	0.288335	300	2.265858	0.288335	315	2.265858	0.288335
Y67	293	2.209555	0.44225	300	2.209555	0.44225	315	2.209555	0.44225
F70	293	2.941128	0.240823	300	2.941128	0.240823	315	2.941128	0.240823
R81	293	1.871149	0.295178	300	1.871149	0.295178	315	1.871149	0.295178
N83	293	1.708534	0.290856	300	1.708534	0.290856	315	1.708534	0.290856
L87	293	0.712975	0.255015	300	0.712975	0.255015	315	0.712975	0.255015
V93	293	1.866166	0.29694	300	1.866166	0.29694	315	1.866166	0.29694
W95	293	2.112743	0.195548	300	2.112743	0.195548	315	2.112743	0.195548

Table 23 $\Delta \bar{C}_p^0$ of the amide sites of β₂-microglobulin at various temperatures.
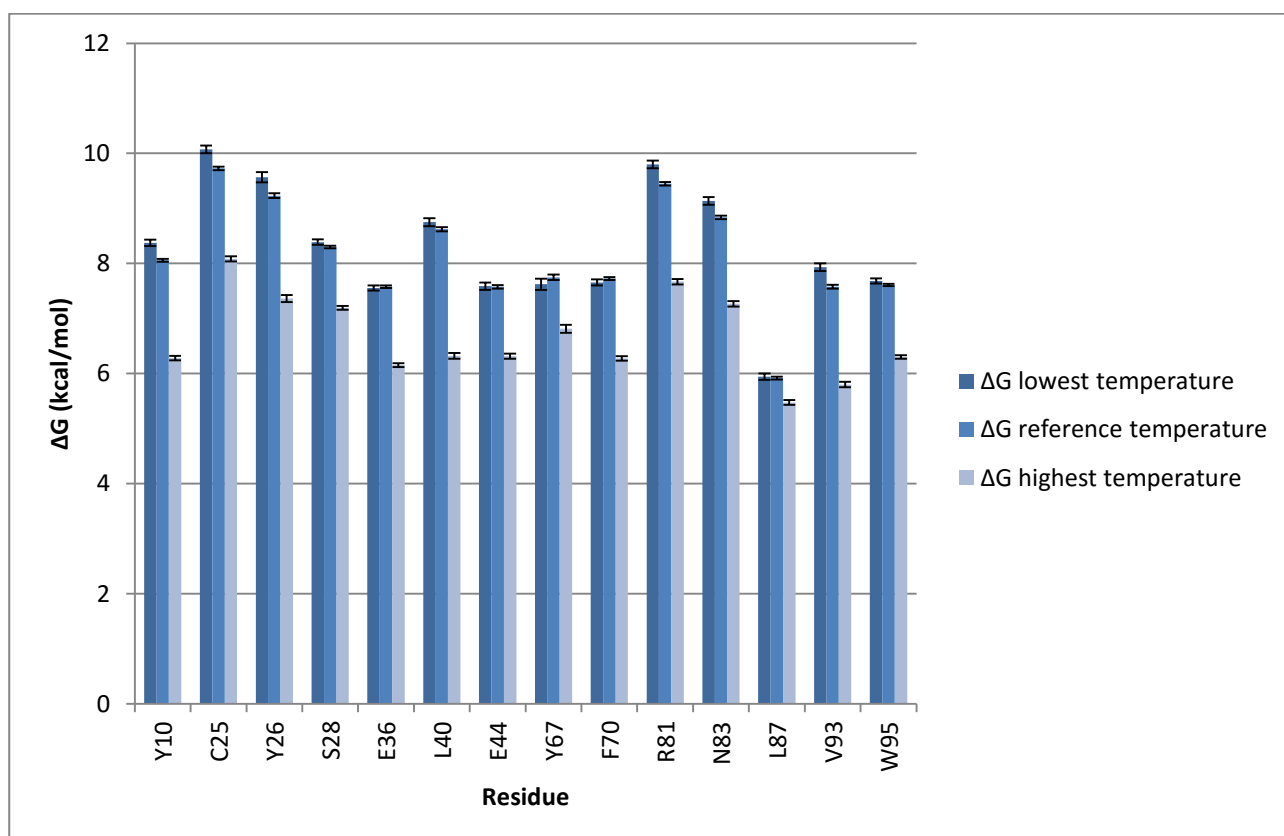
Figure 24 $\Delta \bar{G}^0$ of the amide sites of β₂-microglobulin based on the results of the analysis on the conventional exchange experiments with the addition of an exchange constant per each residue. Half of the error bar corresponds to a standard deviation.

CONVENTIONAL ISOTOPE EXCHANGE EXPERIMENTS WITH ADDED EXCHANGE CONSTANTS
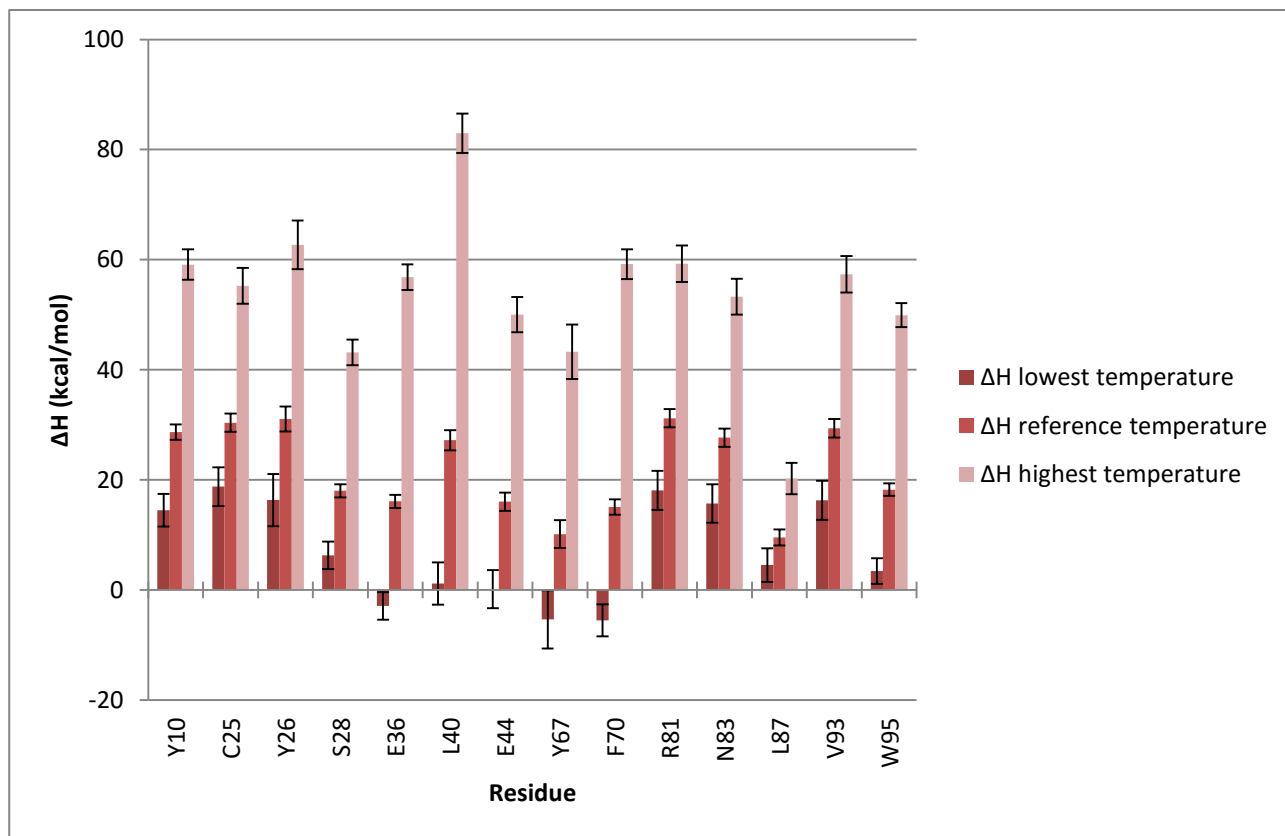
Figure 25 $\Delta\bar{H}^0$ of the amide sites of β$_2$-microglobulin based on the results of the analysis on the conventional exchange experiments with the addition of an exchange constant per each residue. Half of the error bar corresponds to a standard deviation.
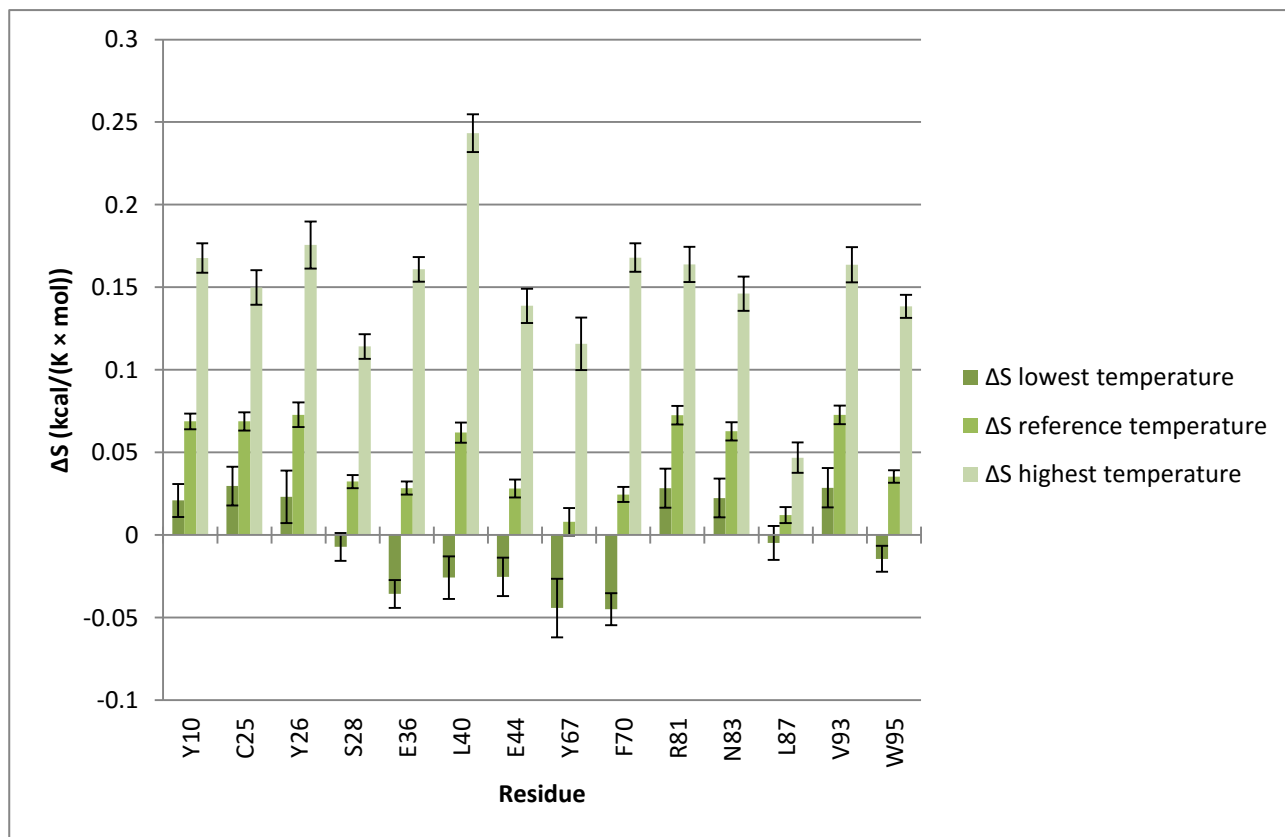
Figure 26 $\Delta\bar{S}^0$ of the amide sites of β$_2$-microglobulin based on the results of the analysis on the conventional exchange experiments with the addition of an exchange constant per each residue. Half of the error bar corresponds to a standard deviation.

CONVENTIONAL ISOTOPE EXCHANGE EXPERIMENTS WITH ADDED EXCHANGE CONSTANTS
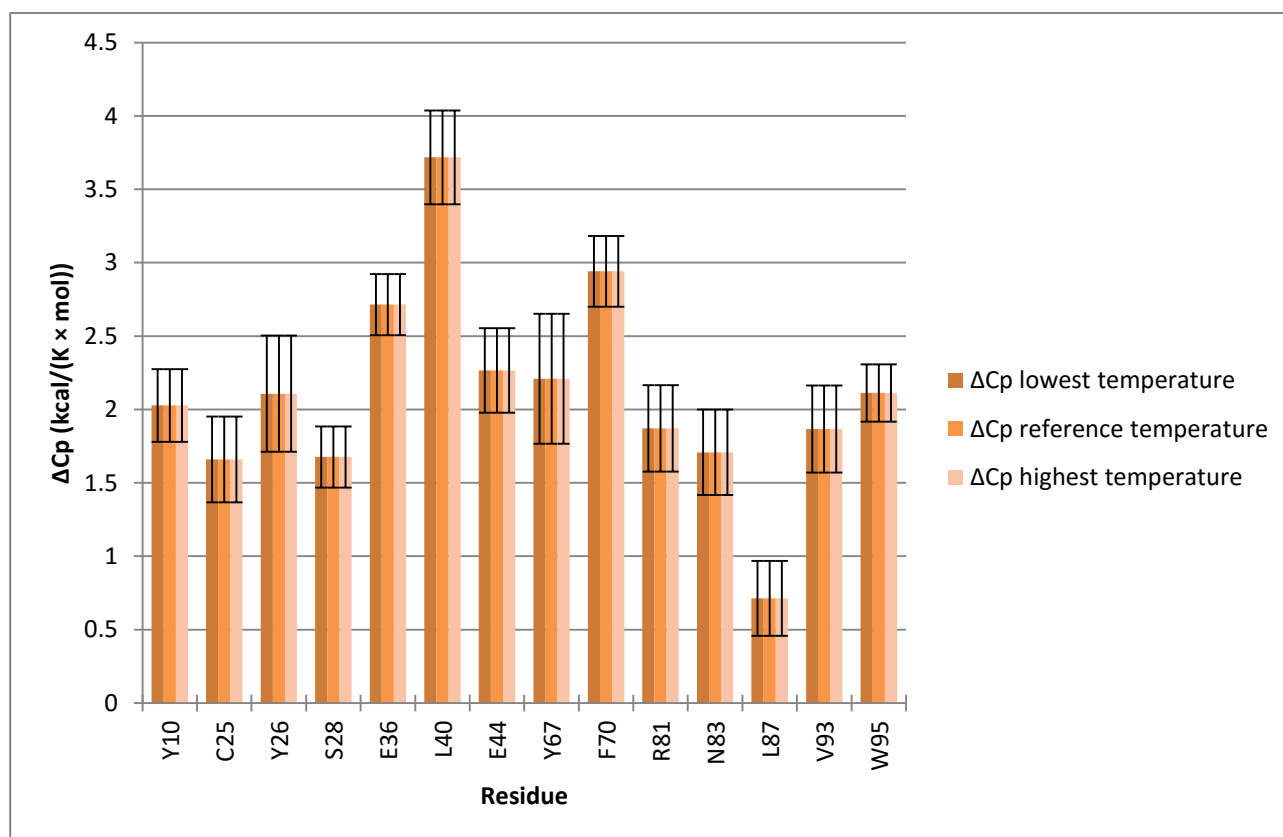
Figure 27 $\Delta \bar{C}_p^0$ **of the amide sites of β$_2$-microglobulin based on the results of the analysis on the conventional exchange experiments with the addition of an exchange constant per each residue. Half of the error bar corresponds to a standard deviation.**

A comparison with the results from the analysis of the BLUU-Tramp experiment at the reference temperature of 300 K shows, apparently, a better consistency of the $\Delta \bar{C}_p^0$ values in the case of the conventional exchange experiments, however the values are significantly different from those obtained from the analysis of the BLUU-Tramp data.
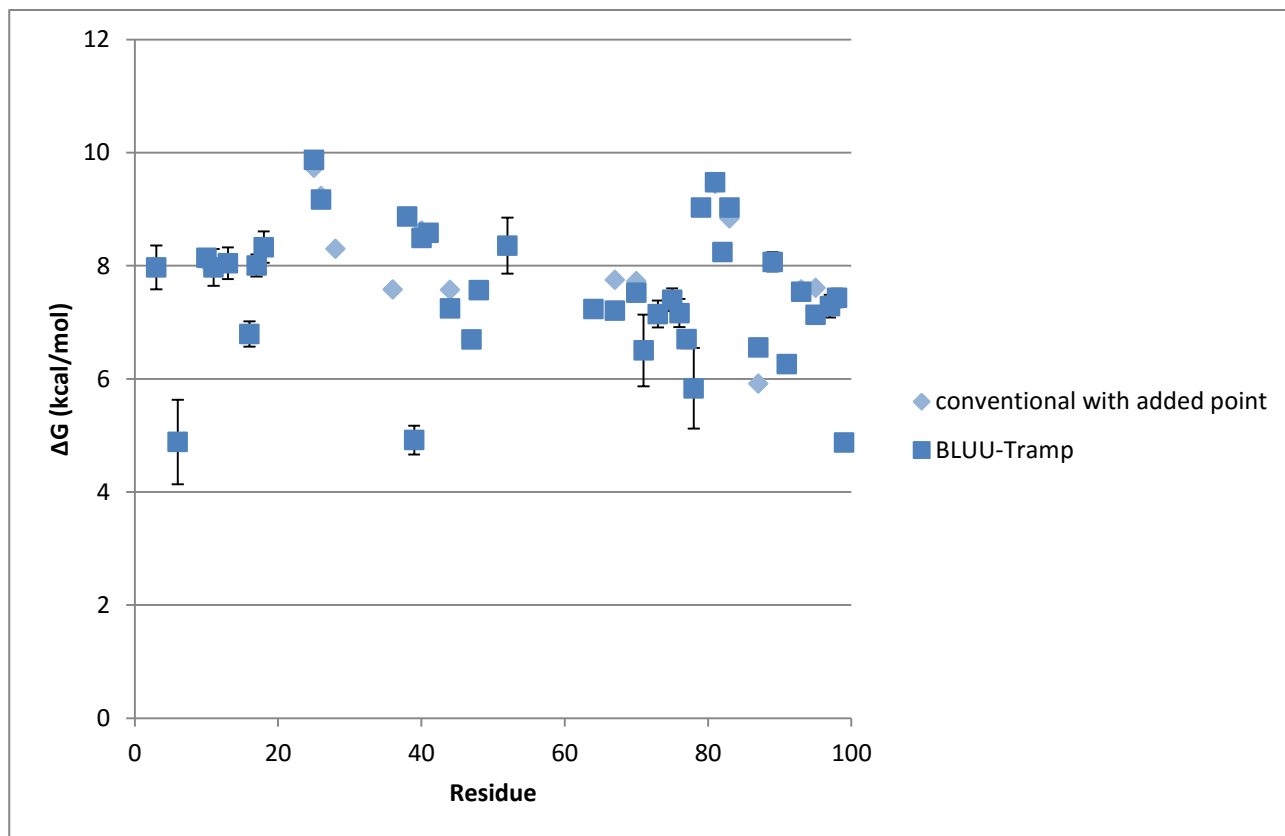
Figure 28 comparison on the $\Delta \bar{G}^0$ at 300 K of the amide sites of β$_2$-microglobulin obtained from the analysis of data from both the conventional isotope exchange experiments with the addition of an exchange constant per each residue (in light blue) and the BLUU-Tramp experiment (in blue). Half of the error bar corresponds to a standard deviation.
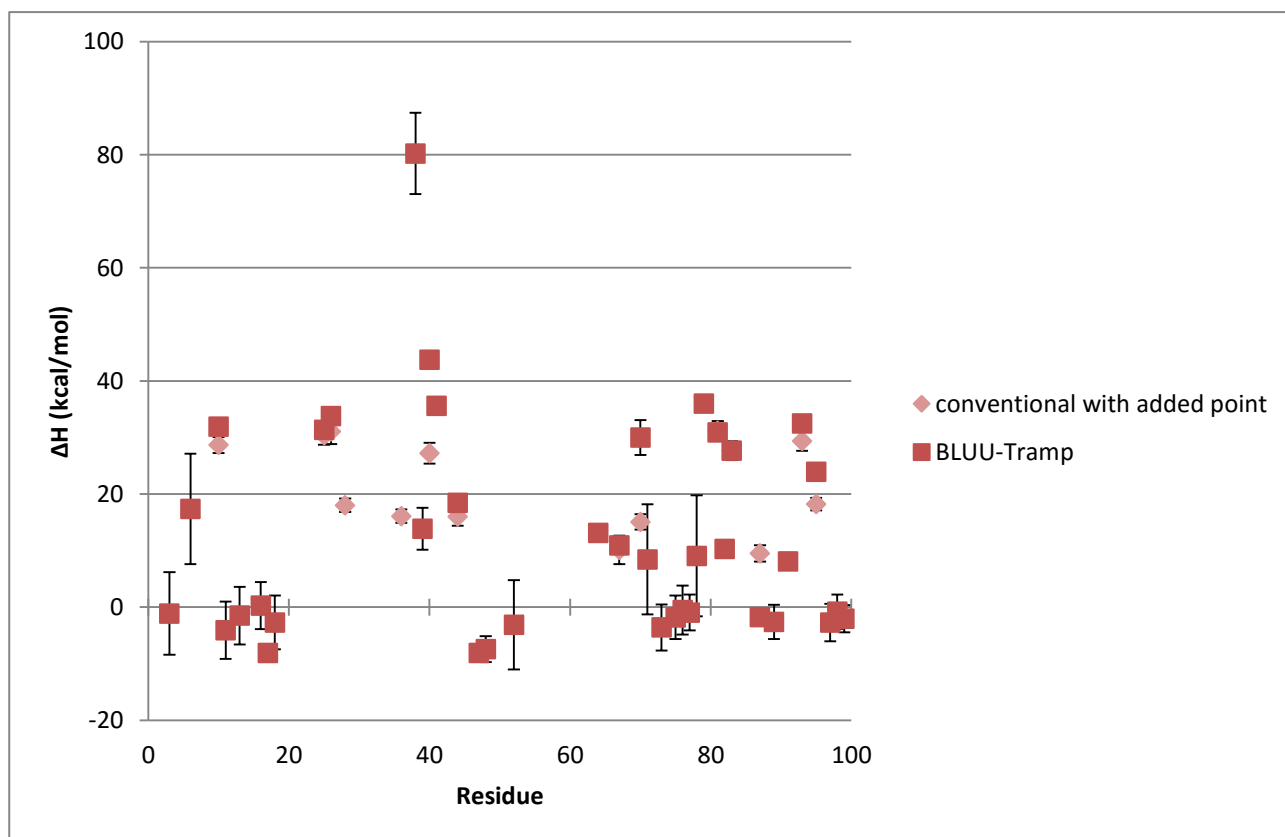
Figure 29 comparison on the $\Delta \bar{H}^0$ at 300 K of the amide sites of β$_2$-microglobulin obtained from the analysis of data from both the conventional isotope exchange experiments with the addition of an exchange constant per each residue (in light red) and the BLUU-Tramp experiment (in red). Half of the error bar corresponds to a standard deviation.

CONVENTIONAL ISOTOPE EXCHANGE EXPERIMENTS WITH ADDED EXCHANGE CONSTANTS
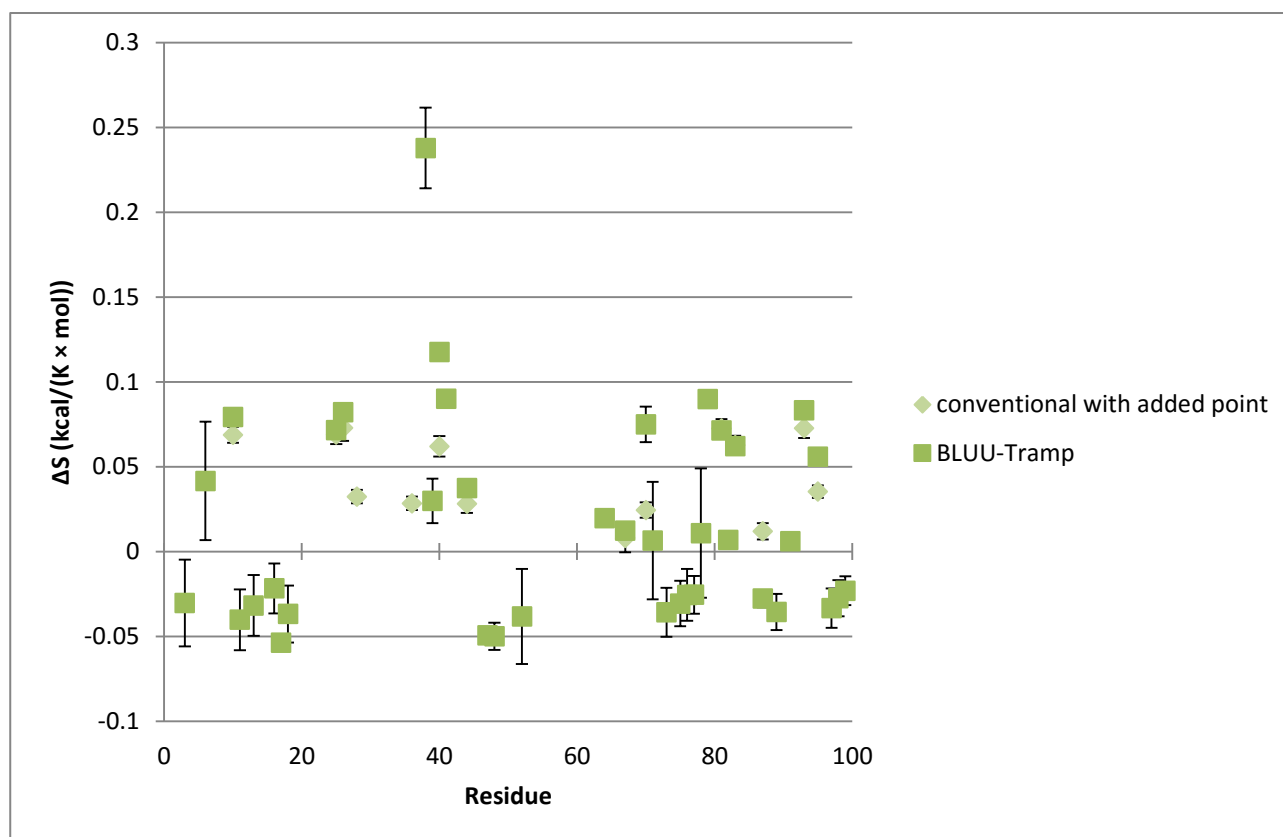
**Figure 30 Comparison on the $\Delta\overline{S}^0$ at 300 K of the amide sites of β$_2$-microglobulin obtained from the analysis of data from both the conventional isotope exchange experiments with the addition of an exchange constant per each residue (in light green) and the BLUU-Tramp experiment (in green). Half of the error bar corresponds to a standard deviation.**
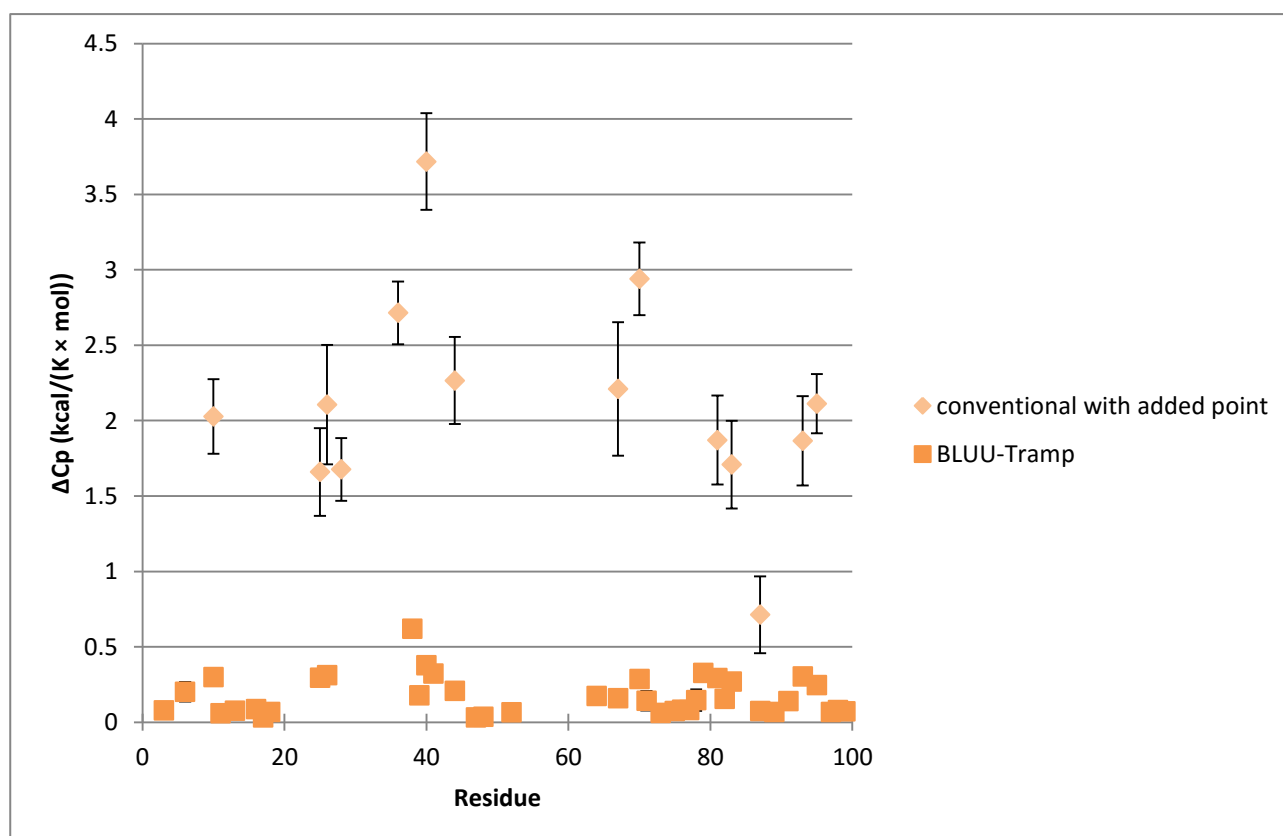
Figure 31 Comparison on the $\Delta\overline{C}_p^0$ at 300 K of the amide sites of β$_2$-microglobulin obtained from the analysis of data from both the conventional isotope exchange experiments with the addition of an exchange constant per each residue (in light orange) and the BLUU-Tramp experiment (in orange). Half of the error bar corresponds to a standard deviation.

DISCUSSION

It is important to note that also in this section the values reported in the tables retain the figures obtained from fitting and calculations, with the actual number of significant figures being three at most, except for temperature values known to an accuracy of four significant figures.

MAPPING OF THE RESULTS TO THE STRUCTURE OF THE PROTEINS

β₂-MICROGLOBULIN

The following images show how the results of the analysis at the reference temperature of 300 K map to the structure of the protein:

MAPPING OF THE RESULTS TO THE STRUCTURE OF THE PROTEINS
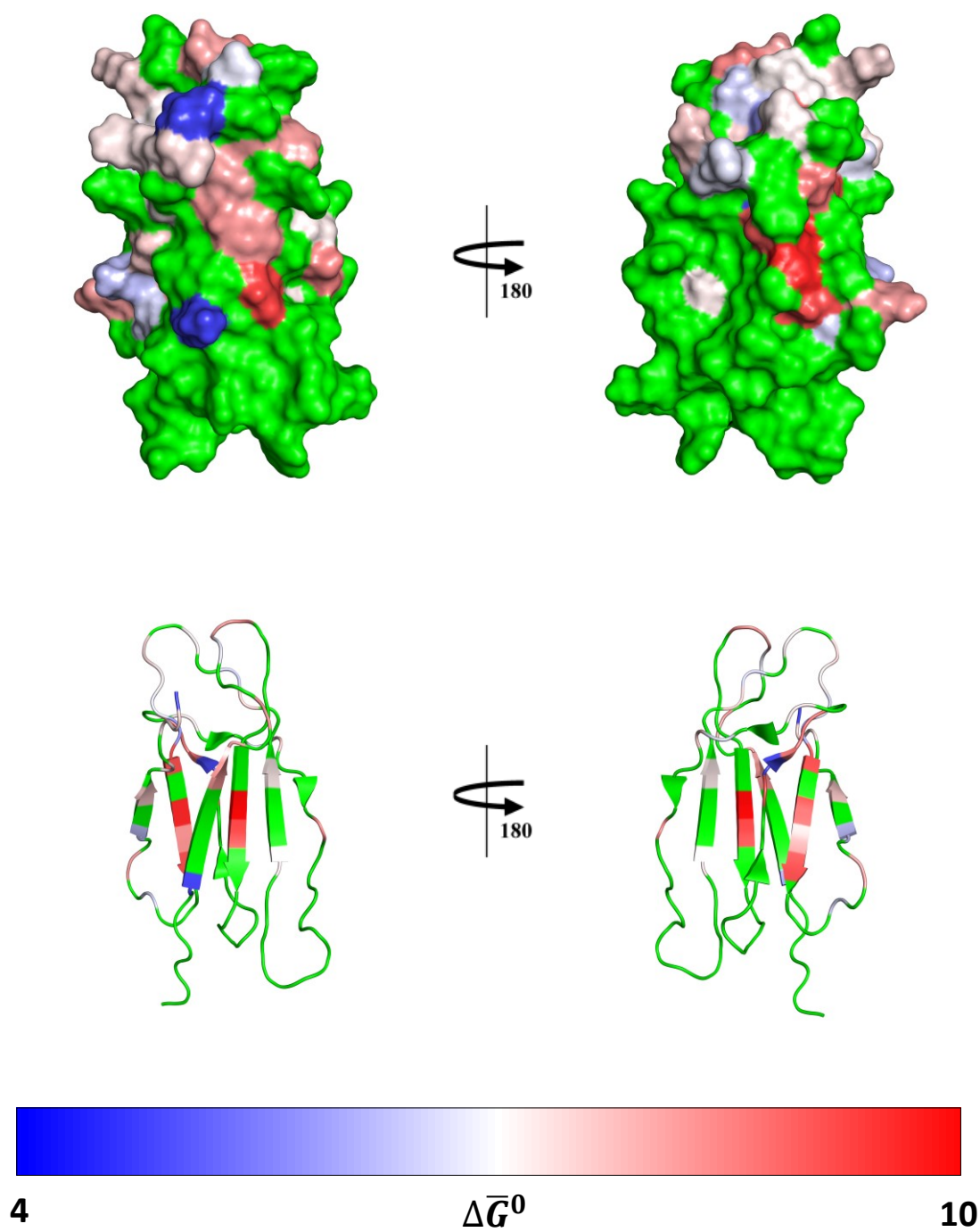
Figure 32 $\Delta\overline{G}^0$ **in kcal/mol of the β$_2$-microglobulin amide sites from the results at 300K of BLUU-Tramp experiment analysis mapped to the structure of the protein. All residues have been uniformly colored according to the $\Delta\overline{G}^0$ obtained for the corresponding amide site. The residues not included in the results are colored in green.**
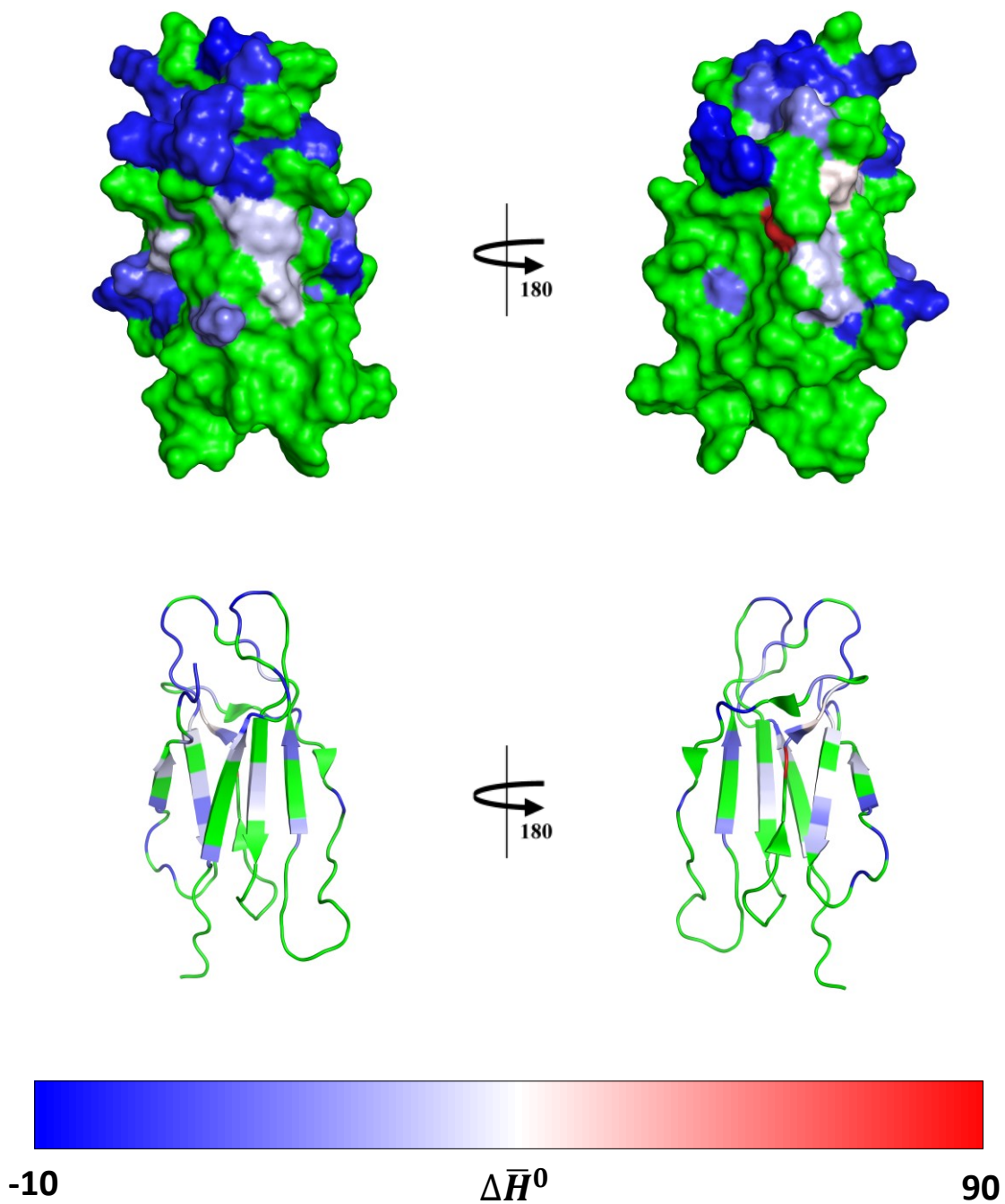
Figure 33 $\Delta\bar{H}^0$ **in kcal/mol of the β₂-microglobulin amide sites from the results at 300K of BLUU-Tramp experiment analysis mapped to the structure of the protein. All residues have been uniformly colored according to the $\Delta\bar{H}^0$ obtained for the corresponding amide site. The residues not included in the results are colored in green.**

MAPPING OF THE RESULTS TO THE STRUCTURE OF THE PROTEINS
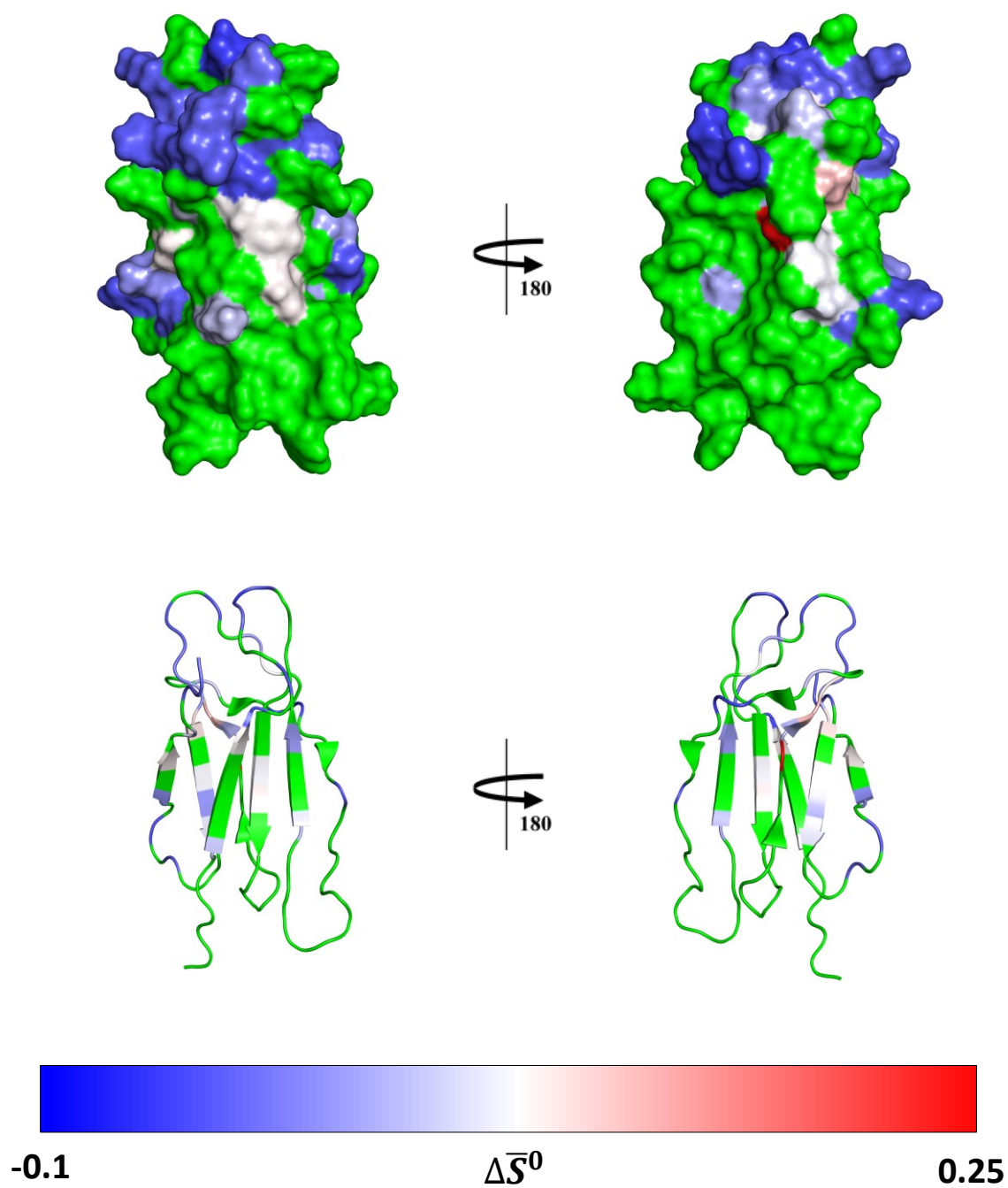
Figure 34 $\Delta\overline{S}^0$ **in kcal/(mol × K) of the β$_2$-microglobulin amide sites from the results at 300K of BLUU-Tramp experiment analysis mapped to the structure of the protein. All residues have been uniformly colored according to the $\Delta\overline{S}^0$ obtained for the corresponding amide site. The residues not included in the results are colored in green.**
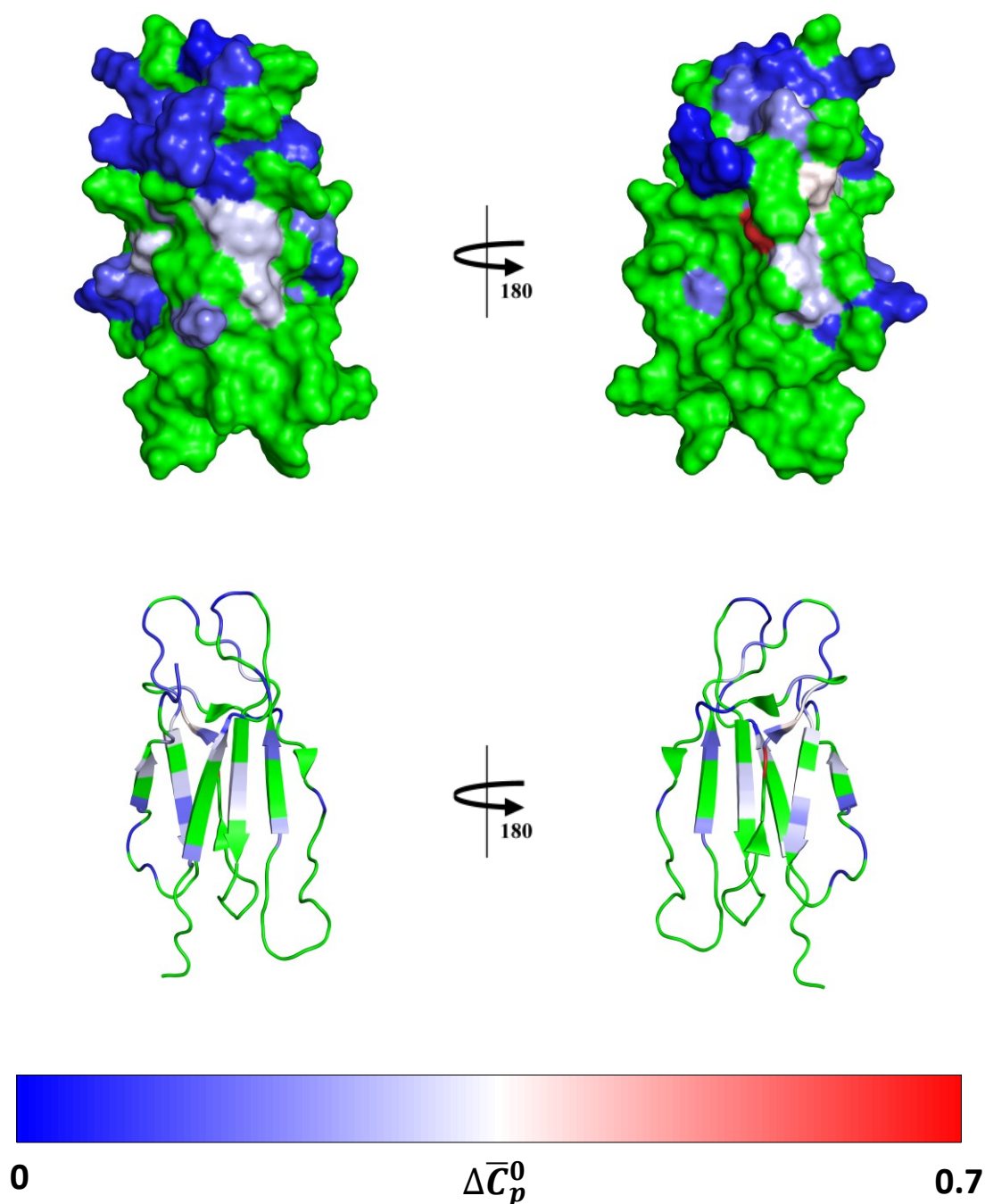
Figure 35 $\Delta\bar{C}_p^0$ **in kcal/(mol × K) of the β$_2$-microglobulin amide sites from the results at 300K of BLUU-Tramp experiment analysis mapped to the structure of the protein. All residues have been uniformly colored according to the $\Delta\bar{C}_p^0$ obtained for the corresponding amide site. The residues not included in the results are colored in green.**

Important trends can be observed by looking at the images and the values from which they are derived.

It is clear that the residues belonging to β strands show a higher $\Delta\bar{G}^0$, especially those near the cysteines involved in the disulfide bridge, like Tyrosine 26, Arginine 81, Valine 82 and Asparagine 83 (see Figure 32 and Table 4). The Cysteine 25 itself, which forms a disulfide bridge with the Cysteine 80, has a relatively high $\Delta\bar{G}^0$ value of 9.87 ± 0.01 kcal/mol. The Methionine 99 at the C-terminal, on the other hand, exhibits a lower $\Delta\bar{G}^0$ value of 4.88 ± 0.13 kcal/mol. Thus, limited conformational flexibility and $\Delta\bar{G}^0$ from the BLUU-Tramp results display signs of mutual correlation.

MAPPING OF THE RESULTS TO THE STRUCTURE OF THE PROTEINS

Interestingly, the first residues of the β strands, namely Arginine 6, first residue of strand A, Leucine 39, first residue of the second part of strand C, and Lysine 91, first residue of strand G, exhibit a $\Delta\bar{G}^0$ value that is lower than that of the other residues of the strand, suggesting that these strands might have a flexible initial part (see Figure 32).

Another interesting case to point out are the three contiguous residues on strand F: Arginine 81, Valine 82 and Asparagine 83. Arginine 81 and Asparagine 83 have a side chain that points toward the solvent, partially protecting the amide site from the isotope exchange, while the side chain of Valine 82 is mostly buried inside the protein core, leaving the amide site more exposed to the solvent (see Figure 36). The $\Delta\bar{G}^0$ of the former two (9.48 ± 0.01 kcal/mol and 9.03 ± 0.01 kcal/mol respectively) is about 1 kcal/mol higher than that of the latter (8.24 ± 0.02 kcal/mol), showing that solvent accessibility might be another important factor affecting the variation of molar Gibbs free energy in standard conditions.
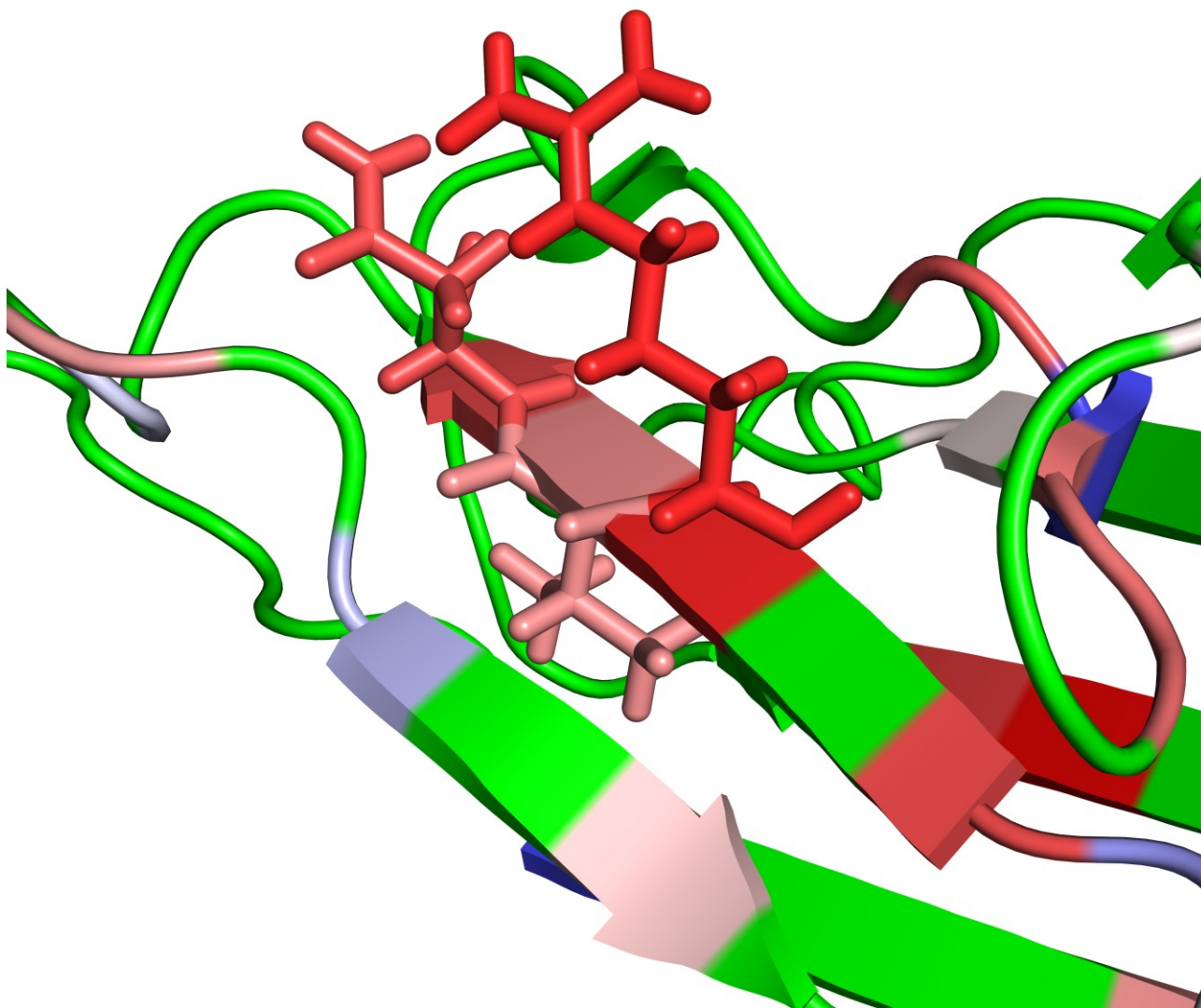
Figure 36 Arginine 81, Valine 82 and Asparagine 83 represented with sticks. The coloring follows the same $\Delta\bar{G}^0$ scale of Figure 32, with Arginine 81 being red, Valine 82 being pink and Asparagine 83 being light red.

DISCUSSION

MAPPING OF THE RESULTS TO THE STRUCTURE OF THE PROTEINS

An important thermodynamic parameter to consider is $\Delta\bar{S}^0$, because negative values lead to an increase in $\Delta\bar{G}^0$ when increasing the temperature, a phenomenon which is actually observed in our results for various residues:

Residue	$\Delta\bar{S}^0$ (kcal/(mol × K))	$\Delta\bar{C}_p^0$ (kcal/(mol × K))
R3	-0.030283 ± 0.025587	0.079236 ± 0.048675
S11	-0.040163 ± 0.017918	0.059476 ± 0.0337
H13	-0.031771 ± 0.017875	0.076761 ± 0.033922
E16	-0.021736 ± 0.014656	0.0885 ± 0.027863
N17	-0.053748 ± 0.003903	0.032525 ± 0.006514
G18	-0.036792 ± 0.016776	0.068616 ± 0.031742
E47	-0.049307 ± 0.00105	0.0327 ± 0.001762
K48	-0.049959 ± 0.007991	0.037205 ± 0.015141
S52	-0.038246 ± 0.028005	0.065876 ± 0.052753
T73	-0.035774 ± 0.014386	0.062754 ± 0.027219
K75	-0.030613 ± 0.013384	0.074768 ± 0.025487
D76	-0.025569 ± 0.015272	0.083278 ± 0.028911
E77	-0.025469 ± 0.011078	0.080397 ± 0.021121
L87	-0.027743 ± 0.005105	0.074901 ± 0.009561
Q89	-0.035602 ± 0.010609	0.069249 ± 0.020112
R97	-0.033343 ± 0.011672	0.068562 ± 0.022019
D98	-0.02748 ± 0.010605	0.081253 ± 0.020149
M99	-0.023103 ± 0.008474	0.07297 ± 0.016099

Table 24 $\Delta\bar{S}^0$ and $\Delta\bar{C}_p^0$ of the amide sites showing a negative value of $\Delta\bar{S}^0$ according to the results of the BLUU_Tramp analysis at 300K.

Those residues are not part of β strands and they also have a lower than variation of molar heat capacity in standard conditions that is lower than 0.1 kcal/(mol × K). It must be remembered that there is an important correlation between the estimated values of $\Delta\bar{S}^0$ and $\Delta\bar{C}_p^0$ in that they have the same derivative with respect to temperature (see equations (17) and (19)), possibly explaining why both values are low. It is nonetheless important to note that areas that are not part of β strands and are exposed to the solvent have low values of both $\Delta\bar{S}^0$ and $\Delta\bar{C}_p^0$ (see Figure 34 and Figure 35). Since negative values of $\Delta\bar{S}^0$ lead to a positive contribution of entropy variation to $\Delta\bar{G}^0$, the $\Delta\bar{H}^0$ is low as well to compensate for this positive contribution (see Figure 33).

MAPPING OF THE RESULTS TO THE STRUCTURE OF THE PROTEINS

It is interesting to look at the residues exhibiting positive values of $\Delta\bar{S}^0$ to evaluate if some common features are found among them:

Residue	Strand	$\Delta\bar{S}^0$ (kcal/(mol × K))	$\Delta\bar{C}_p^0$ (kcal/(mol × K))
K6	A	0.041642 ± 0.034985	0.202521 ± 0.065001
Y10	A	0.07923 ± 0.002918	0.299385 ± 0.005913
C25	B	0.071632 ± 0.002578	0.295762 ± 0.005206
Y26	B	0.082134 ± 0.002888	0.312077 ± 0.00586
D38		0.237816 ± 0.023727	0.621447 ± 0.047828
L39	C	0.029794 ± 0.01313	0.179044 ± 0.02458
L40	C	0.117549 ± 0.002887	0.378384 ± 0.005923
K41		0.09003 ± 0.004053	0.323933 ± 0.008225
E44		0.037322 ± 0.00275	0.209622 ± 0.005396
L64	E	0.01961 ± 0.003754	0.174131 ± 0.007474
Y67	E	0.012408 ± 0.002945	0.159531 ± 0.005699
F70		0.074923 ± 0.01052	0.286659 ± 0.020683
T71		0.00648 ± 0.03458	0.142981 ± 0.064963
Y78		0.010831 ± 0.038108	0.147212 ± 0.071495
A79	F	0.089855 ± 0.002141	0.326587 ± 0.004347
R81	F	0.071374 ± 0.001822	0.292599 ± 0.003684
V82	F	0.006878 ± 0.004693	0.15538 ± 0.00923
N83	F	0.062103 ± 0.001838	0.271048 ± 0.0037
K91	G	0.006135 ± 0.004698	0.140663 ± 0.008845
V93	G	0.083166 ± 0.001817	0.303285 ± 0.00368
W95		0.055979 ± 0.004186	0.246186 ± 0.008237

Table 25 $\Delta\bar{S}^0$ **and** $\Delta\bar{C}_p^0$ **of the amide sites showing a positive value of** $\Delta\bar{S}^0$ **according to the results of the BLUU_Tramp analysis at 300K. The "strand" column indicates the β strand to which the residue belong.**

Many of the residues having positive values of $\Delta\bar{S}^0$ are indeed part of β strands or near such secondary structures, all of them also have $\Delta\bar{C}_p^0$ values greater than 0.1 kcal/(mol × K). An interesting case is that of the Aspartate 38, that has the highest value of $\Delta\bar{S}^0$ (0.24 ± 0.02kcal/(mol × K)) and $\Delta\bar{C}_p^0$ (0.62 ± 0.05 kcal/(mol × K)). Aspartate 38 forms an important salt bridge in the structure, similar to Aspartate 76, whose mutation into Asparagine leads to the highly amyloidogenic D76N mutant form. It is predicted that a mutation of Aspartate 38 even as conservative as that with an asparagine would lead to a highly amyloidogenic species and, indeed, this prediction is confirmed by unpublished results (Kardos, personal communication). Even though this correlation between $\Delta\bar{S}^0$ and $\Delta\bar{C}_p^0$ might again be a consequence of the equations used to estimate those values, it is still important to note that residues that are next to β strands or part of them show high values of $\Delta\bar{S}^0$ and $\Delta\bar{C}_p^0$.

These preliminary observations suggest that it should be possible to correlate the thermodynamic parameters obtained from the results of the analysis of the BLUU-Tramp experiment to structural features of the protein, in particular secondary structures and solvent exposure of the amide sites.

DISCUSSION

MAPPING OF THE RESULTS TO THE STRUCTURE OF THE PROTEINS

LYSOZYME

The following images show how the results at 300 K from the BLUU-Tramp data analysis map to the structure of the protein. It should be mentioned that the information available concerns only 39 residues that represent 30% of the molecule. Therefore the conclusions can only cover a limited part of the structure.

$$5 \qquad \Delta\overline{G}^0 \qquad 17$$
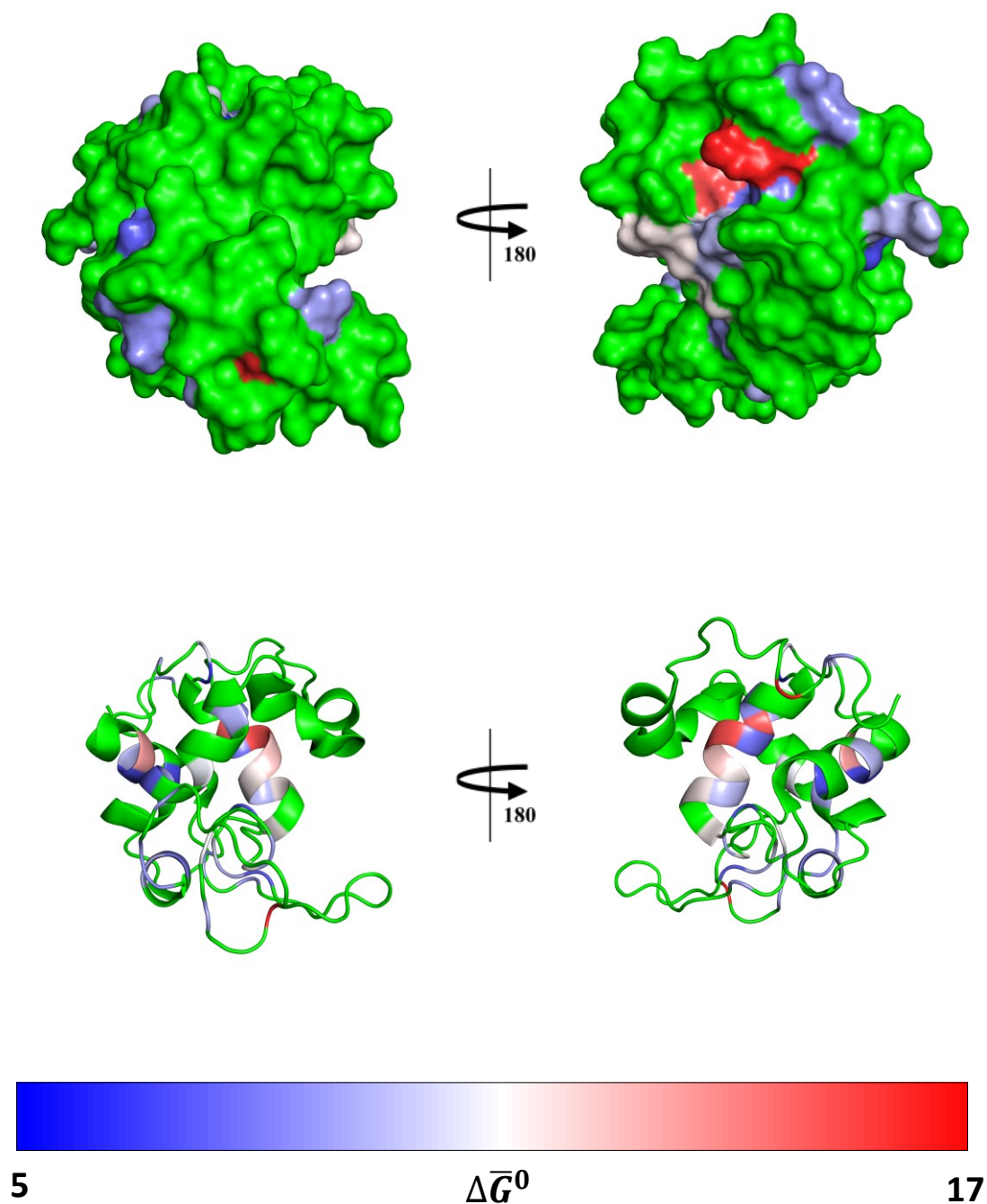
Figure 37 $\Delta\overline{G}^0$ **in kcal/mol of the lysozyme amide sites from the results at 300K of BLUU-Tramp experiment analysis mapped to the structure of the protein. All residues have been uniformly colored according to the $\Delta\overline{G}^0$ obtained for the corresponding amide site. The residues not included in the results are colored in green.**

MAPPING OF THE RESULTS TO THE STRUCTURE OF THE PROTEINS
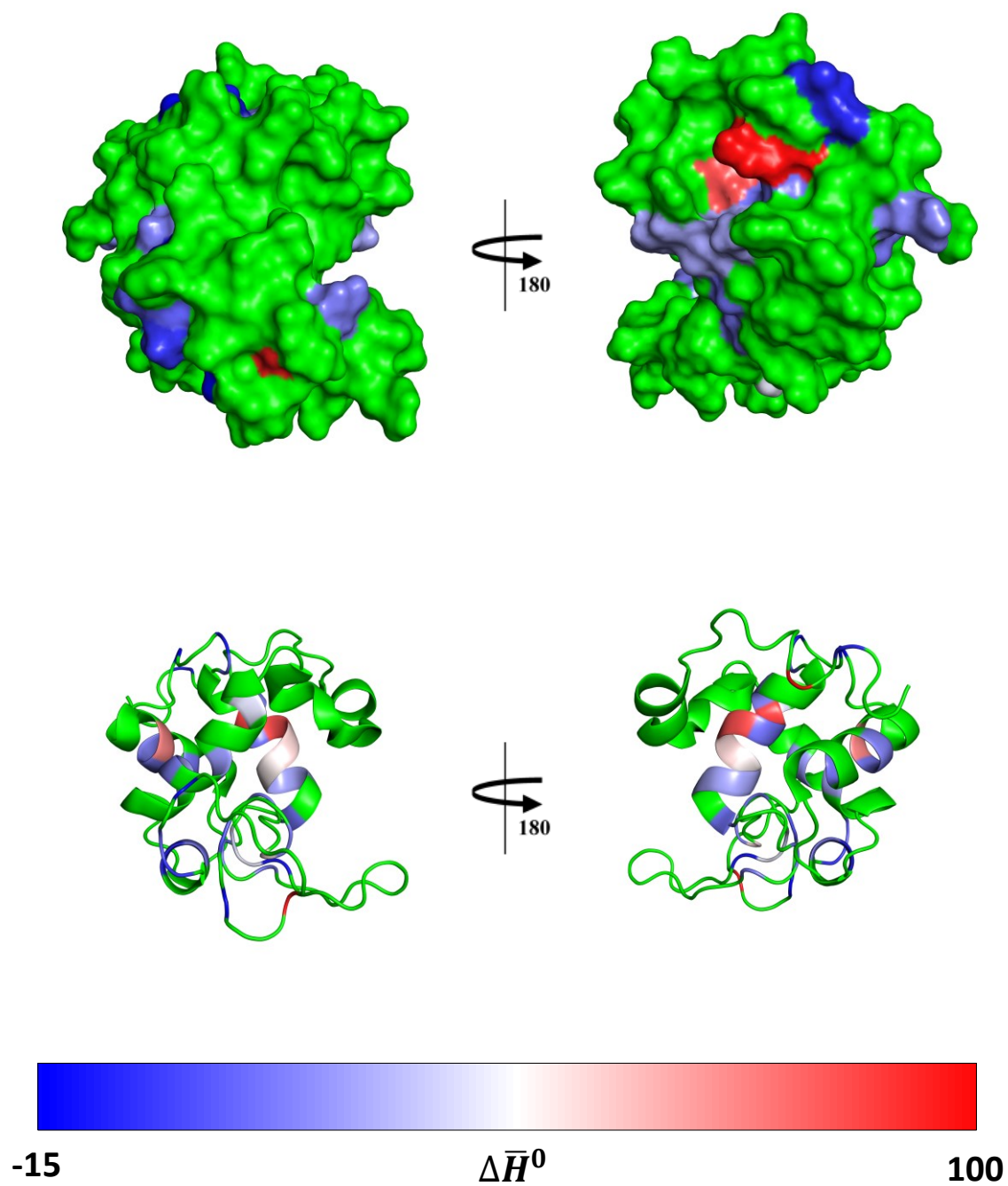
Figure 38 $\Delta \bar{H}^0$ **in kcal/mol of the lysozyme amide sites from the results at 300K of BLUU-Tramp experiment analysis mapped to the structure of the protein. All residues have been uniformly colored according to the** $\Delta \bar{H}^0$ **obtained for the corresponding amide site. The residues not included in the results are colored in green.**
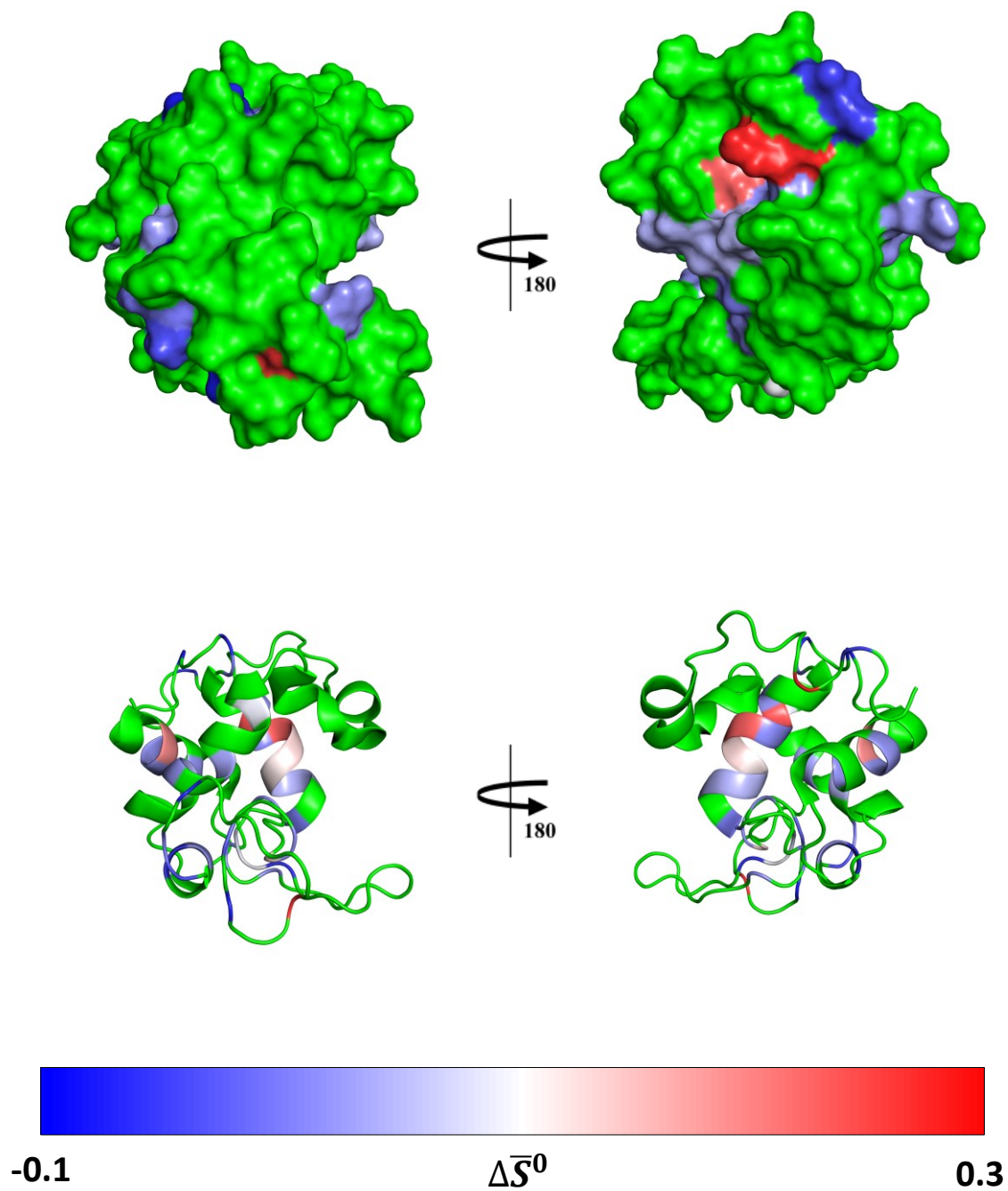
Figure 39 $\Delta\overline{S}^0$ **in kcal/(mol × K) of the lysozyme amide sites from the results at 300K of BLUU-Tramp experiment analysis mapped to the structure of the protein. All residues have been uniformly colored according to the** $\Delta\overline{S}^0$ **obtained for the corresponding amide site. The residues not included in the results are colored in green.**

MAPPING OF THE RESULTS TO THE STRUCTURE OF THE PROTEINS
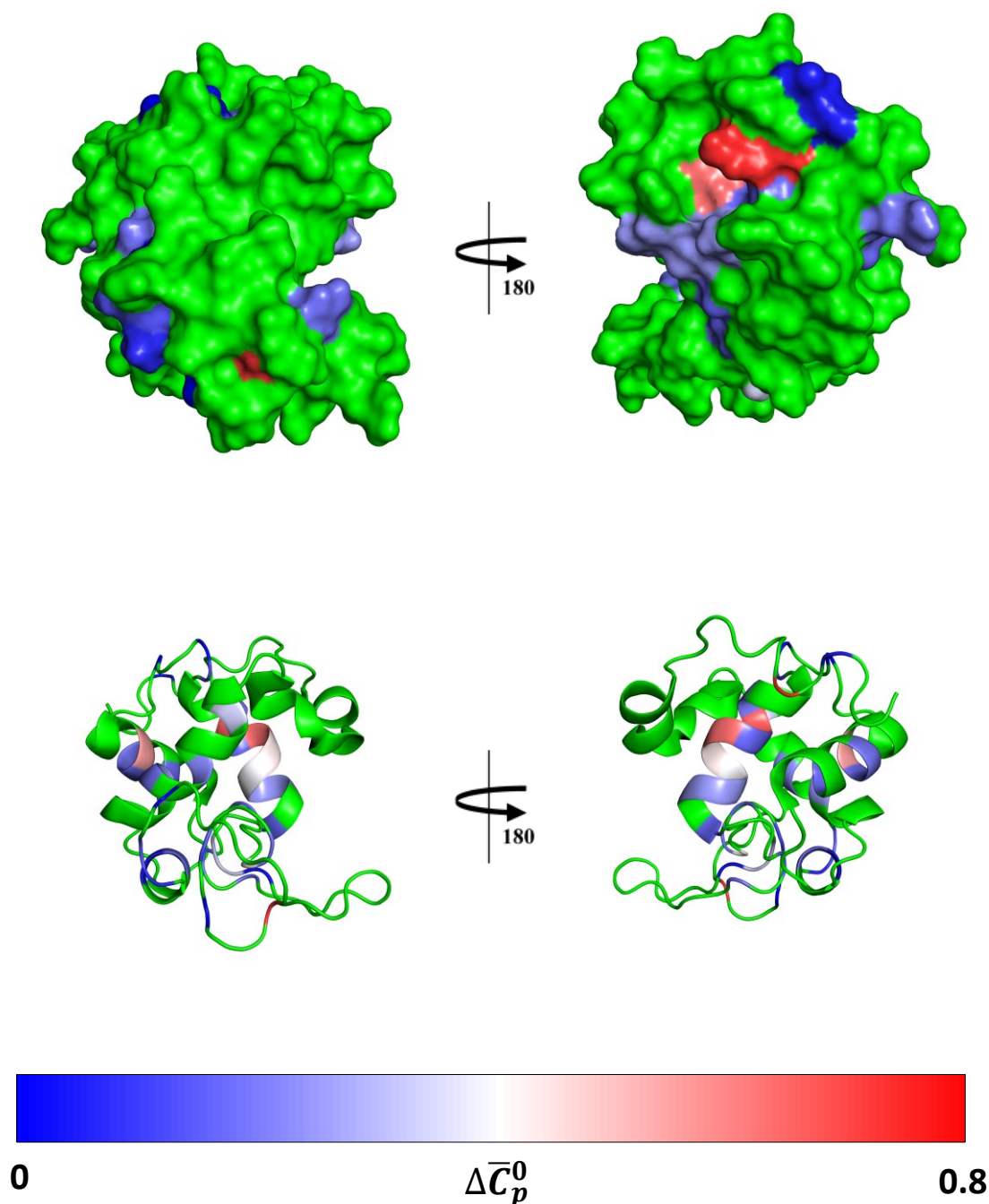
Figure 40 $\Delta\bar{C}_p^0$ in kcal/(mol × K) of the lysozyme amide sites from the results at 300K of BLUU-Tramp experiment analysis mapped to the structure of the protein. All residues have been uniformly colored according to the $\Delta\bar{C}_p^0$ obtained for the corresponding amide site. The residues not included in the results are colored in green.

Overall, the protein presents $\Delta\bar{G}^0$ values at 300 K that are higher than those of human β$_2$-microglobulin reflecting the larger stability of lysozyme. As an example, two of the three Cysteines involved in disulfide bonds that were successfully analyzed, Cysteine 30 and Cysteine 65, present a $\Delta\bar{G}^0$ value of 15.0 ± 0.2 kcal/mol and 10.9 ± 0.5 kcal/mol respectively, higher than those of Cysteine 25 of β$_2$-microglobulin, which is 9.87 ± 0.01 kcal/mol (see Table 4 and Table 9). The remaining lysozyme cysteine involved in a disulfide bond that was analyzed, Cysteine 77, presents a $\Delta\bar{G}^0$ value of 8.74 ± 0.01 kcal/mol. The difference of at least 2 kcal/mol in $\Delta\bar{G}^0$ with respect to the mentioned cysteines might be due to the larger solvent exposure of Cysteine 77 (see Figure 41).
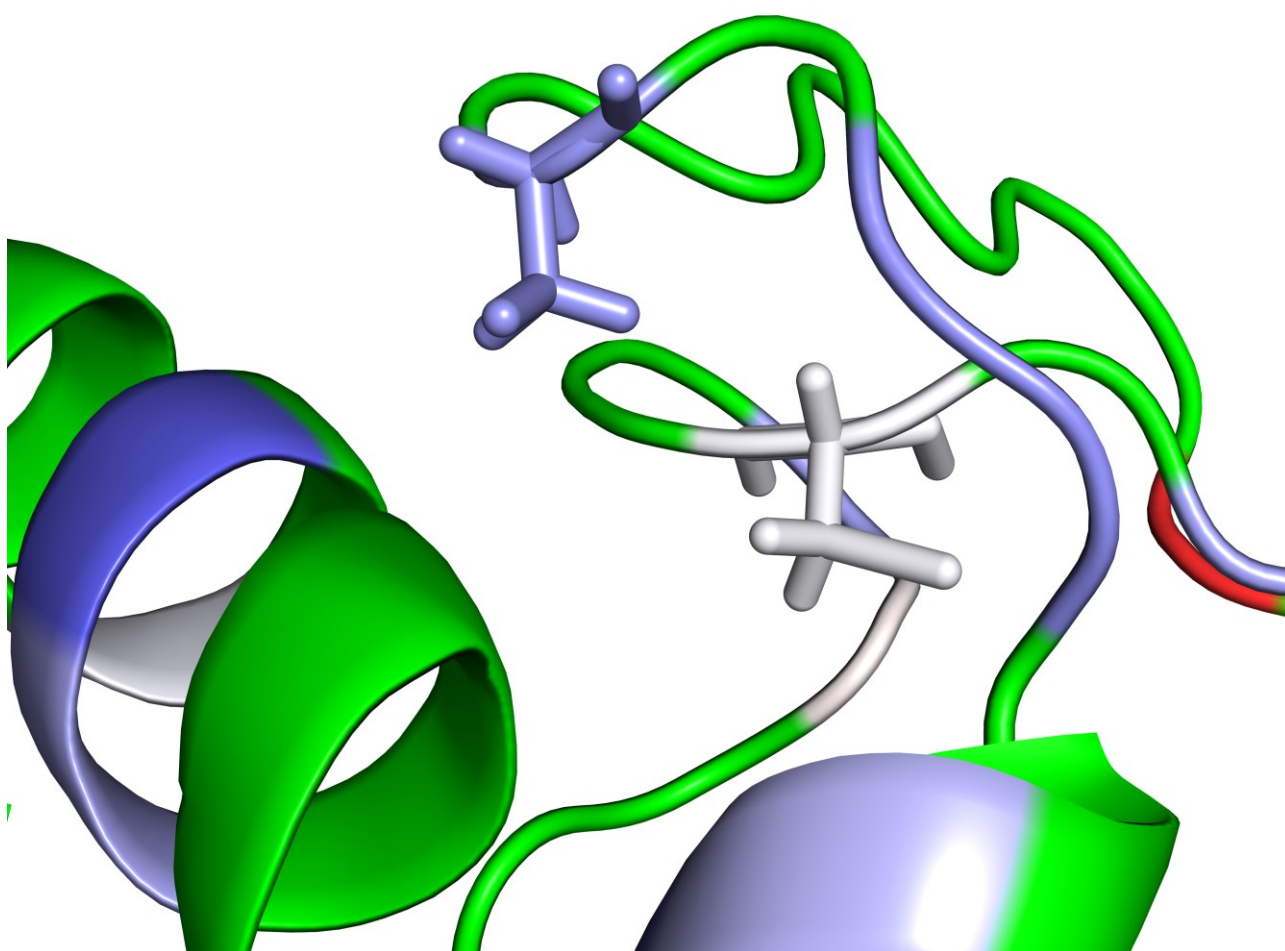
Figure 41 The Cysteines 65 and 77 in sticks representation and colored according to the $\Delta\bar{G}^0$ scale of Figure 37, with Cysteine 65 being white and Cysteine 77 being light blue. The rest of the protein is in cartoon representation and follows the same coloring of Figure 37.

It is also interesting to look at the $\Delta\bar{G}^0$ values of the residues that are part of the active site. The $\Delta\bar{G}^0$ of Aspartate 53, involved in the catalytic reaction of human lysozyme, is 7.42 ± 0.01 kcal/mol, that falls on the lower part of the $\Delta\bar{G}^0$ values range (see Table 9 and Figure 37). Other residues part of the subsites are Phenylalanine 57, part of subsite A with a $\Delta\bar{G}^0$ value of 7.15 ± 0.02 kcal/mol, Tryptophan 34 and Serine 36, part of subsite B and exhibiting $\Delta\bar{G}^0$ values of 11.4 ± 2.6 kcal/mol and 11.2 ± 1.1 kcal/mol, Arginine 62, part of subsite E with a $\Delta\bar{G}^0$ value of 8.95 ± 0.03 kcal/mol. Therefore, only the residue directly involved in the catalytic reaction and the residue in subsite A appear to have a lower value of $\Delta\bar{G}^0$, possibly due to the fact that solvent accessibility of the active site is fundamental for the proper activity of the enzyme.

MAPPING OF THE RESULTS TO THE STRUCTURE OF THE PROTEINS
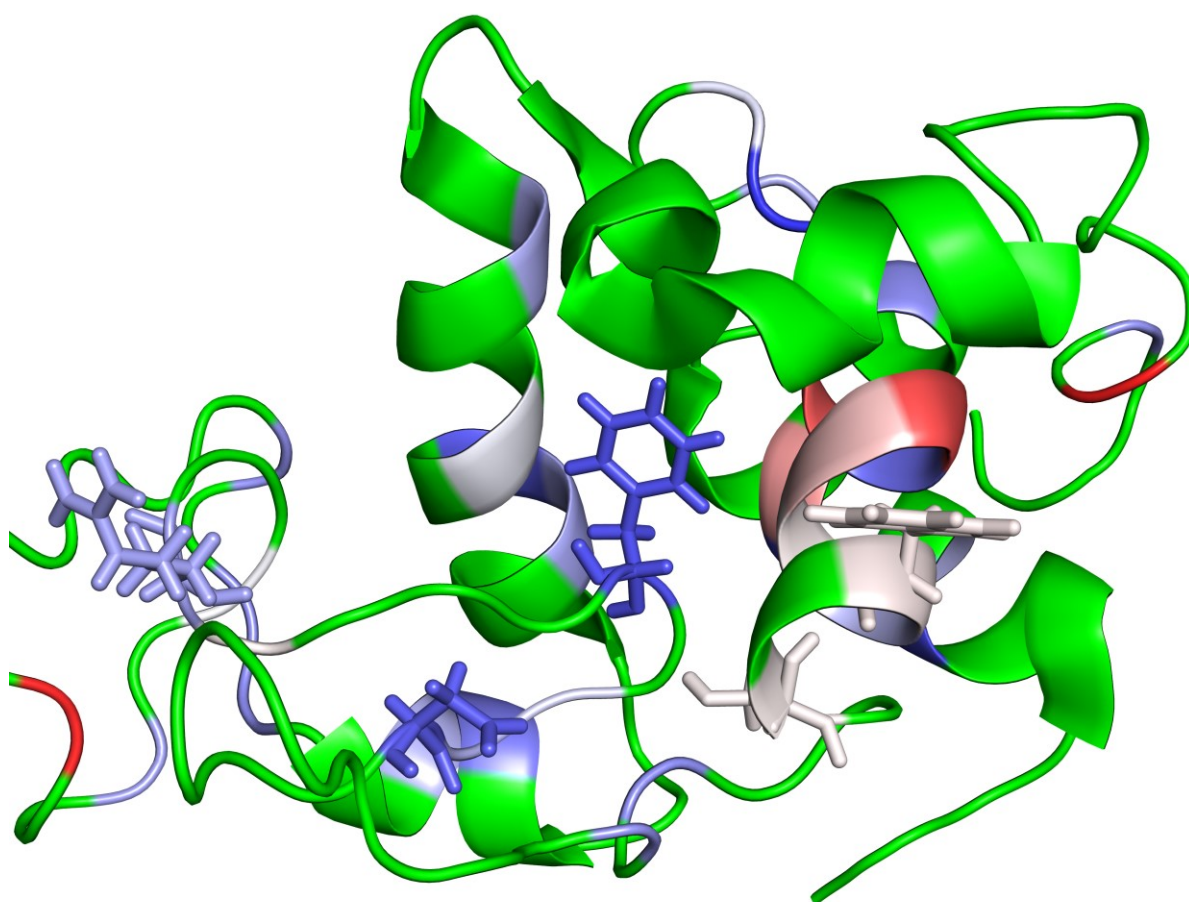
Figure 42 The active site of the lysozyme. The residues that are part of the site or of the subsites and whose results are available are in sticks representation. The coloring follows the same $\Delta\bar{G}^0$ scale as Figure 37, with Aspartate 53 and Phenylalanine 57 being blue, Arginine 62 being light blue and Tryptophan 34 and Serine 36 being light pink.

Generally, the residues that are part of the helices don't necessarily have the highest values of $\Delta\bar{G}^0$ (see Figure 37), nonetheless two of the residues with the highest value of $\Delta\bar{G}^0$, Cysteine 30 and Tryptophan 28, lie in the B-helix . Importantly, the two residues with the highest values of $\Delta\bar{G}^0$, Threonine 70 with a value of 15.9 ± 3.3 kcal/mol and Tyrosine 124 with a value of 16.1 ± 3.1 kcal/mol, also present a considerable uncertainty in the measurement of the value, and lie in the loop region and near the C-terminal region respectively, both of which are region with high segmental motion.

DISCUSSION

MAPPING OF THE RESULTS TO THE STRUCTURE OF THE PROTEINS

It is also important to consider the residues having positive and negative values of $\Delta\bar{S}^0$ to see if those values correlate with structural features of the protein:

Residue	$\Delta\bar{S}^0$ (kcal/(mol × K))	$\Delta\bar{C}_p^0$ (kcal/(mol × K))
E7	-0.057651 ± 0.004871	0.030704 ± 0.010054
G19	-0.06961 ± 0.014639	0.009363 ± 0.030241
G22	-0.062132 ± 0.024376	0.03155 ± 0.050944
D53	-0.051011 ± 0.000612	0.034119 ± 0.001146
C65	-0.01667 ± 0.104324	0.125733 ± 0.205721
D67	-0.069866 ± 0.000513	0.006482 ± 0.000635
C77	-0.067025 ± 0.00015	0.010884 ± 0.000214
S80	-0.034744 ± 0.021999	0.07418 ± 0.043433
A83	-0.051175 ± 0.005061	0.047222 ± 0.010507
Q126	-0.044889 ± 0.003985	0.055436 ± 0.008239

Table 26 $\Delta\bar{S}^0$ and $\Delta\bar{C}_p^0$ of the amide sites having a negative value of $\Delta\bar{S}^0$ according to the results of the BLUU-Tramp analysis at 300K.

Interestingly, two residues, Glutamate 7 and Alanine 83, are actually part of the A-helix and of the first 3_{10} helix respectively. On the other hand, Glutamine 126 lies in the C-terminal region. Furthermore, both Cysteines that do not belong to α helices show negative values of $\Delta\bar{S}^0$. Cysteine 65 also has a $\Delta\bar{C}_p^0$ value higher than 0.1 kcal/(mol × K), while all the other residues with a negative $\Delta\bar{S}^0$ have a $\Delta\bar{C}_p^0$ lower than 0.1 kcal/(mol × K). It is finally important to note that the Aspartate 53, involved in the catalytic reaction, has a negative value of $\Delta\bar{S}^0$ despite being part of the β_2-strand, leading to the observed increase of $\Delta\bar{G}^0$ when increasing the temperature (see Table 10). The $\Delta\bar{H}^0$ again follows a pattern similar to that of the $\Delta\bar{S}^0$ (see Figure 38), with all the residues with a negative value of $\Delta\bar{S}^0$ having a $\Delta\bar{H}^0$ not significantly higher than 0 (seeTable 9).

MAPPING OF THE RESULTS TO THE STRUCTURE OF THE PROTEINS

Residue	Secondary Structure	$\Delta \bar{S}^0$ (kcal/(mol × K))	$\Delta \bar{C}_p^0$ (kcal/(mol × K))
L8	A-helix	0.023 ± 0.001919	0.179512 ± 0.003824
R10		0.0243 ± 0.001147	0.199257 ± 0.002393
T11		0.022633 ± 0.006495	0.178289 ± 0.012523
L12		0.184297 ± 0.004812	0.54257 ± 0.010369
I23		0.004302 ± 0.004315	0.138514 ± 0.008386
N27	B-helix	0.025969 ± 0.004795	0.195865 ± 0.009534
W28	B-helix	0.229748 ± 0.011179	0.644585 ± 0.024148
M29	B-helix	0.015418 ± 0.007033	0.169628 ± 0.013706
C30	B-helix	0.217556 ± 0.007051	0.622045 ± 0.015139
L31	B-helix	0.129616 ± 0.006957	0.427414 ± 0.014958
A32	B-helix	0.11293 ± 0.003461	0.387391 ± 0.007377
K33	B-helix	0.047048 ± 0.004106	0.244724 ± 0.008513
W34	B-helix	0.041522 ± 0.082003	0.245559 ± 0.181173
S36		0.006012 ± 0.037634	0.17346 ± 0.082204
T40		0.0064 ± 0.003097	0.156568 ± 0.006202
A42	β_1-strand	0.014921 ± 0.002162	0.174528 ± 0.004357
Y54	β_2-strand	0.097527 ± 0.004017	0.344933 ± 0.008372
G55	β_2-strand	0.077884 ± 0.00391	0.310366 ± 0.008116
F57		0.017168 ± 0.004441	0.168649 ± 0.008782
S61	β_3-strand	0.126708 ± 0.010063	0.415112 ± 0.020933
R62		0.02001 ± 0.007866	0.18638 ± 0.01554
T70	2nd Loop Region	0.254454 ± 0.131317	0.701727 ± 0.284768
L79		0.000508 ± 0.075229	0.144909 ± 0.152288
L84	3_{10} helix (i)	0.022199 ± 0.001795	0.185345 ± 0.003681
V93	C-helix	0.049171 ± 0.00298	0.246092 ± 0.006232
A94	C-helix	0.026077 ± 0.003026	0.187944 ± 0.005955
A96	C-helix	0.031915 ± 0.015802	0.221744 ± 0.031786
V100		0.092292 ± 0.003717	0.333215 ± 0.007795
Y124	3_{10} helix (ii)	0.265006 ± 0.123106	0.723933 ± 0.266982

Table 27 $\Delta \bar{S}^0$ **and** $\Delta \bar{C}_p^0$ **of the amide sites having a positive value of** $\Delta \bar{S}^0$ **according to the results of the BLUU_Tramp analysis at 300K. The "Secondary Structure" column indicates the secondary structure or the region to which the residue belong.**

The B- and C-helices have many residues with a positive $\Delta \bar{S}^0$ and a $\Delta \bar{C}_p^0$ higher than 0.1 kcal/(mol × K), while the A-helix and the first 3_{10} helix present both residues with and without these features. There are also four residues belonging to β strands with a positive $\Delta \bar{S}^0$ and a $\Delta \bar{C}_p^0$ higher than 0.1 kcal/(mol × K), including two residues that are near Aspartate 53, namely Tyrosine 54 and Glycine 55, suggesting that also in the case of lysozyme residues belonging to β strands and not involved in catalytic activity generally have a positive $\Delta \bar{S}^0$ and a $\Delta \bar{C}_p^0$ higher than 0.1 kcal/(mol × K).

THE COMPARISON BETWEEN THE RESULTS FROM THE ANALYSIS OF BLUU-TRAMP DATA AND THE RESULTS FROM CONVENTIONAL ISOTOPE EXCHANGE EXPERIMENT

Interestingly, among the residues with a positive $\Delta \bar{S}^0$ and a $\Delta \bar{C}_p^0$ higher than 0.1 kcal/(mol × K) also residues that lie in the 2nd loop region, such as the Threonine 70, can be found. Furthermore, all residues that are part of the subsites but don't have catalytic activity have these properties. These residues are Phenylalanine 57, part of subsite B, Tryptophan 34 and Serine 36, part of subsite C, and Arginine 62, part of subsite E. These values might suggest that the subsites have a more rigid structure.

Overall, although some secondary structures, in particular α helices, don't always display similar value ranges of the thermodynamic parameters, and although residues in the loop regions might still have positive values of $\Delta \bar{S}^0$, it is still possible to correlate the thermodynamic parameters to structural features of the protein.

THE COMPARISON BETWEEN THE RESULTS FROM THE ANALYSIS OF BLUU-TRAMP DATA AND THE RESULTS FROM CONVENTIONAL ISOTOPE EXCHANGE EXPERIMENT

When comparing the results from the analysis of the BLUU-Tramp data with the analysis of the conventional exchange experiment it is important to examine the amide sites common to both kinds of experiments:

Residue	$\Delta \bar{G}^0$ BLUU-Tramp (kcal/mol)	$\Delta \bar{G}^0$ conventional exchange (kcal/mol)
Y10	8.138548 ± 0.013714	8.14885 ± 0.051867
C25	9.874799 ± 0.010769	9.850581 ± 0.056428
Y26	9.171372 ± 0.015136	9.375117 ± 0.083553
D38	8.872414 ± 0.061137	8.409392 ± 0.095924
L39	4.918507 ± 0.253261	5.382502 ± 0.037035
L40	8.492698 ± 0.023404	8.707767 ± 0.07451
E44	7.246711 ± 0.018205	7.6506 ± 0.067525
Y67	7.20736 ± 0.030582	7.73804 ± 0.11321
F70	7.522031 ± 0.056281	7.749214 ± 0.060965
R81	9.477786 ± 0.008141	9.558049 ± 0.061334
N83	9.026461 ± 0.006847	8.954296 ± 0.058222
L87	6.55811 ± 0.097877	6.014748 ± 0.052516
V93	7.542878 ± 0.008767	7.568593 ± 0.075961
W95	7.134201 ± 0.022946	7.706903 ± 0.031471

Table 28 Comparison of the $\Delta \bar{G}^0$ obtained from the results at 300 K of the analysis of BLUU-Tramp data and conventional exchange data.

THE COMPARISON BETWEEN THE RESULTS FROM THE ANALYSIS OF BLUU-TRAMP DATA AND THE RESULTS FROM CONVENTIONAL ISOTOPE EXCHANGE EXPERIMENT

Residue	$\Delta \bar{H}^0$ BLUU-Tramp (kcal/mol)	$\Delta \bar{H}^0$ conventional exchange (kcal/mol)
Y10	31.907682 ± 0.887009	37.665053 ± 4.701538
C25	31.364336 ± 0.780935	42.479631 ± 5.114995
Y26	33.81162 ± 0.879046	45.274252 ± 7.573792
D38	80.217098 ± 7.174253	41.083812 ± 8.695144
L39	13.856644 ± 3.687007	11.567684 ± 3.357083
L40	43.757532 ± 0.888471	35.698716 ± 6.754077
E44	18.443332 ± 0.809425	23.42857 ± 6.120902
Y67	10.929707 ± 0.854867	9.191627 ± 10.262065
F70	29.998839 ± 3.102521	17.391252 ± 5.526217
R81	30.889888 ± 0.552528	42.143407 ± 5.559673
N83	27.657226 ± 0.554973	39.159584 ± 5.277556
L87	-1.764791 ± 1.434163	19.130623 ± 4.760364
V93	32.492744 ± 0.552014	28.430278 ± 6.885553
W95	23.927954 ± 1.235592	27.868483 ± 2.85275

Table 29 Comparison of the $\Delta \bar{H}^0$ obtained from the results at 300 K of the analysis of BLUU-Tramp data and conventional exchange data.

Residue	$\Delta \bar{S}^0$ BLUU-Tramp (kcal/(mol × K))	$\Delta \bar{S}^0$ conventional exchange (kcal/(mol × K))
Y10	0.07923 ± 0.002918	0.098387 ± 0.015519
C25	0.071632 ± 0.002578	0.108763 ± 0.016884
Y26	0.082134 ± 0.002888	0.119664 ± 0.025
D38	0.237816 ± 0.023727	0.108915 ± 0.028701
L39	0.029794 ± 0.01313	0.020617 ± 0.011081
L40	0.117549 ± 0.002887	0.08997 ± 0.022294
E44	0.037322 ± 0.00275	0.052593 ± 0.020204
Y67	0.012408 ± 0.002945	0.004845 ± 0.033874
F70	0.074923 ± 0.01052	0.03214 ± 0.018241
R81	0.071374 ± 0.001822	0.108618 ± 0.018352
N83	0.062103 ± 0.001838	0.100684 ± 0.01742
L87	-0.027743 ± 0.005105	0.04372 ± 0.015713
V93	0.083166 ± 0.001817	0.069539 ± 0.022728
W95	0.055979 ± 0.004186	0.067205 ± 0.009417

Table 30 Comparison of the $\Delta \bar{S}^0$ obtained from the results at 300 K of the analysis of BLUU-Tramp data and conventional exchange data.

DISCUSSION

THE COMPARISON BETWEEN THE RESULTS FROM THE ANALYSIS OF BLUU-TRAMP DATA AND THE RESULTS FROM CONVENTIONAL ISOTOPE EXCHANGE EXPERIMENT

Residue	$\Delta\bar{C}_p^0$ BLUU-Tramp (kcal/(mol × K))	$\Delta\bar{C}_p^0$ conventional exchange (kcal/(mol × K))
Y10	0.299385 ± 0.005913	0.945281 ± 0.58762
C25	0.295762 ± 0.005206	0.200861 ± 0.639296
Y26	0.312077 ± 0.00586	0.395621 ± 0.946608
D38	0.621447 ± 0.047828	0.757394 ± 1.086759
L39	0.179044 ± 0.02458	-0.248669 ± 0.419584
L40	0.378384 ± 0.005923	2.694421 ± 0.844156
E44	0.209622 ± 0.005396	1.373873 ± 0.765019
Y67	0.159531 ± 0.005699	2.322137 ± 1.2826
F70	0.286659 ± 0.020683	2.661408 ± 0.690692
R81	0.292599 ± 0.003684	0.552641 ± 0.694874
N83	0.271048 ± 0.0037	0.322299 ± 0.659613
L87	0.074901 ± 0.009561	-0.445434 ± 0.594972
V93	0.303285 ± 0.00368	1.978979 ± 0.860588
W95	0.246186 ± 0.008237	0.950596 ± 0.35655

Table 31 Comparison of the $\Delta\bar{C}_p^0$ obtained from the results at 300 K of the analysis of BLUU-Tramp data and conventional exchange data.

It can be seen that, while the $\Delta\bar{G}^0$ values obtained from the two methods are fairly similar, the $\Delta\bar{H}^0$ and $\Delta\bar{S}^0$ present important differences in the case of the Aspartate 38 and the Leucine 87 and, in general, the results from the conventional exchange data present a higher uncertainty when compared to the results from the BLUU-Tramp data. This uncertainty of the results from conventional exchange data is even higher in the case of the $\Delta\bar{C}_p^0$. It might be due to the low number of exchange constants per residue used to obtain those results and to the relatively narrow temperature range they cover (from 301 K to 315 K). Since the $\Delta\bar{S}^0$ is proportional to the first derivative of $\Delta\bar{G}^0$ with respect to temperature (see equation (14)), while $\Delta\bar{C}_p^0$ is proportional to the second derivate of $\Delta\bar{G}^0$ with respect to temperature(see equation (16)), many exchange constants spanning a wide temperature range are needed to derive an equivalent number $\Delta\bar{G}_{EX2}^0$ values to accurately and precisely estimate them. The addition of an exchange constant measured at 293 K to the previously measured ones could alleviate the uncertainty in the results:

THE COMPARISON BETWEEN THE RESULTS FROM THE ANALYSIS OF BLUU-TRAMP DATA AND THE RESULTS
FROM CONVENTIONAL ISOTOPE EXCHANGE EXPERIMENT

Residue	$\Delta \bar{G}^0$ BLUU-Tramp (kcal/mol)	$\Delta \bar{G}^0$ conventional exchange with addition (kcal/mol)
Y10	8.138548 ± 0.013714	8.057846 ± 0.027566
C25	9.874799 ± 0.010769	9.727909 ± 0.03252
Y26	9.171372 ± 0.015136	9.231186 ± 0.044143
L40	8.492698 ± 0.023404	8.62174 ± 0.035723
E44	7.246711 ± 0.018205	7.57558 ± 0.032164
Y67	7.20736 ± 0.030582	7.747509 ± 0.049333
F70	7.522031 ± 0.056281	7.725689 ± 0.026864
R81	9.477786 ± 0.008141	9.447157 ± 0.032927
N83	9.026461 ± 0.006847	8.837708 ± 0.032445
L87	6.55811 ± 0.097877	5.917322 ± 0.028447
V93	7.542878 ± 0.008767	7.578081 ± 0.033124
W95	7.134201 ± 0.022946	7.609161 ± 0.021813

Table 32 Comparison of the $\Delta \bar{G}^0$ obtained from the results at 300 K of the analysis of BLUU-Tramp data and conventional exchange data with the addition of an exchange constant measured at 293 K.

Residue	$\Delta \bar{H}^0$ BLUU-Tramp (kcal/mol)	$\Delta \bar{H}^0$ conventional exchange with addition (kcal/mol)
Y10	31.907682 ± 0.887009	28.686262 ± 1.411438
C25	31.364336 ± 0.780935	30.376345 ± 1.66508
Y26	33.81162 ± 0.879046	31.07354 ± 2.260193
L40	43.757532 ± 0.888471	27.210941 ± 1.829076
E44	18.443332 ± 0.809425	16.026873 ± 1.646839
Y67	10.929707 ± 0.854867	10.125835 ± 2.525927
F70	29.998839 ± 3.102521	15.070134 ± 1.375471
R81	30.889888 ± 0.552528	31.202418 ± 1.685924
N83	27.657226 ± 0.554973	27.656592 ± 1.661235
L87	-1.764791 ± 1.434163	9.518137 ± 1.456529
V93	32.492744 ± 0.552014	29.366403 ± 1.695982
W95	23.927954 ± 1.235592	18.224973 ± 1.116879

Table 33 Comparison of the $\Delta \bar{H}^0$ obtained from the results at 300 K of the analysis of BLUU-Tramp data and conventional exchange data with the addition of an exchange constant measured at 293 K.

DISCUSSION

THE COMPARISON BETWEEN THE RESULTS FROM THE ANALYSIS OF BLUU-TRAMP DATA AND THE RESULTS
FROM CONVENTIONAL ISOTOPE EXCHANGE EXPERIMENT

Residue	$\Delta\bar{S}^0$ BLUU-Tramp (kcal/(mol × K))	$\Delta\bar{S}^0$ conventional exchange with addition (kcal/(mol × K))
Y10	0.07923 ± 0.002918	0.068761 ± 0.004684
C25	0.071632 ± 0.002578	0.068828 ± 0.005526
Y26	0.082134 ± 0.002888	0.072808 ± 0.007501
L40	0.117549 ± 0.002887	0.061964 ± 0.00607
E44	0.037322 ± 0.00275	0.028171 ± 0.005466
Y67	0.012408 ± 0.002945	0.007928 ± 0.008383
F70	0.074923 ± 0.01052	0.024481 ± 0.004565
R81	0.071374 ± 0.001822	0.072518 ± 0.005595
N83	0.062103 ± 0.001838	0.06273 ± 0.005513
L87	-0.027743 ± 0.005105	0.012003 ± 0.004834
V93	0.083166 ± 0.001817	0.072628 ± 0.005629
W95	0.055979 ± 0.004186	0.035386 ± 0.003707

Table 34 Comparison of the $\Delta\bar{S}^0$ obtained from the results at 300 K of the analysis of BLUU-Tramp data and conventional exchange data with the addition of an exchange constant measured at 293 K.

Residue	$\Delta\bar{C}_p^0$ BLUU-Tramp (kcal/(mol × K))	$\Delta\bar{C}_p^0$ conventional exchange (kcal/(mol × K))
Y10	0.299385 ± 0.005913	2.027322 ± 0.24712
C25	0.295762 ± 0.005206	1.659438 ± 0.291529
Y26	0.312077 ± 0.00586	2.106961 ± 0.395724
L40	0.378384 ± 0.005923	3.71729 ± 0.320242
E44	0.209622 ± 0.005396	2.265858 ± 0.288335
Y67	0.159531 ± 0.005699	2.209555 ± 0.44225
F70	0.286659 ± 0.020683	2.941128 ± 0.240823
R81	0.292599 ± 0.003684	1.871149 ± 0.295178
N83	0.271048 ± 0.0037	1.708534 ± 0.290856
L87	0.074901 ± 0.009561	0.712975 ± 0.255015
V93	0.303285 ± 0.00368	1.866166 ± 0.29694
W95	0.246186 ± 0.008237	2.112743 ± 0.195548

Table 35 Comparison of the $\Delta\bar{C}_p^0$ obtained from the results at 300 K of the analysis of BLUU-Tramp data and conventional exchange data with the addition of an exchange constant measured at 293 K.

In this case, both the $\Delta\bar{G}^0$, $\Delta\bar{H}^0$ and $\Delta\bar{S}^0$ values obtained from the conventional exchange data are more consistent with the values obtained from BLUU-Tramp data with the exception of Leucine 40, Phenylalanine 70 and Leucine 87. Furthermore, the parameter uncertainty is indeed lower than the corresponding obtained from the previously published data without the newly added point (see Table 28 and Table 32, Table 29 and Table 33, Table 30 and Table 34). The $\Delta\bar{C}_p^0$ has a lower uncertainty as well (see Table 31 and Table 35), but the values from the conventional exchange are in disagreement with the values from the BLUU-Tramp experiment. This can be explained by looking at the $\Delta\bar{G}_{EX2}^0$ values that were used as input for the minimization routine:

THE COMPARISON BETWEEN THE RESULTS FROM THE ANALYSIS OF BLUU-TRAMP DATA AND THE RESULTS FROM CONVENTIONAL ISOTOPE EXCHANGE EXPERIMENT
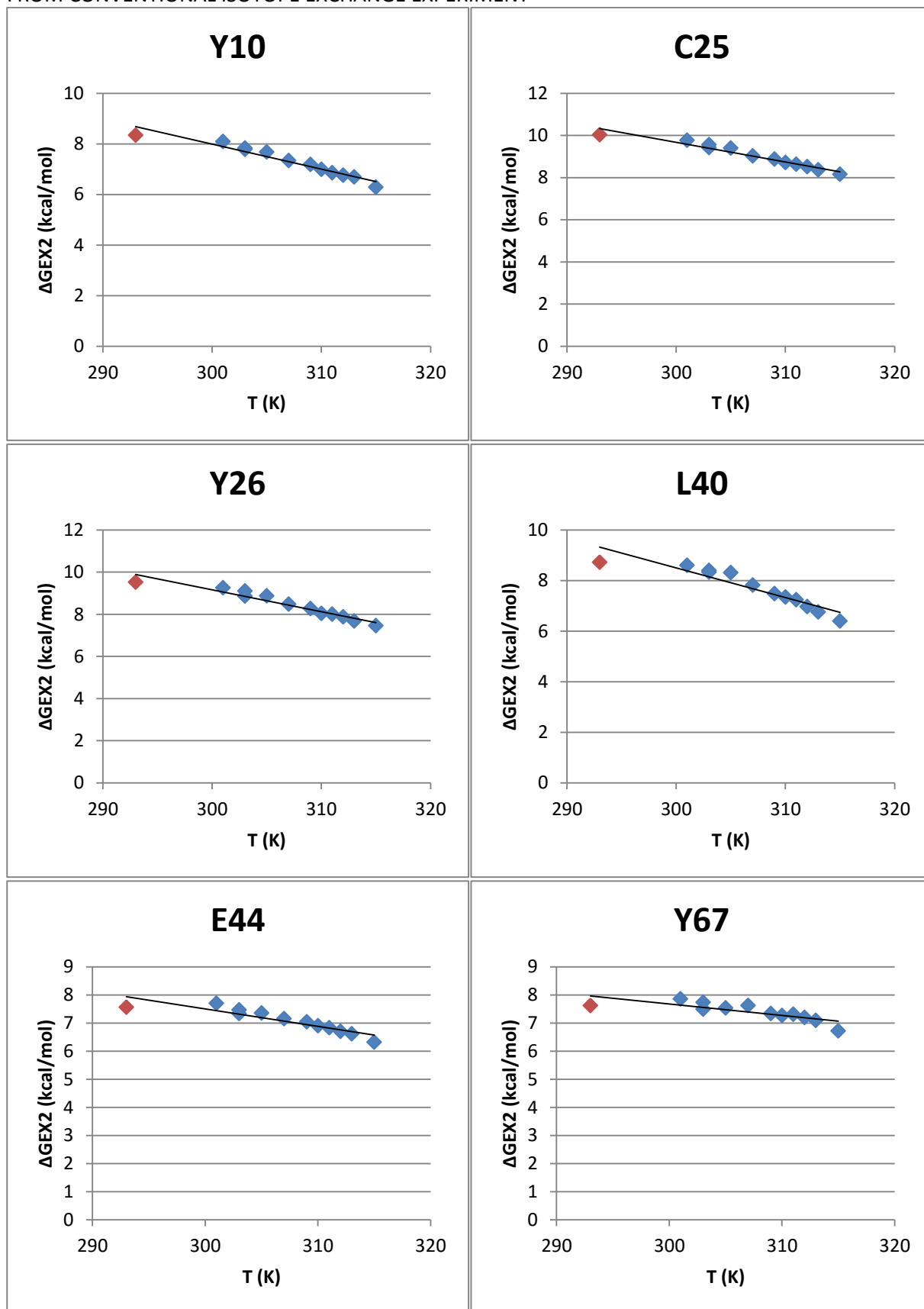
Figure 43 $\Delta \overline{G}^0_{EX2}$ **values of the first six residues of the comparison used as input for the minimization routine. The added value at 293 K is shown in red, the other values are shown in blue. A linear regression of the data has been added to show the nonlinearity forced by the added value.**

THE COMPARISON BETWEEN THE RESULTS FROM THE ANALYSIS OF BLUU-TRAMP DATA AND THE RESULTS FROM CONVENTIONAL ISOTOPE EXCHANGE EXPERIMENT
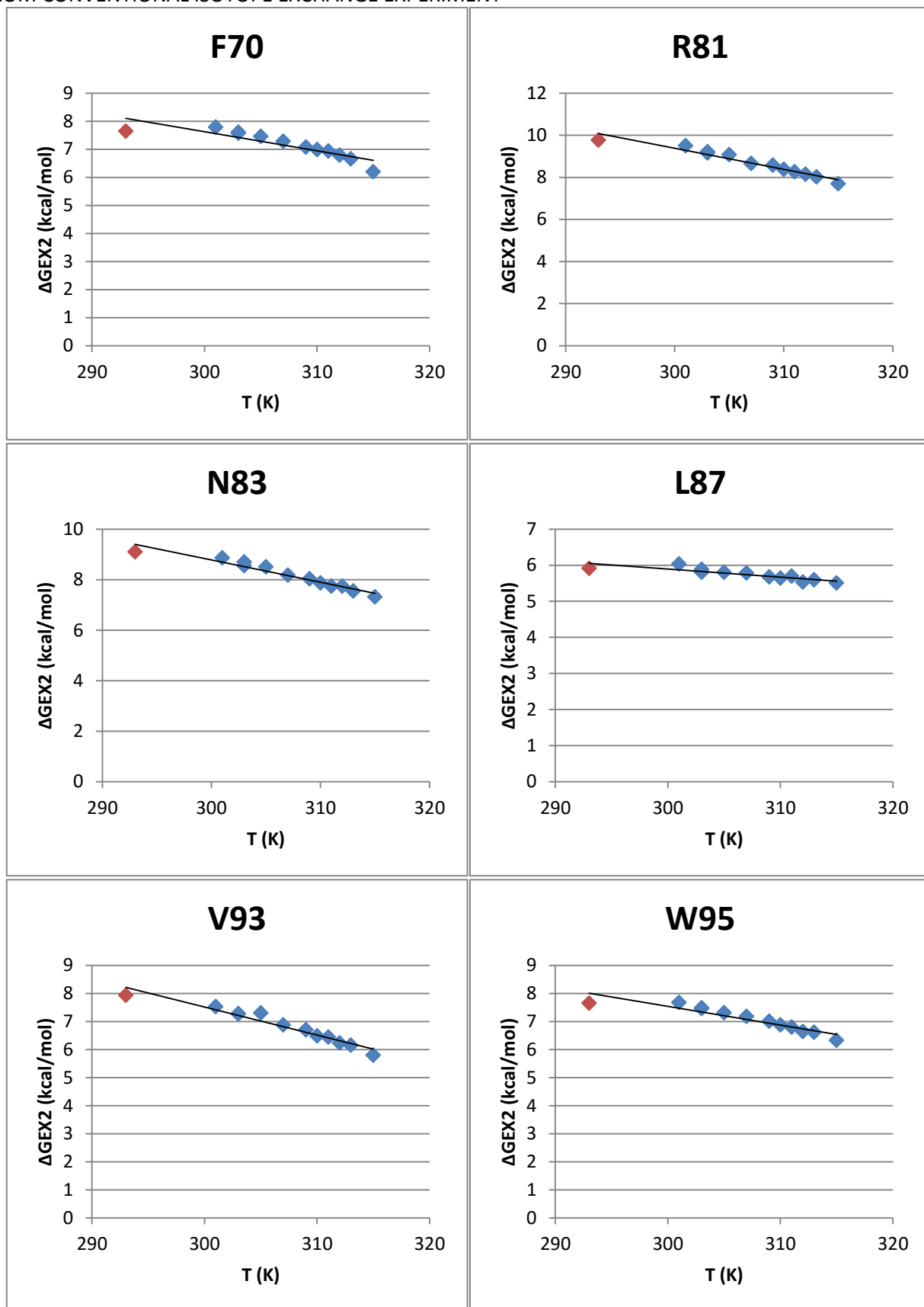
Figure 44 $\Delta\overline{G}^0_{EX2}$ values of the last six residues of the comparison used as input for the minimization routine. The added value at 293 K is shown in red, the other values are shown in blue. A linear regression of the data has been added to show the nonlinearity forced by the added value.

THE COMPARISON BETWEEN THE RESULTS FROM THE ANALYSIS OF BLUU-TRAMP DATA AND THE RESULTS FROM CONVENTIONAL ISOTOPE EXCHANGE EXPERIMENT

It is clear that the added exchange constant at 293 K leads to a $\Delta \bar{G}^0_{EX2}$ value which is consistently lower than the value expected from a linear fitting of the previous points. Since $\Delta \bar{C}^0_p$ is proportional to the second derivative of $\Delta \bar{G}^0$ with respect to temperature, this deviation introduced by the added exchange constant leads to higher values of $\Delta \bar{C}^0_p$ from the minimization routine in order to minimize the residual of the fitting. This nonlinearity is probably an artifact due to different experimental conditions or samples used, because the measured value is higher than the $\Delta \bar{C}^0_p$ measured in the global unfolding reaction, which is 1.3 ± 0.1 kcal/(mol × K)[57], with the only exception of Leucine 87. Since $\Delta \bar{C}^0_p$ is expected to have contributing terms that show additivity[58], it is not much plausible that local exchange phenomena show $\Delta \bar{C}^0_p$ values that are higher than the $\Delta \bar{C}^0_p$ value of global unfolding. On the other hand the values obtained from BLUU-Tramp data might be more correct, as local exchange events do not necessarily need the unfolding of the whole protein in order to happen, but rather only local unfolding events that, as a consequence, are expected to present a $\Delta \bar{C}^0_p$ considerably lower than that of global unfolding. Interestingly, the residues that are part of secondary structures such as β strands, typically show $\Delta \bar{C}^0_p$ values that are higher than those of the residues that are not part of secondary structures, suggesting that the $\Delta \bar{C}^0_p$ value obtained from BLUU-Tramp data might indeed be proportional to the extent of the local unfolding event needed for the exchange to take place.

CONCLUSIONS AND FUTURE PERSPECTIVES

Two routine for the analysis and estimation of $\Delta\bar{G}^0$, $\Delta\bar{H}^0$, $\Delta\bar{S}^0$ and $\Delta\bar{C}_p^0$ from decays obtained from BLUU-Tramp experiments or exchange constants from conventional isotope exchange experiments were developed.

The application of the routine for the analysis of BLUU-Tramp data to experimental data from human β_2-microglobulin and human lysozyme revealed that the estimated thermodynamic parameters appear to be correlated to the local structure where the residues occur. It also showed that secondary structures such as β strands tend to lead to a consistent range of values of $\Delta\bar{H}^0$, $\Delta\bar{S}^0$ and $\Delta\bar{C}_p^0$.

On the other hand, the routine to analyze exchange constants from conventional exchange experiments, when applied to previously published data from human β_2-microglobulin with or without the addition of an additional exchange constant measured at 293 K in order to compare the results with the results from BLUU-Tramp data, revealed how with conventional exchange experiments it is critically important to obtain as many exchange constants as possible, spanning a wide temperature range, in order to estimate $\Delta\bar{H}^0$, $\Delta\bar{S}^0$ and especially $\Delta\bar{C}_p^0$ values with low uncertainty. It also showed how nonlinearity introduced by possible artifacts heavily affects the estimation of $\Delta\bar{C}_p^0$. When comparing $\Delta\bar{G}^0$, $\Delta\bar{H}^0$ and $\Delta\bar{S}^0$ values obtained from the two methods, the results were found to be mostly in agreement with the exception of three residues.

It will be critically important to perform multiple conventional exchange experiments at different temperatures, covering a wider temperature range than the one currently covered by published data, in order to definitely confirm the validity of the results obtained from BLUU-Tramp data and to clarify whether the current correlation that exist between the $\Delta\bar{S}^0$ and $\Delta\bar{C}_p^0$ values from BLUU-Tramp experiments is an artifact or not. If the latter hypothesis is confirmed, the evaluation of other fitting functions that do not lead to the observed correlation will be needed. Nevertheless, if the validity of the results from BLUU-Tramp data is confirmed, these results might be able to give precious insight into the local structural stability and conformational flexibility of protein regions in a variety of systems.

APPENDICES

APPENDIX 1: SOURCE CODE OF THE PROGRAMS

BLUU-TRAMP DATA ANALYSIS PROGRAM

Here the actual source code of the previously described program, devoid of all comments, is presented:

```c
#include <stdio.h>

#include <stdlib.h>

#include <math.h>

#include <cminpack-1/cminpack.h>


#define MAX_RES 1024

#define CH 1024

#define MAX_N_EXP 2048

#define MA 3

#define Ea 13

#define R 0.0019872041

#define Tr 300.00


typedef struct {

        int npunti, lwa, info, ldfjac, ipvt[MA], *esperimento;

        char *nome;

        double *tempo, *temperatura, *dati, *kobs, *dskobs, *keqEX2, *deltaGEX2, *regr, *errore, eqm, x[MA],
*fvec, *fjac, *wa, krc, fnorm, covfac, covar[MA][MA], *regrDG, *dsregrDG, *regrDS, *dsregrDS, *regrDH, *dsregrDH,
*regrDCP, *dsregrDCP, a0i, a1i, a2i, kobsR, DGR, DSR, DHR, DCPR, dskobsR, dsDGR, dsDSR, dsDHR, dsDCPR;} sresiduo;


struct generale{

        int nresidui;

        double Tiniziale, derT, trc;

        };


void lettura(char *filein, sresiduo *residuo, struct generale *g);
```

```c
int fcn(void *p, int m, int n, const double *x, double *fvec, double *fjac, int ldfjac, int iflag);


double fdati[MAX_N_EXP], ftempo[MAX_N_EXP];

int main (int argc, char *argv[]){

        if (argc != 3){

                printf("uso: analisi_completa [file_in_ingresso] [intestazione_files_generati] \n");

                exit (EXIT_FAILURE);

        }

        sresiduo *residui;

        struct generale generale;

        residui = calloc(MAX_RES, sizeof (sresiduo));

        int r;

        for (r = 0; r < MAX_RES; r++){

                residui[r].nome = calloc(CH, sizeof(char));

                residui[r].esperimento = calloc(MAX_N_EXP, sizeof(int));

                residui[r].tempo = calloc(MAX_N_EXP, sizeof(double));

                residui[r].temperatura = calloc(MAX_N_EXP, sizeof(double));

                residui[r].dati = calloc(MAX_N_EXP, sizeof(double));

                residui[r].fvec = calloc(MAX_N_EXP, sizeof(double));

                residui[r].fjac = calloc(MA * MAX_N_EXP, sizeof(double));

                residui[r].wa = calloc(5 * MA * MAX_N_EXP, sizeof(double));

                residui[r].kobs = calloc(MAX_N_EXP, sizeof(double));

                residui[r].regr = calloc(MAX_N_EXP, sizeof(double));

                residui[r].errore = calloc(MAX_N_EXP, sizeof(double));

                residui[r].keqEX2 = calloc(MAX_N_EXP, sizeof(double));

                residui[r].deltaGEX2 = calloc(MAX_N_EXP, sizeof(double));

                residui[r].regrDG = calloc(MAX_N_EXP, sizeof(double));

                residui[r].regrDS = calloc(MAX_N_EXP, sizeof(double));

                residui[r].regrDH = calloc(MAX_N_EXP, sizeof(double));

                residui[r].regrDCP = calloc(MAX_N_EXP, sizeof(double));
```

APPENDIX 1: SOURCE CODE OF THE PROGRAMS

```
                    residui[r].dskobs = calloc(MAX_N_EXP, sizeof(double));

                    residui[r].dsregrDG = calloc(MAX_N_EXP, sizeof(double));

                    residui[r].dsregrDS = calloc(MAX_N_EXP, sizeof(double));

                    residui[r].dsregrDH = calloc(MAX_N_EXP, sizeof(double));

                    residui[r].dsregrDCP = calloc(MAX_N_EXP, sizeof(double));

            }

        lettura (argv[1], residui, &generale);

        double tol, tR;

        int s, o, w, y;

        tol = sqrt(__cminpack_func__(dpmpar)(1));

        for (r = 0; r < generale.nresidui; r++){

                    residui[r].x[0] = residui[r].a0i;

                    residui[r].x[1] = residui[r].a1i;

                    residui[r].x[2] = residui[r].a2i;

                    residui[r].ldfjac = residui[r].npunti;

                    residui[r].lwa = 5 * MA * residui[r].npunti;

                    for (o = 0; o < residui[r].npunti; o++){

                            fdati[o] = residui[r].dati[o];

                            ftempo[o] = residui[r].tempo[o];

                    }

                    residui[r].info = __cminpack_func__(lmder1)(fcn, &residui[r], residui[r].npunti, MA, residui[r].x,
residui[r].fvec, residui[r].fjac, residui[r].ldfjac, tol, residui[r].ipvt, residui[r].wa, residui[r].lwa);

                    residui[r].fnorm = __cminpack_func__(enorm)(residui[r].npunti, residui[r].fvec);

                    residui[r].covfac = pow(residui[r].fnorm, 2);

                    __cminpack_func__(covar1)(residui[r].npunti, MA, residui[r].covfac, residui[r].fjac, residui[r].ldfjac,
residui[r].ipvt, tol, residui[r].wa);

                    for (w = 0; w < MA; w++){

                            for (y = 0; y < MA; y++){

                                    residui[r].covar[w][y] = residui[r].fjac[w * residui[r].ldfjac + y];

                            }

                    }
```

```
                    residui[r].eqm = 0;

                    for (o = 0; o < residui[r].npunti; o++){

                            residui[r].regr[o] = residui[r].x[0] * exp(residui[r].x[1] *
exp(residui[r].x[2]*residui[r].tempo[o]));

                            residui[r].errore[o] = residui[r].dati[o] - residui[r].regr[o];

                            residui[r].eqm = residui[r].eqm + pow (residui[r].errore[o], 2.0);

                            residui[r].kobs[o] = - (residui[r].x[1] * residui[r].x[2]) * exp(residui[r].x[2] *
residui[r].tempo[o]);

                            residui[r].dskobs[o]= sqrt(pow(-(residui[r].x[2]) * exp(residui[r].x[2] * residui[r].tempo[o]),2)
* residui[r].covar[1][1] + pow((-residui[r].x[1] * exp(residui[r].x[2] * residui[r].tempo[o])) - ((residui[r].tempo[o] *
residui[r].x[1] * residui[r].x[2]) * exp(residui[r].x[2] * residui[r].tempo[o])),2) * residui[r].covar[2][2] + (2 * (-
(residui[r].x[2]) * exp(residui[r].x[2] * residui[r].tempo[o])) * ((-residui[r].x[1] * exp(residui[r].x[2] *
residui[r].tempo[o])) - ((residui[r].tempo[o] * residui[r].x[1] * residui[r].x[2]) * exp(residui[r].x[2] *
residui[r].tempo[o]))) * residui[r].covar[1][2]));

                            residui[r].keqEX2[o] = residui[r].kobs[o]/(residui[r].krc * exp(- ((Ea / R
)*((1/residui[r].temperatura[o])-(1/generale.trc)))));

                            residui[r].deltaGEX2[o] = - R * residui[r].temperatura[o] * log(residui[r].keqEX2[o]);

                            residui[r].regrDG[o] = -(R * residui[r].x[2] * pow(residui[r].temperatura[o], 2.0) /
generale.derT ) - ((R * log(-residui[r].x[1] *  residui[r].x[2] / residui[r].krc) - (Ea / generale.trc) - (R * generale.Tiniziale *
residui[r].x[2] / generale.derT)) * residui[r].temperatura[o]) - Ea;

                            residui[r].dsregrDG[o] =  sqrt((pow((- R * residui[r].temperatura[o] / residui[r].x[1]),2) *
residui[r].covar[1][1]) + (pow((((R * residui[r].temperatura[o] * generale.Tiniziale * residui[r].x[2]) - (R *
residui[r].temperatura[o] * residui[r].temperatura[o] * residui[r].x[2]) - (generale.derT * R *
residui[r].temperatura[o]))/(generale.derT * residui[r].x[2])),2) * residui[r].covar[2][2]) + (2 * (- R *
residui[r].temperatura[o] / residui[r].x[1]) * (((R * residui[r].temperatura[o] * generale.Tiniziale * residui[r].x[2]) - (R *
residui[r].temperatura[o] * residui[r].temperatura[o] * residui[r].x[2]) - (generale.derT * R *
residui[r].temperatura[o]))/(generale.derT * residui[r].x[2])) * residui[r].covar[1][2]));

                            residui[r].regrDS[o] = (2 * R * residui[r].x[2] * residui[r].temperatura[o] / generale.derT ) + R
* log(-residui[r].x[1] *  residui[r].x[2] / residui[r].krc) - (Ea / generale.trc) - (R * generale.Tiniziale * residui[r].x[2] /
generale.derT);

                            residui[r].dsregrDS[o] = sqrt((pow((R / residui[r].x[1]),2) * residui[r].covar[1][1]) + (pow((((2
* R * residui[r].temperatura[o] * residui[r].x[2]) - (R * generale.Tiniziale * residui[r].x[2])  + (generale.derT *
R))/(generale.derT * residui[r].x[2])),2) * residui[r].covar[2][2]) + (2 * (R / residui[r].x[1]) * (((2 * R *
residui[r].temperatura[o] * residui[r].x[2]) - (R * generale.Tiniziale * residui[r].x[2])  + (generale.derT *
R))/(generale.derT * residui[r].x[2])) * residui[r].covar[1][2]));

                            residui[r].regrDH[o] = (residui[r].temperatura[o] * residui[r].temperatura[o] * R *
residui[r].x[2] / generale.derT) - Ea;

                            residui[r].dsregrDH[o] = sqrt(pow(residui[r].temperatura[o] * residui[r].temperatura[o] * R /
generale.derT,2) * residui[r].covar[2][2]);

                            residui[r].regrDCP[o] = 2 * residui[r].temperatura[o] * R * residui[r].x[2] / generale.derT;
```

APPENDIX 1: SOURCE CODE OF THE PROGRAMS

```
                    residui[r].dsregrDCP[o] =  sqrt(pow(2 * residui[r].temperatura[o] * R / generale.derT,2) *
residui[r].covar[2][2]);

                }

            tR = (Tr - generale.Tiniziale)/generale.derT;

            residui[r].kobsR = - (residui[r].x[1] * residui[r].x[2]) * exp(residui[r].x[2] * tR);

            residui[r].dskobsR= sqrt(pow(-(residui[r].x[2]) * exp(residui[r].x[2] * tR),2) * residui[r].covar[1][1] +
pow((-residui[r].x[1] * exp(residui[r].x[2] * tR)) - ((tR * residui[r].x[1] * residui[r].x[2]) * exp(residui[r].x[2] * tR)),2) *
residui[r].covar[2][2] + (2 * (-(residui[r].x[2]) * exp(residui[r].x[2] * tR)) * ((-residui[r].x[1] * exp(residui[r].x[2] * tR)) -
((tR * residui[r].x[1] * residui[r].x[2]) * exp(residui[r].x[2] * tR))) * residui[r].covar[1][2]));

            residui[r].DGR = -(R * residui[r].x[2] * pow(Tr, 2.0) / generale.derT ) - ((R * log(-residui[r].x[1] *
residui[r].x[2] / residui[r].krc) - (Ea / generale.trc) - (R * generale.Tiniziale * residui[r].x[2] / generale.derT)) * Tr) - Ea;

            residui[r].DSR = (2 * R * residui[r].x[2] * Tr / generale.derT ) + R * log(-residui[r].x[1] *  residui[r].x[2]
/ residui[r].krc) - (Ea / generale.trc) - (R * generale.Tiniziale * residui[r].x[2] / generale.derT);

            residui[r].DHR = (Tr * Tr * R *residui[r].x[2] / generale.derT) - Ea;

            residui[r].DCPR = 2 * Tr * R * residui[r].x[2] / generale.derT;

            residui[r].dsDGR = sqrt((pow((- R * Tr / residui[r].x[1]),2) * residui[r].covar[1][1]) + (pow((((R * Tr *
generale.Tiniziale * residui[r].x[2]) - (R * Tr * Tr * residui[r].x[2]) - (generale.derT * R * Tr))/(generale.derT *
residui[r].x[2])),2) * residui[r].covar[2][2]) + (2 * (- R * Tr / residui[r].x[1]) * (((R * Tr * generale.Tiniziale *
residui[r].x[2]) - (R * Tr * Tr * residui[r].x[2]) - (generale.derT * R * Tr))/(generale.derT * residui[r].x[2])) *
residui[r].covar[1][2]));

            residui[r].dsDSR = sqrt((pow((R / residui[r].x[1]),2) * residui[r].covar[1][1]) + (pow((((2 * R * Tr *
residui[r].x[2]) - (R * generale.Tiniziale * residui[r].x[2])  + (generale.derT * R))/(generale.derT * residui[r].x[2])),2) *
residui[r].covar[2][2]) + (2 * (R / residui[r].x[1]) * (((2 * R * Tr * residui[r].x[2]) - (R * generale.Tiniziale * residui[r].x[2])
+ (generale.derT * R))/(generale.derT * residui[r].x[2])) * residui[r].covar[1][2]));

            residui[r].dsDHR = sqrt(pow(Tr * Tr * R / generale.derT,2) * residui[r].covar[2][2]);

            residui[r].dsDCPR = sqrt(pow(2 * Tr * R / generale.derT,2) * residui[r].covar[2][2]);

            residui[r].eqm = residui[r].eqm/residui[r].npunti;

        }

    int a, b;

    char risultato[1024];

    FILE *scrittura;

    sprintf(risultato, "%s_risultati", argv[2]);

    remove(risultato);

    printf ("temperatura iniziale %lf derivata %lf \n", generale.Tiniziale, generale.derT);

    for (a = 0; a < generale.nresidui; a++){
```

```c
                if (residui[a].info == 0){

                        printf ("Nel caso del residuo %s i parametri in ingresso non sono appropriati \n",
residui[a].nome);

                }

                else if (residui[a].info == 4){

                        printf ("Nel caso del residuo %s fvec è ortogonale alle colonne della Jacobiana \n",
residui[a].nome);

                }

                else if (residui[a].info == 5){

                        printf ("Nel caso del residuo %s fcn è stata chiamata almeno %d volte \n", residui[a].nome,
200 * (MA +1));

                }

                else if (residui[a].info == 6){

                        printf ("Nel caso del residuo %s non si riesce a ridurre la somma dei quadrati al livello
minimo indicato, %lf \n", residui[a].nome, tol);

                }

                else if (residui[a].info == 7){

                        printf ("Nel caso del residuo %s non si riesce a migliorare la soluzione approssimata fino al
limite indicato, %lf \n", residui[a].nome, tol);

                }

                else {

                        printf ("residuo %s eqm %lf x0 %lf dsx0 %lf x1 %lf dsx1 %lf x2 %lf dsx2 %lf dati a %.0f K: kobs
%lf 1/s dskobs %lf DG %lf kcal/mol dsDG %lf DH %lf kcal/mol dsDH %lf DS %lf kcal/(K x mol) dsDS %lf DCP %lf kcal/(K x
mol) dsDCP %lf\n", residui[a].nome, residui[a].eqm, residui[a].x[0], sqrt(residui[a].covar[0][0]), residui[a].x[1],
sqrt(residui[a].covar[1][1]), residui[a].x[2], sqrt(residui[a].covar[2][2]), Tr, residui[a].kobsR, residui[a].dskobsR,
residui[a].DGR, residui[a].dsDGR, residui[a].DHR, residui[a].dsDHR, residui[a].DSR, residui[a].dsDSR, residui[a].DCPR,
residui[a].dsDCPR);

                        sprintf(risultato, "%s_risultati", argv[2]);

                        scrittura = fopen (risultato, "a");

                        if (scrittura == NULL){

                                printf("uso: analisi_completa [file_in_ingresso] [intestazione_files_generati] \n");

                                exit (EXIT_FAILURE);

                        }
```

APPENDIX 1: SOURCE CODE OF THE PROGRAMS

```
                fprintf (scrittura,"residuo %s eqm %lf x0 %lf dsx0 %lf x1 %lf dsx1 %lf x2 %lf dsx2 %lf dati a
%.0f K: kobs %lf 1/s dskobs %lf DG %lf kcal/mol dsDG %lf DH %lf kcal/mol dsDH %lf DS %lf kcal/(K x mol) dsDS %lf DCP
%lf kcal/(K x mol) dsDCP %lf\n", residui[a].nome, residui[a].eqm, residui[a].x[0],  sqrt(residui[a].covar[0][0]),
residui[a].x[1], sqrt(residui[a].covar[1][1]), residui[a].x[2], sqrt(residui[a].covar[2][2]), Tr, residui[a].kobsR,
residui[a].dskobsR, residui[a].DGR, residui[a].dsDGR, residui[a].DHR, residui[a].dsDHR, residui[a].DSR,
residui[a].dsDSR, residui[a].DCPR, residui[a].dsDCPR);

                fclose (scrittura);

                sprintf(risultato, "%s_residuo%s", argv[2], residui[a].nome);

                scrittura = fopen (risultato, "w");

                if (scrittura == NULL){

                        printf("uso: analisi_completa [file_in_ingresso] [intestazione_files_generati] \n");

                        exit (EXIT_FAILURE);

                        }

                for (b = 0; b < residui[a].npunti; b++){

                        fprintf(scrittura, "%.0lf %.2lf %.6lE %.6lE %.6lE \n", residui[a].tempo[b],
residui[a].temperatura[b], residui[a].dati[b], residui[a].regr[b], residui[a].errore[b]);

                        }

                fclose (scrittura);

                sprintf(risultato, "%s_DG_residuo%s", argv[2], residui[a].nome);

                scrittura = fopen (risultato, "w");

                if (scrittura == NULL){

                        printf("uso: analisi_completa [file_in_ingresso] [intestazione_files_generati] \n");

                        exit (EXIT_FAILURE);

                        }

                for (b = 0; b < residui[a].npunti; b++){

                        fprintf(scrittura, "%.2lf %.6lE %.6lE %.6lE %.6lE %.6lE %.6lE %.6lE %.6lE %.6lE
%.6lE\n", residui[a].temperatura[b], residui[a].kobs[b], residui[a].dskobs[b], residui[a].deltaGEX2[b],
residui[a].regrDG[b], residui[a].dsregrDG[b], residui[a].regrDH[b], residui[a].dsregrDH[b], residui[a].regrDS[b],
residui[a].dsregrDS[b], residui[a].regrDCP[b], residui[a].dsregrDCP[b]);

                        }

                fclose (scrittura);

                }

        }
```

```c
        return 0;

        }


void lettura (char *filein, sresiduo *residuo, struct generale *g){

        FILE *ingresso;

        FILE *tT;

        FILE *res;

        FILE *datidecadimento;

        char *indtT, **indres, *righe, *decadimento, *tempoTEMPERATURA, *primariga, *secondariga;

        int  r, s, u, z;

        double *t, *T, derT, Tiniziale, trc;

        ingresso = fopen (filein, "r");

        if (ingresso == NULL){

                printf("uso: analisi_completa [file_in_ingresso] [intestazione_files_generati] \n");

                exit (EXIT_FAILURE);

                }

        primariga = calloc (CH, sizeof (char));

        if (fgets(primariga, CH, ingresso) != NULL){

                sscanf (primariga, "%*s" "%lf", &trc);

                }

        else{

                printf ("Errore di lettura \n");

                exit (EXIT_FAILURE);

                }

        secondariga = calloc (CH, sizeof (char));

        indtT = calloc (CH, sizeof(char));

        if (fgets(secondariga, CH, ingresso) != NULL){

                sscanf (secondariga, "%*s" "%s", indtT);

                }

        else{
```

96

```c
            printf ("Errore di lettura \n");

            exit (EXIT_FAILURE);

            }

    indres = calloc (MAX_RES, sizeof (char*));

    s = 0;

    righe = calloc (CH, sizeof(char));

    while (fgets(righe, CH, ingresso) != NULL){

            indres[s] = calloc (CH, sizeof (char));

            sscanf (righe, "%*s" "%s" "%s" "%*s" "%lf" "%*s" "%lf" "%*s" "%lf" "%*s" "%lf", residuo[s].nome,
indres[s], &(residuo[s].krc), &(residuo[s].a0i), &(residuo[s].a1i), &(residuo[s].a2i));

            s = s + 1;

            }

    tT = fopen (indtT, "r");

    tempoTEMPERATURA = calloc (CH, sizeof(char));

    t = calloc (MAX_N_EXP, sizeof (double));

    T = calloc (MAX_N_EXP, sizeof (double));

    u = 0;

    while (fgets(tempoTEMPERATURA, CH, tT) != 0){

            sscanf(tempoTEMPERATURA, "%lf" "%lf", &t[u], &T[u]);

            u = u + 1;

            }

    printf ("Letto file tT \n");

    decadimento = calloc (CH, sizeof(char));

    for (r = 0; r < s; r++){

            z = 0;

            residuo[r].npunti = 0;

            datidecadimento = fopen(indres[r], "r");

            while (fgets(decadimento, CH, datidecadimento) != 0){

                    sscanf(decadimento, "%d" "%lf", &residuo[r].esperimento[z], &residuo[r].dati[z]);

                    residuo[r].esperimento[z] = residuo[r].esperimento[z] - 1;
```

```c
                    residuo[r].tempo[z] = t[residuo[r].esperimento[z]];

                    residuo[r].temperatura[z] = T[residuo[r].esperimento[z]];

                    residuo[r].npunti = residuo[r].npunti + 1;

                    z = z + 1;

                    }

            if (residuo[r].npunti <= 1){

                    printf ("Errore con il decadimento di %s. I decadimenti devono consistere di almeno due
punti per poter essere trattati \n", residuo[r].nome);

                    exit (EXIT_FAILURE);

                    }

            printf ("Letto residuo %s \n", residuo[r].nome);

            }

    (*g).nresidui = s;

    (*g).derT = (T[u-1]-T[0])/(t[u-1]-t[0]);

    (*g).Tiniziale = T[0];

    (*g).trc = trc;

    return;

    }


int fcn(void *p, int m, int n, const double *x, double *fvec, double *fjac, int ldfjac, int iflag){

    int i;

    if ( iflag != 2 ) {

            for ( i = 0; i < m; i++){

                    fvec[i] = fdati[i] - x[0] * exp(x[1] * exp(x[2] * ftempo[i]));

                    }

            }

    else{

            for ( i = 0; i < m; i++){

                    fjac[i + ldfjac * 0] = - exp(x[1] * exp(x[2] * ftempo[i]));

                    fjac[i + ldfjac * 1] = - x[0] * exp(x[1] * exp(x[2] * (ftempo[i]))) * exp(x[2] * (ftempo[i]));
```

APPENDIX 1: SOURCE CODE OF THE PROGRAMS

```
                    fjac[i + ldfjac * 2] = - x[0] * exp(x[1] * exp(x[2] * (ftempo[i]))) * x[1] * exp(x[2] * (ftempo[i]))
* (ftempo[i]);

                    }

            }

        return 0;

        }
```

APPENDICES

APPENDIX 1: SOURCE CODE OF THE PROGRAMS

CONVENTIONAL EXCHANGE ANALYSIS PROGRAM

Here the source code of the routine, devoid of the comments, is presented:

```c
#include <stdio.h>

#include <stdlib.h>

#include <math.h>

#include <cminpack-1/cminpack.h>


#define MAX_RES 512

#define CH 512

#define MAX_N_EXP 512

#define MA 3

#define Ea 13.00

#define R 0.0019872041

#define Tr 300.00

#define trc 293.00


typedef struct {

        int locale, npunti, info, ldfjac, lwa, ipvt[MA];

        char *nome;

        double *temperatura, a0i, a1i, a2i, *kobs, *keqEX2, *deltaGEX2, *regr, *errore, *sigma, *sigmaDG, eqm,
x[MA], *fvec, *fjac, *wa, fnorm, covfac, covar[MA][MA], krc, *regrDG, *dsregrDG, *regrDS, *dsregrDS, *regrDH,
*dsregrDH, *regrDCP, *dsregrDCP, DGR, DHR, DSR, DCPR, dsDGR, dsDHR, dsDSR, dsDCPR;} sresiduo;


void lettura(char *filein, sresiduo *residuo, int *nresidui);

int fcn(void *p, int m, int n, const double *x, double *fvec, double *fjac, int ldfjac, int iflag);

double fdati[MAX_N_EXP], ftemperatura[MAX_N_EXP];


int main (int argc, char *argv[]){

        if (argc != 3){

                printf("uso: analisi_completa [file_in_ingresso] [intestazione_files_generati] \n");

                exit (EXIT_FAILURE);
```

APPENDIX 1: SOURCE CODE OF THE PROGRAMS

```
        }
sresiduo *residui;

residui = calloc(MAX_RES, sizeof (sresiduo));

int j, nresidui;

double (tol);

for (j = 0; j < MAX_RES; j++){

        residui[j].nome = calloc(CH, sizeof(char));

        residui[j].temperatura = calloc(MAX_N_EXP, sizeof(double));

        residui[j].kobs = calloc(MAX_N_EXP, sizeof(double));

        residui[j].regr = calloc(MAX_N_EXP, sizeof(double));

        residui[j].errore = calloc(MAX_N_EXP, sizeof(double));

        residui[j].sigma = calloc(MAX_N_EXP, sizeof(double));

        residui[j].sigmaDG = calloc(MAX_N_EXP, sizeof(double));

        residui[j].fvec = calloc(MAX_N_EXP, sizeof(double));

        residui[j].fjac = calloc(MA * MAX_N_EXP, sizeof(double));

        residui[j].wa = calloc(5 * MA * MAX_N_EXP, sizeof(double));

        residui[j].keqEX2 = calloc(MAX_N_EXP, sizeof(double));

        residui[j].deltaGEX2 = calloc(MAX_N_EXP, sizeof(double));

        residui[j].regrDG = calloc(MAX_N_EXP, sizeof(double));

        residui[j].regrDH = calloc(MAX_N_EXP, sizeof(double));

        residui[j].regrDS = calloc(MAX_N_EXP, sizeof(double));

        residui[j].regrDCP = calloc(MAX_N_EXP, sizeof(double));

        residui[j].dsregrDG = calloc(MAX_N_EXP, sizeof(double));

        residui[j].dsregrDH = calloc(MAX_N_EXP, sizeof(double));

        residui[j].dsregrDS = calloc(MAX_N_EXP, sizeof(double));

        residui[j].dsregrDCP = calloc(MAX_N_EXP, sizeof(double));

        }
lettura (argv[1], residui, &nresidui);

tol = sqrt(__cminpack_func__(dpmpar)(1));

int o, w, y;
```

```
        for (j = 0; j < nresidui; j++){

                /*printf("residuo %d parte 2 \n", m+1);*/

                for (o = 0; o < residui[j].npunti; o++){

                        residui[j].keqEX2[o] = residui[j].kobs[o] / (residui[j].krc * exp(-((Ea / R) * ((1 /
residui[j].temperatura[o]) - (1 / trc)))));

                        residui[j].deltaGEX2[o] = - R * residui[j].temperatura[o] * log(residui[j].keqEX2[o]);

                        fdati[o] = residui[j].deltaGEX2[o];

                        ftemperatura[o] = residui[j].temperatura[o];

                        residui[j].sigmaDG[o] = sqrt( pow(-R * residui[j].temperatura[o] * residui[j].sigma[o] /
residui[j].kobs[o], 2));

                }

        residui[j].x[0] = residui[j].a0i;

        residui[j].x[1] = residui[j].a1i;

        residui[j].x[2] = residui[j].a2i;

        residui[j].ldfjac = residui[j].npunti;

        residui[j].lwa = 5 * MA * residui[j].npunti;

        residui[j].info = __cminpack_func__(lmder1)(fcn, &residui[j], residui[j].npunti, MA, residui[j].x,
residui[j].fvec, residui[j].fjac, residui[j].ldfjac, tol, residui[j].ipvt, residui[j].wa, residui[j].lwa);

        residui[j].fnorm = __cminpack_func__(enorm)(residui[j].npunti, residui[j].fvec);

        residui[j].covfac = pow(residui[j].fnorm, 2);

        __cminpack_func__(covar1)(residui[j].npunti, MA, residui[j].covfac, residui[j].fjac, residui[j].ldfjac,
residui[j].ipvt, tol, residui[j].wa);

        for (w = 0; w < MA; w++){

                for (y = 0; y < MA; y++){

                        residui[j].covar[w][y] = residui[j].fjac[w * residui[j].ldfjac + y];

                }

        }

        residui[j].eqm = 0;

        for (o = 0; o < residui[j].npunti; o++){

                residui[j].regr[o] = residui[j].x[0] - (residui[j].temperatura[o] * residui[j].x[1]) + residui[j].x[2]
* (residui[j].temperatura[o] - Tr - (residui[j].temperatura[o] * log(residui[j].temperatura[o]/Tr)));

                residui[j].errore[o] = residui[j].deltaGEX2[o] - residui[j].regr[o];
```

APPENDIX 1: SOURCE CODE OF THE PROGRAMS

```
                    residui[j].eqm = residui[j].eqm + pow (residui[j].errore[o], 2.0);

                    residui[j].regrDG[o] = residui[j].regr[o];

                    residui[j].dsregrDG[o] = sqrt(residui[j].covar[0][0] + (pow(-residui[j].temperatura[o], 2) *
residui[j].covar[1][1]) + (pow(residui[j].temperatura[o] - Tr - (residui[j].temperatura[o] *
log(residui[j].temperatura[o]/Tr)), 2) * residui[j].covar[2][2]) + (2 * (-residui[j].temperatura[o]) * residui[j].covar[0][1])
+ (2 * (residui[j].temperatura[o] - Tr - (residui[j].temperatura[o] * log(residui[j].temperatura[o]/Tr))) *
residui[j].covar[0][2]) + (2 * (-residui[j].temperatura[o]) * (residui[j].temperatura[o] - Tr - (residui[j].temperatura[o] *
log(residui[j].temperatura[o]/Tr))) * residui[j].covar[1][2]));

                        residui[j].regrDS[o] = residui[j].x[1] + (residui[j].x[2] * log(residui[j].temperatura[o]/Tr));

                        residui[j].dsregrDS[o] = sqrt(residui[j].covar[1][1] + (pow(log(residui[j].temperatura[o]/Tr),
2) * residui[j].covar[2][2]) + (2 * log(residui[j].temperatura[o]/Tr) * residui[j].covar[1][2]));

                        residui[j].regrDH[o] = residui[j].x[0] + (residui[j].x[2] * (residui[j].temperatura[o] - Tr));

                        residui[j].dsregrDH[o] =  sqrt(residui[j].covar[0][0] + (pow(residui[j].temperatura[o] - Tr, 2) *
residui[j].covar[2][2]) + (2 * (residui[j].temperatura[o] - Tr) * residui[j].covar[0][2]));

                        residui[j].regrDCP[o] =residui[j].x[2];

                        residui[j].dsregrDCP[o] = sqrt(residui[j].covar[2][2]);

                        }

                residui[j].DGR = residui[j].x[0] - (Tr * residui[j].x[1]);

                residui[j].DSR = residui[j].x[1];

                residui[j].DHR = residui[j].x[0];

                residui[j].DCPR = residui[j].x[2];

                residui[j].dsDGR =  sqrt(residui[j].covar[0][0] + (pow(-Tr,2) * residui[j].covar[1][1]) + (-2 * Tr *
residui[j].covar[0][1]));

                residui[j].dsDHR = sqrt(residui[j].covar[0][0]);

                residui[j].dsDSR =  sqrt(residui[j].covar[1][1]);

                residui[j].dsDCPR = sqrt(residui[j].covar[2][2]);

                residui[j].eqm = residui[j].eqm/residui[j].npunti;

                }

        int a, b;

        char risultato[1024];

        FILE *scrittura;

        sprintf(risultato, "%s_risultati", argv[2]);

        remove(risultato);
```

```
        for (a = 0; a < nresidui; a++){

                if (residui[a].info == 0){

                        printf ("Nel caso del residuo %s i parametri in ingresso non sono appropriati \n",
residui[a].nome);

                }

                else if (residui[a].info == 4){

                        printf ("Nel caso del residuo %s fvec è ortogonale alle colonne della Jacobiana \n",
residui[a].nome);

                }

                else if (residui[a].info == 5){

                        printf ("Nel caso del residuo %s fcn è stata chiamata almeno %d volte \n", residui[a].nome,
200 * (MA +1));

                }

                else if (residui[a].info == 6){

                        printf ("Nel caso del residuo %s non si riesce a ridurre la somma dei quadrati al livello
minimo indicato, %lf \n", residui[a].nome, tol);

                }

                else if (residui[a].info == 7){

                        printf ("Nel caso del residuo %s non si riesce a migliorare la soluzione approssimata fino al
limite indicato, %lf \n", residui[a].nome, tol);

                }

                else {

                        printf ("residuo %s eqm %lf a0 %lf dsa0 %lf a1 %lf dsa1 %lf a2 %lf dsa2 %lf dati a %.0f K: DG
%lf kcal/mol dsDG %lf DH %lf kcal/mol dsDH %lf DS %lf kcal/(K x mol) dsDS %lf DCP %lf kcal/(K x mol) dsDCP %lf\n",
residui[a].nome, residui[a].eqm, residui[a].x[0], sqrt(residui[a].covar[0][0]), residui[a].x[1], sqrt(residui[a].covar[1][1]),
residui[a].x[2], sqrt(residui[a].covar[2][2]), Tr, residui[a].DGR, residui[a].dsDGR, residui[a].DHR, residui[a].dsDHR,
residui[a].DSR, residui[a].dsDSR, residui[a].DCPR, residui[a].dsDCPR);

                        sprintf(risultato, "%s_risultati", argv[2]);

                        scrittura = fopen (risultato, "a");

                        if (scrittura == NULL){

                                printf("uso: analisi_completa [file_in_ingresso] [intestazione_files_generati] \n");

                                exit (EXIT_FAILURE);

                        }
```

APPENDIX 1: SOURCE CODE OF THE PROGRAMS

```c
                fprintf (scrittura,"residuo %s eqm %lf a0 %lf dsa0 %lf a1 %lf dsa1 %lf a2 %lf dsa2 %lf dati a
%.0f K: DG %lf kcal/mol dsDG %lf DH %lf kcal/mol dsDH %lf DS %lf kcal/(K x mol) dsDS %lf DCP %lf kcal/(K x mol) dsDCP
%lf\n", residui[a].nome, residui[a].eqm, residui[a].x[0], sqrt(residui[a].covar[0][0]),residui[a].x[1],
sqrt(residui[a].covar[1][1]), residui[a].x[2], sqrt(residui[a].covar[2][2]), Tr, residui[a].DGR, residui[a].dsDGR,
residui[a].DHR, residui[a].dsDHR, residui[a].DSR, residui[a].dsDSR, residui[a].DCPR, residui[a].dsDCPR);

                fclose (scrittura);

                sprintf(risultato, "%s_residuo%s", argv[2], residui[a].nome);

                scrittura = fopen (risultato, "w");

                if (scrittura == NULL){

                        printf("uso: analisi_completa [file_in_ingresso] [intestazione_files_generati] \n");

                        exit (EXIT_FAILURE);

                        }

                for (b = 0; b < residui[a].npunti; b++){

                        fprintf(scrittura, "%.2lf %.6lE %.6lE %.6lE %.6lE \n", residui[a].temperatura[b],
residui[a].kobs[b], residui[a].keqEX2[b], residui[a].deltaGEX2[b], residui[a].regr[b], residui[a].errore[b]);

                        }

                fclose (scrittura);

                sprintf(risultato, "%s_DG_residuo%s", argv[2], residui[a].nome);

                scrittura = fopen (risultato, "w");

                if (scrittura == NULL){

                        printf("uso: analisi_completa [file_in_ingresso] [intestazione_files_generati] \n");

                        exit (EXIT_FAILURE);

                        }

                for (b = 0; b < residui[a].npunti; b++){

                        fprintf(scrittura, "%.2lf %.6lE %.6lE %.6lE %.6lE %.6lE %.6lE %.6lE %.6lE
%.6lE\n", residui[a].temperatura[b], residui[a].deltaGEX2[b], residui[a].sigmaDG[b], residui[a].regrDG[b],
residui[a].dsregrDG[b], residui[a].regrDH[b], residui[a].dsregrDH[b], residui[a].regrDS[b], residui[a].dsregrDS[b],
residui[a].regrDCP[b], residui[a].dsregrDCP[b]);

                        }

                fclose (scrittura);

                }

        }

    return 0;
```

```
        }


void lettura (char *filein, sresiduo *residuo, int *nresidui){

        FILE *ingresso;

        FILE *datidecadimento;

        char **indres, *righe, *decadimento;

        int  q, r, s;

        ingresso = fopen (filein, "r");

        if (ingresso == NULL){

                printf("uso: analisi_completa [file_in_ingresso] [intestazione_files_generati] \n");

                exit (EXIT_FAILURE);

                }

        indres = calloc (MAX_RES, sizeof (char*));

        r = 0;

        righe = calloc (CH, sizeof(char));

        while (fgets(righe, CH, ingresso) != NULL){

                indres[r] = calloc (CH, sizeof (char));

                sscanf (righe, "%*s" "%s" "%s" "%*s" "%lf" "%*s" "%lf" "%*s" "%lf" "%*s" "%lf", residuo[r].nome,
indres[r], &(residuo[r].krc), &(residuo[s].a0i), &(residuo[s].a1i), &(residuo[s].a2i));

                r = r + 1;

                }

        decadimento = calloc (CH, sizeof(char));

        for (q = 0; q < r; q++){

                s = 0;

                residuo[q].npunti = 0;

                datidecadimento = fopen(indres[q], "r");

                while (fgets(decadimento, CH, datidecadimento) != 0){

                        sscanf(decadimento, "%lf" "%lf" "%lf", &(residuo[q].temperatura[s]), &(residuo[q].kobs[s]),
&(residuo[q].sigma[s]));

                        s = s + 1;

                        residuo[q].npunti = residuo[q].npunti + 1;
```

APPENDIX 1: SOURCE CODE OF THE PROGRAMS

```c
                    }

            if (residuo[q].npunti <= 1){

                    printf ("Errore con il decadimento di %s. I decadimenti devono consistere di almeno due
punti per poter essere trattati \n", residuo[q].nome);

                    exit (EXIT_FAILURE);

                    }

            }

    *nresidui = r;

    return;

    }


int fcn(void *p, int m, int n, const double *x, double *fvec, double *fjac, int ldfjac, int iflag){

    int i;

    if ( iflag != 2 ) {

            for ( i = 0; i < m; i++){

                    fvec[i] = fdati[i] - (x[0] - (ftemperatura[i] * x[1]) + x[2] * (ftemperatura[i] - Tr -
(ftemperatura[i] * log(ftemperatura[i]/Tr))));

                    }

            }

    else{

            for ( i = 0; i < m; i++){

                    fjac[i + ldfjac * 0] = -1;

                    fjac[i + ldfjac * 1] = ftemperatura[i];

                    fjac[i + ldfjac * 2] = -(ftemperatura[i] - Tr -(ftemperatura[i] * log(ftemperatura[i]/Tr)));

                    }

            }

    return 0;

    }
```

APPENDIX 2: HUMAN β₂-MICROGLOBULIN MUTANT FORM D76N BLUU-TRAMP EXPERIMENT

An attempt at performing a BLUU-Tramp experiment on the mutant form D76N of human β₂-microglobulin was made, but problems with the intensity of the peaks in the exchange ramp emerged, prompting a correction based on assumptions yet to be verified. Therefore, the data relative to this form are only indicative.

SAMPLE USED

The protein used presents a methionine added at the N-terminal. The protein was deuterated and lyophilized. By adding an aqueous solution containing phosphate buffer and D_2O, a 550 μl aqueous sample having a pH of 7.17 and containing the ^{15}N-enriched D76N mutant form of human β₂-microglobulin at a concentration of 279 μM, along with D_2O at a concentration of 5% v/v and phosphate buffer at a concentration of 20 mM was prepared and put in an NMR samples tube for the BLUU-Tramp experiment. The tube was inserted in an NMR spectrometer and the acquisition was started 276 seconds after the addition of the protein to the aqueous solution.

ACQUISITION

191 best-TROSY[48],[49] experiments with sensitivity improvement and using Echo-Antiecho to obtain quadrature detection in the indirect dimension were performed per temperature ramp. The starting temperature was 283 K and the temperature was increased by 0.18 K between one experiment and the next. The overall temperature range was therefore 283 K – 302.1 K. After increasing the temperature, at most 50 seconds of delay were introduced to allow equilibration at the new temperature.

The parameters used in the acquisition were the following:

PARAMETER	F1 (^{15}N)	F2 (^{1}H)
Number of dummy scans		32
Number of scans		32
Number of points	80	768
Base Frequency (MHz)	60.810645	600.13
Offset (Hz)	7175.66	2818.2
Spectral Width (Hz)	1946.28260023355	9009.00900900901

PROCESSING

After being converted in the NMRPipe input format, the raw data was processed with NMRPipe[54] using the following parameters:

PARAMETER	F1 (^{15}N)	F2 (^{1}H)
Baseline correction	4th order polynomial subtract (only in the Frequency Domain)	4th order polynomial subtract (both in the Time Domain and Frequency Domain)
Window Function	Gaussian with g1= 10 and g2=25	Gaussian with g1= 10 and g2=25 and c=0.5
Linear prediction	Forward-backward linear prediction, 80 more points predicted	none
Number of points after zero filling	1024	1536

APPENDIX 2: HUMAN β2-MICROGLOBULIN MUTANT FORM D76N BLUU-TRAMP EXPERIMENT

ANALYSIS

The processed data were analyzed using the TinT routine. A peculiar behavior of the intensity of the peaks in the exchange ramp was observed, in that the intensity is higher in the exchange ramp until a certain temperature is reached. After that temperature, the intensity gradually decreases until it becomes of the same magnitude as the intensity in the reference ramp.
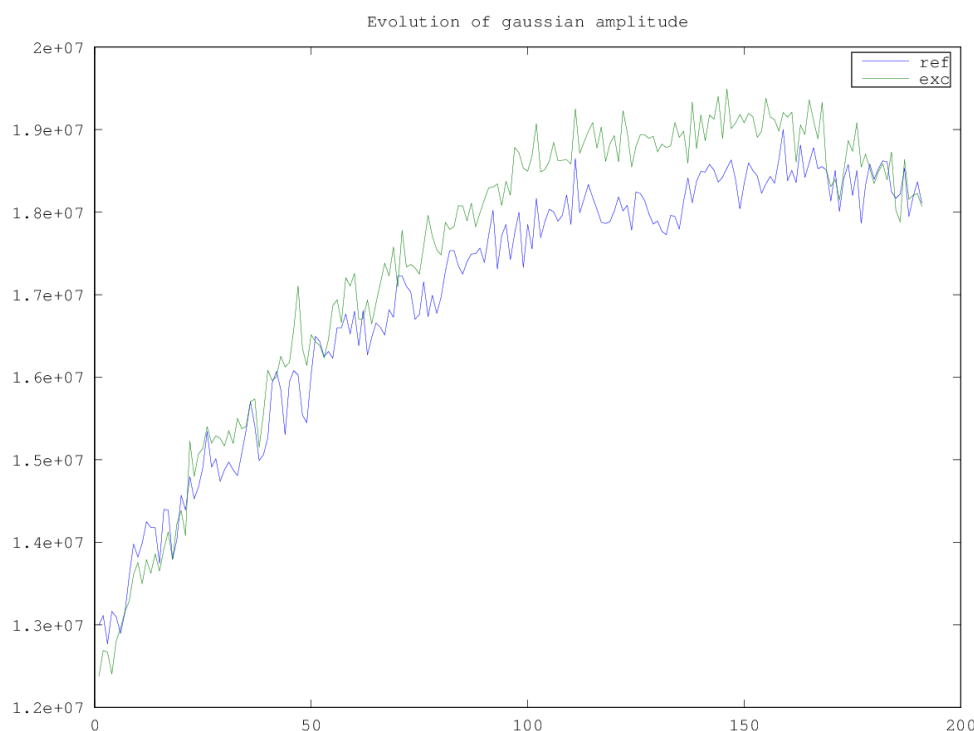

Figure 45 The intensity profile of the amide peak of residue D98 in both the exchange ramp (green) and the reference ramp (blue) as an example of the observed behavior. The horizontal axis represents the number of the spectrum at which the intensity was measured, while the vertical axis represents the intensity measured in arbitrary units.

This was interpreted as a precipitation phenomenon occurring only in the late phase of the exchange ramp and not in the reference ramp. Unfortunately, it was not possible to experimentally verify this hypothesis.

To correct this bias, the ratio between the intensity the exchange ramp versus the intensity of the reference ramp was estimated using a minimization routine in all the decays, the largest value was found and the intensity in the reference ramp was multiplied by this value. Furthermore, only the first 125 spectra of both ramps were considered in the subsequent analysis.

The obtained decays were then calculated and assigned using Sparky[55].

RESULTS

In this and in the following section the values reported in the tables retain the figures obtained from fitting and calculations, with the actual number of significant figures being three at most, except for temperature values known to an accuracy of four significant figures.

From the analysis the thermodynamic parameters of 20 residues were obtained. The results are summarized in the following tables and graphs.

APPENDIX 2: HUMAN β2-MICROGLOBULIN MUTANT FORM D76N BLUU-TRAMP EXPERIMENT

Residue	$\Delta \bar{G}^0$ (kcal/mol)	$\Delta \bar{H}^0$ (kcal/mol)	$\Delta \bar{S}^0$ (kcal/(mol × K))	$\Delta \bar{C}_p^0$ (kcal/(mol × K))
Y10	7.316314 ± 0.073865	17.450617 ± 2.250547	0.033781 ± 0.007745	0.203004 ± 0.015004
F22	6.90709 ± 0.060414	-0.871911 ± 0.584781	-0.02593 ± 0.002151	0.080854 ± 0.003899
C25	9.143374 ± 0.062821	12.344703 ± 1.844744	0.010671 ± 0.006356	0.168965 ± 0.012298
Y26	8.347078 ± 0.107727	13.72887 ± 3.247952	0.017939 ± 0.011181	0.178192 ± 0.021653
L40	7.323636 ± 0.086922	8.661078 ± 2.582355	0.004458 ± 0.008894	0.144407 ± 0.017216
K41	7.486839 ± 0.059366	17.976407 ± 1.806928	0.034965 ± 0.006218	0.206509 ± 0.012046
E44	5.445308 ± 0.186226	25.762261 ± 3.851504	0.067723 ± 0.013458	0.258415 ± 0.025677
V49	6.683935 ± 0.83114	8.774471 ± 24.137679	0.006968 ± 0.083205	0.145163 ± 0.160918
Y67	7.035555 ± 0.059148	7.19528 ± 1.422468	0.000532 ± 0.004937	0.134635 ± 0.009483
T68	7.075936 ± 0.049585	16.533731 ± 1.26666	0.031526 ± 0.004386	0.196892 ± 0.008444
F70	6.671061 ± 0.062541	9.821402 ± 1.497556	0.010501 ± 0.005199	0.152143 ± 0.009984
E77	6.613335 ± 1.223491	5.620934 ± 25.277805	-0.003308 ± 0.088327	0.12414 ± 0.168519
A79	7.98919 ± 0.05638	16.230953 ± 1.707631	0.027473 ± 0.005878	0.194873 ± 0.011384
C80	6.814769 ± 0.965433	90.618484 ± 40.054027	0.279346 ± 0.136704	0.69079 ± 0.267027
R81	8.686849 ± 0.055386	14.014054 ± 1.650367	0.017757 ± 0.005684	0.180094 ± 0.011002
V82	7.622254 ± 0.060754	6.498621 ± 1.756904	-0.003745 ± 0.006056	0.129991 ± 0.011713
N83	8.365878 ± 0.050026	13.209567 ± 1.468804	0.016146 ± 0.005061	0.17473 ± 0.009792
K91	6.119254 ± 0.025169	7.082009 ± 0.302969	0.003209 ± 0.001094	0.13388 ± 0.00202
V93	6.821477 ± 0.052953	10.677008 ± 1.558297	0.012852 ± 0.005369	0.157847 ± 0.010389
W95	6.639875 ± 0.068933	13.713964 ± 1.654285	0.02358 ± 0.005742	0.178093 ± 0.011029

Table 36 Results of the analysis on the BLUU-Tramp experiment performed on the β₂-microglobulin mutant form D76N. Data are reported as value ± standard deviation and are relative to the reference temperature of 300 K.

Residue	Lowest Temperature			Reference Temperature			Highest Temperature		
	T (K)	$\Delta \bar{G}^0$ (kcal/mol)	$\sigma_{\Delta \bar{G}^0}$ (kcal/mol)	T (K)	$\Delta \bar{G}^0$ (kcal/mol)	$\sigma_{\Delta \bar{G}^0}$ (kcal/mol)	T (K)	$\Delta \bar{G}^0$ (kcal/mol)	$\sigma_{\Delta \bar{G}^0}$ (kcal/mol)
Y10	283	7.792811	0.052759	300	7.316314	0.073865	295.4	7.464547	0.039583
F22	283	6.427335	0.025752	300	6.90709	0.060414	295.4	6.78496	0.050662
C25	283	9.243398	0.041223	300	9.143374	0.062821	295.4	9.186502	0.034653
Y26	283	8.566217	0.075096	300	8.347078	0.107727	295.4	8.423314	0.058202
L40	283	7.329868	0.05853	300	7.323636	0.086922	295.4	7.33905	0.047492
K41	283	7.981779	0.042307	300	7.486839	0.059366	295.4	7.640396	0.031841
E44	283	6.472132	0.032849	300	5.445308	0.186226	295.4	5.747722	0.125415
V49	285.3	6.734091	0.357814	300	6.683935	0.83114	295.4	6.710871	0.459914
Y67	283	6.979757	0.02208	300	7.035555	0.059148	295.4	7.033256	0.037074
T68	283	7.517041	0.022518	300	7.075936	0.049585	295.4	7.214012	0.03004
F70	283	6.776298	0.022954	300	6.671061	0.062541	295.4	6.714	0.039286
E77	283	6.497305	0.218475	300	6.613335	1.223491	295.4	6.59374	0.824672
A79	283	8.36236	0.039729	300	7.98919	0.05638	295.4	8.108691	0.030357
C80	283	11.230916	1.244355	300	6.814769	0.965433	295.4	8.075397	0.360317
R81	283	8.901979	0.037602	300	8.686849	0.055386	295.4	8.762181	0.03021
V82	283	7.495969	0.038389	300	7.622254	0.060754	295.4	7.600441	0.033884
N83	283	8.556192	0.032823	300	8.365878	0.050026	295.4	8.433986	0.0276
K91	283	6.109325	0.007584	300	6.119254	0.025169	295.4	6.129295	0.020213
V93	283	6.963927	0.034904	300	6.821477	0.052953	295.4	6.875028	0.029155
W95	283	6.954959	0.025441	300	6.639875	0.068933	295.4	6.742064	0.043239

Table 37 $\Delta \bar{G}^0$ of the amide sites of β₂-microglobulin mutant form D76N at various temperatures.

APPENDIX 2: HUMAN β2-MICROGLOBULIN MUTANT FORM D76N BLUU-TRAMP EXPERIMENT

Residue	Lowest Temperature			Reference Temperature			Highest Temperature		
	T (K)	$\Delta\bar{H}^0$ (kcal/mol)	$\sigma_{\Delta\bar{H}^o}$ (kcal/mol)	T (K)	$\Delta\bar{H}^0$ (kcal/mol)	$\sigma_{\Delta\bar{H}^o}$ (kcal/mol)	T (K)	$\Delta\bar{H}^0$ (kcal/mol)	$\sigma_{\Delta\bar{H}^o}$ (kcal/mol)
Y10	283	14.097327	2.002711	300	17.450617	2.250547	295.4	16.523957	2.182059
F22	283	-2.207483	0.520383	300	-0.871911	0.584781	295.4	-1.240988	0.566985
C25	283	9.553688	1.641597	300	12.344703	1.844744	295.4	11.573424	1.788606
Y26	283	10.785427	2.890281	300	13.72887	3.247952	295.4	12.915469	3.149112
L40	283	6.275712	2.29798	300	8.661078	2.582355	295.4	8.001898	2.50377
K41	283	14.565216	1.607945	300	17.976407	1.806928	295.4	17.033747	1.751941
E44	283	21.493674	3.427368	300	25.762261	3.851504	295.4	24.582665	3.734297
V49	285.3	6.692853	21.830141	300	8.774471	24.137679	295.4	8.11184	23.403132
Y67	283	4.971331	1.265823	300	7.19528	1.422468	295.4	6.580706	1.37918
T68	283	13.281411	1.127173	300	16.533731	1.26666	295.4	15.634973	1.228113
F70	283	7.308259	1.332642	300	9.821402	1.497556	295.4	9.126912	1.451983
E77	283	3.570355	22.494157	300	5.620934	25.277805	295.4	5.05427	24.508562
A79	283	13.011976	1.519583	300	16.230953	1.707631	295.4	15.34141	1.655666
C80	283	79.207786	35.643188	300	90.618484	40.054027	295.4	87.465212	38.83512
R81	283	11.039207	1.468625	300	14.014054	1.650367	295.4	13.191975	1.600144
V82	283	4.35139	1.56343	300	6.498621	1.756904	295.4	5.905248	1.703438
N83	283	10.323311	1.307056	300	13.209567	1.468804	295.4	12.411969	1.424106
K91	283	4.870534	0.269605	300	7.082009	0.302969	295.4	6.470882	0.293749
V93	283	8.069644	1.386694	300	10.677008	1.558297	295.4	9.95648	1.510876
W95	283	10.772163	1.472112	300	13.713964	1.654285	295.4	12.901017	1.603943

Table 38 $\Delta\bar{H}^0$ of the amide sites of β₂-microglobulin mutant form D76N at various temperatures.

APPENDIX 2: HUMAN β2-MICROGLOBULIN MUTANT FORM D76N BLUU-TRAMP EXPERIMENT

Residue	Lowest Temperature			Reference Temperature			Highest Temperature		
	T (K)	$\Delta \bar{S}^0$ (kcal/(mol × K))	$\sigma_{\Delta \bar{S}^0}$ (kcal/(mol × K))	T (K)	$\Delta \bar{S}^0$ (kcal/(mol × K))	$\sigma_{\Delta \bar{S}^0}$ (kcal/(mol × K))	T (K)	$\Delta \bar{S}^0$ (kcal/(mol × K))	$\sigma_{\Delta \bar{S}^0}$ (kcal/(mol × K))
Y10	283	0.022277	0.006895	300	0.033781	0.007745	295.4	0.030668	0.007515
F22	283	-0.030512	0.00193	300	-0.02593	0.002151	295.4	-0.02717	0.002091
C25	283	0.001096	0.005659	300	0.010671	0.006356	295.4	0.00808	0.006167
Y26	283	0.007842	0.009954	300	0.017939	0.011181	295.4	0.015207	0.010849
L40	283	-0.003725	0.007919	300	0.004458	0.008894	295.4	0.002244	0.00863
K41	283	0.023263	0.005536	300	0.034965	0.006218	295.4	0.031799	0.006034
E44	283	0.05308	0.012003	300	0.067723	0.013458	295.4	0.063761	0.013064
V49	285.3	-0.000145	0.07532	300	0.006968	0.083205	295.4	0.004743	0.080738
Y67	283	-0.007097	0.0044	300	0.000532	0.004937	295.4	-0.001532	0.004792
T68	283	0.020369	0.003907	300	0.031526	0.004386	295.4	0.028507	0.004256
F70	283	0.00188	0.004633	300	0.010501	0.005199	295.4	0.008168	0.005045
E77	283	-0.010343	0.078777	300	-0.003308	0.088327	295.4	-0.005211	0.085743
A79	283	0.01643	0.005233	300	0.027473	0.005878	295.4	0.024484	0.005703
C80	283	0.240201	0.121572	300	0.279346	0.136704	295.4	0.268754	0.132609
R81	283	0.007552	0.00506	300	0.017757	0.005684	295.4	0.014996	0.005515
V82	283	-0.011112	0.005393	300	-0.003745	0.006056	295.4	-0.005739	0.005877
N83	283	0.006244	0.004506	300	0.016146	0.005061	295.4	0.013466	0.004911
K91	283	-0.004377	0.000979	300	0.003209	0.001094	295.4	0.001156	0.001063
V93	283	0.003907	0.00478	300	0.012852	0.005369	295.4	0.010431	0.005209
W95	283	0.013488	0.005117	300	0.02358	0.005742	295.4	0.02085	0.005573

Table 39 $\Delta \bar{S}^0$ of the amide sites of β₂-microglobulin mutant form D76N at various temperatures.

APPENDIX 2: HUMAN β2-MICROGLOBULIN MUTANT FORM D76N BLUU-TRAMP EXPERIMENT

Residue	Lowest Temperature			Reference Temperature			Highest Temperature		
	T (K)	$\Delta \bar{C}_p^0$ (kcal/(mol × K))	$\sigma_{\Delta \bar{C}_p^0}$ (kcal/(mol × K))	T (K)	$\Delta \bar{C}_p^0$ (kcal/(mol × K))	$\sigma_{\Delta \bar{C}_p^0}$ (kcal/(mol × K))	T (K)	$\Delta \bar{C}_p^0$ (kcal/(mol × K))	$\sigma_{\Delta \bar{C}_p^o}$ (kcal/(mol × K))
Y10	283	0.191501	0.014153	300	0.203004	0.015004	295.4	0.199891	0.014774
F22	283	0.076272	0.003678	300	0.080854	0.003899	295.4	0.079614	0.003839
C25	283	0.15939	0.011601	300	0.168965	0.012298	295.4	0.166374	0.01211
Y26	283	0.168095	0.020426	300	0.178192	0.021653	295.4	0.17546	0.021321
L40	283	0.136224	0.01624	300	0.144407	0.017216	295.4	0.142193	0.016952
K41	283	0.194807	0.011364	300	0.206509	0.012046	295.4	0.203343	0.011861
E44	283	0.243772	0.024222	300	0.258415	0.025677	295.4	0.254453	0.025283
V49	285.3	0.13805	0.153033	300	0.145163	0.160918	295.4	0.142937	0.15845
Y67	283	0.127006	0.008946	300	0.134635	0.009483	295.4	0.132571	0.009338
T68	283	0.185734	0.007966	300	0.196892	0.008444	295.4	0.193873	0.008315
F70	283	0.143521	0.009418	300	0.152143	0.009984	295.4	0.14981	0.009831
E77	283	0.117105	0.158969	300	0.12414	0.168519	295.4	0.122236	0.165935
A79	283	0.18383	0.010739	300	0.194873	0.011384	295.4	0.191885	0.01121
C80	283	0.651645	0.251895	300	0.69079	0.267027	295.4	0.680198	0.262932
R81	283	0.169888	0.010379	300	0.180094	0.011002	295.4	0.177332	0.010834
V82	283	0.122625	0.011049	300	0.129991	0.011713	295.4	0.127998	0.011533
N83	283	0.164829	0.009237	300	0.17473	0.009792	295.4	0.172051	0.009642
K91	283	0.126294	0.001905	300	0.13388	0.00202	295.4	0.131827	0.001989
V93	283	0.148902	0.0098	300	0.157847	0.010389	295.4	0.155426	0.010229
W95	283	0.168001	0.010404	300	0.178093	0.011029	295.4	0.175362	0.010859

Table 40 $\Delta \bar{C}_p^0$ of the amide sites of β₂-microglobulin mutant form D76N at various temperatures.

APPENDIX 2: HUMAN β2-MICROGLOBULIN MUTANT FORM D76N BLUU-TRAMP EXPERIMENT
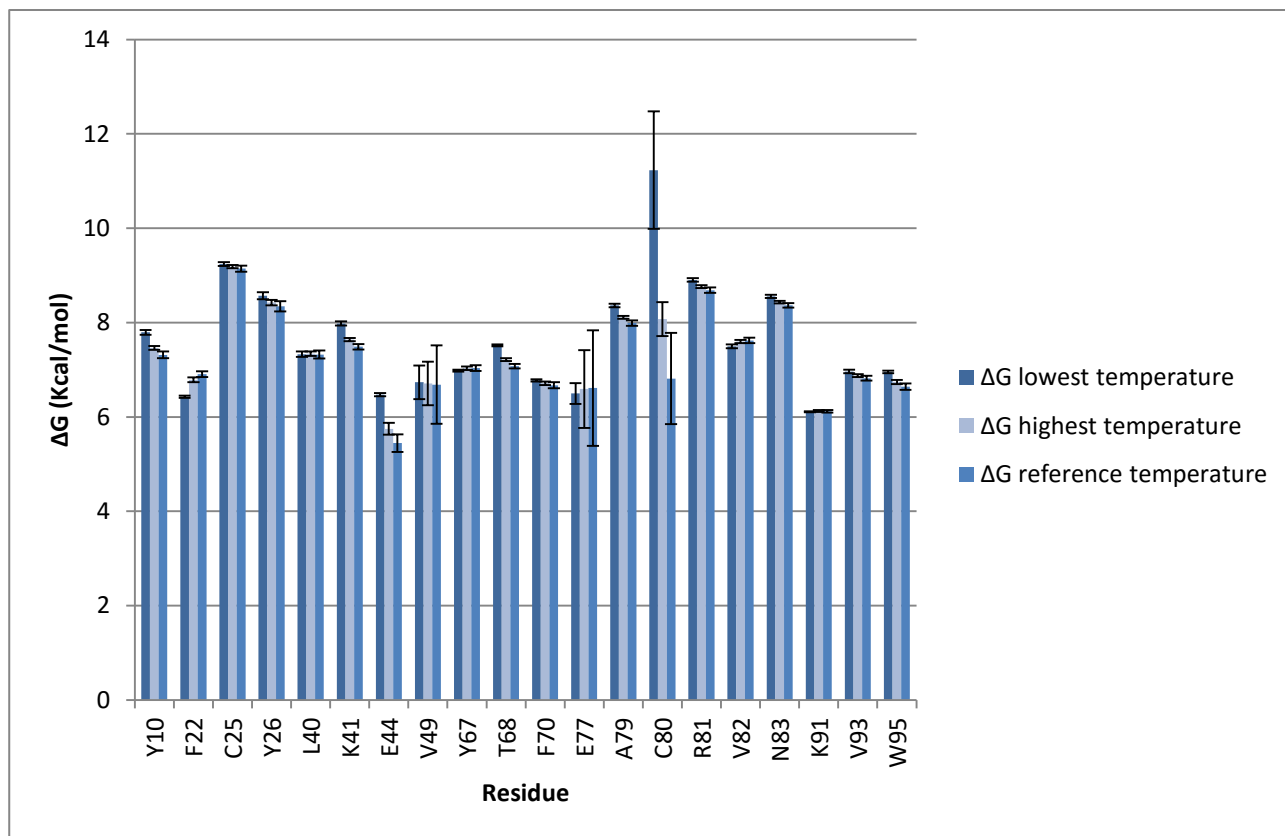

Figure 46 $\Delta\overline{G}^0$ **of the amide sites of β$_2$-microglobulin mutant form D76N based on the results of the analysis on the BLUU-Tramp experiment. Half of the error bar corresponds to a standard deviation.**
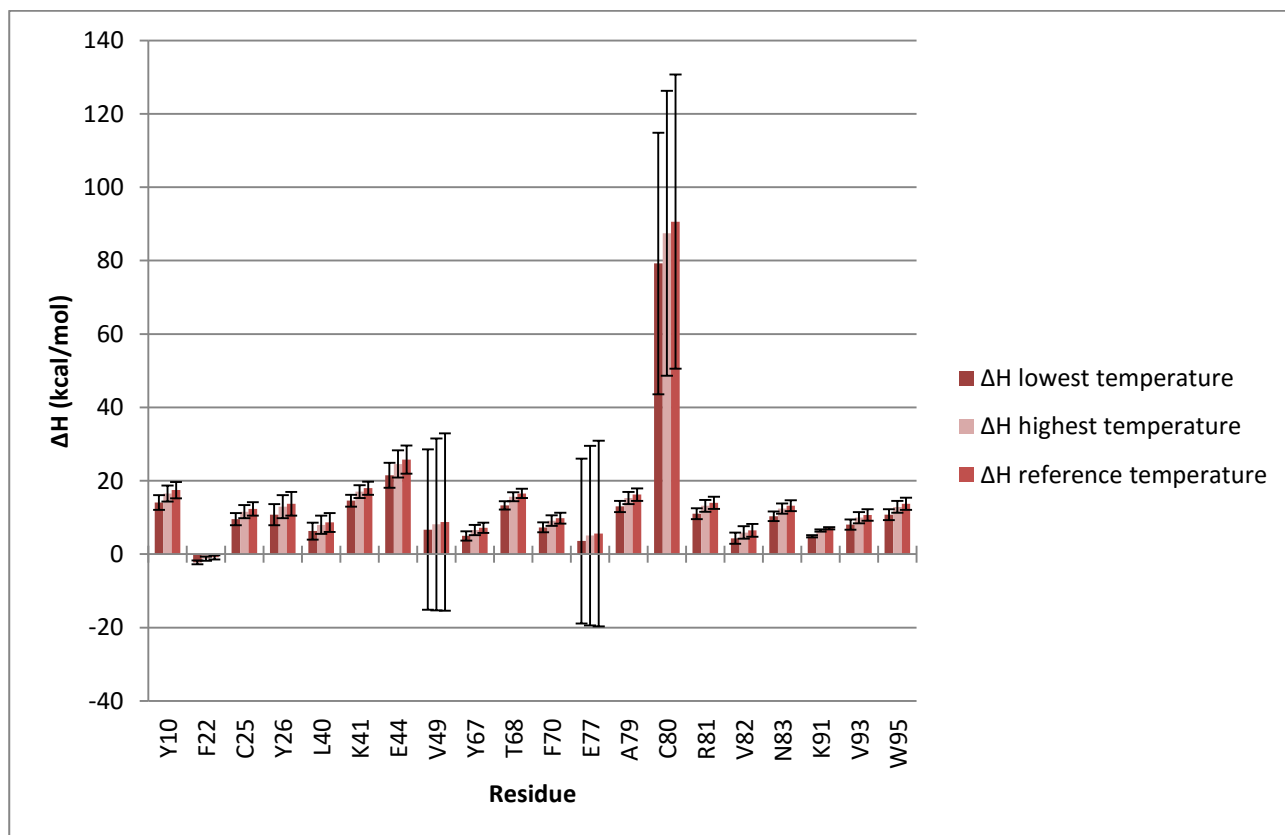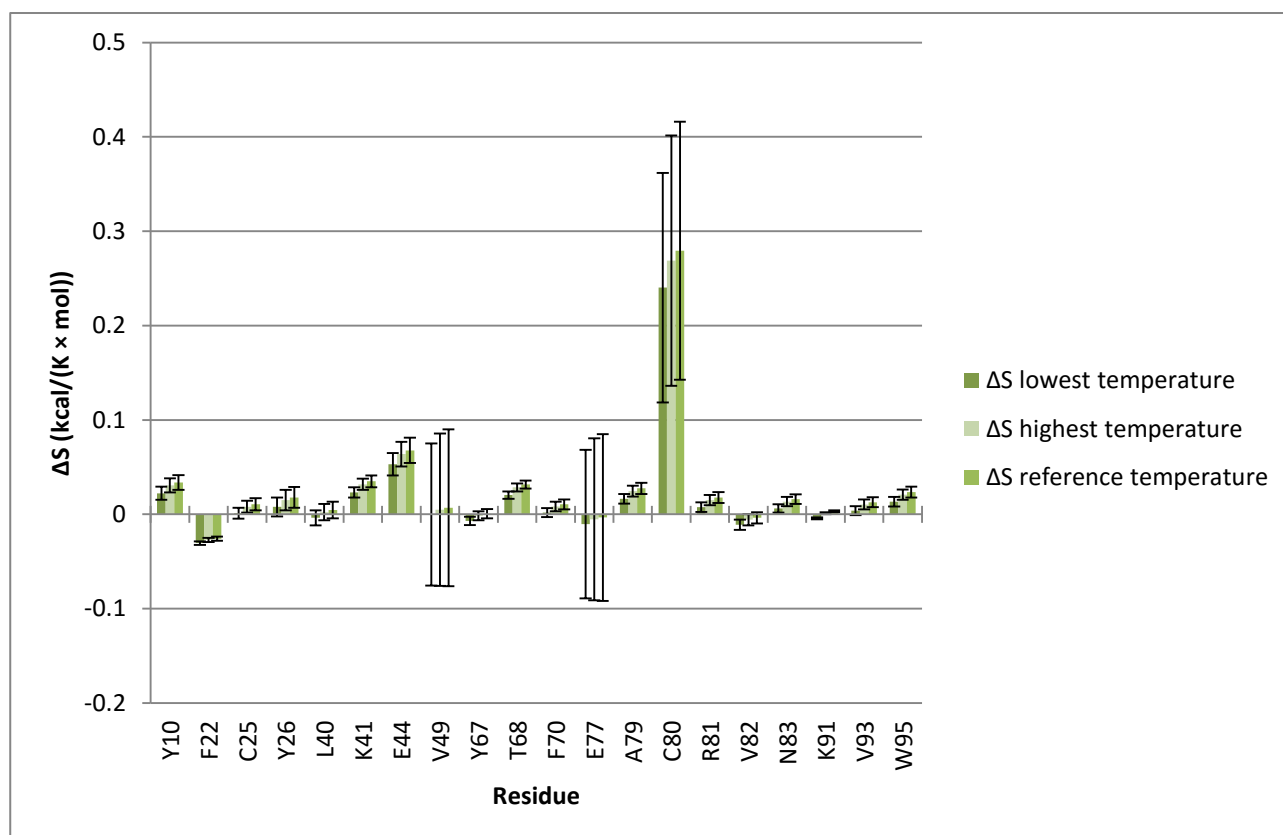

Figure 47 $\Delta\overline{H}^0$ **of the amide sites of β$_2$-microglobulin mutant form D76N based on the results of the analysis on the BLUU-Tramp experiment. Half of the error bar corresponds to a standard deviation.**

APPENDIX 2: HUMAN β2-MICROGLOBULIN MUTANT FORM D76N BLUU-TRAMP EXPERIMENT

Figure 48 $\Delta \overline{S}^0$ **of the amide sites of β₂-microglobulin based on the results of the analysis on the BLUU-Tramp experiment. Half of the error bar corresponds to a standard deviation.**
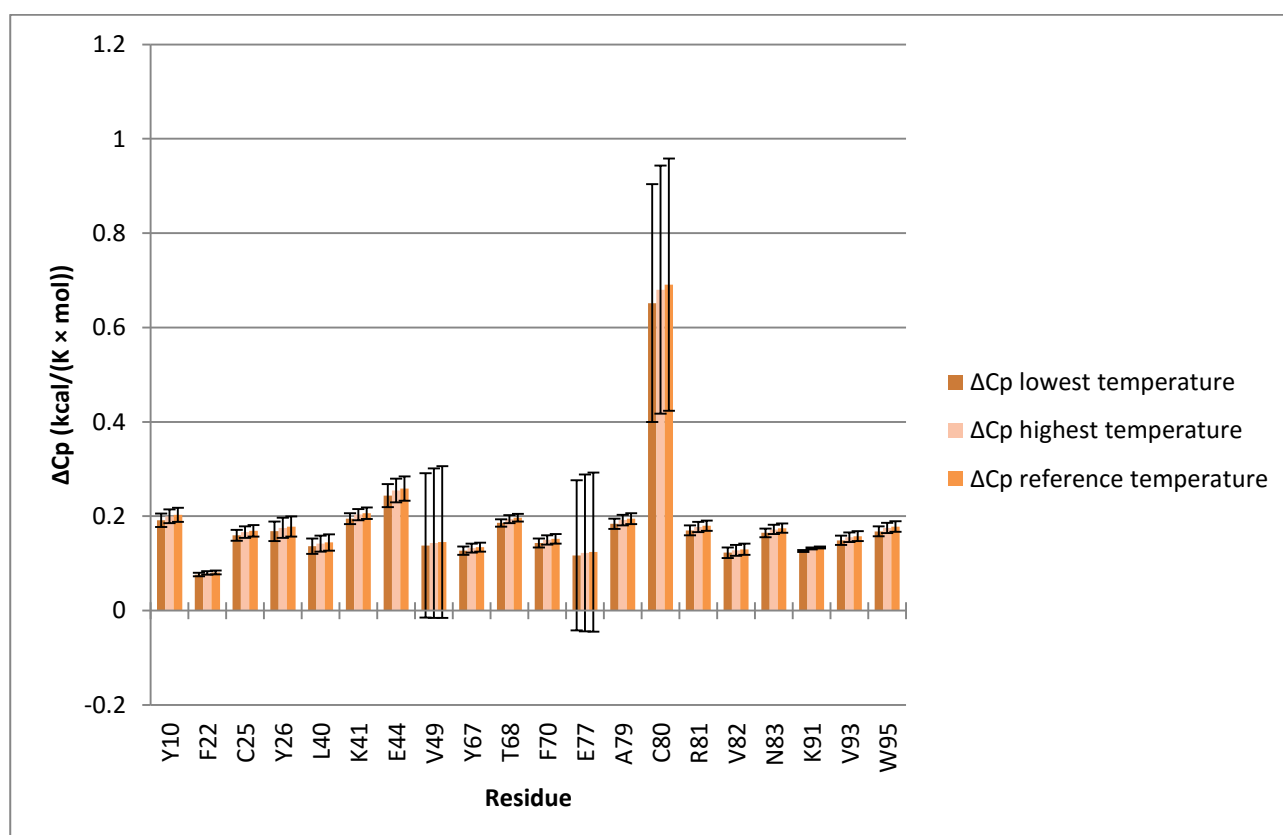

Figure 49 $\Delta \overline{C}_p^0$ **of the amide sites of β₂-microglobulin mutant form D76N based on the results of the analysis on the BLUU-Tramp experiment. Half of the error bar corresponds to a standard deviation.**

APPENDIX 2: HUMAN β2-MICROGLOBULIN MUTANT FORM D76N BLUU-TRAMP EXPERIMENT

A comparison between the results of the BLUU-Tramp analysis at the reference temperature 300 K for the wild type form and the mutant form D76N of β2-microglobulin reveals that the mutant form has consistently lower values for the thermodynamic parameters, especially in the case of the $\Delta \bar{G}^0$. It is important to note the parameters other than the $\Delta \bar{G}^0$ in the case of the cysteine 80, which was not analyzed in the case of the wild type form.
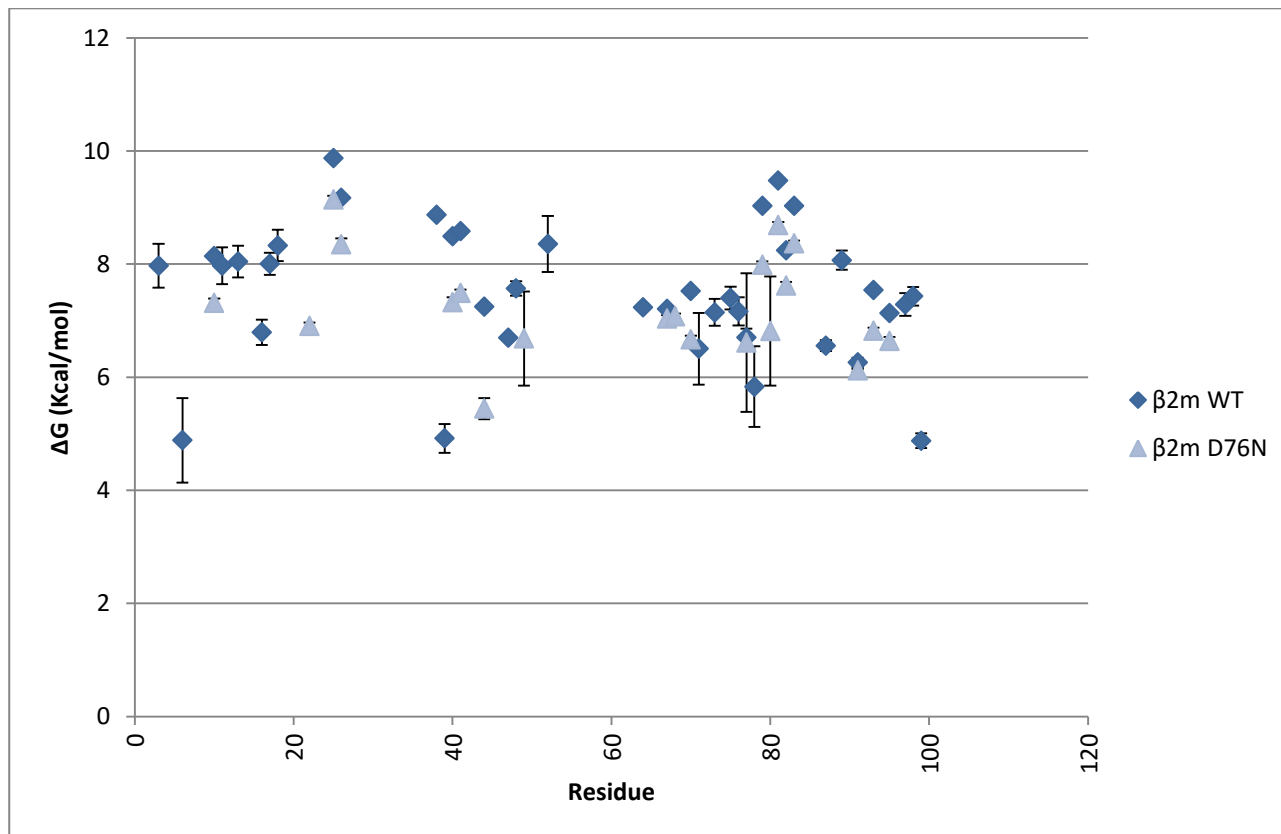

Figure 50 comparison on the $\Delta \bar{G}^0$ at 300 K of the amide sites of β2-microglobulin obtained from the analysis of BLUU-Tramp data from the mutant form D76N (in light blue) and the wild type form (in blue). Half of the error bar corresponds to a standard deviation.
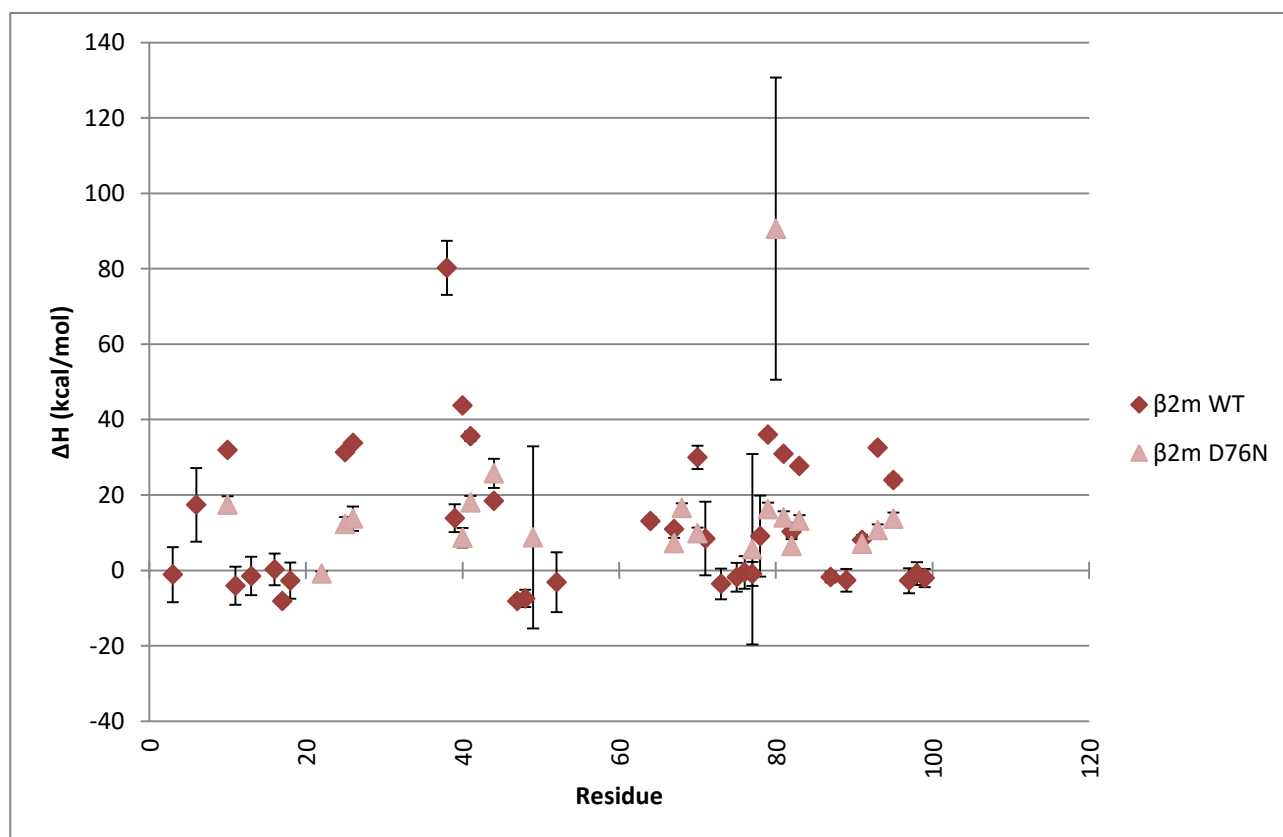
APPENDIX 2: HUMAN β2-MICROGLOBULIN MUTANT FORM D76N BLUU-TRAMP EXPERIMENT

Figure 51 comparison on the $\Delta\bar{H}^0$ at 300 K of the amide sites of β2-microglobulin obtained from the analysis of BLUU-Tramp data from the mutant form D76N (in light red) and the wild type form (in red). Half of the error bar corresponds to a standard deviation.
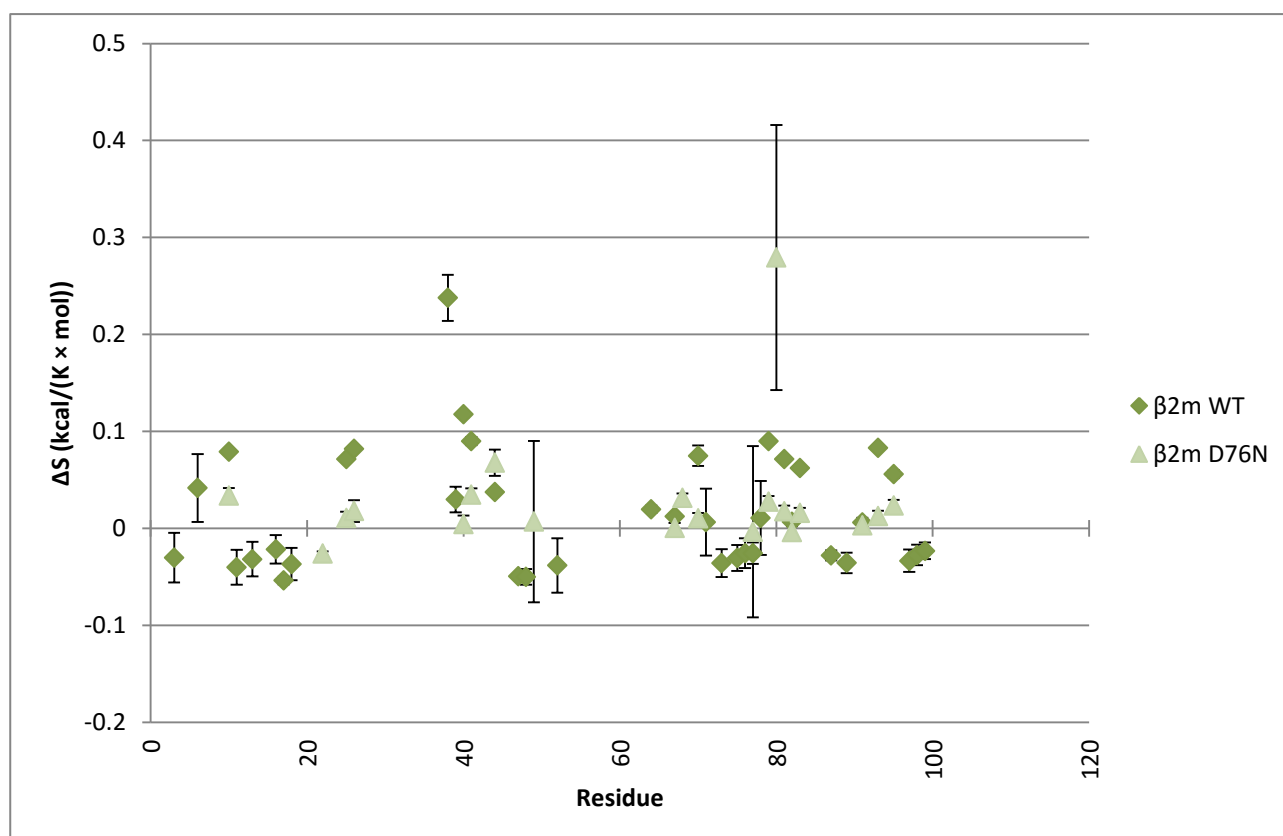

Figure 52 comparison on the $\Delta\bar{S}^0$ at 300 K of the amide sites of β2-microglobulin obtained from the analysis of BLUU-Tramp data from the mutant form D76N (in light green) and the wild type form (in green). Half of the error bar corresponds to a standard deviation.
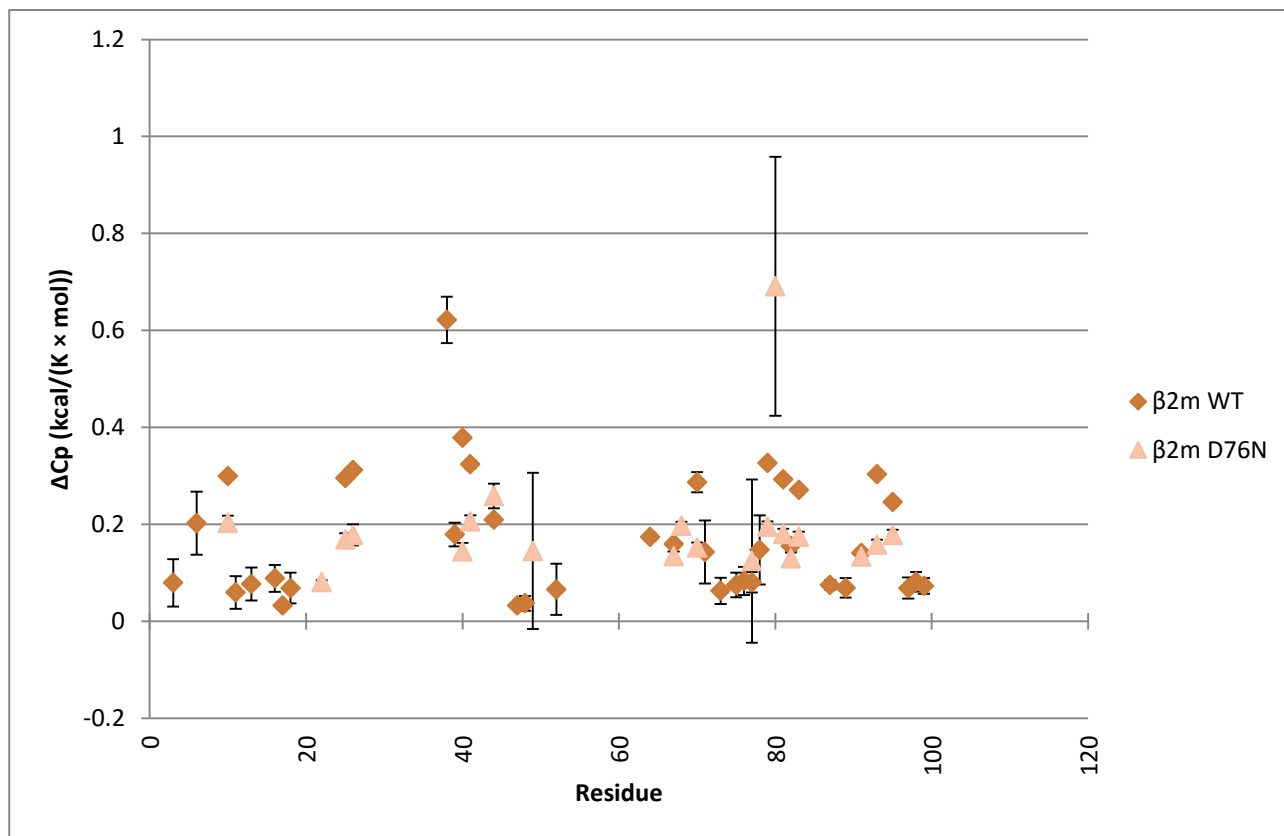
Figure 53 comparison on the $\Delta \overline{C}_p^0$ at 300 K of the amide sites of β2-microglobulin obtained from analysis of BLUU-Tramp data from the mutant form D76N (in light orange) and the wild type form (in orange). Half of the error bar corresponds to a standard deviation.

APPENDIX 2: HUMAN β2-MICROGLOBULIN MUTANT FORM D76N BLUU-TRAMP EXPERIMENT

DISCUSSION

It is important to map the results to the structure of the protein in order to properly correlate them with the structural information:
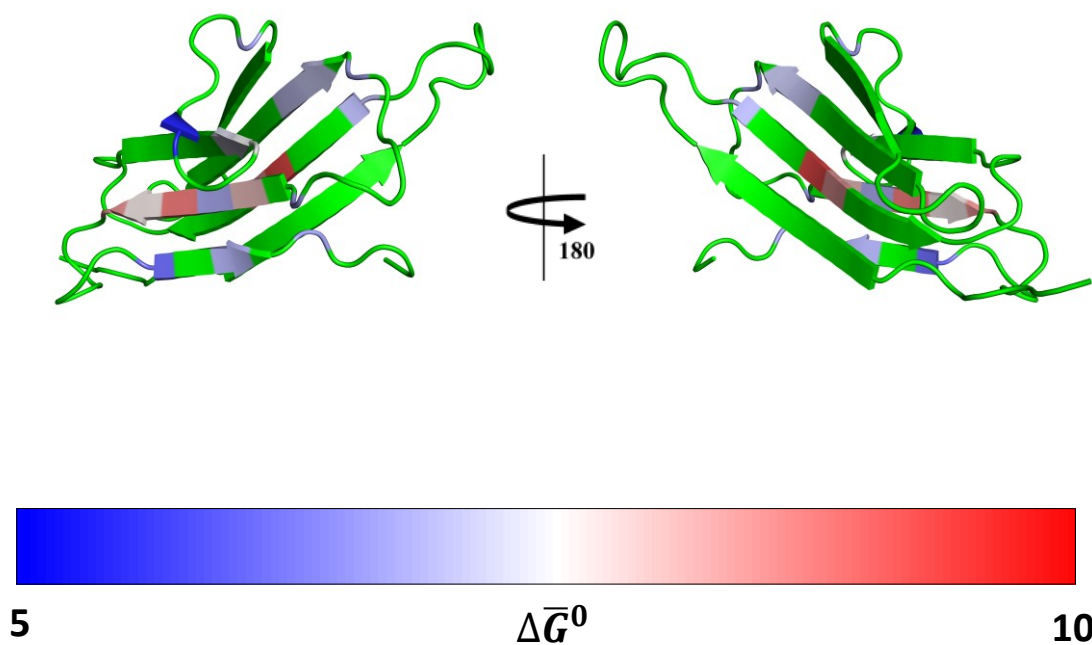

Figure 54 $\Delta\overline{G}^0$ **in kcal/mol of the β$_2$-microglobulin mutant D76N amide sites from the results at 300K of BLUU-Tramp experiment analysis mapped to the structure of the protein. The whole residues have been uniformly colored according to the $\Delta\overline{G}^0$ of the amide site. The residues not included in the results are colored in green.**

Figure 55 $\Delta\bar{H}^0$ **in kcal/mol of the β$_2$-microglobulin mutant D76N amide sites from the results at 300K of BLUU-Tramp experiment analysis mapped to the structure of the protein. The whole residues have been uniformly colored according to the** $\Delta\bar{H}^0$ **of the amide site. The residues not included in the results are colored in green.**
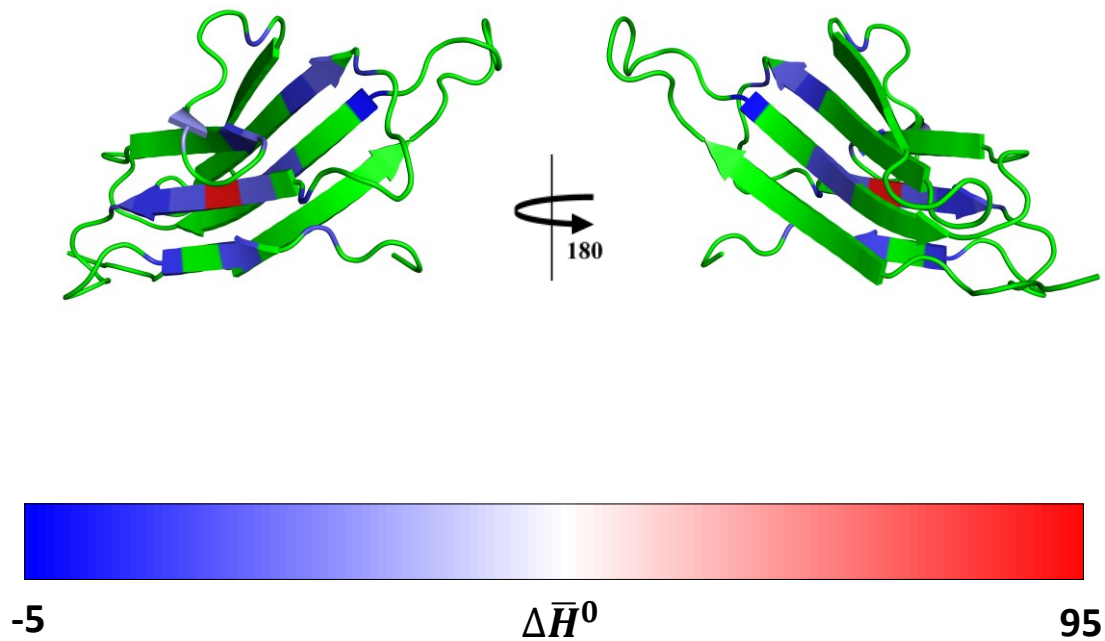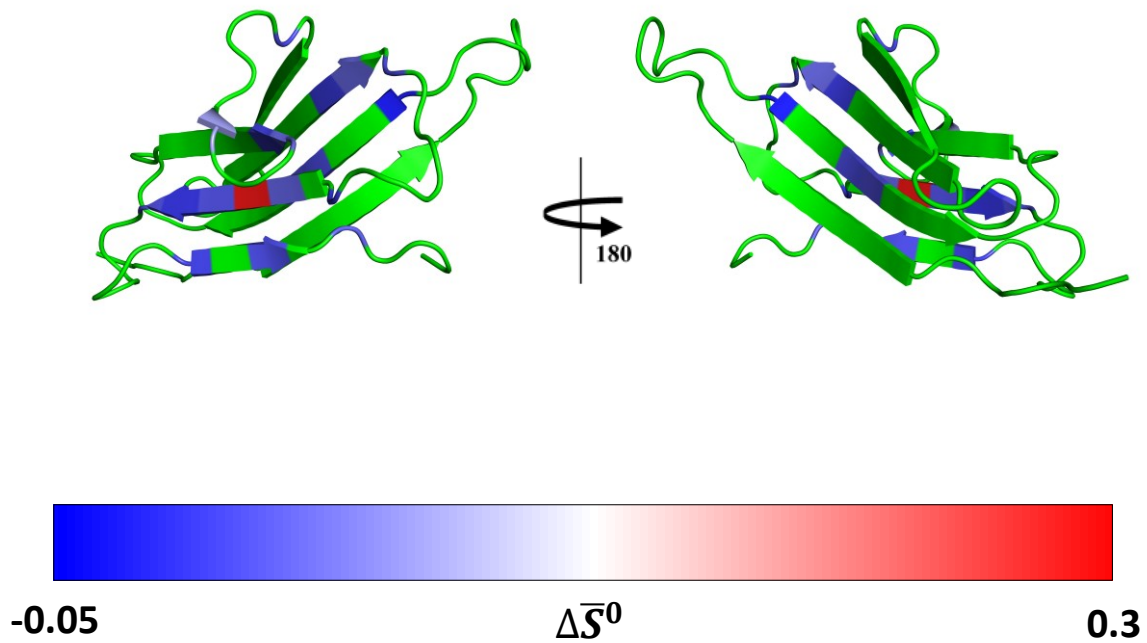

Figure 56 $\Delta\bar{S}^0$ **in kcal/(mol × K) of the β$_2$-microglobulin mutant D76N amide sites from the results at 300K of BLUU-Tramp experiment analysis mapped to the structure of the protein. The whole residues have been uniformly colored according to the** $\Delta\bar{S}^0$ **of the amide site. The residues not included in the results are colored in green.**

Figure 57 $\Delta\bar{C}_p^0$ **in kcal/(mol × K) of the β$_2$-microglobulin mutant D76N amide sites from the results at 300K of BLUU-Tramp experiment analysis mapped to the structure of the protein. The whole residues have been uniformly colored according to the** $\Delta\bar{C}_p^0$ **of the amide site. The residues not included in the results are colored in green.**
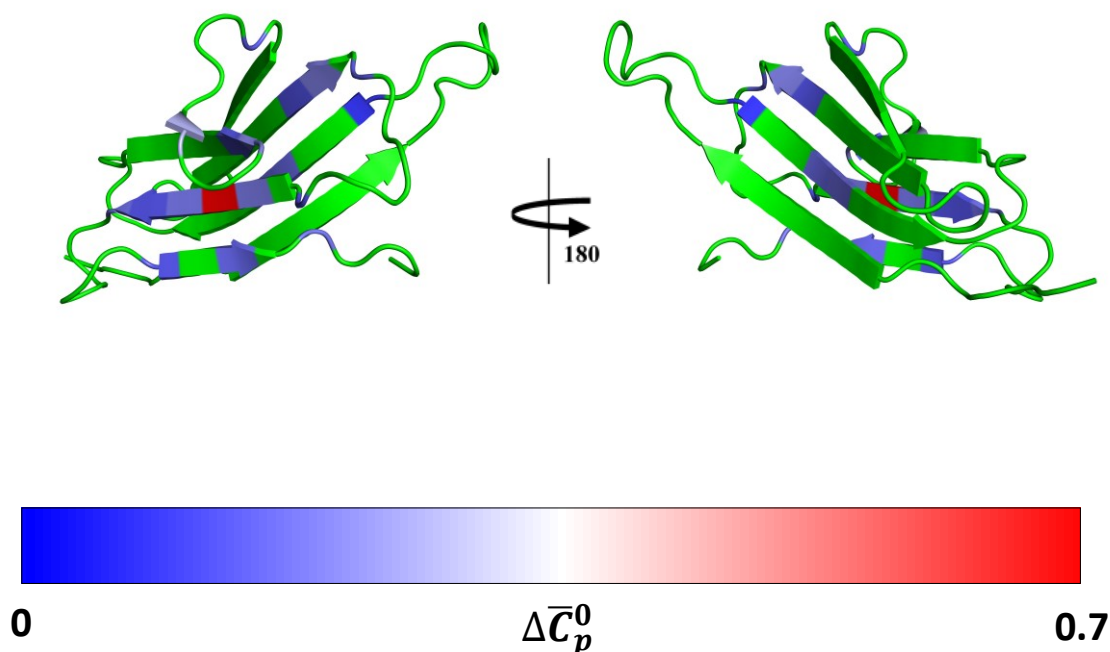
In this case the results at 300 K from both the cysteine residues involved in the disulfide bridge, Cysteine 25 and Cysteine 80, are present, but the results from Cysteine 80 show a higher uncertainty (see Table 36). Cysteine 25 has the highest value of $\Delta\bar{G}^0$, 9.14 ± 0.06 kcal/mol , while Cysteine 80 has an apparently lower value of 6.81 ± 0.97, which might be due to the higher uncertainty in the results. The first residues of strand B, C' and G, namely Phenylalanine 22, Glutamine 44 and Lysine 91, have $\Delta\bar{G}^0$ values of 6.91 ± 0.06 kcal/mol, 5.45 ± 0.19 kcal/mol and 6.12 ± 0.03 kcal/mol respectively, all of which are relatively low when compared to the values of other residues of their strands (see Figure 54). Finally, Valine 82 has a $\Delta\bar{G}^0$ of 7.62 ± 0.06 kcal/mol, which is around 1 kcal/mol lower than that of Arginine 81 (8.69 ± 0.06 kcal/mol) and Asparagine 83 (8.37 ± 0.05 kcal/mol), a feature that was already observed in the wild type form of β$_2$-microglobulin and that might be due to the amide site being more exposed to the solvent (see Figure 58).
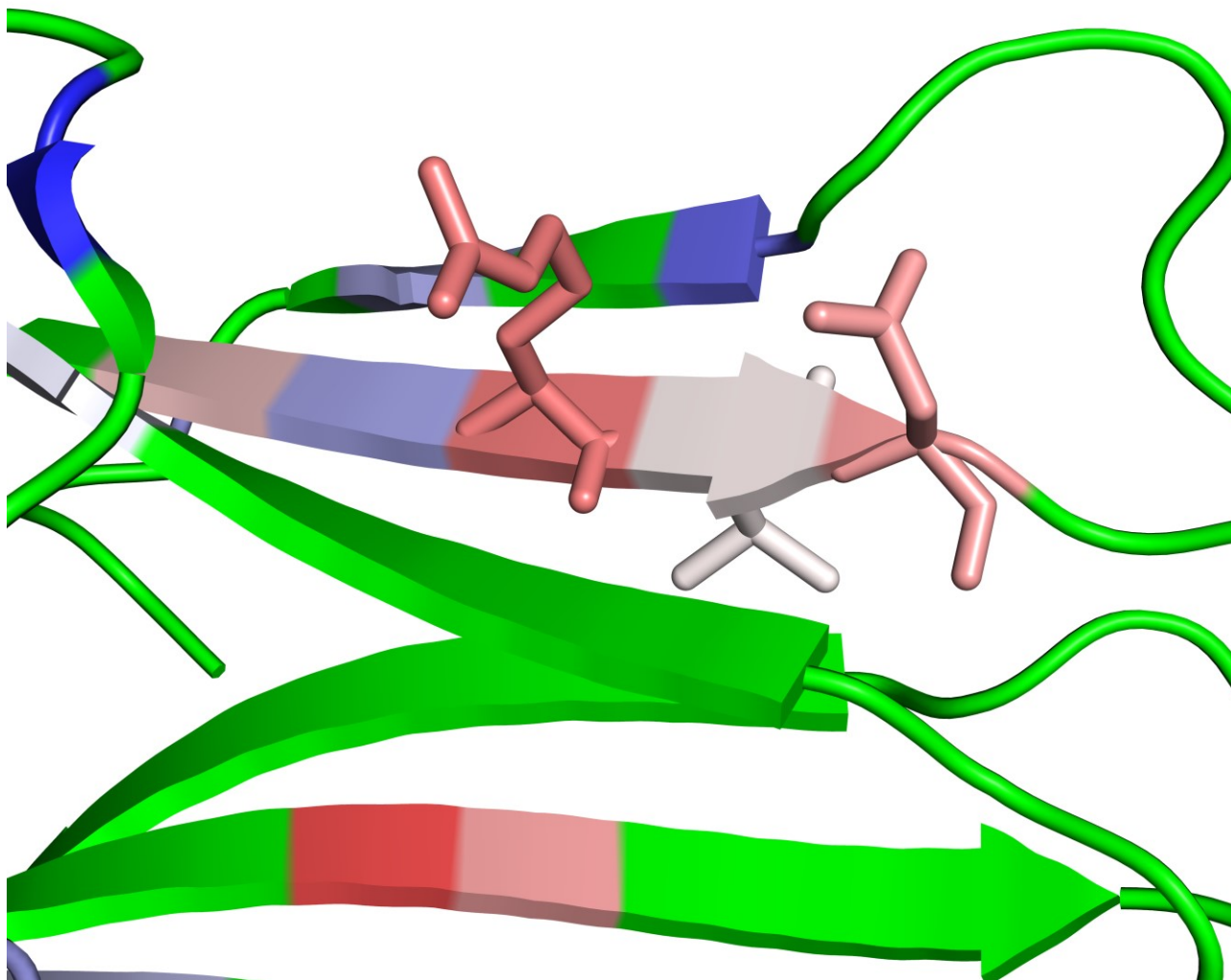
Figure 58 Arginine 81, Valine 82 and Asparagine 83 represented with sticks. The coloring follows the same $\Delta \bar{G}^0$ scale of Figure 54, with Arginine 81 being red, Valine 82 being white and Asparagine 83 being pink.

In the case of the mutant D76N, only the Phenylalanine 22 has a $\Delta \bar{S}^0$ significantly lower than 0 (-0.03 ± 0.00 kcal/(mol × K)), as well as a $\Delta \bar{C}_p^0$ lower than 0.1 kcal/mol × K (0.08 ± 0.00 kcal/(mol × K)). Interestingly, this residue is also the first residue of strand B, according to the crystal structure[32], suggesting that the first residue of strand B might lie in a more flexible region than the other first residues of the other strands. It is important to note, on the other hand, that Cysteine 80 has both the highest value of $\Delta \bar{S}^0$ (0.28 ± 0.14 kcal/(mol × K))and the highest value of $\Delta \bar{C}_p^0$ (0.69 ± 0.27 kcal/mol × K), since however the uncertainty in those value is quite high, these values might be just artifacts due to imprecise measurement.

Thus, similar considerations as those made for the wild type form of β₂-microglobulin can be made for the D76N form as well, even though only one residue showing a negative $\Delta \bar{S}^0$ value was considered.

APPENDIX 2: HUMAN β2-MICROGLOBULIN MUTANT FORM D76N BLUU-TRAMP EXPERIMENT

It is therefore interesting to compare the actual values of the thermodynamic parameters obtained in the two forms:

Residue	$\Delta\bar{G}^0$ Wild Type (kcal/mol)	$\Delta\bar{G}^0$ D76N (kcal/mol)
Y10	8.138548 ± 0.013714	7.316314 ± 0.073865
C25	9.874799 ± 0.010769	9.143374 ± 0.062821
Y26	9.171372 ± 0.015136	8.347078 ± 0.107727
L40	8.492698 ± 0.023404	7.323636 ± 0.086922
K41	8.580887 ± 0.021221	7.486839 ± 0.059366
E44	7.246711 ± 0.018205	5.445308 ± 0.186226
Y67	7.20736 ± 0.030582	7.035555 ± 0.059148
F70	7.522031 ± 0.056281	6.671061 ± 0.062541
E77	6.700189 ± 0.160867	6.613335 ± 1.223491
A79	9.031541 ± 0.011572	7.98919 ± 0.05638
R81	9.477786 ± 0.008141	8.686849 ± 0.055386
V82	8.243707 ± 0.027014	7.622254 ± 0.060754
N83	9.026461 ± 0.006847	8.365878 ± 0.050026
K91	6.258958 ± 0.083409	6.119254 ± 0.025169
V93	7.542878 ± 0.008767	6.821477 ± 0.052953
W95	7.134201 ± 0.022946	6.639875 ± 0.068933

Table 41 Comparison between the $\Delta\bar{G}^0$ values at 300 K obtained from the BLUU-Tramp experiments performed on the wild type and mutant D76N forms of β₂-microglobulin.

Residue	$\Delta\bar{H}^0$ Wild Type (kcal/mol)	$\Delta\bar{H}^0$ D76N (kcal/mol)
Y10	31.907682 ± 0.887009	17.450617 ± 2.250547
C25	31.364336 ± 0.780935	12.344703 ± 1.844744
Y26	33.81162 ± 0.879046	13.72887 ± 3.247952
L40	43.757532 ± 0.888471	8.661078 ± 2.582355
K41	35.59002 ± 1.233741	17.976407 ± 1.806928
E44	18.443332 ± 0.809425	25.762261 ± 3.851504
Y67	10.929707 ± 0.854867	7.19528 ± 1.422468
F70	29.998839 ± 3.102521	9.821402 ± 1.497556
E77	-0.940461 ± 3.168113	5.620934 ± 25.277805
A79	35.987977 ± 0.652086	16.230953 ± 1.707631
R81	30.889888 ± 0.552528	14.014054 ± 1.650367
V82	10.307075 ± 1.384427	6.498621 ± 1.756904
N83	27.657226 ± 0.554973	13.209567 ± 1.468804
K91	8.099468 ± 1.326706	7.082009 ± 0.302969
V93	32.492744 ± 0.552014	10.677008 ± 1.558297
W95	23.927954 ± 1.235592	13.713964 ± 1.654285

Table 42 Comparison between the $\Delta\bar{H}^0$ values at 300 K obtained from the BLUU-Tramp experiments performed on the wild type and mutant D76N forms of β₂-microglobulin.

APPENDIX 2: HUMAN β2-MICROGLOBULIN MUTANT FORM D76N BLUU-TRAMP EXPERIMENT

Residue	$\Delta \bar{S}^0$ Wild Type (kcal/(mol × K))	$\Delta \bar{S}^0$ D76N (kcal/(mol × K))
Y10	0.07923 ± 0.002918	0.033781 ± 0.007745
C25	0.071632 ± 0.002578	0.010671 ± 0.006356
Y26	0.082134 ± 0.002888	0.017939 ± 0.011181
L40	0.117549 ± 0.002887	0.004458 ± 0.008894
K41	0.09003 ± 0.004053	0.034965 ± 0.006218
E44	0.037322 ± 0.00275	0.067723 ± 0.013458
Y67	0.012408 ± 0.002945	0.000532 ± 0.004937
F70	0.074923 ± 0.01052	0.010501 ± 0.005199
E77	-0.025469 ± 0.011078	-0.003308 ± 0.088327
A79	0.089855 ± 0.002141	0.027473 ± 0.005878
R81	0.071374 ± 0.001822	0.017757 ± 0.005684
V82	0.006878 ± 0.004693	-0.003745 ± 0.006056
N83	0.062103 ± 0.001838	0.016146 ± 0.005061
K91	0.006135 ± 0.004698	0.003209 ± 0.001094
V93	0.083166 ± 0.001817	0.012852 ± 0.005369
W95	0.055979 ± 0.004186	0.02358 ± 0.005742

Table 43 Comparison between the $\Delta \bar{S}^0$ values at 300 K obtained from the BLUU-Tramp experiments performed on the wild type and mutant D76N forms of β₂-microglobulin.

Residue	$\Delta \bar{C}_p^0$ Wild Type (kcal/(mol × K))	$\Delta \bar{C}_p^0$ D76N (kcal/(mol × K))
Y10	0.299385 ± 0.005913	0.203004 ± 0.015004
C25	0.295762 ± 0.005206	0.168965 ± 0.012298
Y26	0.312077 ± 0.00586	0.178192 ± 0.021653
L40	0.378384 ± 0.005923	0.144407 ± 0.017216
K41	0.323933 ± 0.008225	0.206509 ± 0.012046
E44	0.209622 ± 0.005396	0.258415 ± 0.025677
Y67	0.159531 ± 0.005699	0.134635 ± 0.009483
F70	0.286659 ± 0.020683	0.152143 ± 0.009984
E77	0.080397 ± 0.021121	0.12414 ± 0.168519
A79	0.326587 ± 0.004347	0.194873 ± 0.011384
R81	0.292599 ± 0.003684	0.180094 ± 0.011002
V82	0.15538 ± 0.00923	0.129991 ± 0.011713
N83	0.271048 ± 0.0037	0.17473 ± 0.009792
K91	0.140663 ± 0.008845	0.13388 ± 0.00202
V93	0.303285 ± 0.00368	0.157847 ± 0.010389
W95	0.246186 ± 0.008237	0.178093 ± 0.011029

Table 44 Comparison between the $\Delta \bar{C}_p^0$ values at 300 K obtained from the BLUU-Tramp experiments performed on the wild type and mutant D76N forms of β₂-microglobulin.

The values of all the four thermodynamic parameters ($\Delta \bar{G}^0$, $\Delta \bar{H}^0$, $\Delta \bar{S}^0$ and $\Delta \bar{C}_p^0$) are generally lower in the mutant D76N form, with the only exception of Glutammate 44, whose $\Delta \bar{G}^0$ is lower in the mutant form, but whose $\Delta \bar{S}^0$, $\Delta \bar{C}_p^0$ and $\Delta \bar{H}^0$ are higher in the mutant form. Furthermore, due to the increased uncertainty, the Glutamate 77 has a $\Delta \bar{S}^0$ value that is no longer significantly lower than 0.

APPENDIX 2: HUMAN β2-MICROGLOBULIN MUTANT FORM D76N BLUU-TRAMP EXPERIMENT

Overall, this comparison shows a decreased stability and possibly greater conformational flexibility of the whole protein structure of the mutant form, as shown by generally decreased $\Delta \bar{G}^0$ values as well as generally decreased $\Delta \bar{S}^0$ and $\Delta \bar{C}_p^0$ values.

APPENDIX 3: ARTICLE PUBLISHED DURING THE COURSE

Probing the Influence of Citrate-Capped Gold Nanoparticles on an Amyloidogenic Protein

Giorgia Brancolini,[*,†] Alessandra Corazza,[‡,¶] Marco Vuano,[‡] Federico Fogolari,[‡,¶] Maria Chiara Mimmi,[‡] Vittorio Bellotti,[§,¶,‖] Monica Stoppini,[§,¶] Stefano Corni,[*,†] and Gennaro Esposito[*,‡,¶,⊥]

Center S3, CNR Institute Nanoscience, Via Campi 213/A, 41125 Modena, Italy, Dipartimento di Scienza Mediche e Biologiche (DSMB), University of Udine, Piazzale Kolbe 3, 33100 Udine, Italy, Istituto Nazionale Biostrutture e Biosistemi, Viale medaglie d'Oro 305 - 00136 Roma, Italy, Dipartimento di Medicina Molecolare, Universita' di Pavia, Via Taramelli 3, 27100 Pavia, Italy, Division of Medicine, University College of London, London NW3, 2PF, UK, and Science and Math Division, New York University at Abu Dhabi, Abu Dhabi, UAE

E-mail: giorgia.brancolini@nano.cnr.it; stefano.corni@nano.cnr.it; gennaro.esposito@uniud.it

---

[*]To whom correspondence should be addressed
[†]CNR-NANO-S3
[‡]UniUd
[¶]INBB
[§]UniPv
[‖]UK
[⊥]NYUAD

1

ABSTRACT

Nanoparticles (NPs) are known to exhibit distinct physical and chemical properties compared with the same materials in bulk form. NPs have been repeatedly reported to interact with proteins and this interaction can be exploited to affect processes undergone by proteins, such as fibrillogenesis. Fibrillation is common to many proteins and in living organisms it causes tissue-specific or systemic amyloid diseases. The nature of NPs and their surface chemistry is crucial in assessing their affinity for proteins and their effects on them. Here we present the first detailed structural characterization and molecular mechanics model of the interaction between a fibrillogenic protein, β_2-microglobulin, and a NP, 5 nm hydrophilic citrate-capped gold nanoparticles. NMR measurements and simulations at multiple levels (enhanced sampling molecular dynamics, Brownian dynamics and Poisson-Boltzman electrostatics) explain the origin of the observed protein perturbations mostly localized at the amino-terminal region. Experiments show that the protein-NP interaction is weak in the considered, physiological-like, conditions, and do not induce protein fibrillation. Simulations reproduce these findings and reveal instead the role of the citrate in destabilizing the lower pH, protonated form of β_2-microglobulin. The results offer possibile strategies for controlling the desired effect of NPs on the conformational changes of the proteins, which have significant roles in the fibrillation process.

KEYWORDS: nanoparticles; amyloid; fibrillogenesis; docking; molecular dynamics, nuclear magnetic resonance

The interaction between proteins and nanoparticles (NPs)[1–5] is central to many aspects of nanoscience and several nanotechnological applications.[6] Among these, examples of relevant areas of interest are the nanoparticle-based medical imaging and drug delivery.[7–10] These applications entail the administration of NPs to living organisms, which raises a number of issues concerning immunology, toxicology, biochemistry, biophysics, etc., often leading to assess and analyze NP/protein interaction processes that are central also in nanoscale

2

127

bioanalytics.[11,12] The subject of NP/protein interaction has been addressed by several investigators over the last decades and recent reviews are available to summarize the state of the art.[4,13,14] From a general viewpoint, nanoparticles have been reported to either affect or leave unchanged protein structure and function, depending on the specific properties of the nanoparticle surface and dimensions, the environmental conditions, the actual protein characteristics.[4,14,15] The basic pattern that proteins elicit on interacting with NPs is the formation of tightly and/or loosely bound layers around the NPs. These layers are referred to as corona and represent the very essence of the relationship between the NPs and the surrounding biological environment.[16]

Particular relevance has been attributed to the interaction of NPs with amyloidogenic proteins due to the interest in possible therapeutic approaches[17–20] for a class of pathologies with poor treatment, if any. Most of the available evidence, however, point to an enhanced amyloid fibril formation in the presence of NPs.[19,20] In particular it was shown[21] that different types of NPs, such as copolymer particles, cerium oxide particles, quantum dots and carbon nanotubes, enhance the fibril nucleation rate of β_2-microglobulin (β_2m) *i.e.* the light-chain of class I major histocompatibility complex (MHC-I) that is responsible for a tissue-specific amyloidosis in long-term hemodialysed patients.[22] Secondary and tertiary structure and topology of β_2m are reported in Fig. 1.

As β_2m fibrils did not appear physically linked to any of the NPs accelerating their onset, the faster growth was attributed to increased protein concentration in the vicinity of the NP surface, with a mechanism that had already been proposed to account for the protein tissue-specific deposition in collagen-rich regions.[23] However, a microscopic characterization of the β_2m-NP interaction is still lacking, preventing a chemical understanding of the mechanisms that govern the fate of the protein. We present here a comprehensive investigation of on β_2m in the presence of citrate-coated gold NPs that, by combining synergically experiments and simulations, unravel such microscopic picture. Citrate anions reduce gold ions to atoms and stabilize colloidal AuNPs formed from clustered atoms,[24] and the so-formed citrate-capped
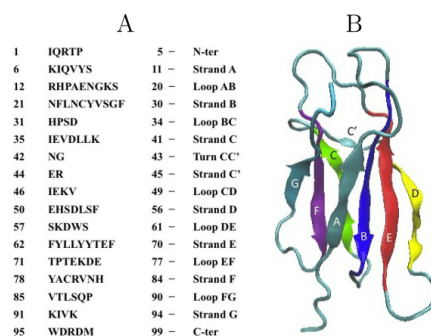
3

Figure 1: Panel A: Protein Sequence. Panel B: Tertiary structure and Topology of β_2-Microglobulin.

gold nanoparticles (Cit-AuNPs) are among the most investigated in this field.[3,25–28] Despite the large number of experimental investigation exploiting Cit-AuNPs, the structural details of citrate anions adsorbed on the AuNP surface are still poorly understood.[29] Yet, they certainly constitute and array of negative charges that can interact with proteins. This is particularly relevant for β_2m because for its tissue specific deposition, a mechanism has been proposed based on the effects of the collagen[23] and heparin[30] charge arrays in promoting local concentration increase and fibril nucleation.

To advance the understanding of the mechanisms driving the adsorption/deposition of amyloidogenic proteins to charged surfaces and the potential influence on fibrillogenesis, we present a comprehensive study based on the protein structural characterization by NMR and molecular simulations of the protein/nanoparticle system. Both simulations and experimental results support the conclusions that Cit-AuNPs, in the physiological-like experimental conditions probed here, have a quite labile interaction with β_2m, that does not lead to fibrillation. Our combined experimental&simulation approach reveals the protein patch interacting with the NP, and suggests that conformational rearrangements associated with protein protonation are accentuated by the interaction with the citrate ad-layer.

Not surprisingly, our findings on the NP effects on fibrillation are different from those previ-

4

ously obtained with other NPs and in other environmental conditions on this amyloidogenic protein. The previously reported results[21] have been paradigmatic and rather influential for most of the successive interpretations, but, as pointed out in a commentary to the original report[31] different scenarios can be envisaged because of the enormous variability that is possible for the NP size, shape, surface coating and composition. By learning how to exploit that variability, we aim at specifically fine-tuning the NP properties to rescue protein fibrillation or revert their amyloid deposition.[18]

RESULTS AND DISCUSSION

Docking of β_2m on Negative Gold

In this section, we investigate the nature of the binding of β_2m to a citrate-coated gold surface by means of Brownian dynamics docking.

Among the various crystal surfaces, we have considered the (111) plane (*i.e.*, Au(111)) which is the most stable and the most commonly occurring in nanoparticles.[32] In this section we shall consider extended gold surfaces, larger than the crystal faces that can be found on the experimental 5 nm gold NP. This simplifying assumption might create differences on the extent of the electrostatic interaction felt by the protein. The role of the finite particle size on electrostatic will be specifically tested by a continuum electrostatic model in Section "Role of Nanoparticle Actual Size on the Electrostatic Interaction". Finally, for a surfactant-covered nanoparticle, possibily reactive edges and vertexes are certainly passivated by the surfactant itself.

The nature of the binding of β_2m to a citrate-coated gold surface, as well as the effect of a negative surface potential, has been initially investigated by introducing a small negative charge density per gold surface atom.

The charge density of (Au_{chg}^{net} = -0.05 e) per surface atom used in the calculation was determined assuming an ordered monolayer of fully deprotonated citrate molecules on gold, as

5

shown in Fig. 2. The regular citrate ad-layer on the top of Au(111) was generated with a ratio of the surface gold ion and citrate concentrations suitable to reproduce experimental electrochemical data on the cit-AuNPs system under aqueous conditions and at physiological pH.[33,39]
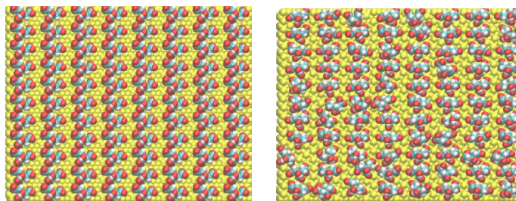

Figure 2: Initial (on the left) and final (on the right) citrate anion distribution on positively charged Au(111) after 20 ns of classical MD with GolP and OPLS/AA in SPCE water.

In short, we generated the structures of protein-surface encounter complexes by running Brownian dynamics simulations during which the internal structure of the protein was kept rigid (rigid docking). The interaction (free) energy of the protein with the surface was obtained using the ProMetCS protein-metal continuum solvent model,[40] and adsorption free energies of β_2m on the Au(111) surface were computed for the structures resulting from the docking. The protein-surface encounter complexes obtained during a BD simulation trajectory were clustered to identify genuinely different protein orientations. For each of the most populated complexes, which were ranked by size, a representative structure was selected.

During docking, the interaction energy of the protein with the Au(111) surface is described by three main terms:[40] van der Waals energy described by site-site Lennard-Jones, E_{LJ}, interactions, adsorbate-metal electrostatic interaction energy, U_{EP} and the desolvation energy of the protein, U_{ds}^p, and of the metal surface, U_{ds}^m (see Tab. 1). The electrostatic term arises from surface polarization and includes an image-charge term.[41]

When this docking procedure was applied to the β_2m-AuNP system with negatively charged gold surface atoms (Au_{chg}^{net} = -0.05 e), it yielded a single orientation accounting for more than

6

98 per cent of the total encounter complexes. The representative structure of the resulting complex is shown in Fig. 3. The complex stability and the protein residues contacting the surface are listed in Fig. 1.

Table 1: Resultant encounter complex from rigid-body BD docking of β_2m (1JNJ) to an Au (111) surface. A hierarchical clustering algorithm (based on a minimum distance linkage function) was applied to the diffusional encounter complexes after docking to a bare negative gold (Au_{chg}^{neg} = -0.05 e) surface. The reported complexes represent 98 per cent of the encounter complexes obtained by BD simulation.

Label	RelPop % (a)	U_{Repr} (b)	E_{LJ} (c)	E_{LJ}+U_{ds}^p+U_{ds}^m (d)	U_{EP} (e)	spread (f)	Contact Residues (g)
A	98	-41.380	-44.020	-10.278	-31.100	0.322	ARG3 LYS58 ASP59 TRP60

Å [(a)] Relative population of this cluster
[(b)] U_{Repr}: total interaction energy of the representative of the given cluster in kT with T= 300 K
[(c)] E_{LJ}: Lennard-Jones energy term for the representative complex, U_{ds}^p: non-polar (hydrophobic) desolvation energy of the representative complex, in kT
[(d)] U_{ds}^m: surface desolvation energy of the representative complex, in kT
[(e)] U_{EP}: total electrostatic energy of the representative complex, in kT
[(f)] RMSD of the structures within the cluster with respect to the representative complex
[(g)] Residues with atoms contacting gold at distances $\leq$ 3 Å

The binding in complex A is stabilized mostly by the electrostatic terms. The preferred orientation involves the residues at the N-terminal (ARG3) tail and DE-loop (LYS58, ASP59 and TRP60). The strong and highly populated binding seems to be associated with the total charge of the gold surface atoms and the amount of charged residues contacting the surface (see Tab. 1) and this is due to the fact that in presence of negatively charged gold the protein is able to use simultaneously more than one charged contact in order to optimize the binding. For completeness, we extended the docking to surfaces with five-fold lower surface charge density (Au_{chg}^{net} = -0.01 e). Complex A remains the most populated, but other complexes also appear (results are reported Fig. 1 and Tab. 1 of Supplementary Information).
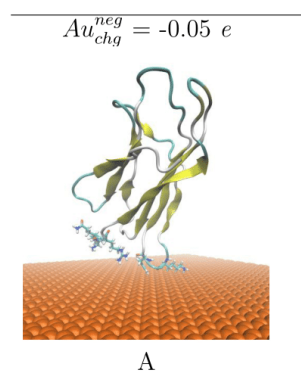
7

$$Au^{neg}_{chg} = \text{-0.05 } e$$

A

Figure 3: Most populated encounter complex of β_2m on negatively charged gold nanocluster obtained by BD simulation. For Au^{neg}_{chg} = -0.05 e, the structure of a single complex is representative for the 98 per cent of the total encounter complexes. The protein backbone is shown in cartoon representation. The residues contacting the gold surface are shown in stick representation.

Atomistic MD Simulations of β_2m on Citrate-Covered Au

In order to disclose the possible conformational changes induced on the structure of the protein by the adsorption on cit-AuNPs, which may have significant roles in the fibrillation process, the stability of the encounter complexes resulting from the rigid docking was assessed performing atomistic MD simulations.

As an atomistic molecular mechanics model for Cit-AuNPs, we propose a surface in which the fully deprotonated citrate anions $(C_3H_5O(COO)_3^{3-})$ are described as interacting adsorbed species on a positively charged AuNPs. For the sake of completeness, we also consider the comparison with a different citrate-covered surface model based on a neutral gold core and the counter ions included in aqueous solution over the citrate, namely Cit3Na-AuNPs (*i.e.*, three Na+ ions released from each sodium citrate when it is put in aqueous solution). Simulations results are summarized in the Supporting Information (section "Validation of the Au surface with a positive charge density" and Fig. 3). Such results are qualitatively similar to those presented later in the main text for the positive gold core model, although somewhat in less good agreement with NMR data than the main text model. In fact, we believe that the

8

choice of a positive gold core is more in line with current understading of citrate covered gold nanoparticles. For instance in ref.[33] the authors reported an open circuit potential for freshly formed colloids (460-560 mV vs SCE) corresponding to positive gold core for both pH=1 and pH=3 accompanied with a modest tendence of the gold core to be pH sensitive in passing from pH=1 to pH=3. In our opinion, the latter results support the assumption of a positive gold core even at higher pH. More importantly, in ref.,[34] a positive gold NP cores at pH 7.5 was proposed on the basis of experiments. Additionally, in ref.[35] the authors reported a zeta potential of $-40\,\text{mV} \div -50\,\text{mV}$ for 10 nm nanoparticles, in a pH range from 5 to 12. The ionic strength was not clearly reported there, but it was reasonable to assume that it was about 20-30 mM at neutral pH. Based on a Poisson-Boltzman estimate, this zeta potential would require a surface charge density of $\sim -0.2\,\text{e/nm}^2$. Such values must be reproduced with a citrate surface concentration which in previous works was reported to be in the range from $1.4 \cdot 10^{-10}\,\text{mole/cm}^2$ [36] to $5 \cdot 10^{-10}\,\text{mole/cm}^2$.[37] Our atomistic model satisfies these experimental constraints, by using a reasonable citrate surface concentration of $2.8 \cdot 10^{-10}\,\text{mole/cm}^2$ and by including a positive gold core to obtain a surface charge density of $-0.3\,\text{e/nm}^2$.

To our knowledge, the formation of a citrate adsorption layer (ad-layer) composed of interacting citrate molecules as a stabilizing layer has never been incorporated in simulations due to the lack of suitable force-fields (FFs) able to describe the citrate anion, as well as their interfacial physisorption on the top of the gold nanoparticle. Such FFs were developed only recently.[38]

At first, the stability of the citrate ad-layer on the top of Au(111) in aqueous solution was assessed by using 20 ns of standard MD simulations at 300 K. The initial and final distributions of citrate anion on the positively charged AuNP are shown in Fig. 2. None of the citrate was displaced from the surface during the entire lenght of the simulation in explicit water, in line with experimental knowledge. The distribution of citrate was stabilized on the top of the AuNP surface by direct contact with the surface gold atoms and no large

9

distortion of the ad-layer from the initial conformation have been observed.

In order to enhance the effective sampling space of our protein-citAuNP system, we have applied REMD involving multiple independent simulations at different temperatures (T-REMD). In the present simulation protocol the system periodically attempts an exchange in temperature space,[42,43] thus enabling replicas at low temperature to exchange to a higher temperature where energy barriers may be more easily crossed. In this way we overcome the limit of straight MD simulations which are known to suffer from the quasi-ergodic problem *i.e.* simulations at low temperature tend to get trapped in a local-minimum-energy state.[42] Given the experimental evidence demonstrating that the neutral nonprotonated wildtype β_2m does not form amyloid fibrils *in vitro*,[44–46] we have generated the effect of both non-protonating and protonating conditions by using two fully solvated systems, which were equilibrated under constant temperature for 20 ns with standard MD: (i) nonprotonated normal β_2m (PDB code 1JNJ *i.e.* with only HIS51 and HIS84 protonated); (ii) protonated normal β_2m (PDB code 1JNJ with also HIS31 protonated). The present experimental pH conditions are correctly described by a nonprotonated regime for the protein but given the presence of the negative citrate ad-layer which may stabilize the protonated regime, both regimes may be relevant and should be investigated. The comparison of the two protonation states is very important here, since the protonation state has been found to be relevant in determining the stability of the protein and of the barrier-crossing energies between normal and amyloidogenic form of βm.[47–51] For example, a very low pH was used in ref.,[21] at which HIS31 is certainly protonated.

Before starting the T-REMD, we applied to both systems an equilibration protocol which consists of various steps of optimization of atomic coordinates and restrained finite-temperature dynamics during which the restraints on protein atoms were gradually weakened and eventually released, according to a previously reported procedure.[52–54] At the end of the equilibration, the trajectories were stable in terms of density, temperature, potential energy and other macroscopic properties. The equilibration phases of the nonprotonated and protonated

10

protein were followed by 20 ns of unrestrained T-REMD in which 32 replicas on the top of
cit-Au(111) surface for each systems were used, yielding an aggregated simulation time of
640 ns. During the 20 ns of T-REMD the proteins of each replica were fully flexible and the
water molecules, ions, and citrates were treated explicity in the simulations.

Simulations results are summarized in Fig. 4 in which panel (a) is referring to nonprotonated
protein and panel (b) is referring to protonated protein.

Figure 4: Panels (a) refers to the nonprotonated protein and panel (b) to the protonated pro-
tein. Top panels (a) report the most representative structures of the nonprotonated protein
during T-REMD and top panel (b) the orientation for the protonated protein on cit-AuNPs.
In both cases the results are obtained following the Replica at the lowest temperature dur-
ing 20 ns of T-REMD. Lowest panels (a-b) report the time evolution of contacting residues
(*i.e.*, residues with atoms within 0.6 nm from the Au surface) for the nonprotonated and
protonated protein with respect to the surface of the nanoparticle, extracted from the last
10 ns of the total 20 ns T-REMD.
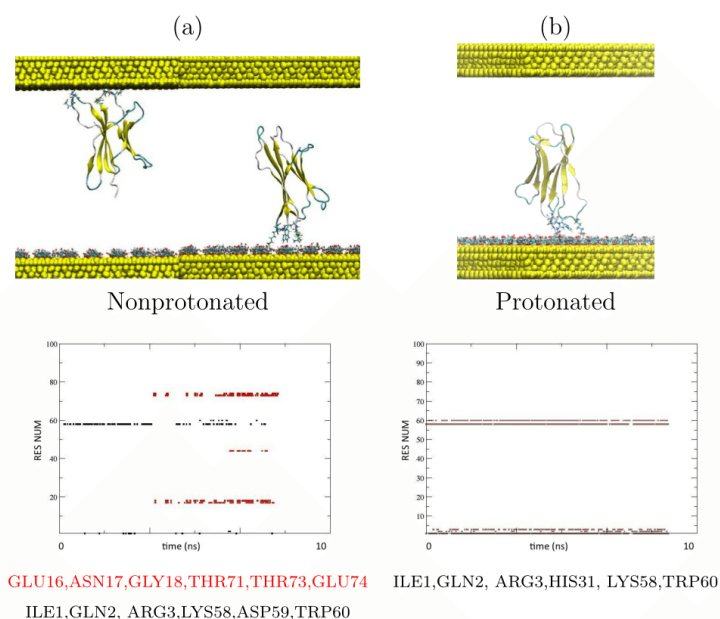
Top panel of Fig. 4(a) report the final representative structures of the two most recurrent
orientations found for the nonprotonated protein and Fig. 4(b) the unique stable orientation
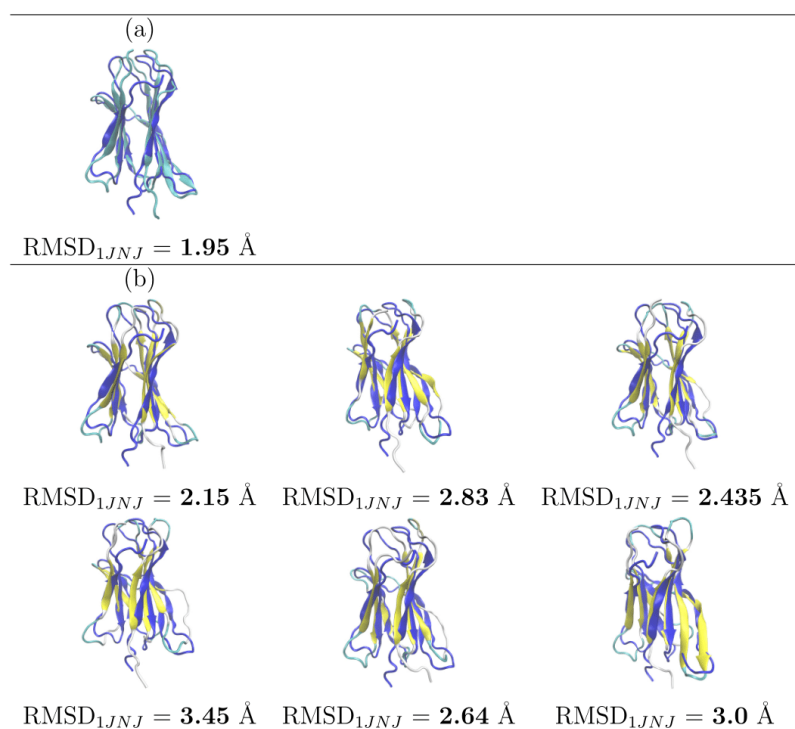
11

for the protonated protein. In both cases the results were obtained following the replica at the lowest temperature during the 20 ns of T-REMD. Lowest panels of Fig. 4(a-b) report the time evolution of contacting residues for the nonprotonated (a) and protonated (b) protein with respect to the surface of the nanoparticle, along the last 10 ns of T-REMD. In the case of the nonprotonated protein the patch contacting the citrate surface is not conserved during the simulation which point to a loosely bound neutral protein on the top of cit-AuNPs. On the contrary, for the protonated protein, Fig. 4(b) the contact patch is unique and well conserved during the entire 20 ns lenght of T-REMD since the protein is never able to detach from the citrate layer during the 20 ns but it remains anchored through the N-Terminal residues (ILE1, GLN2, ARG3) and DE-loop residues (LYS58, TRP60). The capability of the nonprotonated protein to detach from the citrate surface during T-REMD is in line with the labile, transient interaction measured by the experiments (as will be discussed in the next Sections).

The structural impact on (i) nonprotonated and (ii) protonated protein upon adsorption on the top of cit-Au(111) surface, were analyzed with an additional conformational analysis (sorting and averaging of the trajectories) of the simulated systems to select a few representative structures of the proteins contacting the cit-Au(111) through the N-Terminal tail. Clustering with a simple means algorithm was applied during the last 5 ns of the 20 ns T-REMD, extracting (i) 1 relevant representative structure for the nonprotonated protein and (ii) 6 relevant representative structures for the protonated protein, (shown in Fig. 5) covering the 50 per cent of the total population in both cases.

The unique nonprotonated structure has a RMSD value of 1.96 Å with respect to the NMR reference structure (PDB:1JNJ), pointing to modest internal rearrangements of the nonprotonated protein. On the contrary, protonated structures have RMSD with respect to NMR reference (PDB:1JNJ modified by protonation of HIS31 residue) ranging from 2.15 to 3.45 Å referring to local rearrangments of loops AB, DE, BC and strand D (see Fig. 5). In all cases the internal rearrangements of the proteins suggest the absence of unfolding events in

12

Figure 5: Cluster analysis of the conformational rearrangements of the protein on cit-AuNP during the last 5 ns of the 20 ns of T-REMD following replica at the lowest temperature and computed RMSD respect to the NMR reference structure. Panels (a) refers to the nonprotonated protein and panel (b) to the protonated protein. Resulting structures are covering the 50 per cent of the total population in both cases.

(a)

$RMSD_{1JNJ} = \mathbf{1.95}$ Å

(b)

$RMSD_{1JNJ} = \mathbf{2.15}$ Å $RMSD_{1JNJ} = \mathbf{2.83}$ Å $RMSD_{1JNJ} = \mathbf{2.435}$ Å

$RMSD_{1JNJ} = \mathbf{3.45}$ Å $RMSD_{1JNJ} = \mathbf{2.64}$ Å $RMSD_{1JNJ} = \mathbf{3.0}$ Å

the short term able to destructure the secondary structure of the native protein. However, the larger RMSD and the larger variety of structures observed for the protonated protein point to a lower stability of the system under acidic conditions upon adsorption on cit-Au. Moreover, a deeper analysis showed that among the structures with the largest RMSD with respect to the NMR reference, the largest deviations were localized at the BC loop region which is belonging to the hydrophobic pocket formed by the N-Terminus, BC and FG loop, as discussed in reference.[47] To quantify, the RMSD restricted to the atoms of the BC loop (residues 31-34) were evaluated and found to range from (i) 2.5 Å for the nonprotonated

13

case, to (ii) 3.4 Å for the protonated case, respect to the NMR reference. For the sake of comparison, the same RMSD restricted to the BC loop (for the nonprotonated β_2m) were compared with that of the same protein interacting with a hydrophobic nanoparticle $(Au_{25}L_{18}{}^-(L{=}S(CH_2)_2Ph))$ through the same hydrophobic patch.[55] In that case the RMSD value was only 1.6 Å. The reported behaviour points to an induced larger exposure of the protonated HIS31 side-chains upon adsorption to hydrophilic respect to hydrophobic surfaces. Native *cis*-prolyl peptide bond (between HIS31 and PRO32) switches into *trans* as part of the transition to the amyloidogenic state. It is well known that the conversion of the HIS31-PRO32 peptide bond from *cis* to *trans* requires the breaking of a network of hydrogen bonds[56] and of the interactions stabilizing the hydrophobic pocket.[47] This transition may therefore be catalyzed by the interactions of N-terminal residues with the ad-layer of citrate. We were not able to observe the *cis-trans* transition in our simulations, due to the low probability of the event and the length of the simulations. To understand if the citrate ad-layer has a role in the conformational rearrangements of the protonated protein, we have repeated the same 20 ns TREMD simulation for the protein in bulk solution (same number of replicas). Focusing on the BC loop, the RMSD was observed to decrease from 3.4 Å on cit-AuNP to 2.2 Å in solution for the protonated case (the RMSD of the entire protein also decreased). These findings indicate that the citrate ad-layer magnifies the conformational changes related to protein protonation. To investigate this point further, we additionally performed configurational Principal Component Analysis (PCA) to reveal the structures underlying the atomic fluctuations and the region of the protein with the highest degree of correlation, which may be directly connected through bonds or move in a concerted manner. In Fig. 6, we report a direct comparison between the first three dominant fluctuations of the (i) nonprotonated and (ii) protonated protein in solvent and upon interaction with the cit-AuNPs. In the case of (i) nonprotonated protein the largest collective motions of atoms are localized at the N-Terminal tail and DE-loop regions, whereas in the (ii) protonated case fluctuations of the BC loop, involving the HIS31-PRO32 peptide bond, are more relevant

14

especially in the vicinity of the ad-layer of citrate (see mode 1 and 2 in Fig. 6) and appear to be sligthly correlated to the fluctuation of the proximal DE loop belonging to the same hydrophobic pocket. More in detail, fluctuations at the BC loop appear to be larger when fluctuations at DE loop are larger. On the contrary, fluctuations at the BC and DE loop appear to be larger when fluctuations at AB loop are smaller, and viceversa. The comparison clearly shows the role of the interaction with the charged surface of cit-AuNPs on the induced conformational changes of the protonated protein which are absent in water, and much more limited for the nonprotonated case.

Figure 6: Principal Component Analysis: direct comparison between the first three dominant fluctuations of the (a) nonprotonated protein and (b) protonated protein in solvent and upon interaction with the cit-AuNPs. Protonated and non-protonated proteins in solvent exhibit very similar dynamics, while the protonated protein on the surface has notably larger distortions than the non-protonated one

(a) (b)

Protein in solvent   Protein in solvent

Protein on cit-Au and solvent   Protein on cit-Au and solvent
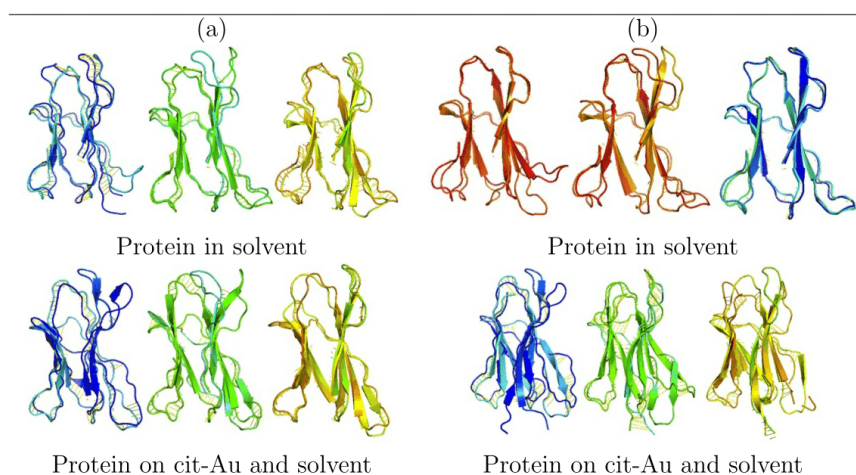
To summarize, with a number of T-REMD refining runs, we were able to assess the global stability of complex A already predicted by rigid-body BD docking, on the top of negatively charged AuNPs. The protein was always contacting the nanoparticle through the apical region representing the edges of the D, E β-strand and N-terminal tail. The protonated and nonprotonated forms of the proteins showed quite different stability when interacting with

15

the citrate layer (largest changes and fluctuations for the protonated). In particular, the comparison between the protonated β_2m behavior in solution and interacting with the citrates suggests that the latter accentuate the structural destabilization following protonation.

Role of Nanoparticle Actual Size on the Electrostatic Interaction

In order to support the assumption based on a flat surface, the nanoparticle coated by citrate was additionally simulated by a dielectric sphere with a diameter of 5 nm (as in the experiments), and with the same density of negative charge as in the Brownian Dynamics model (-1.38 e/nm^2).

Because the goal of this model was to test the effect of finite particle size on electrostatic, only electrostatic interactions were considered. It was also assumed, based on explicit computations for a few randomly selected rotamers, that the generalized Born radii of the atoms are not changed significantly by the presence of the nanoparticle, as long as the two systems remain well separated.

Generalized Born radii have been computed according to the GBR6 model which was shown to be extremely accurate for proteins.[57] The set of 10 rotamers leading to the system's lowest electrostatic energy are superimposed and displayed in Fig. 7 for the neutral and positively charged states of β2-microglobulin.

The number of favorable orientations and the computed interaction energies depend on the distance between the centers of mass, on the radius assumed for the citrate particles and on the charge state of the protein. For the neutral state there are 384 favorably interacting orientations out of 800, whereas for the positively charged state the same figure rises to 425. Notwithstanding these differences it is seen that for all orientations the N-terminal region is pointing towards the negative nanoparticle. The same conclusion holds for all the possible sixteen protonation states of the four histidines, although the number of favorably interacting orientations and the interaction energy depends on the histidines protonation state (data not shown).
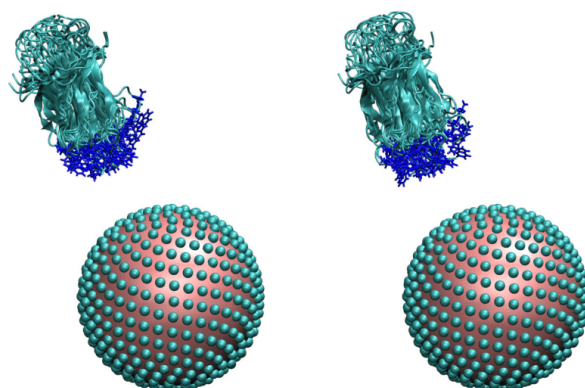
16

Figure 7: 10 lowest energy arrangements of β2-microglobulin (shown together) and a model of citrate coated nanoparticle for the neutral protein (left panel) and positively charged protein (right panel). Citrate moieties are modeled as 3 Å spheres on the surface of 25 Å sphere representing the nanoparticle. The sidechains of residues 1, 3, 31, 59, 60 of the protein are shown in blue.

NMR Experimental Evidence

1D ^{1}H and 2D [^{1}H, ^{15}N] HSQC NMR experiments have been used to characterize, at amino acid residue level, the interaction between β_2m and gold nanoparticles at various molar ratios. Different samples containing 130 nM of 5nm AuNP (Sigma-Aldrich) and variable β_2m concentrations ranging from 4 to 36 μM were analysed.

A general decrease of β_2m signal intensity in ^{1}H monodimensional experiments when Au nanoparticles were added is highlighted in Fig. 8 whereas chemical shifts are only marginally affected.

In fact, the presence of nanoparticles affects the protein signal intensities much more than chemical shifts. The attenuation tends to decrease as the protein concentration increases and arises from exchange average between the free molecule and the species transiently in contact with the nanoparticle. Due to the slower tumbling of the protein nanoparticle adduct with respect to the free molecule, the resulting larger extent of dipolar broadening propagates to the free species because of fast exchange, thereby attenuating the overall sampled signal. This behaviour is consistent with protein-nanoparticles interaction also confirmed by a surface

17

plasmon resonance absorption red shift of 3.4 nm shown in Fig. 9.

Similar shifts were reported for hUbq and azurin.[26] The comparison of 1D spectra of β_2m alone and with AuNP presence suggests the absence of any significant chemical shift perturbation that is confirmed by the complete cross-peaks overlap of HN signals in 2D [^{1}H, ^{15}N] HSQC maps acquired with and without nanoparticles (results are shown in Fig. 2 of Supplementary Information).

This is the signature of a conserved protein fold also when the protein interacts with the gold-citrate surface. On the contrary, the analysis of the normalised cross-peaks intensities, shown in Fig. 10, reveals differential behaviours of the observed HN connectivity signals suggesting variable dipolar contributions to relaxation for the various amide locations that approach more closely the surface of the AuNPs.

Simple steric consideration, based on the protein modeled as a sphere or with an oblate shape, has lead to speculate that some 15 to 25 molecules can be accommodated in a layer surrounding a 5 nm diameter nanoparticle. These estimates are probably in excess because a very close packing is implied, but tell us that in the present experimental conditions, even at the lowest tested β_2m concentration, the number of protein molecules is largely exceeding the amount required to cover the particle surface. Therefore the present results reflect the fast exchange between the bound and free state of the protein, in the context of a labile protein-nanoparticle adduct. This, in turn, suggests a weakly bound protein layer surrounding the NPs, also referred to as soft corona,[13] even if the corresponding hard corona would be poorly observable by NMR because of an expected rather slow rotational tumbling rate, there are a few elements that make unlikely the occurrence of a tightly bound layer of β_2m around the small AuNPs used. First, the size of the NPs is not that large to support a tightly bound first corona layer.[13] The actual interaction between the citrate-coated surface of the NPs and the protein should be electrostatic, as confirmed by simulation, but the overall protein charge should be around zero or slightly negative, which definitely attenuates the layer tightness. The substantial agreement between simulation and experiment for the

18

NP close approach or contact points on the protein surface suggests that the loosely bound layer of protein molecules we observe experimentally does not establish contacts with any hard corona layer of protein molecules. The experimental differential attenuation pattern, on the other hand, can not be attributed to the citrate because control experiments (not shown) confirm the absence of any correlation between the pattern oberved with citrate-coated AuNPs and that obtained with citrate alone. The described weak interaction regime appears also consistent with the experimentally observed attenuation pattern of the protein signals. The normalised intensities in Fig.10 for the backbone amide peaks obtained from the 26 μM sample are highlighted on the β_2m molecular structure in Fig. 11 (pdb code: 1JNJ) through appropriate colour coding.

The picture renders the involvement in the interaction with Au-NP of the N-ter apical part of the protein, and in particular GLN2, ARG3 in the N-terminus, and LYS58 and ASP59 in loop D-E, in good agreement to complex A of simulations as already discussed in Fig. 3. In addition we could also identify other close interaction sites, in loop D-E, SER55 and PHE56, in strand B, residues TYR26, SER28, GLY29, PHE30 and SER33 in the following BC loop. This interaction pattern is proved to be independent from the experimental protein/nanoparticle molar ratio. Very similar pictures emerged, in fact, also when the β_2m concentration was lowered to 4 μM with a β_2m/AuNP ratio of about 30. The same residues involvement was assessed with the addition of LYS6, ASN42 and LEU65. These additional involvements may reflect the less-populated binding modes which are expected to occur from rigid docking (see Supporting Information) and whose occurrence should be more easily observed at low protein concentration excess with respect to AuNPs. To test a long term effect of AuNP on β_2m stability we repeatedly acquired HSQC spectra over 4 to 7 days from sample preparation - and more recently over about a month with an analogous system - without revealing any significant variation (data not shown). This result establishes over macroscopically - accessible time frames the conformational stability elements observed in T-REMD analysis.

19

Figure 8: 1D 1H NMR spectra: In blue and red are the traces of the protein alone and in the presence of gold nanoparticles at 130nM, pH 6.47 and 298K. The protein concentration is 36 and 17 μM in (a) and (b), respectively. A few limited changes are seen upon adding Au nanoparticles. Among these, we can identify shifts of the phenyl hydrogens of F56 around 6.5 and 6.9 ppm (the corresponding amide resonances, however, do not undergo any shift - see the HSQC map in Supplementary Information). In addition we see the intensity loss of N42 side chain amide around 8 ppm and the slight chemical shift changes of S28 and L40 backbone amides at about 9 ppm. On the other hand, the differences that are seen in the aliphatic region are due to citrate and stabilizing surfactants that occur in the nanoparticle preparations.
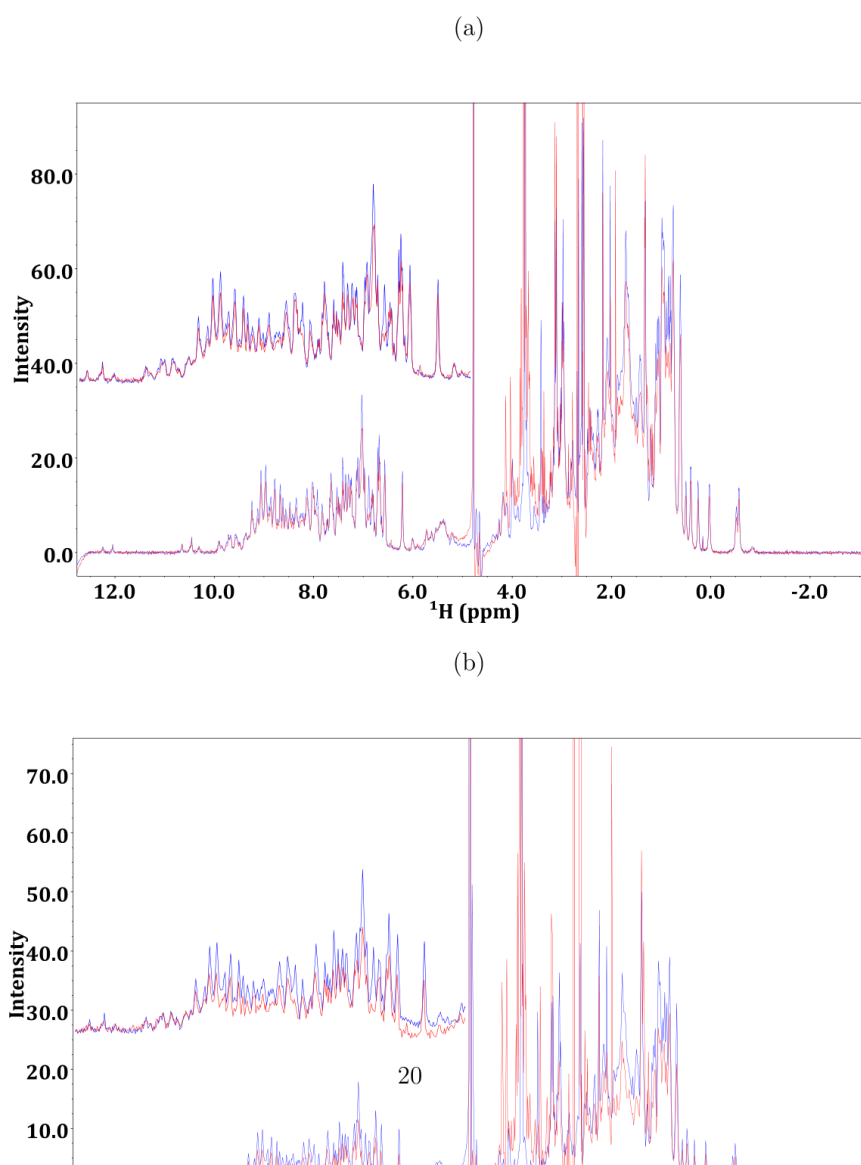
(a)

(b)

Figure 9: UV-Vis spectra of AuNP free and bound to β_2m in red and blue, respectively. AuNP and β_2m are at a concentration of 130 nM and 26 μM. In a) the UV-Vis spectrum and in b) the spectrum derivative highlights the surface plasmon resonance red shift of 3.4 nm.
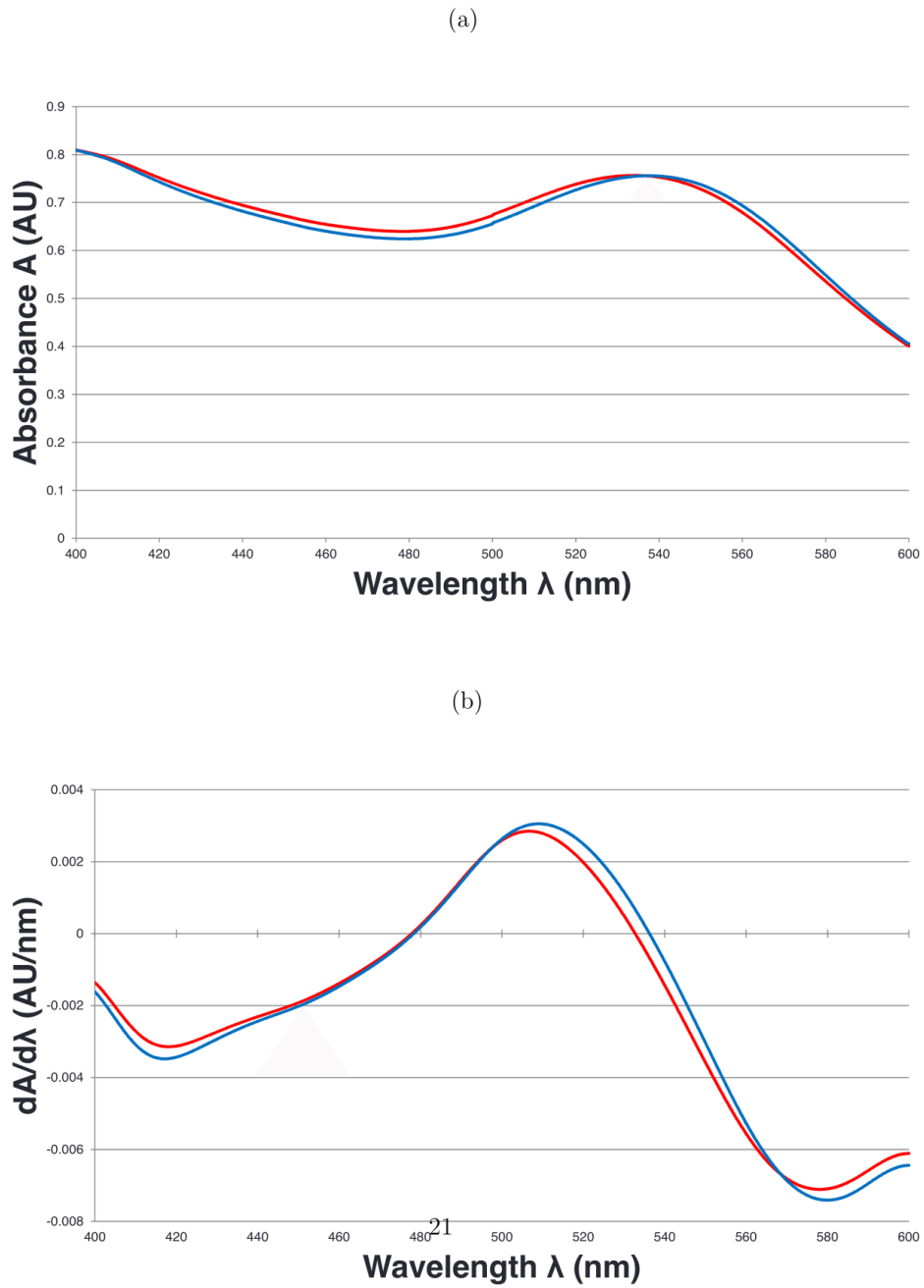
(a)

(b)

Figure 10: Relative intensities of β_2m HSQC cross peaks in the free and bound state at a protein concentration of 17μM.
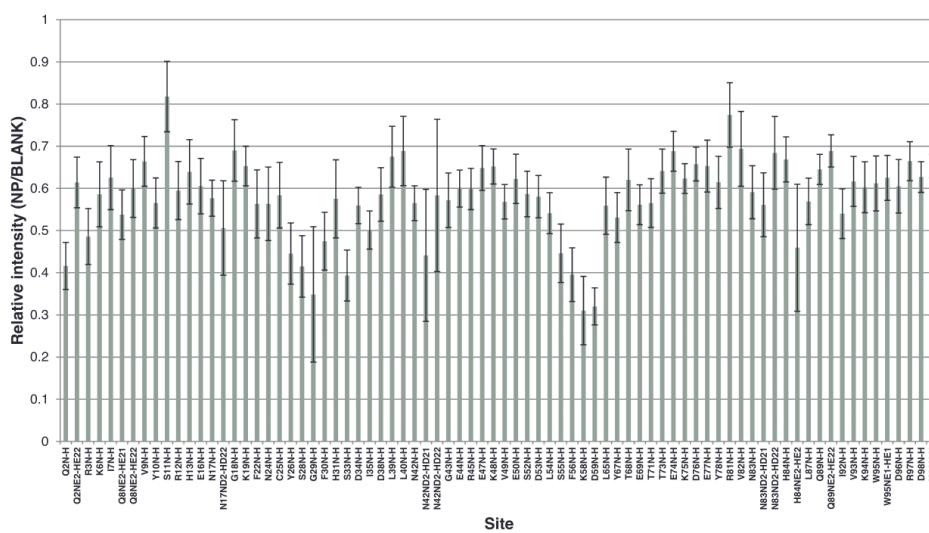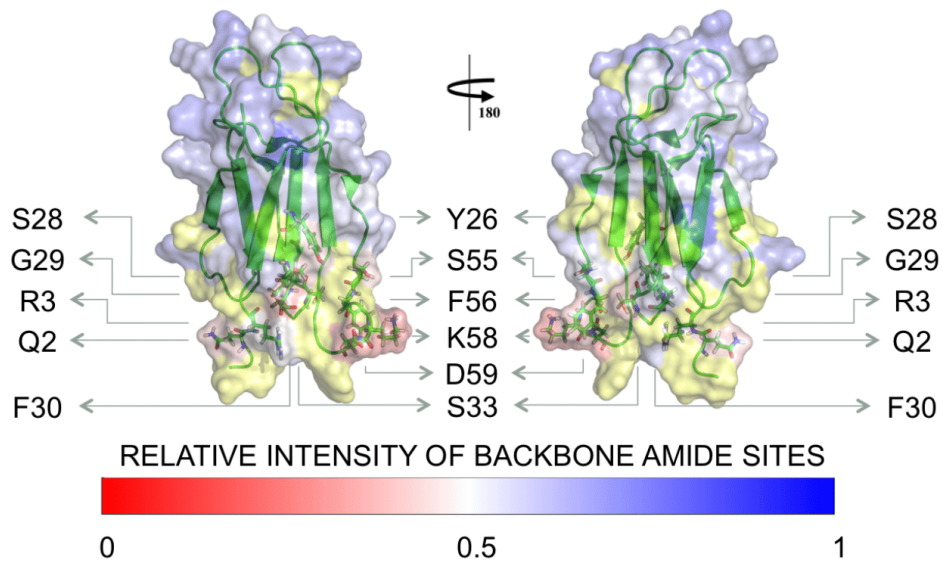

22

Figure 11: β_2m surface coloured according to the relative intensity scale. The residues whose backbone amide sites have less than 0.5 relative intensities are highlighted. In yellow the amide residues not measured in the analysis.

Conclusions

In this article, we have presented an extensive set of experimental and computational study of the interaction between β_2m and citrate-capped gold NPs. We have used atomically detailed simulations at multiple levels of theory, including docking by Brownian dynamics, Poisson Boltzmann electrostatics and enhanced atomistic MD. From these simulations, we could provide molecular insights into the β_2m-cit-AuNP interactions that are not directly accessible from experiments. In particular, on the basis of our results on protein-surface docking and implicit solvation modeling, we discussed the nature of the interactions that guide the binding of β_2m to the citrate-capped gold nanoparticle, finding that long range, electrostatic interactions are the leading terms for the encounter complex. In fact, the orientation of the protein relative to the particle surface is determined by such interactions and is in agreement with the experimental results from NMR spectroscopy. Moreover, the comparison between docking results obtained mimicking the experimental conditions clearly states that the ad-layer of citrate molecules does remain on the surface of the NP, coexisting with the adsorbed protein, similarly to what previously shown for other proteins on cit-AuNP.[27,58] Both experiments and simulations suggest that the internal rearrangements of the protein induced by the interaction with the charged surface of cit-AuNPS are not able to disrupt the secondary structure of the native protein thus do not lead to unfolded amyloidogenic intermediates. The overall picture is consistent with the small dimensions of the AuNPs and the labile interaction regime that occurs between β_2m and the AuNPs. Our MD results also suggest that the effect of protonation of HIS31, known to destabilize the protein toward amyloidogenic intermediates, are enhanced by the interaction with the negative surface. Our work also offers a fresh view on the interaction of the protein with biomolecules comprising negative charge arrays.

The results presented here, combined with our previous findings on hydrophobic NPs,[55] suggests that by properly balancing the extent of electrostatic and hydrophobic interactions, the NP surface may provide stabilization/destabilization to amyloidogenic proteins as shown

24

in the comparison between nonprotonating and protonating conditions. Therefore NP-based approaches to treat amyloid pathologies may be definitely conceived once the available ingredients for NP performance are adapted to the properties of the specific protein surface.

25

Methodology

Electrostatic model

The structure of $\beta2$-microglobulin (pdb id. 1jnj) was preprocessed using the program pdb2pqr[59] using the CHARMM set of radii and charges. In view of the high negative potential due to the nanoparticle, HIS51 for which a pKa of 6.6 is predicted using the program BLUUES[57] was assigned a protonated state. The overall charge of the protein is important for the absolute value of the interaction with the nanoparticle, but the best orientations are less sensitive to it. In the presence of a negatively charged nanoparticle (and consequent local pH lowering) it is expected that the overall charge state of the protein should be close to zero at measured pH 6.5. The structure of $\beta2$-microglobulin was placed at 65 Å distance from the center of the nanoparticle rotated around 100 axes uniformly distributed in the solid angle and identified by the polar angular coordinates θ and ϕ. The rotation angle ψ about the axis was taken from a distribution with probability density:

$$\frac{2}{\pi}\sin^2(\frac{\psi}{2}) = \frac{1}{\pi}(1 - \cos(\psi)) \tag{1}$$

for uniformly sampling the rotation space. The total number of rotations sampled was 800.

NMR Spectroscopy

The interaction between β_2m and AuNP was studied by NMR experiments and UV-Vis absorption spectroscopy on samples containing Au-nanoparticles at a concentration of 130 nM. NMR experiments were performed at β_2m concentrations of 4, 17, 26, 36 μM. All the samples analysed were buffered with 25 mM sodium phosphate, pH 6.4 and contained 5% D2O for lock purposes. NMR experiments were recorded on a Bruker Avance spectrometer operating at 500 MHz (^{1}H). 1D ^{1}H spectra were acquired with 4096 data point, a spectral width of 16

26

ppm and 4096 scans. The water suppression was achieved by excitation sculpting scheme.[60] 2D and [^{1}H, ^{15}N] HSQC were acquired with 1024 and 128 points in the direct and indirect dimensions, respectively, and 400-1600 scans depending on the sample concentration, over spectral widths of 16 and 37 ppm in the 1H and 15N dimension, respectively. The data were processed with Topspin 2.1 and analysed with NMRViewJ.[61] The β_2m assignment was based on the file deposited on the Biological Magnetic Resonance Data Bank (Accession Code: 17165). AuNPs, 5nm in diameter, 0.01% in HAuCl$_4$ (around 130 nM in NP concentration) were purchased by Sigma-Aldrich (Product Code: G1402) and used without further purification after UV-vis test to verify that no aggregation has taken place.

UV-Vis Absorption Spectroscopy

A spectrum in the range from 400 to 600 nm was acquired with a JASCO UV-530 spectrophotometer on samples containing Au-nanoparticles and β_2m at a concentration of 130 nM and 26 μM, respectively. The experimental condition for the solutions were the same as those for NMR samples. 1001 points were acquired with a band-width of 2.0 nm, a data pitch of 0.2 nm and a speed of 40 nm/min.

Brownian Dynamics Simulations

Rigid-body docking simulations were carried out using Brownian dynamics (BD) techniques with the ProMetCS continuum solvent model for protein-gold surface interactions.[40] The calculations were performed using the SDA version 6 software.[62,63] The Au(111) surface was constructed with a surface area of 100 Å x 100 Å and three atomic layers.[64] The β_2m structure was taken from the NMR solution structure (PDB id: 1JNJ). Human β_2m is a 99-residue-long, 11.9 kDa protein, with a single disulphide bridge between the two CYS residues of the sequence at positions 25 and 80. The protein folds into the classical β-sandwich motif of the immunoglobulin superfamily, *i.e.* seven antiparallel β-strands (A, B,..., G) forming two facing sheets (ABED and CFG).[65]

27

5000 BD trajectories were computed starting with the protein positioned randomly with its center at a distance of 70 Å from the surface where the protein-surface interaction energy is negligible. The specified number of docked complexes was extracted directly from the runs and clustered with a clustering algorithm. Experimental salt concentration of 30 mM was included as a non-specific screening effects on the electrostatic potential of the protein which was calculated using the APBS program.[66] The relative translational diffusion coefficient was 0.0123 Å^2/ps and the rotational diffusion coefficient for the protein was 1.36 x e-4 in radian^2/ps. The simulation timestep was set to 0.50 ps. Parameters for the calculation of hydrophobic desolvation energy and forces was set to -0.019 kcal/mole/Å^2 and for the electrostatic desolvation energy and forces to 1.67 according to ref.[67] BD trajectories were generated in a rectangular box (ibox=1); the dimensions of the (x, y) plane, describing the symmetry of the simulation volume as well as the surface size, were given as input parameters. At each BD step, the protein-surface interaction energy and forces acting on the protein were computed using the implicit-solvent ProMetCS force field,[40] developed and parametrized for protein-gold surface interactions. The energy terms included in ProMetCS have been described in the main text.

Two clustering algorithms were tested and evaluated for this system. These were top-down splitting (hierarchical based on a reference structure) and bottom-up aggregating (single-linkage based on RMSD). The results of docking were preprocessed by translating the protein coordinates parallel to the surface in order to superimpose the protein stuctures before applying the clustering algorithm. Finally, we applied a single-linkage clustering method (based on CA atoms, with RMSD= 3.0 Å) for the results given in the manuscript.

Molecular Dynamics Simulations

We have implemented new force field parameters for the citrate anions based on *ab initio* calculations (that take into account the quantum nature of such small chemical species) in a consistent and compatible way with the existing GolP force field for the protein-AuNP

surface interactions.

The regular citrate ad-layer on the top of Au(111) was generated with a ratio of the surface gold ion and citrate concentrations suitable to reproduce experimental data.[39] The positive atomic charges of the gold surface atoms were set to fit the electronic charges / cm^2 on the surface of the AuNPs in the electrochemical experiments under aqueous conditions and at physiological pH.[33]

For the (i) nonprotonated β_2m: all titratable protein side chains, were assigned their standard protonation state at pH 6.8 using the H++ pK-calculation program;[68] (ii) for the protonated protein, additional protonation at HIS31 was performed.

At the beginning of the simulation the protein was moved away from the surface of the cit-AuNPs by 6 Å, without changing the orientation resulted from docking. Various tests that we performed showed that the protein in direct contact with the surface is in a kinetically trapped state were only minor relaxation can take place on the time-scale of tens of ns.

For each (i) nonprotonated and (ii) protonated protein, 32 replicas of a rectangular simulation box of dimension (82 Å x 64 Å x 82 Å) including SPC water molecules, the protein, the citrate ad-layer and the gold surface was built.

Before adding the solvent in the box the protein was moved away from the surface of the cit-AuNPs by 6 Å, without changing the orientation resulted from docking. Various tests that we performed showed that the protein in direct contact with the surface is in a kinetically trapped state were only minor relaxation can take place on the time-scale of tens of ns.

All simulations were performed with the Gromacs 4.5.4 package.[69] GolP[64] and OPLS/AA parameters[70] were used for the surface and the protein and the SPC/E water model[71] was applied. The lengths of bonds were constrained with the LINCS algorithm. Surface gold atoms and bulk gold atoms were frozen during all simulations but gold dipole charges were left free. Periodic boundary conditions and the Particle-Mesh-Ewald algorithm were used. A 2 fs integration time step was used.

We performed a total of 4 independent T-REMD simulations of 20 ns in explicit water

29

for both (i) nonprotonated and (ii) protonated protein in solvent and on the top of the cit-Au(111) surface in the temperature range 290-320 K.

Trajectories were analyzed in terms of density, temperature, potential energy and other macroscopic properties with the Gromacs tools (*e.g.* g_traj, g_rms, g_clusters *etc.*). Principal component analysis was also performed using GROMACS and to compare principal component obtained from independent runs, the covariance matrix was calculated. The eigenvectors and eigenvalues were obtained from diagonalization of the combined covariance matrix, after which coordinates from each independent trajectory were projected along eigenvectors of interest to obtain projection values for given modes.

Acknowledgement

References

1. Lundqvist, M.; Stigler, J.; Elia, G.; Lynch, I.; Cedervall, T.; Dawson, K. A. Nanoparticle Size and Surface Properties Determine the Protein Corona with Possible Implications for Biological Impacts. *Proc. Natl. Acad. Sci. U.S.A.* **2008**, *105*, 14265-14270.

2. Maiorano, G.; Sabella, S.; Sorce, B.; Brunetti, V.; Malvindi, M. A.; Cingolani, R.;

30

Pompa, P. P. Effects of Cell Culture Media on the Dynamic Formation of Protein-Nanoparticle Complexes and Influence on the Cellular Response. *ACS Nano* **2010**, *4*, 7481-7491.

3. Lacerda, S. H. D. P.; Park, J. J.; Meuse, C.; Pristinski, D.; Becker, M. L.; Karim, A.; Douglas, J. F. Interaction of Gold Nanoparticles with Common Human Blood Proteins. *ACS Nano* **2010**, *4*, 365-379.

4. Mahmoudi, M.; Lynch, I.; Ejtehadi, M. R.; Monopoli, M. P.; Bombelli, F. B.; Laurent, S. Protein-Nanoparticle Interactions: Opportunities and Challenges. *Chem. Rev.* **2011**, *111*, 5610-5637.

5. Moyano, D. F.; Rotello, V. M. Nano meets Biology: Structure and Function at the Nanoparticle Interface. *Langmuir* **2011**, *27*, 10376-10385.

6. Pelaz, B.; Jaber, S.; de Aberasturi, D. J.; Wulf, V.; Aida, T.; de la Fuente, J. M.; Feldmann, J.; Gaub, H. E.; Josephson, L.; Kagan, C. R. *et al.* The State of Nanoparticle-based Nanoscience and Biotechnology: Progress, Promises, and Challenges. *ACS Nano* **2012**, *6*, 8468-8483.

7. Gobin, A.; Lee, M.; Halas, N.; James, W.; Drezek, R.; West, J. L. Near-Infrared Resonant Nanoshells for Combined Optical Imaging and Photothermal Cancer Therapy. *Nano Lett.* **2007**, *7*, 1929-1934.

8. Lu, F.; Doane, T. L.; Zhu, J.-J.; Burda, C. Gold Nanoparticles for Diagnostic Sensing and Therapy. *Inorganica Chimica Acta* **2012**, *3006*, 1-12.

9. Wright, J. Deliver on a Promise. *Nature* **2013**, *509*, S58-S59.

10. Gibbs, B. F.; Yasinska, I. M.; Calzolai, L.; Gilliland, D.; Sumbayev, V. V. Highly Specific Targeting of Human Leukocytes Using Gold Nanoparticle-Based Biologically Active Conjugates. *Journal of Biomedical Nanotechnology* **2014**, *10*, 1259-1266.

31

11. Nel, A. E.; Mädler, L.; Velegol, D.; Xia, T.; Hoek, E. M. V.; Somasundaran, P.; Klaessig, F.; Castranova, V.; Thompson, M. Understanding Biophysicochemical Interactions at the Nano-Bio Interface. *Nat. Mater.* **2009**, *8*, 543-557.

12. Dawson, K. A.; Salvati, A.; Lynch, I. Nanotoxicology: Nanoparticles Reconstruct Lipids *Nat. Nanotechnol.* **2009**, *4*, 84-85.

13. Rahaman, M.; Laurent, S.; Tawil, N.; Yahia, L.; Mahmoudi, M. Protein-Nanoparticle Interactions. *Springer-Verlag, Berlin Heidelberg* **2013**, *Ch. 2*, 21-44.

14. Saptarshi, S. R.; Duschl, A.; Lopara A. L. Interaction of Nanoparticles with Proteins: Relation to Bio-Reactivity of the Nanoparticle. *J. Nanobiotech.* **2013**, *11*, 26-37.

15. Cabaleiro-Lago, C.; Quinlan-Pluck, F.; Lynch, I.; Dawson, K. A.; Linse, S. Dual Effect of Amino Modified Polystyrene Nanoparticles on Amyloid β Protein Fibrillation. *ACS Chem. Neurosci.* **2010**, *1*, 279-287.

16. Lynch, I.; Dawson, K. A. Protein-Nanoparticle Interactions. *Nanotoday*, **2008**, *3*, 40-47.

17. Liao, Y.-H.; Chang, Y.-J.; Yoshiike, Y.; Chang, Y.-C.; Chen, Y.-R. Negatively Charged Gold Nanoparticles Inhibit Alzheimer's Amyloid-β Fibrillization, Induce Fibril Dissociation, and Mitigate Neurotoxicity. *Small* **2012**, *8*, 3631-3639.

18. Zhang, M.; Mao, X.; Yu, Y.; Wang, C.-X.; Yang, Y.-L.; Wang, C. Nanomaterials for Reducing Amyloid Cytotoxicity. *Adv. Mat.* **2013**, *25*, 3780-3801.

19. Mahmoudi, M.; Kalhor, H. R.; Laurent, S.; Lynch, I. Protein Fibrillation and Nanoparticle Interactions: Opportunities and Challenges. *Nanoscale* **2013**, *5*, 2570-2588.

20. Zaman, M.; Ahmad, E.; Qadeer, A.; Rabbani, G.; Khan, R. H. Nanoparticles in Relation to Peptide and Protein Aggregation. *Int. J. of Nanomed.* **2014**, *9*, 899-912.

32

21. Linse, S.; Cabaleiro-Lago, C.; Xue, W.-F.; Lynch, I.; Lindman, S.; Thulin, E.; Radford, S.E; Dawson, K.A. Nucleation of Protein Fibrillation by Nanoparticles. *Proc. Natl. Acad. Sci. USA* **2007**, *104*, 8691-8696.

22. Gejyo F.; Yamada T.; Odani S.; Nakagawa Y.; Arakawa M.; Kunitomo T.; Kataoka H.; Suzuki M.; Hirasawa Y.; Shirahama T.; *et al.* A new Form of Amyloid Protein Associated with Hemodialysis was Identified as β2-Microglobulin. *Biochem. Biophys. Res. Commun.* **1985**, 129, 701-706.

23. Relini, A.; Canale, C.; De Stefano, S.; Rolandi, R.; Giorgetti, S.; Stoppini, M; Rossi, A.; Fogolari, F.; Corazza, A.; Esposito, G.; *et al.* Collagen Plays an Active Role in the Aggregation of β2-Microglobulin Under Physiopathological Conditions of Dialysis-related Amyloidosis. *J. Biol. Chem.* **2006**, *281*, 16521-16529.

24. Xia, Y.; Xiong, Y.; Lim, B.; Skrabalak, S. E. Shape-Controlled Synthesis of Metal Nanocrystals: Simple Chemistry Meets Complex Physics? *Angewandte Chemie (International ed. in English)* **2009**, *48*, 60-103.

25. Sperling, R.; Gil, P.; Zhang, F.; Zanella, M.; Parak, W. J. Biological Applications of Gold Nanoparticles. *Chem. Soc. Rev.* **2008**, *37*, 1896-1908

26. Calzolai, L.; Franchini, F.; Gilliland, D.; Rossi, F. Protein-Nanoparticle Interaction: Identification of the Gold Nanoparticle Interaction Site. *Nano Lett.* **2010**, *10*, 3101-3105.

27. Brancolini, G.; Kokh, D. B.; Calzolai, L.; Wade,R. C.; Corni, S. Docking of Ubiquitin to Gold Nanoparticles. *ACS Nano* **2012**, *6*, 9863-9878.

28. Sabella, S.; Carney, R. P.; Brunetti, V.; Malvindi, M. A.; Al-Juffali, N.; Vecchio, G.; Janes, S. M.; Bakr, O. M.; Cingolani, R.; Stellacci, F. *et al.* A General Mechanism for Intracellular Toxicity of Metal-Containing Nanoparticles. *Nanoscale* **2014**, *6*, 7052-7061.

33

29. Park, J.-W.; Shumaker-Parry, J. S. Structural Study of Citrate Layers on Gold Nanoparticles: Role of Intermolecular Interactions in Stabilizing Nanoparticles. *J. Am. Chem. Soc.* **2014**, *136*, 1907-1921.

30. Relini, A.; De Stefano, S.; Torrassa, S.; Cavalieri, O.; Rolandi, R.; Gliozzi, A.; Giorgetti, S.; Raimondi, S.; Marchese, L.; Verga, L.; *et al.* Heparin Strongly Enhances the Formation of β2-Microglobulin Amyloid Fibrils in the Presence of Type I Collagen. *J. Biol. Chem.* **2008**, *283*, 4912-4920.

31. Colvin, V. M.; Kulinowski, K. M. Nanoparticles as Catalysts for Protein Fibrillation. *Proc. Natl. Acad. Sci. USA* **2007**, *104*, 8679-8680.

32. Elechiguerra, J. L.; Reyes-Gasga, J.; Yacaman, M. J. The Role of Twinning in Shape Evolution of Anisotropic Noble Metal Nanostructures *J. Mater. Chem.* **2006**, *16*, 3906-3919.

33. Kunze, J.; Burgess, I., Nichols, R., Buess-Herman, I., Lipkowski, J. Electrochemical Evaluation of Citrate Adsorption on Au(111) and the Stability of Citrate-Reduced Gold Colloids. *J. Electroanal. Chem.* **2007**, *599*, 147-159.

34. Vivek, J. P. and Burgess, I. J. Insight into Chloride Induced Aggregation of DMAP-Monolayer Protected Gold Nanoparticles Using the Thermodynamics of Ideally Polarized Electrodes *J. Phys. Chem. C* **2008**, *112*, 2872-2880.

35. Scott H. Brewer, S. H.; Glomm, W. R.; Marcus C. Johnson, M. C.; Magne K. Knag, M. K.; Franzen, S. Probing BSA Binding to Citrate-Coated Gold Nanoparticles and Surfaces. *Langmuir* **2005**, *21*, 9303-9307.

36. Lin, Y.; Pan, G.-B.; Su, G.-J.; Fang, X.-H.; Wan, L.-J.; Bai, C.-L. Study of Citrate Adsorbed on the Au(111) Surface by Scanning Probe Microscopy. *Langmuir* **2003**, *19*, 10000-10003.

37. Rostek, A.; Mahl, D.; Epple, M. Chemical Composition of Surface-Functionalized Gold Nanoparticles. *J. Nanoparticle Res.* **2011**, *13*, 4809-4814.

38. Wright, L. B.; Rodgera, P. M.; Walsh, T. R. Aqueous Citrate: a First-Principles and Force-Field Molecular Dynamics Study. *RSC Adv.* **2013**, *3*, 16399-16409.

39. Lin, Y.; Pan, G.; Su, G.-J.; Fang, X.-H.; Wan, L.-J.; Bai, C.-L. Study of Citrate Adsorbed on the Au(111) Surface by Scanning Probe Microscopy. *Langmuir* **2003**, *19*, 10000-10003.

40. Kokh, D. B.; Corni, S; Winn, P.J.; Hoefling, M.; Gottschalk, K. E.; Wade R. C. ProMetCS: An Atomistic Force Field for Modeling Protein-Metal Surface Interactions in a Continuum Aqueous Solvent. *J. Chem. Theory Comput.* **2010**, *6*, 1753-1768.

41. Gabdoulline, R. R.; Wade, R. C. Effective Charges for Macromolecules in Solvent. *J. Phys. Chem.* **1996**, *100*, 3868-3878.

42. Sugita Y.; Okamoto Y. Replica-Exchange Molecular Dynamics Method for Protein Folding. *Chem. Phys. Lett.* **1999**, *314*, 141-151.

43. Hansmann, U. H. E. Parallel Tempering Algorithm for Conformational Studies of Biological Molecules. *Chem. Phys. Lett.* **1997**, *281*, 140-150.

44. Eichner, T.; Kalverda, A. P.; Thompson, G. S.; Homans, S. W.; Radford, S. E. Conformational Conversion During Amyloid Formation at Atomic Resolution. *Mol. Cell* **2011**, *41*, 161-172.

45. Esposito, G.; Ricagno, S.; Corazza, A.; Rennella, E.; Gumral, D.; Mimmi, M.; Betto, E.; Pucillo, C.; Fogolari, F.; Viglino, P.; *et al.* NMR Spectroscopy Reveals Unexpected Structural Variation at the Protein-Protein Interface in MHC Class I Molecules. *J. Mol. Biol.* **2008**, *378*, 887-897.

46. Eichner, T.; Radford, S. E. A Generic Mechanism of β_2-Microglobulin Amyloid Assembly at Neutral pH Involving a Specific Proline Switch. *J. Mol. Biol.* **2009**, *386*, 1312-1326.

35

47. Stober, T. S.; Abrams, F. C. Energetics and Mechanism of the Normal-to-Amyloidogenic Isomerization of β_2-Microglobulin: On-the-Fly String Method Calculations. *J. Phys. Chem. B* **2012**, *116*, 9371-9375.

48. Verdone, G.; Corazza, A.; Viglino, P.; Pettirossi, F.; Giorgetti, S.; Mangione, P.; Andreola, A.; Stoppini, M.; Bellotti, V.; and Esposito, G. The Solution Structure of Human β_2-Microglobulin Reveals the Prodromes of its Amyloid Transition. *Protein Sci.* **2002**, *11* 487–499.

49. Corazza, A.; Pettirossi, F.; Viglino, P.; Verdone, G.; Garcia, J.; Dumy, P.; Giorgetti, S.; Mangione, P.; Raimondi, S.; Stoppini, M.; *et al.* Properties of Some Variants of Human β2-Microglobulin and Amyloidogenesis. *J. Biol. Chem.* **2004**, *279*, 9176-9189.

50. Esposito, G.; Corazza, A.; Viglino, P.; Verdone, G.; Pettirossi, F.; Fogolari, F.; Makek, A.; Giorgetti, S.; Mangione, P.; Stoppini, M.; *et al.* Solution Structure of β2-Microglobulin and Insights into Fibrillogenesis. *Biochim. Biophys. Acta* **2005**, *1753*, 76-84.

51. Giorgetti, S.; Rossi, A.; Mangione, P.; Raimondi, S.; Marini, S.; Stoppini, M; Corazza, A.; Viglino, P.; Esposito, G.; Cetta, G.; *et al.* β2-Microglobulin Isoforms Display an Heterogeneous Affinity for Type I Collagen. *Protein Sci.* **2005**, *14*, 696-702.

52. Brancolini, G.; Migliore, A.; Corni, S.; Fuentes-Cabrera, M.; Luque, F. J.; Di Felice, R. Dynamical Treatment of Charge Transfer Through Duplex Nucleic Acids Containing Modified Adenines. *ACS Nano* **2013**, *7*, 9396-9406.

53. Soliva, R.; Sherer, E.; Luque, F. J.; Laughton, C. A.; Orozco, M. Molecular Dynamics Simulations of PNA3DNA and PNA3RNA Duplexes in Aqueous Solution. *J. Am. Chem. Soc.* **2000**, *122*, 5997-6008.

54. Spector, T. I.; Cheatham, T. E.; Kollman, P. A. Unrestrained Molecular Dynamics of Photodamaged DNA in Aqueous Solution. *J. Am. Chem. Soc.* **1997**, *119*, 7095-7104.

36

55. Brancolini, G.; Toroz, D.; Corni, S. Can Small Hydrophobic Gold Nanoparticles Inhibit β_2-Microglobulin Fibrillation? *Nanoscale* **2014**, *6*, 7903-7911.

56. Fogolari, F.; Corazza, A.; Varini, N.; Rotter, M.; Gumral, D.; Codutti, L.; Rennella, E.; Viglino, P.; Bellotti, V.; Esposito, G. Molecular Dynamics Simulations of β_2-Microglobulin in Denaturing and Stabilizing Conditions. *Proteins* 2011 **79**, 986-1001.

57. Fogolari, F.; Corazza, A.; Yarra, V.; Jalaru, A.; Esposito, G. Bluues: a Program for the Analysis of the Electrostatic Properties of Proteins Based on Generalized Born Radii. *BMC Bioinformatics* **2012**, *13 Suppl 4*, S18

58. Brewer, S. H.; Glomm, W. R.; Johnson, M. C.; Knag, M. K.; Franzen, S.; Gold, D. L. M. Probing BSA Binding to Citrate-Coated Gold Nanoparticles and Surfaces. *Langmuir* **2005**, *62*, 9303-9307.

59. Dolinsky, TJ, Czodrowski, P, Li, H, Nielsen, JE, Jensen, JH, Klebe, G, Baker, NA PDB2PQR: Expanding and Upgrading Automated Preparation of Biomolecular Structures for Molecular Simulations. *Nucleic Acids Res.* **2007**, *35*, W522–525.

60. Hwang T.L., Shaka A.J.; Water Suppression that Works. Excitation Sculpting using Arbitrary Waveforms and Pulsed Field Gradients. *J. Magn. Res. Series A* **1995**, *112*, 275-279.

61. Johnson, B. A. and Blevins, R. A. NMR View: A Computer Program for the Visualization and Analysis of NMR Data. *J. Biomol. NMR* **1994**, *4*, 603-614.

62. Gabdoulline, R. R.; Wade, R. C. Simulation of the Diffusional Association of Barnase and Barstar. *Biophys. J.*, **1997**, *72*, 1917-1929.

63. www.h-its.org/mcm

64. Iori, F; Di Felice, R.; Molinari, E.; Corni, S. GolP: An Atomistic Force-Field to Describe

37

the Interaction of Proteins with Au(111) Surfaces in Water. *J. Comp. Chem.* **2009**, *30*, 1465-1476.

65. Esposito, G.; Corazza, A.; Bellotti, V. Pathological Self-Aggregation of β_2-Microglobulin: A Challenge for Protein Biophysics. *Subcell Biochem.* 2012, **65**, 1917-1929.

66. Baker, N. A.; Sept, D.; Joseph, S.; Holst, M. J.; McCammon, J. A. Electrostatics of Nanosystems: Application to Microtubules and the Ribosome. *Proc. Natl. Acad. Sci. U.S.A* **2001**, *98*, 10037-10041.

67. Elcock, A. H.; Gabdoulline, R.R.; Wade, R. C. and McCammon, J. A. Computer Simulation of Protein-Protein Association Kinetics: Acetylcholinesterase-Fasciculin. *J. Mol. Biol.* **1999**, *291*, 149-162.

68. http://biophysics.cs.vt.edu/H++

69. van der Spoel, D.; Lindahl, E.; Hess, B.; Groenhof, G.; Mark, A. E.; Berendsen, H. J. C. GROMACS: Fast, Flexible, and Free. *J. Comp. Chem.* **2005**, *26*, 1701-1718.

70. Jorgensen, W. L.; Maxwell, D. S.; TiradoRives, J. Development and Testing of the OPLS All-Atom Force Field on Conformational Energetics and Properties of Organic Liquids. *J. Am. Chem. Soc.* **1996**, *118*, 11225-11236.

71. Hess, B. and van der Vegt, N. F. Hydration Thermodynamic Properties of Amino Acid Analogues: A Systematic Comparison of Biomolecular Force Fields and Water Models. *J. Phys. Chem. B* **2006**, *110*, 17616-17626.

38

Supplementary Information - Probing the Influence of Citrate-Capped Gold Nanoparticles on an Amyloidogenic Protein

Giorgia Brancolini,[*,†] Alessandra Corazza,[‡,¶] Marco Vuano,[‡] Federico Fogolari,[‡,¶] Maria Chiara Mimmi,[‡] Vittorio Bellotti,[§,¶,‖] Monica Stoppini,[§,¶] Stefano Corni,[*,†] and Gennaro Esposito[*,‡,¶,⊥]

Center S3, CNR Institute Nanoscience, Via Campi 213/A, 41125 Modena, Italy, Dipartimento di Scienza Mediche e Biologiche (DSMB), University of Udine, Piazzale Kolbe 3, 33100 Udine, Italy, Istituto Nazionale Biostrutture e Biosistemi, Viale medaglie d'Oro 305 - 00136 Roma, Italy, Dipartimento di Medicina Molecolare, Universita' di Pavia, Via Taramelli 3, 27100 Pavia, Italy, Division of Medicine, University College of London, London NW3, 2PF, UK, and Science and Math Division, New York University at Abu Dhabi, Abu Dhabi, UAE

E-mail: giorgia.brancolini@nano.cnr.it; stefano.corni@nano.cnr.it; gennaro.esposito@uniud.it

---

*To whom correspondence should be addressed
†CNR-NANO-S3
‡UniUd
¶INBB
§UniPv
‖UK
⊥NYUAD

1

Validation of the Docking Model

To investigate the nature of the binding between β_2m and a citrate-coated gold surface, as well as the effect of a negative surface potential, we looked for the possible adsorption orientations of β_2m on citAu(111) (and the corresponding driving forces) by initially using an implicit electrostatic effects of negatively charged citrate molecules on the surface assigning a small negative charge density of $(Au_{chg}^{net} = \text{-0.01 } e)$ per surface atom.

When this docking procedure was applied to the system, it yielded three different orientations accounting for more than 92 per cent of the total encounter complexes when the negative Au surface was considered (see Tab. 1). The representative structure of each computed complex is shown in Fig. 1. The protein residues contacting the surface differ in the various complexes, and are listed in Tab. 1.

In the case of the negatively charged state of the gold surface the preferred orientation are complex A which is still involving the residues at the N-terminal (ILE1, ARG3) tail and DE-loop (LYS58, ASP59 and TRP60) of the protein but complexes B (driven mostly by E_{LJ} interactions) and C (driven both by E_{LJ} and electrostatic terms) are also present. In both cases of a small negative charge density of $(Au_{chg}^{net} = \text{-0.01 } e)$ per surface atom and a larger charge density of $(Au_{chg}^{net} = \text{-0.05 } e)$ reported in the main text, pose A is present and it is the most populated, therefore suggesting a picture in which the layer of citrate covering the surface of the GNP does remain on the surface of the gold and interacts with the protein, as already predicted by the proposed atomistic model in Fig.1.
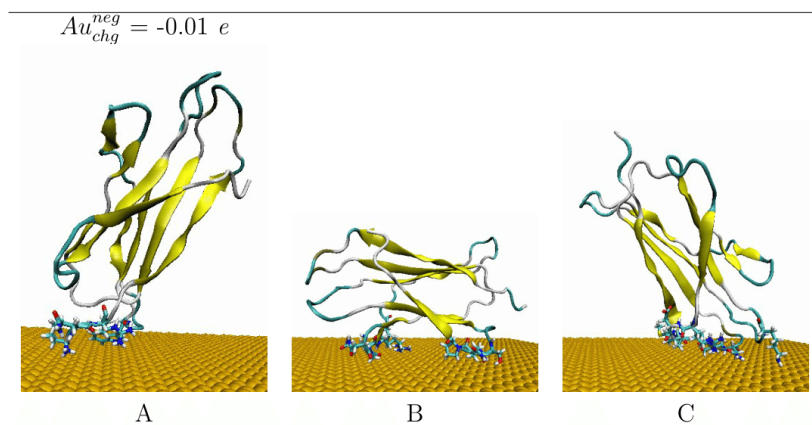
2

Au_{chg}^{neg} = -0.01 e

| | A | B | C |

Figure 1: Most populated encounter complexes of β_2m on negatively charged gold nanocluster obtained by BD simulation. In the case of Au_{chg}^{neg} = -0.01 e, the structures of representative complexes for each of the three clusters are shown, ordered by decreasing cluster size. The reported complexes represent the 92 per cent obtained by BD simulation. The protein backbone is shown in cartoon representation. The residues contacting the gold surface are shown in stick representation.

Table 1: Resultant encounter complexes from rigid-body BD docking of β_2m (1JNJ) to an Au (111) surface. A hierarchical clustering algorithm (based on a minimum distance linkage function) was applied to the diffusional encounter complexes after docking to a bare negative gold (Au_{chg}^{neg} = -0.01 e) surface. The reported complexes represent 92 per cent obtained by BD simulation.

Label $Au_{chg}^{neg} = -0.01e$	RelPop % (a)	U_{Repr} (b)	$E_{LJ}+U_{ds}^{p}+U_{ds}^{m}$ (c)	U_{EP} (d)	spread (e)	Contact Residues (f)
A	45	-5.280	-0.053	-5.226	5.401	ILE1, ARG3, TRP60
B	28	-24.380	-30.71	6.294	0.128	ASN42, GLY43, GLU44, ARG45,
						GLU47, SER88, GLN89, PRO90
C	22	-30.260	-24.38	-5.879	5.545	PRO14, ALA15, GLU16, ASN17
						GLU74, LYS75, ARG97

Å $^{(a)}$ Relative population of this cluster
$^{(b)}$ U_{Repr}: total interaction energy of the representative of the given cluster in kT with T= 300 K
$^{(c)}$ E_{LJ}: Lennard-Jones energy term for the representative complex, U_{ds}^{p}: non-polar (hydrophobic) desolvation energy of the representative complex, U_{ds}^{m}: surface desolvation energy of the representative complex, in kT
$^{(d)}$ U_{EP}: total electrostatic energy of the representative complex, in kT
$^{(e)}$ RMSD of the structures within the cluster with respect to the representative complex
$^{(f)}$ Residues with atoms contacting gold at distances $\leq$ 3 Å

3

# 2D [^{1}H, ^{15}N] HSQC Experiments

2D [^{1}H, ^{15}N] HSQC NMR experiments have been used to characterize, at amino acid residue level, the interaction between β_2m and gold nanoparticles at various molar ratios. Different samples containing 130 nM of 5nm AuNP (Sigma-Aldrich) and variable β_2m concentrations ranging from 4 to 36 μM were analysed.

Figure 2: 2D [^{1}H, ^{15}N] HSQC: In blue and red are depicted the HN cross peaks of the protein 17μM in the absence and in the presence of 130 mM of gold nanoparticles, respectively. β_2m is dissolved in 25 mM phosphate buffer, pH 6.47 and at 298K.

4

Validation of the Au surface with a positive charge density

As described in the main text, Section "Atomistic MD Simulations of β_2m on Citrate-Covered Au" we proposed an atomistic molecular mechanics surface model namely Cit-AuNPs, in which the fully deprotonated citrate anions ($\mathrm{C_3H_5O(COO)_3^{3-}}$) are described as interacting adsorbed species on a positively charged AuNPs with few neutralizing counterions. To support the choice of a positively charged gold core of the AuNPs which was taken line with current experimental understanding and for the sake of completeness, we conducted a 10 ns MD simulation at 300 K of the protonated protein in the presence of a different surface model based on a neutral gold core with the counter ions included in aqueous solution over the citrate, namely Cit3Na-AuNPs (*i.e.*, three Na+ ions released from each sodium citrate when it is put in aqueous solution). Simulations results are summarized in Fig. 3 in which panel (a) is referring to protein on Cit-AuNPs and panel (b) is referring to protein on Cit3NA-AuNPs.

Top panel of Fig. 3(a) report the unique stable orientation for the protonated protein during the last 10 ns of 20 ns T-REMD and Fig. 3(b) report the final representative structures of the orientations found for the protonated protein during the 10 ns of standard MD preceded by 2 ns equilibration. Lowest panels of Fig. 3(a-b) report the time evolution of contacting residues for the same protonated protein with respect to the two model surfaces, (a) cit-AuNPs along 10 ns of T-REMD and (b) Cit3Na-AuNP along 10 ns of standard MD. Results are qualitatively the same showing that in both cases, there is an unique and well conserved binding patch lowest panels in Fig. 3(a-b), involving the same N-Terminal residues (ILE1, GLN2, ARG3) and DE-loop residues (LYS58, TRP60) proving that the charge of the gold core is not really crucial in determing the binding of the protein to the surface in the present case. In details, contacts in regions of residues 58-60 are lost with the ral gold core but they are clearly highlighted by NMR results shown here. Therefore, we believe that a positive

5

Figure 3: Panels (a) refers to the protein on Cit-AuNPs and panel (b) to the protein on Cit3NA-AuNPs. Top panels (a) report the orientation of the protein on Cit-AuNPs during T-REMD and top panel (b) the orientation for the protein on cit3Na-AuNPs during MD. Lowest panels (a-b) report the time evolution of contacting residues for the protein with respect to the surface of Cit-AuNPs and Cit3NA-AuNPs, extracted from the last 10 ns of T-REMD and MD, respectively.
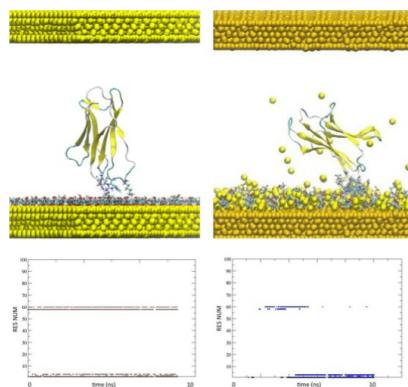
Positive Au vs Neutral Au

ILE1,GLN2, ARG3,HIS31, PRO32, LYS58,ASP59,TRP60

gold core is a more realistic model being in line with current understanding of citrate covered

nanoparticles, as discussed in the main text and supported by references.

6

ACKNOWLEDGEMENTS

REFERENCES

[1] Enrico Rennella et al., "Single-Shot NMR Measurement of Protein Unfolding Landscapes," *Biochimica et Biophysica Acta (BBA) - Proteins and Proteomics* 1824, no. 6 (June 2012): 842–49, doi:10.1016/j.bbapap.2012.04.002.

[2] Paul Schanda, Ēriks Kupče, and Bernhard Brutscher, "SOFAST-HMQC Experiments for Recording Two-Dimensional Deteronuclear Correlation Spectra of Proteins within a Few Seconds," *Journal of Biomolecular NMR* 33, no. 4 (December 2005): 199–211, doi:10.1007/s10858-005-4425-x.

[3] Giuliana Verdone et al., "The Solution Structure of Human β2-Microglobulin Reveals the Prodromes of Its Amyloid Transition," *Protein Science* 11, no. 3 (April 13, 2009): 487–99, doi:10.1110/ps.29002.

[4] The PyMOL Molecular Graphics System, Version 1.8 Schrödinger, LLC.

[5] P. N. Goodfellow et al., "The β2-Microglobulin Gene Is on Chromosome 15 and Not in the HL-A Region," *Nature* 254, no. 5497 (March 20, 1975): 267–69, doi:10.1038/254267a0.

[6] George F. Gao et al., "Crystal Structure of the Complex between Human CD8αα and HLA-A2," *Nature* 387, no. 6633 (June 5, 1997): 630–34, doi:10.1038/42523.

[7] M Colonna and J Samaridis, "Cloning of Immunoglobulin-Superfamily Members Associated with HLA-C and HLA-B Recognition by Human Natural Killer Cells," *Science* 268, no. 5209 (April 21, 1995): 405–8, doi:10.1126/science.7716543.

[8] M.A. Saper, P.J. Bjorkman, and D.C. Wiley, "Refined Structure of the Human Histocompatibility Antigen HLA-A2 at 2.6 Å Resolution," *Journal of Molecular Biology* 219, no. 2 (May 20, 1991): 277–319, doi:10.1016/0022-2836(91)90567-P.

[9] Yinan Zhang and David B. Williams, "Assembly of MHC Class I Molecules within the Endoplasmic Reticulum," *Immunologic Research* 35, no. 1–2 (2006): 151–62, doi:10.1385/IR:35:1:151.

[10] J. Floege et al., "Clearance and Synthesis Rates of Beta 2-Microglobulin in Patients Undergoing Hemodialysis and in Normal Subjects," *The Journal of Laboratory and Clinical Medicine* 118, no. 2 (August 1991): 153–65.

[11] A. R. Mezo et al., "X-Ray Crystal Structures of Monomeric and Dimeric Peptide Inhibitors in Complex with the Human Neonatal Fc Receptor, FcRn," *Journal of Biological Chemistry* 285, no. 36 (September 3, 2010): 27694–701, doi:10.1074/jbc.M110.120667.

[12] Stephan D. Gadola et al., "Structure of Human CD1b with Bound Ligands at 2.3 Å, a Maze for Alkyl Chains," *Nature Immunology*, July 15, 2002, doi:10.1038/ni821.

[13] J.N. Feder et al., "The Hemochromatosis Gene Product Complexes with the Transferrin Receptor and Lowers Its Affinity for Ligand Binding," *Proceedings of the National Academy of Sciences* 95, no. 4 (1998): 1472.

[14] S. Otsubo et al., "Characteristics of Dialysis-Related Amyloidosis in Patients on Haemodialysis Therapy for More than 30 Years," *Nephrology Dialysis Transplantation* 24, no. 5 (May 1, 2009): 1593–98, doi:10.1093/ndt/gfn706.

[15] F. Gejyo et al., "A New Form of Amyloid Protein Associated with Chronic Hemodialysis Was Identified as Beta 2-Microglobulin," *Biochemical and Biophysical Research Communications* 129, no. 3 (June 28, 1985): 701–6.

[16] P. D. Gorevic et al., "Polymerization of Intact Beta 2-Microglobulin in Tissue Causes Amyloidosis in Patients on Chronic Hemodialysis," *Proceedings of the National Academy of Sciences of the United States of America* 83, no. 20 (October 1986): 7908–12.

[17] T Miyata et al., "Beta 2-Microglobulin Modified with Advanced Glycation End Products Is a Major Component of Hemodialysis-Associated Amyloidosis.," *Journal of Clinical Investigation* 92, no. 3 (September 1, 1993): 1243–52, doi:10.1172/JCI116696.

[18] C. Capeillere-Blandin, T. Delaveau, and B. Descamps-Latscha, "Structural Modifications of Human β2 Microglobulin Treated with Oxygen-Derived Radicals," *Biochemical Journal* 277, no. 1 (July 1, 1991): 175–82, doi:10.1042/bj2770175.

[19] R. P. Linke et al., "Beta 2-Microglobulin, Different Fragments and Polymers Thereof in Synovial Amyloid in Long-Term Hemodialysis," *Biological Chemistry Hoppe-Seyler* 368, no. 2 (February 1987): 137–44.

[20] Vittorio Bellotti et al., "Beta 2-Microglobulin Can Be Refolded into a Native State from Ex Vivo Amyloid Fibrils," *European Journal of Biochemistry* 258, no. 1 (November 15, 1998): 61–67, doi:10.1046/j.1432-1327.1998.2580061.x.

[21] Sarah L. Myers et al., "A Systematic Study of the Effect of Physiological Factors on β2-Microglobulin Amyloid Formation at Neutral pH," *Biochemistry* 45, no. 7 (February 1, 2006): 2311–21, doi:10.1021/bi052434i.

[22] C. J. Morgan et al., "Kidney Dialysis-Associated Amyloidosis: A Molecular Role for Copper in Fiber Formation," *Journal of Molecular Biology* 309, no. 2 (June 1, 2001): 339–45, doi:10.1006/jmbi.2001.4661.

[23] Suguru Yamamoto et al., "Glycosaminoglycans Enhance the Trifluoroethanol-Induced Extension of β2-Microglobulin–Related Amyloid Fibrils at a Neutral pH," *Journal of the American Society of Nephrology* 15, no. 1 (January 1, 2004): 126–33, doi:10.1097/01.ASN.0000103228.81623.C7.

REFERENCES

[24] Henriett Pál-Gábor et al., "Mechanism of Lysophosphatidic Acid-Induced Amyloid Fibril Formation of β2-Microglobulin in Vitro under Physiological Conditions," *Biochemistry* 48, no. 24 (June 23, 2009): 5689–99, doi:10.1021/bi900356r.

[25] A. Relini et al., "Collagen Plays an Active Role in the Aggregation of beta2-Microglobulin under Physiopathological Conditions of Dialysis-Related Amyloidosis," *Journal of Biological Chemistry* 281, no. 24 (June 16, 2006): 16521–29, doi:10.1074/jbc.M513827200.

[26] Annalisa Relini et al., "Heparin Strongly Enhances the Formation of β2-Microglobulin Amyloid Fibrils in the Presence of Type I Collagen," *Journal of Biological Chemistry* 283, no. 8 (February 22, 2008): 4912–20, doi:10.1074/jbc.M702712200.

[27] G. Esposito et al., "Removal of the N-Terminal Hexapeptide from Human β2-Microglobulin Facilitates Protein Aggregation and Fibril Formation," *Protein Science* 9, no. 5 (2000): 831–45, doi:10.1110/ps.9.5.831.

[28] Timo Eichner et al., "Conformational Conversion during Amyloid Formation at Atomic Resolution," *Molecular Cell* 41, no. 2 (January 2011): 161–72, doi:10.1016/j.molcel.2010.11.028.

[29] T A Waldmann and W D Terry, "Familial Hypercatabolic Hypoproteinemia. A Disorder of Endogenous Catabolism of Albumin and Immunoglobulin.," *Journal of Clinical Investigation* 86, no. 6 (December 1, 1990): 2093–98, doi:10.1172/JCI114947.

[30] M. A. Wani et al., "Familial Hypercatabolic Hypoproteinemia Caused by Deficiency of the Neonatal Fc Receptor, FcRn, due to a Mutant beta2-Microglobulin Gene," *Proceedings of the National Academy of Sciences* 103, no. 13 (March 28, 2006): 5084–89, doi:10.1073/pnas.0600548103.

[31] Chaity Chaudhury et al., "The Major Histocompatibility Complex–related Fc Receptor for IgG (FcRn) Binds Albumin and Prolongs Its Lifespan," *The Journal of Experimental Medicine* 197, no. 3 (February 3, 2003): 315–22, doi:10.1084/jem.20021829.

[32] Sophie Valleix et al., "Hereditary Systemic Amyloidosis Due to Asp76Asn Variant β2-Microglobulin," *New England Journal of Medicine* 366, no. 24 (June 14, 2012): 2276–83, doi:10.1056/NEJMoa1201356.

[33] Hiroyuki Kumeta et al., "Low-Temperature-Induced Structural Changes in Human Lysozyme Elucidated by Three-Dimensional NMR Spectroscopy," *Biochemistry* 42, no. 5 (February 1, 2003): 1209–16, doi:10.1021/bi026730w.

[34] Wolfgang Kabsch and Christian Sander, "Dictionary of Protein Secondary Structure: Pattern Recognition of Hydrogen-Bonded and Geometrical Features," *Biopolymers* 22, no. 12 (December 1983): 2577–2637, doi:10.1002/bip.360221211.

[35] P.J. Artymiuk and C.C.F. Blake, "Refinement of Human Lysozyme at 1.5 Å Resolution Analysis of Non-Bonded and Hydrogen-Bond Interactions," *Journal of Molecular Biology* 152, no. 4 (November 1981): 737–62, doi:10.1016/0022-2836(81)90125-X.

[36] François Niyonsaba and Hideoki Ogawa, "Protective Roles of the Skin against Infection: Implication of Naturally Occurring Human Antimicrobial Agents β-Defensins, Cathelicidin LL-37 and Lysozyme," *Journal of Dermatological Science* 40, no. 3 (December 2005): 157–68, doi:10.1016/j.jdermsci.2005.07.009.

[37] Hisham R Ibrahim, Tetsuji Matsuzaki, and Takayoshi Aoki, "Genetic Evidence That Antibacterial Activity of Lysozyme Is Independent of Its Catalytic Function," *FEBS Letters* 506, no. 1 (September 28, 2001): 27–32, doi:10.1016/S0014-5793(01)02872-1.

[38] P. LeMarbre et al., "Lysozyme Enhances Monocyte-Mediated Tumoricidal Activity: A Potential Amplifying Mechanism of Tumor Killing," *Blood* 58, no. 5 (November 1, 1981): 994–99.

[39] M. B. Pepys et al., "Human Lysozyme Gene Mutations Cause Hereditary Systemic Amyloidosis," *Nature* 362, no. 6420 (April 8, 1993): 553–57, doi:10.1038/362553a0.

[40] Sophie Valleix et al., "Hereditary Renal Amyloidosis Caused by a New Variant Lysozyme W64R in a French Family," *Kidney International* 61, no. 3 (March 2002): 907–12, doi:10.1046/j.1523-1755.2002.00205.x.

[41] Masahide Yazaki, Sandra A. Farrell, and Merrill D. Benson, "A Novel Lysozyme Mutation Phe57Ile Associated with Hereditary Renal Amyloidosis," *Kidney International* 63, no. 5 (May 2003): 1652–57, doi:10.1046/j.1523-1755.2003.00904.x.

[42] Christoph Röcken et al., "ALys Amyloidosis Caused by Compound Heterozygosity in Exon 2 (Thr70Asn) and Exon 4 (Trp112Arg) of the Lysozyme Gene," *Human Mutation* 27, no. 1 (January 2006): 119–20, doi:10.1002/humu.9393.

[43] Mireille Dumoulin, Janet R. Kumita, and Christopher M. Dobson, "Normal and Aberrant Biological Self-Assembly: Insights from Studies of Human Lysozyme and Its Amyloidogenic Variants," *Accounts of Chemical Research* 39, no. 9 (September 2006): 603–10, doi:10.1021/ar050070g.

[44] Denis Canet et al., "Mechanistic Studies of the Folding of Human Lysozyme and the Origin of Amyloidogenic Behavior in Its Disease-Related Variants," *Biochemistry* 38, no. 20 (May 1, 1999): 6419–27, doi:10.1021/bi983037t.

[45] S. W. Englander and N. R. Kallenbach, "Hydrogen Exchange and Structural Dynamics of Proteins and Nucleic Acids," *Quarterly Reviews of Biophysics* 16, no. 4 (November 1983): 521–655.

[46] Frédéric Devernay, *C/C++ Minpack*, 2007, http://devernay.free.fr/hacks/cminpack/.

[47] Wayne J. Becktel and John A. Schellman, "Protein Stability Curves," *Biopolymers* 26, no. 11 (November 1987): 1859–77, doi:10.1002/bip.360261104.

[48] Thomas Schulte-Herbrüggen and Ole Winneche Sørensen, "Clean TROSY: Compensation for Relaxation-Induced Artifacts," *Journal of Magnetic Resonance* 144, no. 1 (May 2000): 123–28, doi:10.1006/jmre.2000.2020.

[49] Ewen Lescop, Paul Schanda, and Bernhard Brutscher, "A Set of BEST Triple-Resonance Experiments for Time-Optimized Protein Resonance Assignment," *Journal of Magnetic Resonance* 187, no. 1 (July 2007): 163–69, doi:10.1016/j.jmr.2007.04.002.

[50] Arthur G Palmer et al., "Sensitivity Improvement in Proton-Detected Two-Dimensional Heteronuclear Correlation NMR Spectroscopy," *Journal of Magnetic Resonance (1969)* 93, no. 1 (June 1991): 151–70, doi:10.1016/0022-2364(91)90036-S.

[51] Lewis Kay, Paul Keifer, and Tim Saarinen, "Pure Absorption Gradient Enhanced Heteronuclear Single Quantum Correlation Spectroscopy with Improved Sensitivity," *Journal of the American Chemical Society* 114, no. 26 (December 1992): 10663–65, doi:10.1021/ja00052a088.

[52] Stephan Grzesiek and Ad Bax, "The Importance of Not Saturating Water in Protein NMR. Application to Sensitivity Enhancement and NOE Measurements," *Journal of the American Chemical Society* 115, no. 26 (December 1993): 12593–94, doi:10.1021/ja00079a052.

[53] J. Schleucher et al., "A General Enhancement Scheme in Heteronuclear Multidimensional NMR Employing Pulsed Field Gradients," *Journal of Biomolecular NMR* 4, no. 2 (March 1994), doi:10.1007/BF00175254.

[54] Frank Delaglio et al., "NMRPipe: A Multidimensional Spectral Processing System Based on UNIX Pipes," *Journal of Biomolecular NMR* 6, no. 3 (November 1995), doi:10.1007/BF00197809.

[55] T. D. Goddard and D. G. Kneller, *SPARKY 3* (University of California, San Francisco, n.d.).

[56] Enrico Rennella et al., "Equilibrium Unfolding Thermodynamics of β2-Microglobulin Analyzed through Native-State H/D Exchange," *Biophysical Journal* 96, no. 1 (January 2009): 169–79, doi:10.1529/biophysj.108.142448.

[57] J. Kardos et al., "Direct Measurement of the Thermodynamic Parameters of Amyloid Formation by Isothermal Titration Calorimetry," *Journal of Biological Chemistry* 279, no. 53 (December 31, 2004): 55308–14, doi:10.1074/jbc.M409677200.

[58] Javier Gómez et al., "The Heat Capacity of Proteins," *Proteins: Structure, Function, and Genetics* 22, no. 4 (August 1995): 404–12, doi:10.1002/prot.340220410.